

NNT : 2016SACLE007



THESE DE DOCTORAT
de
L'UNIVERSITE DE COLOGNE
et de
L'UNIVERSITE PARIS-SACLAY,
préparée à l'Université d'Evry Val d'Essonne

ÉCOLE DOCTORALE N° 577
Structure et dynamique des systèmes vivants
Spécialité de doctorat Sciences de la Vie et de la Santé
MATHEMATISCH-NATURWISSENSCHATLICHE FAKULTAET

Par

M^{elle} Florence Jacob

**Cell death and transcriptional signalling mediated by
the coiled-coil domain of the barley resistance protein MLA**

Thèse présentée et soutenue à Cologne, le 25/04/2016.

Composition du Jury :

Pr. Döhlemann, Gunther	Professor, Institut für Botanik, Köln	Président
Pr. Hofmann, Kay	Professor, Institut für Genetik, Köln	Rapporteur
Pr. Panstruga, Ralph	Professor, RTWH Aachen	Rapporteur
Pr. Dron, Michel	Professor, Université Paris Sud	Examineur
Dr. Somssich, Imre	Research Group Leader, MPIPZ	Examineur
Pr. Hirt, Heribert	Research Group Leader, IPS2, Paris Saclay	Directeur de thèse
Pr. Schulze-Lefert, Paul	Professor, Institut für Genetik, Köln	Co-directeur de thèse



Cell death and transcriptional signalling mediated by the coiled-coil domain of the barley resistance protein MLA

Inaugural-Dissertation

zur

Erlangung des Doktorgrades

der Mathematisch-Naturwissenschaftlichen Fakultät

der Universität zu Köln

vorgelegt von

Florence Jacob

Aus Aix-en-Provence

Köln, April 2016

Die vorliegende Arbeit wurde am Max-Planck-Institut für
Pflanzenzüchtungsforschung in Köln in der Abteilung für Pflanze-Mikroben
Interaktionen (Direktor: Prof. Dr. P. Schulze-Lefert) und am Institute of Plant Sciences
Paris-Saclay in Orsay in der Abteilung für Physiology and Signalling (previously
URGV, Direktor: Prof. Dr. M. Crespi) angefertigt.

Berichterstatter: Prof. Dr. Kay Hofmann
Prof. Dr. Ralph Panstruga
Prof. Dr. Jürgen Zeier

Tag der mündlichen Prüfung: 25.04.2016

*Savoir s'étonner à propos
est le premier pas fait
sur la route de la découverte.*

*To know how to wonder and question
is the first step of the mind
toward discovery*

Louis Pasteur

Cell death and transcriptional signalling mediated by the coiled-coil domain of the barley resistance protein MLA

Abstract

Plants rely entirely on innate immunity to prevent infection by pathogens. Extracellular perception of evolutionarily conserved pathogen/microbe-associated molecular patterns (P/MAMP) by membrane-resident pattern recognition receptors (PRRs) leads to pattern-triggered immunity (PTI). Host-adapted pathogens intercept PRR-mediated immunity by delivering effectors into host cells. These polymorphic effectors can be recognized by intracellular immune receptors of the nucleotide-binding domain leucine-rich repeat (NLR) family. Upon effector recognition, NLRs trigger a rapid immune response, termed effector-triggered immunity (ETI), which is typically associated with a host cell death response. In barley, the NLR MLA confers ETI against the pathogenic powdery mildew fungus, *Blumeria graminis* f. sp. *hordei*. Although *MLA* orthologues are present only in the Triticeae family of monocotyledonous plants, barley *MLA* is functional in transgenic dicotyledonous *A. thaliana*, indicating that the underlying disease resistance mechanism has been evolutionarily conserved for at least 150 Mya in monocot and dicot plants. In dicotyledonous *Nicotiana benthamiana*, transient gene expression of the coiled-coil (MLA_{CC}) domain, consisting of the N-terminal 160 amino acids of the MLA receptor, was sufficient to activate a cell death response, raising the possibility that MLA initiates a conserved signalling mechanism through the MLA_{CC} domain. This thesis aimed at identifying signalling mechanism(s) acting downstream of the MLA_{CC} module in transgenic *A. thaliana*. Conditional MLA_{CC} expression triggered immune-related responses, characterized by a rapid onset of massive changes in gene expression at ~2 h post induction (hpi), followed by cell death at ~4 hpi. These MLA_{CC}-triggered responses are retained in *A. thaliana* plants simultaneously lacking the immune components PAD4, SAG101, PEN2, and all major defence phytohormones, i.e. ethylene, jasmonic acid, and salicylic acid. A comparison of time-resolved and genome-wide transcript profiles in MLA_{CC}-expressing transgenic plants with expression profiles induced during ETI and PTI by endogenous *A. thaliana* NLRs or PRRs revealed at early time points highly similar patterns. This suggests that early signalling mediated by MLA_{CC}, ETI, and PTI converges on a common transcriptional machinery that activates immune response genes,

implying that the barley MLA_{CC} domain is sufficient to stimulate an ETI-like response in *A. thaliana*. This also suggests that activation of these immune response genes can occur independently of PTI. Most (> 74.7%) of the 562 genes that were significantly upregulated at 2 hpi in MLA_{CC}-expressing plants are immediate early response genes since their induction does not depend on *de novo* protein synthesis, suggesting that these genes are activated by the removal of short-lived repressors. In the 5' regulatory regions of the early induced genes, I found a striking enrichment of *cis*-acting motifs that serve as binding sites for Ca²⁺-responsive transcription factors, including the calmodulin-binding transcription activator 3 (CAMTA3) which is known to be rapidly degraded during ETI. This might explain complete inhibition of MLA_{CC}-mediated responses by the Ca²⁺ channel inhibitor LaCl₃, which was previously also reported for several NLR-mediated and P/MAMP-triggered responses. Using chemical mutagenesis, I identified three candidate suppressor mutants of MLA_{CC}-mediated responses. Affinity purification of MLA_{CC} complexes and a yeast two-hybrid screen identified several MLA_{CC} candidate interacting proteins. Together this has revealed novel candidate components engaged in MLA_{CC} signalling.

Keywords: plant biology, phytopathology, immune system, resistance protein, immune signalling, hypersensitive response

Régulation transcriptionnelle et induction de la mort cellulaire par le domaine coiled-coil de MLA, protéine de résistance de l'orge

Résumé

La réponse immunitaire des plantes contre les pathogènes végétaux dépend entièrement du système immunitaire inné. La perception extracellulaire de motifs moléculaires conservés associés aux pathogènes/microbes (P/MAMP) par des récepteurs de reconnaissance de motifs moléculaires (PRR) induit un type de réponse immunitaire dénommé PTI (pattern-triggered immunity). Certains pathogènes interceptent cette réponse en injectant, dans les cellules hôtes, des protéines appelées effecteurs. Ces effecteurs, souvent polymorphiques, peuvent être détectés par des récepteurs immunitaires intracellulaires de la famille des NLR (nucleotide-binding domain leucine-rich repeat containing). En cas de détection, les NLRs induisent une réponse immunitaire rapide, appelée ETI (effector-triggered immunity), souvent associée à la mort des cellules hôtes. Un des NLRs présents chez l'orge, MLA, confère une ETI protectrice contre *Blumeria graminis* f. sp. *hordei*, l'agent pathogène du mildiou. Bien que MLA n'ait d'homologues qu'au sein de la famille monocotylédone des Triticeae, MLA est fonctionnel dans une lignée transgénique chez l'espèce dicotylédone *A. thaliana*. Ceci indique que le mécanisme de résistance sous-jacent a été conservé depuis plus de 150 Ma chez les plantes dicotylédones et monocotylédones. Chez la plante dicotylédone *Nicotiana benthamiana*, l'expression transitoire du domaine coiled-coil (MLA_{CC}) qui correspond aux 160 premiers acides aminés en N-terminus de MLA, suffit à induire la mort cellulaire. Cette observation suggère que MLA pourrait initier un mécanisme de signalisation conservé, via son domaine MLA_{CC}. Le but de cette thèse a été de décrire le(s) mécanisme(s) de signalisation en aval de MLA_{CC} dans des lignées transgéniques d'*A. thaliana*. L'expression conditionnelle de MLA_{CC} induit une réponse similaire à la réponse immunitaire, et caractérisée par l'initiation d'une reprogrammation transcriptionnelle massive à ~2 h post-induction (hpi) suivie par la mort des cellules à ~4 hpi. Cette réponse est aussi induite par MLA_{CC} chez une lignée transgénique d'*A. thaliana* qui est simultanément dépourvue de trois composants (PEN2, PAD4 et SAG101) et des trois principales phytohormones (éthylène, acide jasmonique et acide salicylique) impliqués dans la régulation immunitaire. La comparaison des profils d'expression au cours du temps chez des plantes exprimant MLA_{CC}, avec ceux induits au

cours de l'ETI et de la PTI chez *A. thaliana*, a révélé des patterns largement similaires lors de la réponse précoce. Ceci suggère que la signalisation initiée par MLA_{CC}, l'ETI et la PTI pourrait converger rapidement vers une machinerie de transcription commune qui active les gènes de la réponse immunitaire. De plus, ces données indiquent que le domaine MLA_{CC} de l'orge suffit à induire la réponse immunitaire normalement associée à l'ETI chez *A. thaliana*, et que l'activation des gènes de la réponse immunitaire peut se produire indépendamment de la PTI. La plupart (> 74.7%) des 562 gènes significativement induits à 2 hpi chez des plantes exprimant MLA_{CC} sont caractéristiques des gènes de type « immediate early response » puisqu'ils sont induits rapidement sans nécessiter la synthèse *de novo* de protéine. Ces gènes pourraient donc être activés par élimination d'un répresseur à courte durée de vie. Dans les régions régulatrices en 5' de ces gènes, des motifs sont fortement enrichis qui correspondent à des sites de liaison pour des facteurs de transcription sensibles au Ca²⁺, tels que le calmodulin-binding transcription activator 3 (CAMTA3) qui est rapidement dégradé au cours de l'ETI. Ceci pourrait expliquer l'inhibition totale de la réponse médiée par MLA_{CC} en présence de LaCl₃, un inhibiteur des canaux calciques, inhibition qui a aussi été décrite par le passé concernant les réponses induites par plusieurs NLRs et P/MAMPs. J'ai effectué un crible génétique de mutants obtenus par mutagenèse chimique et identifié par ce biais trois candidats suppresseurs de la réponse médiée par MLA_{CC}. La purification des complexes protéiques associés à MLA_{CC}, ainsi qu'un crible en double-hybride chez la levure ont permis d'identifier plusieurs candidats interagissant avec MLA_{CC}. Ces approches ont révélé de nouveaux candidats impliqués dans la signalisation médiée par MLA_{CC}.

Mots-clés : biologie végétale, phytopathologie, système immunitaire, protéine de résistance, signalisation immunitaire, réponse hypersensible

Zelltod- und transkriptionelle- Signalisierung aktiviert durch die Coiled-Coil Domäne von der Gersten-R-Protein MLA

Zusammenfassung

Pflanzen sind voll und ganz auf ihr angeborenes Immunsystem angewiesen um Infektionen durch Krankheitserreger zu verhindern. Extrazelluläre Erkennung von evolutionär konservierten Pathogenen/Mikroben-assoziierten molekularen Mustern (microbe/pathogen-associated molecular patterns; P/MAMP) durch membranassoziierte P/MAMP-Rezeptoren (pattern recognition receptors, PRRs), was zur sogenannten Muster-ausgelösten Immunität (pattern-triggered immunity, PTI) führt. Wirtsadaptierte Krankheitserreger hemmen diese Immunität durch die Sekretion von Effektoren in die Wirtszelle. Als Folge der Effektor-Erkennung, lösen NLRs eine rasche Immunantwort aus, welche als Effektor-ausgelöste Immunität (effector-triggered immunity, ETI) bekannt ist, und oft einen programmierten Zelltode beinhaltet. In Gerste vermitteln die MLA NLRs Resistenz gegenüber dem Mehltau Pilz *Blumeria graminis* f. sp. *hordei*. Obwohl *MLA*-Orthologe nur in anderen Mitgliedern der *Triticeae* Familie von Monokotyledonen Pflanzen bekannt sind, ist *MLA* in der Dikotyledonen Pflanze *Arabidopsis thaliana* voll funktionsfähig; was heißt, dass die *MLA*-zugrundeliegenden Widerstandsmechanismen über mindestens die letzten 150 Millionen Jahre evolutionär konserviert wurden. Transiente Genexpression der *MLA* Coiled-Coil‘ (*MLA_{CC}*) Domäne, bestehend aus den 160 N-terminalen Aminosäuren von *MLA*, in der Dikotyledonen Pflanze *Nicotiana benthamiana* ist ausreichend um den Zelltod auszulösen. Daher besteht die Möglichkeit, dass die *MLA_{CC}* Domäne verantwortlich für die Auslösung der konservierten Signalmechanismen ist. Diese Doktorarbeit bezweckt die Signalwege zu identifizieren, welche durch das *MLA_{CC}* Modul in *A. thaliana* ausgelöst werden. Konditionale *MLA_{CC}* Expression führt zu immunähnlichen Reaktionen, welche durch die rasche und gewaltige Änderung der Genexpression nach ca. zwei Stunden, und den Zelltod nach ca. vier Stunden gekennzeichnet sind. Diese von *MLA_{CC}* ausgelösten Reaktionen werden auch in der *A. thaliana* Mutante ausgelöst, welche nicht-funktionelle Mutationen in *PAD4*, *SAG101*, *PEN2*, und den Signalwegen der wichtigsten Verteidigungs-Phytohormone Ethylen, Jasmonsäure, und Salicylsäure trägt. Der zeitabhängige Vergleich von genomweiten Transkriptionsprofilen endogener *A. thaliana* NLRs und PRRs mit denen von *MLA_{CC}*

exprimierenden, transgenen Pflanzen, zeigte eine erhebliche Überschneidung der Transkriptionsprofile in den frühen Phasen nach Expressierung und Aktivierung der jeweiligen Rezeptoren. Dies weist darauf hin, dass die frühen, durch MLA_{CC}, ETI und PTI induzierten Signalwege zu einem gemeinsamen Transkriptionsmechanismus konvergieren, welcher zur Aktivierung von Immunitätsgenen führt. Diese Resultate deuten auch darauf hin, dass die MLA Coiled-Coil Domäne von Gerste tatsächlich ausreichend ist um in *A. thaliana* ETI-ähnliche Reaktionen herbeizuführen, was auch bedeutet, dass diese Immunreaktionen PTI-unabhängig sind. Die meisten (>74,7%) der 562 Gene, welche ca. zwei Stunden nach Induktion der MLA_{CC} Expression signifikant höher exprimiert sind, gehören zu den sogenannten „immediate early“ Genen, da deren Expression unabhängig von der *de novo* Proteinbiosynthese ist. Das wiederum bedeutet, dass die Expression dieser Gene durch den Verlust eines Transkriptionsrepressors ist. In der 5' Regulationsregion der früh induzierten Reaktionsgenen, identifizierte ich eine auffällige Anreicherung von *cis*-Regulationselementen, welche als Motive für Ca²⁺-regulierte Signal-Transkriptionsfaktoren dienen. Einer dieser Faktoren ist der calmodulin-binding transcription-activator 3 (CAMTA3), welcher während ETI abgebaut wird. Das wiederum könnte erklären warum Reaktionen von MLA_{CC} und anderen NLRs, durch den Kalziumkanalblocker LaCl₃ komplett gehemmt werden. Zusätzliche habe ich durch chemische Mutation drei Mutanten identifiziert welche auch die von MLA_{CC} herbeigeführten Reaktionen inhibieren. Eine Affinitätsreinigung von MLA_{CC} Proteinkomplexen und eine Hefe-Zwei-Hybrid-Suche (yeast-2-hybrid screen) identifizierten zusätzliche, mit MLA-assoziierende Proteine. Diese bisher nicht charakterisierten Kandidaten fungieren möglicherweise als Komponenten für die MLA_{CC} Signalwege.

Stichwörter: Pflanzenbiologie, Phytopathologie, Immunsystem, Resistenz-Protein, Immun-Signalweg, Hypersensitive Response

Preface and Acknowledgements

This thesis concludes my PhD work conducted jointly at the Max Planck Institute for Plant Breeding research (Cologne) and at the URGV-IPS2 (Evry/Orsay), in the frame of a “cotutelle”. This work has benefited from several contributions. Takaki Maekawa provided me with some of the starting material such as pENTR clones and later *A. thaliana* transgenic lines expressing full-length MLA variants. Several students performed under my supervision some work related to the project: Betel Endeshaw, Sebastian Böckmann and Parmida Jamali. Barbara Kracher provided a major contribution in the bioinformatics analysis of the raw RNA-seq data, the whole-genome resequencing data, and in the SHOREmap analysis. Xiangchao Gan supported the mapping of the MLA_{CC} suppressor mutation by analyzing the sequence information with a pipeline which he developed. The Y2H screen for MLA_{CC} interaction partners was performed in the group of Nobutaka Mitsuda (AIST, Japan). The group of Kenichi Tsuda and the group of Jane Parker shared some unpublished RNA-seq data which I integrated into a comparative transcriptomic analysis. Iris Finkemeier, Katharina Kramer and Anne Harzen from the MPIPZ proteomics facility performed the LC-MS-MS analysis of the affinity-purified protein complexes and provided scientific advising and support for the data analysis. All sequencing reactions were performed by the MPIPZ Genome Center. The French-German University financially supported the extra travel and accommodation costs related to the “cotutelle”.

Parts of the introduction have been taken from my review „Evolution and conservation of plant NLR functions“, published in *Frontiers*, in accordance with *Frontiers* terms and conditions.

I would like to thank Paul and Heribert for the opportunity to work in their groups, for their constant support, and all the very helpful scientific discussions. They were both a formidable source of inspiration and conveyed scientific enthusiasm in their own manner.

Many thanks to Takaki Maekawa for his daily support during my PhD, for being always there when needed to answer questions and solve problems. I not only learned a lot from him, on

both a scientific and a personal point of view, but also had a lot of pleasure working together with him.

Many thanks go to Pr. Ralph Panstruga and Pr. Kay Hofmann for reviewing my thesis as well as to the other members of my defence jury: Pr. Gunther Döhlemann, Dr. Imre Somssich, and Pr. Michel Dron.

I would like to thank Pr. Thomas Kufer for being part of my PhD committee and Jean Colcombet for both his involvement in my PhD committee and as a PhD co-director.

Many thanks to Takaki Maekawa, Isabel Saur, Eva Willing and Johan Zicola for their conscientious correcting of my thesis.

To the group members at the MPIPZ: Takaki, Xunli, Makoto, Stéphane, Hyeran, Saskia V. and B., Isabel, Sabine, Petra, lots of thanks for the great work atmosphere, the nice discussions, and the help provided. Without you, it would not have been the same great adventure.

To the group members at the URGV (now IPS2 Saclay): Jean B., Jean C., Marie, Marie-Lu, Cécile, Baptiste, Eleonora, Sebastian, Santiago, Tiffany, Ana, Yunhe, and Axel; a big merci for everything and for accommodating my presence over all the short periods of intensive work. I still owe you quite many cakes for this. Special thanks go to Jean Bigeard for sharing with me his knowledge and experience on tandem affinity purification.

I would like to thank my beloved partner in life, Vipul, for his patience and for standing by me during the ups and downs alike, and my parents for their useful advice and support despite the geographical distance.

Table of content

ABSTRACT	I
RESUME	III
ZUSAMMENFASSUNG	V
PREFACE AND ACKNOWLEDGEMENTS	VII
TABLE OF CONTENT	IX
INDEX OF TABLES.....	XV
INDEX OF FIGURES.....	XVI
INDEX OF SUPPLEMENTARY DATA	XVIII
INDEX OF SUPPLEMENTARY FIGURES.....	XVIII
INDEX OF SUPPLEMENTARY TABLES.....	XIX
ABBREVIATIONS	XX
INTRODUCTION.....	1
1. THE PLANT IMMUNE SYSTEM.....	1
1.1. AN OVERVIEW OF THE MULTI-LAYERED PLANT INNATE IMMUNE SYSTEM	1
1.2. DIVERSITY OF PATHOGENS AND DIVERSITY OF PATHOGEN DETECTION MECHANISMS	1
1.3. INNATE IMMUNE SIGNALLING	3
1.3.1 The early events downstream of pathogen recognition.....	3
1.3.2 Transcriptional reprogramming in immunity	5
1.4. HYPERSENSITIVE RESPONSE AND OTHER DEFENCE OUTPUTS.....	7
2. EFFECTOR-TRIGGERED IMMUNITY AND PLANT NLRs	9
2.1. NLR PROTEINS REPRESENT THE LARGEST CLASS OF R PROTEINS.....	9
2.2. FUNCTION OF THE DIFFERENT NLR MODULES	10
2.3. COMPARTMENTALIZATION OF NLRs AND NLR FUNCTIONS	12
2.4. KEY COMPONENTS REQUIRED FOR NLR FUNCTION	13
2.5. CONSERVATION OF THE NLR SIGNALLING MECHANISMS ACROSS PLANT SPECIES.....	14
3. CASE STUDY ON THE ETI MEDIATED BY THE BARLEY MLA.....	15
4. THE AIM OF THIS THESIS.....	17

RESULTS.....	19
CHAPTER 1. FUNCTIONAL CHARACTERIZATION OF THE MLA COILED-COIL MODULE IN <i>A. THALIANA</i>	21
1.1. INTRODUCTION.....	22
1.2. EXPRESSION OF THE MLA_{CC} MODULE INDUCES HR-LIKE RESPONSES IN <i>A. THALIANA</i>.....	23
1.2.1. Growth phenotype of stable transgenic lines expressing MLA _{CC}	23
1.2.2. Selection and characterization of a <i>DEXp:MLA_{CC}-mYFP</i> line conferring stable transgene expression over multiple generations.....	25
1.2.3. Conditional expression of MLA _{CC} induces a rapid cell death response and MAPK activation.....	25
1.2.4. MLA _{CC} -mediated cell death requires extracellular calcium influx but not NADPH-dependent oxidase activity.....	31
1.2.5. MLA _{CC} -mediated cell death is homodimer-dependent and similar to the HR induced by the autoactive full length MLA in <i>A. thaliana</i>	33
1.2.6. The MLA _{CC} domain induces cell death but not MAPK activation in partially immunocompromised <i>pen2 pad4 sag101 dde2 ein2 sid2</i> sextuple mutant plants	34
1.3. BARLEY MLA_{CC} JUMP-STARTS AN IMMUNE TRANSCRIPTIONAL PROGRAM INDEPENDENT OF MAPK ACTIVATION AND DEFENCE PHYTOHORMONES IN <i>A. THALIANA</i>	36
1.3.1. MLA _{CC} rapidly induces a transcriptional reprogramming which does not require the major defence phytohormones and MAPK activation.....	36
1.3.2. The MLA _{CC} -mediated transcriptional response is similar to several other NLR mediated- and P/MAMP-triggered early responses.....	41
1.3.3. Investigation of the 562 genes rapidly induced by MLA _{CC} and identification of immediate early immune response genes.....	48
1.4. ROBUSTNESS OF THE MLA_{CC}-TRIGGERED SIGNALLING MECHANISM.....	55
1.4.1. <i>RARI</i> is dispensable for MLA _{CC} -mediated responses	55
1.4.2. Robustness of MLA _{CC} -triggered responses in diverse environmental conditions.....	57
CHAPTER 2. A GENETIC SUPPRESSOR SCREEN TO UNRAVEL EVOLUTIONARILY CONSERVED SIGNALLING COMPONENTS REQUIRED FOR THE MLA_{CC}-TRIGGERED IMMUNE RESPONSES IN <i>A. THALIANA</i>	61
2.1. INTRODUCTION.....	62
2.2. THE SCREENING PROCEDURE: FROM PRIMARY SCREENING TO CONFIRMED CANDIDATE SUPPRESSORS....	64
2.2.1. Mutagenesis and generation of the M ₂ seed batches	64
2.2.2. Primary suppressor screening of the M ₂ population.....	66
2.2.2.1. Primary screening on MS plates.....	66
2.2.2.2. Primary screening on soil	66
2.2.3. Secondary screening of the ~1,900 primary M ₂ suppressor mutants.....	66

2.2.4. Parallel screening of the ~1,900 M ₂ suppressor candidates for hyper-responsivity to <i>Pst</i> DC3000 AvrRpm1	67
2.2.5. Integration of the different screening data and selection of 58 candidates for further characterization	69
2.2.6. Validation of the 58 mutant candidates by analysis of their M ₃ progeny phenotype.....	70
2.3. PRELIMINARY MUTATION MAPPING BASED ON THE WHOLE GENOME SEQUENCES OF THE M₂ MUTANT POPULATION	72
2.3.1. Introduction.....	72
2.3.2. Determination of the SNP profile of 21 M ₂ candidates using whole genome resequencing	73
2.3.3. Targeted analysis of prospective suppressor loci	76
2.3.4. Genome-wide analysis of the mutant allele frequencies	77
2.4. MAPPING OF THE CAUSAL MUTATIONS BY CLASSICAL “MAPPING BY SEQUENCING”	78
2.4.1. Generation and analysis of the segregating F ₂ populations	78
2.4.2. Mapping by sequencing applied to candidates 1A, 1E, 2B and 2H	80
2.5. CHARACTERIZATION OF <i>AT3G02840</i>, A CANDIDATE GENE ENCODING AN ARM-CONTAINING PROTEIN SHARING HIGH SIMILARITY WITH <i>AtCMPG1/PUB20</i> AND <i>AtPUB21</i>.....	85
 CHAPTER 3. IDENTIFICATION OF THE MLA_{CC}-ASSOCIATED SIGNALLING PARTNERS IN <i>A. THALIANA</i>	 93
3.1. INTRODUCTION.....	94
3.2. SCREENING FOR PHYSICAL INTERACTION BETWEEN MLA_{CC} AND <i>A. THALIANA</i> TRANSCRIPTIONAL REGULATORS BY YEAST TWO HYBRID.....	94
3.3. ISOLATION AND CHARACTERIZATION OF MLA_{CC}-ASSOCIATED PROTEIN COMPLEXES IN <i>A. THALIANA</i>.....	98
3.3.1. Design of the experimental setup and material preparation	98
3.3.1.1. Aims of the approach and experimental setup	98
3.3.1.2. Generation and characterization of the transgenic plant material	101
3.3.2. Optimization of the tandem affinity purification protocol	102
3.3.2.1. Optimization of the affinity purification procedure.....	102
3.3.2.2. Processing of the TAP samples	105
3.3.2.3. Analysis of the pull down input fractions for quality control and investigation of the proteome-wide MLA _{CC} -dependent responses.....	107
3.3.3. Quantitative MS data analysis of the pull downs leads to the identification of a MLA _{CC} candidate interactor list	109
3.3.3.1. Quantitative MS data analysis and identification of MLA _{CC} interactor candidates	109
3.3.3.2. Assessment of the biological relevance of the MLA _{CC} candidate interactors by data mining	114
3.3.3.3. Preliminary data for the functional characterization of PLA2A	116
3.3.4. MLA _{CC} might reside within large SDS-resistant protein polymers.....	117

DISCUSSION	119
1. MLA_{CC} INDUCES EFFECTOR-TRIGGERED IMMUNITY-LIKE RESPONSES IN <i>A. THALIANA</i>	120
2. THE EARLY TRANSCRIPTIONAL RESPONSES DURING PTI, ETI AND THOSE MEDIATED BY MLA_{CC} AND TEMPERATURE-DEPENDENT RPS4 ARE LARGELY OVERLAPPING	124
3. EARLY TRANSCRIPTIONAL REPROGRAMMING JUMP-STARTED BY NLRs IN THE ABSENCE OF ET, JA, SA AND EDS1. 129	
4. FORWARD SUPPRESSOR SCREENING OF MLA_{CC}-MEDIATED RESPONSES: OUTCOME AND CONCLUSIONS....	130
5. IDENTIFICATION OF CANDIDATE MLA_{CC} INTERACTION PARTNERS.....	133
CONCLUSION AND PERSPECTIVES.....	137
MATERIALS AND METHODS.....	139
1. MATERIAL.....	139
1.1. PLANT MATERIALS	139
1.1.1. <i>Arabidopsis thaliana</i>	139
1.1.2. <i>Nicotiana benthamiana</i>	140
1.2. BACTERIAL STRAINS.....	140
1.3. VECTORS.....	141
1.4. OLIGONUCLEOTIDES	143
1.5. ENZYMES	148
1.5.1. Restriction endonucleases	148
1.5.2. Nucleic acid modifying enzymes	148
1.6. CHEMICALS.....	149
1.7. ANTIBIOTICS.....	149
1.8. MEDIA 149	
1.9. ANTIBODIES	150
1.10. BUFFERS AND SOLUTIONS.....	150
2. METHODS	152
2.1. MAINTENANCE AND CULTIVATION OF <i>A. THALIANA</i> PLANTS	152
2.2. GENERATION OF <i>A. THALIANA</i> F₁, F₂, AND F₃ PROGENY.....	152
2.3. AGROBACTERIUM-MEDIATED STABLE TRANSFORMATION OF <i>A. THALIANA</i> (FLORAL DIP).....	152
2.4. <i>A. THALIANA</i> SEED SURFACE STERILIZATION.....	153
2.4.1. Standard seed surface sterilization	153
2.4.2. Vapor phase seed surface sterilization	153
2.5. PSEUDOMONAS SYRINGAE PV. TOMATO INOCULATION.....	153
2.5.1. <i>Pst</i> spray-infection	153
2.5.2. <i>Pst</i> detached leaf dipping	153
2.5.3. <i>Pst</i> infiltration assay for ion leakage measurement.....	154
2.5.4. <i>Pst</i> infiltration assay for RNA-seq	154
2.6. TEMPERATURE SHIFT	154
2.6.1. Temperature shift for analysis of the phenotype of the <i>p35S:MLA_{CC}-mYFP</i> lines.....	154

2.6.2. Temperature shift for RNA-seq.....	155
2.7. EMS-INDUCED MUTAGENESIS.....	155
2.8. YEAST TWO HYBRID (Y2H) SCREENING	155
2.8.1. Y2H screening for AT3G02840 interaction partners	155
2.8.2. Y2H screening for ML _{ACC} interaction partners (AIST system).....	156
2.9. DEXAMETHASONE (DEX)-INDUCIBLE EXPRESSION IN STABLE <i>A. THALIANA</i> TRANSGENIC LINES.....	156
2.9.1. Leaf disc assays.....	156
2.9.2. Leaf infiltration	157
2.10. ESTRADIOL (ER)-INDUCIBLE EXPRESSION IN STABLE <i>A. THALIANA</i> TRANSGENIC LINES.....	157
2.10.1. Seedling assays.....	157
2.10.2. Large scale induction of older plants	158
2.11. SCREENING FOR SUPPRESSORS OF ML_{ACC}-MEDIATED SIGNALLING.....	158
2.11.1. Primary screening on plates	158
2.11.2. Primary screening on soil.....	158
2.11.3. Secondary screening.....	158
2.11.4 Analysis of the M ₃ and F ₂ .BC _T progeny.....	159
2.11.4.1. Scoring and selection of mutant plants	159
2.11.4.2. Selection of wild-type plants in the F ₂ .BC _T progeny (negative segregant bulk).....	159
2.12. TRYPAN BLUE STAINING.....	159
2.13. BIOCHEMICAL METHODS.....	159
2.13.1. <i>A. thaliana</i> total protein extraction for immunoblot analysis.....	159
2.13.2. Denaturing SDS-polyacrylamide gel electrophoresis (SDS-PAGE).....	159
2.13.3. Immunoblot analysis (Western Blot)	160
2.13.4. Detection of phosphorylated MAPK by Western Blot.....	160
2.13.4.1. MAPK extraction	160
2.13.4.2. Immunodetection of phosphorylated MAPKs	161
2.13.5. Semi-Denaturing Detergent-Agarose Gel Electrophoresis (SDD-AGE).....	161
2.13.6. Tandem affinity purification (TAP) of protein complexes.....	162
2.13.7. Mass spectrometry (MS) analysis of <i>A. thaliana</i> protein extracts.....	162
2.13.7.1. Proteolytic digestion and desalting.....	162
2.13.7.2. LC-MS/MS data acquisition.....	163
2.13.7.3. Data analysis.....	163
2.14. MOLECULAR BIOLOGICAL METHODS	164
2.14.1. Isolation of genomic DNA from <i>A. thaliana</i> (Edwards method)	164
2.14.2. Isolation of high molecular weight genomic DNA from <i>A. thaliana</i>	164
2.14.3. Isolation of total RNA from <i>A. thaliana</i>	164
2.14.4. Polymerase chain reaction (PCR).....	164
2.14.5. Plasmid DNA isolation from bacteria	165
2.14.6. Restriction endonuclease digestion of DNA	165
2.14.7. Cloning of DNA fragments into pENTR/D-TOPO vector.....	165
2.14.8. Site specific recombination of DNA in Gateway®-compatible vectors.....	165

2.14.9. Agarose gel electrophoresis of DNA.....	165
2.14.10. Isolation of DNA fragments from agarose gel	166
2.14.11. Transformation of chemically competent <i>E. coli</i> cells	166
2.14.12. Transformation of electro-competent <i>A. tumefaciens</i> cells	166
2.14.13. Genome Walking	166
2.15. CONFOCAL LASER SCANNING MICROSCOPY (CLSM)	166
2.16. MICROARRAY DATA ANALYSIS.....	167
2.17. RNA-SEQ ASSAY	167
2.18. RNA-SEQ DATA ANALYSIS.....	167
2.19. PROMOTER ELEMENT ENRICHMENT ANALYSIS.....	168
2.20. GENE ONTOLOGY (GO) TERM ENRICHMENT ANALYSIS.....	168
2.21. HEATMAPS	168
2.22. VISUALIZATION AND ANALYSIS OF COEXPRESSION NETWORKS	169
2.23. COMPARATIVE TRANSCRIPTOMIC ANALYSIS.....	169
2.24. VENN DIAGRAMS	169
2.25. ANALYSIS OF SINGLE NUCLEOTIDE POLYMORPHISMS (SNP) IN THE CANDIDATE MUTANTS.....	169
2.25.1. Whole genome resequencing	169
2.25.2. SNP mapping and analysis in the M ₂ candidates	169
2.25.3. SNP mapping and analysis in the F ₂ .BC _T bulks	170
REFERENCES	171
SUPPLEMENTARY DATA.....	193
1. SUPPLEMENTARY FIGURES.....	193
2. SUPPLEMENTARY TABLES	212
ERKLÄRUNG.....	219
CURRICULUM VITAE	221

Index of tables

Table 1-1: Overrepresentation of cis-regulatory sequences in the promoter of the 562 MLACC early-induced genes.....	52
Table 2-1: Calculation method for the candidate mutant score.....	70
Table 2-2: Description of the 21 M ₂ mutant candidates selected for characterization.....	71
Table 2-3: Analysis of the SNPs number and their effects in the 21 M ₂ candidate mutants ..	76
Table 2-4: Candidate SNPs with significant impact on genes identified on chromosome 1 of candidate mutants 2B and 2H. A, SNP description. B, gene description.....	84
Table 2-5: AT3G02840 candidate interactors identified by Y2H.....	92
Table 3-1: Description of the clone libraries used for yeast two hybrid screening.....	95
Table 3-2: Number of candidate interactions identified by Y2H.....	95
Table 3-3: Description of the MLACC candidate interactors identified by Y2H.....	96
Table 3-4: TF family representation in the 31 MLACC candidate interactors	97
Table 3-5: Summary of the samples processed by TAP and analysed by MS.....	105
Table 3-6: Protein groups identified by MS analysis exclusively in the MLACC-PC2 pull down fractions but not in the pull down controls.....	110
Table 3-7: MLACC candidate interactors identified by MS analysis of MLACC pull down..	111

Index of figures

Figure 1-1: Plant growth phenotype and leaf chlorosis of <i>DEXp:MLACC-mYFP</i> expressing transgenic lines.....	24
Figure 1-2: Timing of <i>MLACC</i> -dependent activation of cell death and MAPKs in leaves.	27
Figure 1-3: Subcellular localization of <i>MLACC-mYFP</i> fusion protein in <i>A. thaliana</i>	28
Figure 1-4: Time series of confocal images of epidermal cells expressing <i>MLACC-mYFP</i> ...	30
Figure 1-5: Effect of the calcium channel blocker LaCl_3 and the NADPH oxidase inhibitor DPI on <i>MLACC</i> -mediated cell death.....	32
Figure 1-6: <i>MLACC</i> -mediated MAPK activation is abolished in the <i>ppsdes</i> mutant background.....	35
Figure 1-7: <i>MLACC</i> rapidly induces a similar transcriptional reprogramming in wild type <i>A. thaliana</i> (Col-0) and <i>ppsdes</i> mutant background.	39
Figure 1-8: GO term enrichment analysis of <i>MLACC</i> -upregulated genes at 2 hours after induction.....	42
Figure 1-9: Transcriptome-wide correlation analysis among <i>MLACC</i> -, ETI- and PTI-associated gene expression patterns.	45
Figure 1-10: Expression profile of the genes rapidly induced upon <i>MLACC</i> expression in the early response to diverse biotic, abiotic, hormone and chemical treatments.	50
Figure 1-11: Analysis of CAMTA binding motif frequency and distribution in 5' <i>cis</i> -regulatory sequences.	54
Figure 1-12: <i>RARI</i> is dispensable for <i>MLACC</i> function.....	56
Figure 1-13: <i>MLACC</i> -mediated growth phenotype is only partially temperature sensitive. ...	58
Figure 2-1: DEX-inducible expression of <i>MLACC-mYFP</i> leads to growth arrest.....	62
Figure 2-2: Flowchart of the genetic suppressor screen for <i>MLACC</i> -dependent growth arrest.	63
Figure 2-3: Nomenclature used in this chapter to identify each analysed generation and lineage.	65
Figure 2-4: Examples of <i>M</i> ₂ candidates displaying enhanced symptoms after inoculation with <i>Pst</i> DC3000 AvrRpm1.	67
Figure 2-5: Position of the confirmed and putative loss of function mutations identified in RPM1.	68
Figure 2-6: Number of homozygous SNPs identified in each of the 22 <i>M</i> ₂ plants.....	74
Figure 2-7: Overall SNP analysis before and after curation for background SNPs.....	75
Figure 2-8: Segregation ratio of the <i>F</i> ₂ .BC _T progeny of the candidate mutants.	79

Figure 2-9: Allele frequencies identified by sequencing of segregant bulks for the candidate mutants 1A, 2B and 2H.	83
Figure 2-10: Candidate SNPs identified on chromosome 1 by analysis of positive and negative segregant bulks of the mutant candidates 2B and 2H.	83
Figure 2-11: Comparison of AT3G02840 and <i>AtCMPG1</i> protein structure and domain composition.	85
Figure 2-12: AT3G02840 sequence analysis.	86
Figure 2-13: Analysis of <i>AT3G02840</i> expression in <i>A. thaliana</i> upon <i>MLA_{CC}</i> expression or <i>MLA1</i> activation.	88
Figure 2-14: Effect of AT3G02840 deficiency on HR cell death triggered by RPM1.	90
Figure 3-1: Overview of the TAP strategy and the construct used.	99
Figure 3-2: Bait constructs expressed in the <i>A. thaliana</i> transgenic lines for the TAP analysis.	100
Figure 3-3: Characterization of the bait-PC2 constructs used for TAP.	102
Figure 3-4: Abundance-based ranking of the proteins identified in the different pull downs.	104
Figure 3-5: Immunoblot analyses of tandem affinity-purified plant extracts expressing <i>MLA_{CC}-PC2</i> , <i>mYFP-PC2</i> and <i>MLA_{CC}L36E-PC2</i>	106
Figure 3-6: Volcano plot of the protein groups identified in the TAP input samples of the <i>MLA_{CC}</i> line and the <i>mYFP</i> line.	108
Figure 3-7: Overview of the protein groups identified by MS analysis in the TAP samples.	110
Figure 3-8: Volcano plot of the protein groups identified by MS analysis in <i>MLA_{CC}-PC2</i> pull down versus the control pull downs.	112
Figure 3-9: Abundance-based ranking of the protein groups confirms the enrichment of several candidate interactors in the <i>MLA_{CC}</i> pull down compared to the control pull downs.	114
Figure 3-10: Expression profile of the <i>MLA_{CC}</i> candidate interactors in <i>A. thaliana</i> upon <i>MLA_{CC}</i> expression.	116
Figure 3-11: Effects of PLA2A inhibitors on <i>MLA_{CC}</i> -mediated cell death.	117
Figure 3-12: <i>MLA_{CC}</i> predominantly resides in large SDS-resistant protein complexes.	118

Index of supplementary data

Index of supplementary figures

Figure S1-1: Genomic location of the <i>DEXp:MLACC-mYFP</i> transgene in line #5.1 as defined by sequencing of the flanking regions.....	193
Figure S1-2: Ion leakage measure in the <i>DEXp:MLACC-mYFP</i> line upon DEX treatment...	193
Figure S1-3: Cell death induction by MLACC and MLAMHD in <i>A. thaliana</i>	195
Figure S1-4: Analysis of the top 3,153 differentially expressed genes upon MLACC expression in wild-type or <i>ppsdes</i> mutant background.	197
Figure S1-5: Expression profile of EDS1, SA and, ET/JA marker genes upon MLACC expression in wild-type and <i>ppsdes</i> mutant.....	198
Figure S1-6: GO term enrichment analysis in genes differentially expressed upon MLACC expression in wild type <i>A. thaliana</i> (Col-0) and <i>ppsdes</i> mutant background.	199
Figure S1-7: Expression profile of various gene clusters after inoculation with different pathogens and MLACC inducible expression.	200
Figure S1-8: Extended expression profile of the genes rapidly induced upon MLACC expression in the early response to diverse biotic, abiotic, hormone and chemical treatments.	201
Figure S1-9: Effect of sucrose concentration and day length on the MLACC-mediated growth phenotype.	202
Figure S2-1: Pictures of four representative screening plates.....	203
Figure S2-2: Pictures of the pilot screen conducted on soil.....	204
Figure S2-3: Distribution of the suppressor candidate scores.....	204
Figure S2-4: Effect of DZNep and Zeb on transgene silencing.....	205
Figure S2-5: Segregation analysis of the F ₂ .BC _T progeny.....	206
Figure S3-1: Plasmid maps of the estradiol inducible vectors used in this study.	207
Figure S3-2: Optimization of the TAP extraction buffer composition.	208
Figure S3-3: Clustering analysis of the TAP input and eluate samples.....	210
Figure S3-4: Multi scatterplot showing the correlation in protein group abundance (LFQ intensities) between all samples of the TAP input fractions.	211

Index of supplementary tables

Table S1-1: Description of the transcriptomic datasets used for comparative transcriptomic analysis together with the MLACC-related transcriptomic profiling.....	213
Table S2-1: List of loci selected for the targeted analysis of the 21 M ₂ candidate mutants sequenced.....	214
Table S2-2: SNPs isolated by the targeted (A) and the untargeted (B) analysis in the 21 M ₂ suppressor mutants sequenced	215
Table S2-3: Mutations identified in the candidate mapping intervals for the candidate mutants 1A, 2B and 2H.....	216
Table S3-1: Top 16 differentially expressed protein groups (DEPGs) in lines expressing MLACC-PC2 compared to lines expressing mYFP-PC2.....	217
Table S3-2: Comparison of proteomic and transcriptomic data.....	217
Table S3-3: Protein abundance of the 9 MLACC candidate interactors.....	218
Table S3-4: Co-expression degree between the candidates.	218
Table S3-5: Ortholog search for the nine MLACC candidate interactors in Phytozome v10.3.	218

Abbreviations

-	translational fusion (in the context of protein fusion constructs)
∅	diameter
°C	degree Celsius
A.A	amino acid
ABA	abscissic acid
AIST	National Institute of Advanced Industrial Science and Technology
ARA	aristolochic acid
ARM	armadillo
Avr	avirulence
BEL	bromo-enol lactone
BLAST	basic local alignment search tool
bp	base pair
C-terminal	carboxy-terminal
CaMV	cauliflower mosaic virus
CC	coiled-coil
CHAPS	3-[(3-Cholamidopropyl)dimethylammonio]-1-propanesulfonate
CMPG	protein family Cys, Met, Pro and Gly
CNL	CC-NBS-LRR
cpm	count per million
DAMP	damage-associated molecular pattern
DDM	β-D-Maltopyranoside
DEG	differentially expressed gene(s)
DEPG	differentially expressed protein group(s)
DEX	dexamethasone
DEXp	dexamethasone-inducible promoter
DMSO	dimethylsulfoxid
DNA	deoxyribonucleic acid
dpg	day(s) post germination
DPI	diphenylene iodonium
DZNep	3-Deazaneplanocin A
EDS1	Enhanced disease resistance 1
EMS	ethyl methanesulfonate
ER	estradiol
ET	ethylene
FC	fold change
FDR	false discovery rate
Fig.	figure
FL	full length
FW	fresh weight
g	gram(s)
gDNA	genomic DNA
GO	gene ontology
GVG	GAL4-binding domain-VP16 activation domain-GR fusion
h	hour(s)

Het	heterozygous
Hom	homozygous
hpi	hour(s) post inoculation/induction/infiltration
HR	hypersensitive response
HRP	horseradish peroxidase
iBAQ	intensity-based absolute quantification
JA	jasmonic acid
KO	knock out
L	litre
LaCl ₃	lanthanum(III) chloride
LC	liquid chromatography
LFQ	label free quantification
log	logarithm
log ₂	logarithm base two
LRR	leucine-rich repeats
m	milli
M	molar (mol/L)
MAMP	microbe-associated molecular pattern (=PAMP)
MAPK	mitogen-activated protein kinase(s)
max.	maximum
min	minute(s)
min.	minimum
MLAcc	MLA coiled-coil domain
MPIPZ	Max Planck Institute for Plant Breeding Research
mRNA	messenger ribonucleic acid
MS	Murashige and Skoog medium, or mass spectrometry
MW	molecular weight
mYFP	monomeric yellow fluorescent protein
NB-ARC	nucleotide-binding adaptor shared by APAF-1, R proteins, and CED-4
NBS	nucleotide binding-site
NDR1	Non race-specific disease resistance 1
NLR	nucleotide-binding domain and leucine rich repeats-containing protein(s)
N-terminal	amino-terminal
ng	nanogram(s)
NP-40	nonidet P-40
OD	optical density
ON	overnight
PAGE	polyacrylamide gel-electrophoresis
PAMP	pathogen-associated molecular pattern (=MAMP)
PCD	plant cell death
PCR	polymerase chain reaction
pH	negative decimal logarithm of the H ⁺ concentration
<i>Pst</i>	<i>Pseudomonas syringae</i> pv. <i>tomato</i>
PUB	plant U-box protein(s)
pv.	pathovar
qRT-PCR	quantitative reverse transcription-polymerase chain reaction

R-gene	resistance gene
RNA	ribonucleic acid
RNAseq	RNA sequencing
rpm	round per minute
RPM	resistance to <i>Pseudomonas syringae</i> pv. <i>maculicola</i>
RPS	resistant to <i>Pseudomonas syringae</i>
RT	room temperature
s	second(s)
SA	salicylic acid
SDS	sodium dodecyl sulphate
SNP	single nucleotide polymorphism
Stdev	standard deviation
T-DNA	transfer DNA
TAP	tandem affinity purification
TBS	tris buffered saline
TF	transcription factor
TIR	Toll/interleukine-1 receptor homology domain
TNL	TIR-NBS-LRR
TR	transcription regulator
Tris	Tris-(hydroxymethyl)-aminomethane
TUM	Technische Universität München
U	unit(s)
UCSD	University California, San Diego
URGV/IPS2	Unité de Recherche en Génomique Végétale/Institute of Plant Science - Paris Saclay
UTR	untranslated region
V	Volt(s)
v/v	volume per volume
w/v	weight per volume
WB	western blot (immunoblot)
WT	wild-type
Y2H	yeast two hybrid
Zeb	zebularine

Introduction

1. The plant immune system

1.1. An overview of the multi-layered plant innate immune system

Contrary to vertebrates, plants possess neither an adaptive immune system nor specialized immune cells. Therefore each plant cell relies entirely on its own innate immunity to defend itself against pathogens (Maekawa et al., 2011a). To achieve a specific and localized immune response, plants have evolved several lines of defence against pathogens. Plasma membrane-localized pattern-recognition receptors detect in the extracellular space the presence of conserved pathogen-derived epitopes, such as bacterial flagellin and fungal chitin, and stimulate an immune response which limits pathogen proliferation (Boller and Felix, 2009). However, host-adapted pathogens can suppress this immune response by delivering highly polymorphic effector arsenals inside host cells (Jones and Dangl, 2006; Rafiqi et al., 2012). As a counter mechanism, plants deploy resistance (R) proteins to detect the presence of the effectors, which in turn trigger a potent immune response that terminates pathogen growth (Chisholm et al., 2006; Jones and Dangl, 2006). The former type of immune response is called “pattern-triggered immunity” (PTI), whereas the latter is called “effector-triggered immunity” (ETI). ETI is often associated with a local and rapid host cell death at sites of attempted pathogen ingress, designated the hypersensitive response (HR) (Maekawa et al., 2011a).

1.2. Diversity of pathogens and diversity of pathogen detection mechanisms

Plants can be threatened by a wide range of taxonomically diverse pathogens such as viruses, bacteria, fungi, oomycetes, and nematodes. The site of pathogen challenge can be either at aerial organs (e.g. leaves) or at underground organs (e.g. roots). Plant pathogens are also diverse in terms of host range, pathogenicity, and life style. Whereas some “generalists” can colonize a large host range (e.g. the root pathogenic fungus *Rhizoctonia solani*), others behave as “specialists” with a restricted host range (e.g. the powdery mildew fungus *Blumeria graminis* whose eight distinct *formae speciales* each infects a distinct genus of grasses). Different strategies are employed by pathogens to exploit the plants. For instance, a group of

1. The plant immune system

pathogens, denoted as biotrophs, can engage in a feeding process only with living plant cells. This strategy implies the capacity to inhibit host defence and host death. In the more specific case of obligate biotrophy, the pathogen can grow and complete its reproductive cycle only on its living host. Thus biotrophs, and to an even higher degree obligate biotrophs, are tightly co-evolving with their hosts and usually display a narrow host range. In contrast, necrotrophic pathogens kill host cells in order to feed on dead plant tissues (e.g. the fungus *Fusarium oxysporum*, causal agent of vascular wilt disease in many species such as banana tree, cotton, melon, and tomato). Other pathogens have adopted an intermediate strategy referred to as hemibiotrophy which starts with a biotrophic phase followed by a shift to a necrotrophic phase. From the plant side, such pathogen diversity implies the activation of specific defence responses.

Upon pathogen challenge, plants recognize pathogens via pattern recognition receptors (PRRs). Plant PRRs are surfaced-localized receptor kinases or receptor-like proteins which recognize a wide range of microbe- or plant-derived molecules (Zipfel, 2014). Since the molecules recognized by PRRs are not specific to phytopathogens, PRR-triggered immunity (PTI) is activated by, and efficiently limits the growth of various pathogenic and non-pathogenic organisms in contact with the plant. PRRs can be either broadly conserved across flowering plants, such as FLS2 (FLAGELLIN-SENSITIVE-2), or present only in restricted taxa, such as EFR (EF-TU RECEPTOR) in Brassicacea. FLS2 recognizes an epitope consisting of 22 amino acids of the bacterial flagellin (flg22). Among the other recognized bacterial-derived molecules are the elongation factor Tu (EF-Tu, recognized by EFR), HrpZ, peptidoglycans and lipopolysaccharides (LPS). On the fungus and oomycete side, chitin and NPP1 (NECROSIS-INDUCING PHYTOPHTORA PROTEIN-1) induce PTI. Mechanisms for recognition of viruses and insects have been so far less documented. In addition to non-self-sensing, PRRs also detect self-molecules, so-called DAMPs (damage-/danger- associated molecular patterns) which are released upon cell damage or pathogen detection. Three DAMPs have been documented so far: the Pep peptide family, oligogalacturonides, and extracellular ATP. The green leaf volatile E-2-hexenal is produced upon wounding, herbivory and pathogen infection, and act as a potent inducer of general defence response (Mirabella et al., 2015). Thus, hexenal is also a potential DAMP. DAMP perception can activate defence responses similar to PTI and contributes to amplification of the PTI in a positive feedback loop (Zipfel, 2014).

1. The plant immune system

A key for successful pathogen invasion is the release of effector proteins which can sabotage the PTI and manipulate the host cell to promote efficient colonization. Therefore, plants have evolved a highly specific pathogen recognition mechanism mediated by so-called resistance (R) proteins which can sense the presence of pathogen effectors. The recognition results in a potent immune response designated effector triggered immunity (ETI). The corollary of this system is that pathogen effectors are under selection pressure to escape recognition whereas selection pressure promotes allelic diversification of R proteins to expand the recognition repertoire and keep up with effector evolution. This layer of the plant immune system has been at the beginning genetically described as a “gene for gene” interaction, since ETI is controlled by a pair of matching genes: the plant *R* gene on one side, and its cognate pathogen avirulence (*Avr*) gene on the other side (Flor, 1955). This model has set the basis for the definition of virulence/avirulence and compatible/incompatible interaction: a virulent pathogen is a pathogen whose effectors are not recognized by any of the R proteins of the host plant and thus does not trigger the ETI (compatible interaction). By opposition, an avirulent pathogen has at least one effector recognized by at least one R protein of the host plant and does trigger the ETI (incompatible interaction). The highly pathogen-specific property of ETI makes it resemble to some extent the acquired immunity in mammals. The mechanisms of effector recognition by plant R proteins has been well established. Plant R proteins utilize two major modes of effector recognition: a direct and an indirect recognition mode (Chisholm et al., 2006; DeYoung and Innes, 2006; van der Hoorn and Kamoun, 2008; Jones and Dangl, 2006). In case of a direct recognition, an effector is detected by direct physical interaction with its cognate R protein, whereas during the indirect recognition, an R protein senses modifications of host proteins caused by the cognate effector action. Experimental evidence supports that the indirect recognition enables a single R protein to recognize multiple effectors irrespective of effector structures when effectors target the same host protein (Chisholm et al., 2006; Jones and Dangl, 2006). However, detection of multiple effectors by a single R protein is not exclusive to the indirect recognition mode. Recently it was demonstrated that the rice R protein pair RGA4/RGA5 detects at least two sequence-unrelated effectors of *Magnaporthe oryzae* by direct binding (Cesari et al., 2013).

1.3. Innate immune signalling

1.3.1 The early events downstream of pathogen recognition

Although the knowledge in this field remains largely incomplete, qualitatively similar signalling mechanisms seem to occur upon ETI and PTI activation. It has been proposed that quantitative and temporal differences mainly account for the distinct outputs of ETI and PTI, and that different types of R proteins also trigger similar responses (Jones and Dangl, 2006; Maleck et al., 2000; Navarro et al., 2004; Tao et al., 2003; Tsuda and Katagiri, 2010). Pathogen perception induces a rapid and transient increase of calcium (Ca^{2+}) concentration in the cytosol or other subcellular compartments. This elevation of Ca^{2+} concentration represents one of the earliest common signalling events downstream of all modes of pathogen detection. Ca^{2+} signals are decoded by calcium sensors (calmodulin [CaM], calmodulin-like proteins, calcium dependent protein kinases [CDPK], and calcineurin B-like proteins [CBL]), and regulate several pathways involved in immune signalling (Poovaiah et al., 2013). CDPKs are important players in immunity (Boudsocq and Sheen, 2013). For example, CDPKs can directly regulate the NADPH oxidase RBOHB (RESPIRATORY BURST OXIDASE HOMOLOG B) leading to the production of reactive oxygen species which act as both antimicrobial compounds and signalling molecules further contributing in the immune signalling (Baxter et al., 2013). Pathogen recognition also activates a signalling cascade mediated by mitogen-activated protein kinases (MAPKs). In *A. thaliana*, functionally redundant AtMPK3 and AtMPK6 are activated upon several stresses including pathogen detection by a partially unknown mechanism. The immune signalling also involves a complex interplay between several plant hormones. Salicylic acid (SA), jasmonic acid (JA), and ethylene (ET) are considered as the three major defence phytohormones but abscisic acid (ABA), gibberellins (GA), auxin, cytokinins, brassinosteroids and nitric oxide can also modulate the immune signalling network (Pieterse et al., 2012). In a simple model, SA and ET/JA act antagonistically to positively regulate plant defence against biotrophic pathogens and against necrotrophic pathogens and herbivorous insects, respectively (Bari and Jones, 2009; Glazebrook, 2005). However, accumulating evidence suggests a more complex hormone cross-talk whose molecular bases are being gradually resolved (Pieterse et al., 2012; Tsuda and Somssich, 2015).

Two interesting facts have emerged from the study of the immune signalling network. First, many of the recruited components are not specific to immunity and can be involved in other stress responses such as response to abiotic stresses. Second, all the above-mentioned

1. The plant immune system

signalling pathways converge on transcription factor regulation. It has been proposed that transcription factors (TFs) act as convergence points which integrate the signals from a complex signalling network, and that integration of the multiple inputs defines the response specificity at the transcriptional level. Transcriptional reprogramming, which is crucial for plant immunity, thus acts as a major effector arm in immunity. The mechanisms involved in the immune transcriptional reprogramming are detailed in the next section.

1.3.2 Transcriptional reprogramming in immunity

A rapid and massive transcriptional reprogramming occurs upon pathogen detection (Boudsocq et al., 2010; Eulgem et al., 2004; Gao et al., 2011; Maekawa et al., 2012; Maleck et al., 2000; Navarro et al., 2004; Ramonell et al., 2005; Tao et al., 2003). Transcriptional reprogramming is an essential process in plant immunity. This is supported by the facts that several TFs are required for resistance (Ando et al., 2014; Padmanabhan et al., 2013; Shimono et al., 2007; Xu et al., 2014; Zheng et al., 2006), a large part of the induced genes are involved in critical defence processes, and transcription factors are frequently targeted by pathogen effectors (Kazan and Lyons, 2014). For example, in *A. thaliana*, synthesis of camalexin, an antimicrobial compound critical for resistance to the hemibiotroph *Botrytis cinerea*, is induced via WRKY33-dependent activation of the camalexin biosynthesis genes, and the TF WRKY33 is a target of pathogen effectors (Mao et al., 2011; Sarris et al., 2015). The main TF families involved in immunity are AP2/ERF, bHLH, bZIP, MYC, NAC, WRKY and CAMTA (Tsuda and Somssich, 2015).

How are then the different immune signalling pathways integrated into a specific immune response at the transcriptional level?

MAPK cascades regulate directly or indirectly several TFs by phosphorylation. Direct phosphorylation by MAPK(s) has been shown for *At*WRKY33, *Nb*WRKY8, *At*ERF6 (ETHYLENE RESPONSE FACTOR6), *At*ERF104 (ETHYLENE RESPONSE FACTOR104), *At*VIP1 (VIRE2 INTERACTING PROTEIN 1), and *At*MYB44, and the biological relevance of the MAPK-mediated phosphorylations in term of immunity has been demonstrated in most cases (Tsuda and Somssich, 2015).

Ca²⁺-mediated signalling also regulate transcription via several means. The activity of several defence-related TFs, such as *At*CAMTA3, *At*CBP60g, *At*CBP60a, *At*TGA3 and *At*CBNAC, is

1. The plant immune system

directly regulated by CaM proteins (Poovaiah et al., 2013; Tsuda and Somssich, 2015). For example the CAMTA (CALMODULIN-BINDING TRANSCRIPTION ACTIVATOR) family of TF is regulated by Ca²⁺ via interaction to CaM, and CAMTA3 is involved in the transcriptional regulation of *EDS1* (*ENHANCED DISEASE SUSCEPTIBILITY-1*) and NDR1 (NON DISEASE RACE SPECIFIC DISEASE RESISTANCE 1), two major regulators of plant immunity (Du et al., 2009; Nie et al., 2012). Similarly, CDPKs can regulate defence-related TFs as exemplified by the phosphorylation of *AtWRKY8*, 28 and 48 by *AtCDPK4,5,6* and 11 (Gao et al., 2013).

Plant hormones also mediate defence-related transcriptional reprogramming. It has been proposed that *AtNPR1* (NON-EXPRESSOR OF PATHOGENESIS-RELATED GENES1), which can indirectly sense SA accumulation, interacts with TFs of the TGA family to drive expression of most of the SA-responsive genes (Tsuda and Somssich, 2015). Similarly, the JA-dependent regulation of the TF *AtMYC2* and its role in defence have been well described (Chini et al., 2007; Thines et al., 2007) as well as the ET-mediated regulation of *AtEIN3* (ETHYLENE INSENSITIVE3) and *AtEIL1* (EIN3-LIKE1) which control expression of some defence genes such *PDF1.2* (Tsuda and Somssich, 2015).

Interestingly, TFs can also be the site of convergence for signals coming from different pathways. For instance, the activity of *AtEIN3* and *AtEIL1* is synergistically regulated by both JA and ET whereas *AtMYC2* and *AtEIN3* antagonize each other. Several other convergence points important for immunity have been described (Tsuda and Somssich, 2015).

Recent reports indicate direct interactions between R proteins and transcription factors. The barley NLR MLA10 interacts with three transcription factors upon activation (*HvWRKY1*, *HvWRKY2*, *HvMYB6*), and the interaction releases *HvMYB6* from the *HvWRKY1*-mediated repression (Chang et al., 2013; Shen et al., 2007). Pb1, a rice R protein, has been shown to interact with the transcription factor *OsWRKY45*. However, in contrast to the MLA-*HvMYB6* interaction, the transcriptional activity is regulated via *OsWRKY45* abundance, since Pb1 protects *OsWRKY45* from degradation upon pathogen attack (Inoue et al., 2013). A third example aiding in our understanding of nuclear activity of R proteins is the interaction of N with the transcription factor SPL6 (SQUAMOSA PROMOTER BINDING PROTEIN-LIKE 6) in *Nicotiana benthamiana* (Padmanabhan et al., 2013). The association of N and SPL6 at subnuclear bodies occurs only in the presence of the cognate effector. A genetic requirement for SPL6 was shown in *N. benthamiana* for N-mediated disease resistance as well as in *A. thaliana* for RPS4-mediated immunity. A number of RPS4-mediated defence

1. The plant immune system

responsive genes are differentially regulated upon *AtSPL6* silencing (Padmanabhan et al., 2013). The bHLH TF *AtbHLH84* and its homologs interact with two R proteins, RPS4 and SNC1, and all three homologues act redundantly in the ETI mediated by the R protein RPS4 and in the constitutive ETI-like response mediated by *snc1* (Xu et al., 2014). The R protein RRS1 possesses a WRKY domain which can bind DNA in vitro (Noutoshi et al., 2005) and RRS1 might directly contribute to transcriptional regulation (Heidrich et al., 2013). Close re-examination of yeast-two-hybrid data generated by Mukhtar et al., 2011, indicate at least 14 other potential R protein-TF in *A. thaliana*, further supporting that R protein-TF interactions constitute a more common mechanism of R protein actions. Interaction between transcriptional regulators and NLRs has also been demonstrated, such as the interaction between the transcriptional co-repressor *AtTPR1* (Topless-related 1) and the *A. thaliana* R protein SNC1 (Zhu et al., 2010). Taken together, these studies draw an emerging picture in which nuclear localized R proteins mediate transcriptional reprogramming via interaction with transcription factors in various plants species. Interaction with transcriptional regulators appears not to be limited to just a few specialized R proteins. Instead, this type of interactions might be a more common phenomenon, implying a possible general mechanism of direct regulation of transcriptional reprogramming via plant R proteins. Nonetheless, among the TFs found to interact with R proteins, none of them seems to be commonly targeted by multiple R proteins. Therefore the existence of TFs which act as signalling targets for multiple R proteins is still debated.

Overall, TFs appear to integrate several immune signals and the network of recruited TFs likely defines and fine tunes the response output. However the current knowledge still needs to be integrated into a finer spatio-temporal model to accurately determine the specific pattern of immune transcriptional regulation at different time and in local or distant cells.

Furthermore, the predictable common immune mechanisms downstream of ETI and PTI prompts a question: how can R proteins reboot a signalling mechanism which has been sabotaged by pathogen effectors? It is unlikely that plant R proteins rely on a single immune signalling pathway, which could be easily disarmed by pathogens. In an attempt to solve this paradox, it was proposed that a single R protein can directly regulate several nodes of the immune network to achieve its robust reactivation (Maekawa et al., 2012), since it is difficult for pathogens to evolve an effector which simultaneously hampers multiple signalling branches.

1.4. Hypersensitive response and other defence outputs

Interestingly, both ETI and PTI converge on qualitatively similar defence outputs. Quantitative differences seem to account for most differences between PTI and ETI. ETI is indeed considered as an accelerated and amplified PTI (Jones and Dangl, 2006). ETI and PTI result in a wide range of defence outputs: cell wall thickening, lignification, callose deposition, alkalinisation of the extracellular space, production of antimicrobial or repellent compounds, production of pathogen-degrading enzymes and reactive oxygen intermediates, activation of systemic acquired resistance, and stomatal closure. Defence against viruses is mainly mediated by activation of RNA silencing which is targeted against the viral RNAs, and suppression of the virus replication. These responses can occur not only locally but also in distant cells since some immune signals are spread via hormones or other mobile signalling mechanisms, and induce a fitness cost for the plant (Walters and Heil, 2007). Typically, ETI also results in the induction of a hypersensitive response (HR), which is a specific type of cell death occurring at the site of attempted infection. The HR is usually used as readout for the ETI activation. However the HR does not occur in all incompatible interactions and can be uncoupled from disease resistance, indicating that the HR is not always required to confer disease resistance to certain pathogens and that other defence outputs can be more efficient in conferring disease resistance (Bai et al., 2012; Bendahmane et al., 1999; Chang et al., 2013; Coll et al., 2010; Yu et al., 1998, 2000). Whilst the HR can in some cases contribute to restricting the growth of biotrophs, it can on the contrary promote infection by necrotrophs. Necrotrophic pathogens secrete toxins, which function as effectors to promote host cell death response. These toxins are often host-plant species-specific, thus called host-selective toxins and mediate effector-triggered susceptibility (ETS), which mirrors ETI to some extent (Laluk and Mengiste, 2010). It has been implicated that susceptibility to necrotrophic pathogens or sensitivity to their host-selective toxins is associated with *R* loci in diverse plant species such as *A. thaliana* (Lorang et al., 2007), sorghum (Nagy and Bennetzen, 2008), and wheat (Faris et al., 2010). This indicates that some necrotrophic pathogens hijack the ETI to trigger an HR, thereby promoting virulence. Therefore, resistance to host specific necrotrophs is mainly mediated by PTI, detoxification of toxins, loss of toxin recognitions, or restricting toxin-mediated cell death response (Mengiste, 2012). Plant *R* proteins seem to play minor roles in disease resistance to necrotrophic pathogens. However the *A. thaliana* *RLM3* *R* locus confers resistance to a broad range of necrotrophs by unknown mechanisms (Staal et al., 2008).

2. Effector-triggered immunity and plant NLRs

The HR-like response triggered by the pathogen-derived protein harpin requires an active metabolism and *de novo* protein synthesis indicating that the HR is likely transcriptionally controlled (He et al., 1994). It is still debated whether HR cell death results from the activation of a cell death-specific program or simply from exaggerated defence responses, especially since the HR can be uncoupled from disease resistance (see above). The current understanding of the mechanisms involved in the HR is not complete. Divergent results suggest that several distinct cell death mechanisms are involved and that different R proteins trigger an HR via distinct processes. Cell death processes similar to the well-studied mammalian apoptosis have not been observed in plant cells. According to a morphological classification, there are at least two types of plant cell death: vacuolar cell death involving autophagic-like processes, and necrosis (van Doorn et al., 2011). Vacuolar and autophagic processes as well as regulation by the defence phytohormone salicylic acid have been associated to the HR cell death (Coll et al., 2011; Hatsugai et al., 2004, 2015; Hofius et al., 2009; Munch et al., 2015; Yoshimoto et al., 2009). However the HR fails to be assigned to any type of plant cell death since it displays mixed features of both vacuolar and necrotic cell death (van Doorn et al., 2011). A conductivity increase in the extracellular fluids can be measured rapidly after HR induction. Such phenomenon can be explained by several processes including a massive cation efflux and the fusion of the plasma membrane with the vacuolar membrane leading to the release of the vacuolar content into the extracellular space (Atkinson et al., 1985; Hatsugai et al., 2009). The release of intracellular molecules and the conductivity increase occur before the apparition of obvious cell death symptoms such as cell shrinkage, vacuolization and cytoplasmic aggregation (Hatsugai et al., 2009). Therefore conductivity measure of the extracellular fluid is a marker routinely used to follow ETI and HR development.

2. Effector-triggered immunity and plant NLRs

2.1. NLR proteins represent the largest class of R proteins

R proteins activate responses leading to ETI upon recognition of pathogen effectors or effector-induced host perturbations. Most of R proteins belong to the NLR (nucleotide-binding domain and leucine-rich repeats) family of intracellular receptors. A minority of R proteins is encoded by other classes of proteins such as receptor-like proteins or receptor-like kinases which likely act as cell surface immune receptors. Similar to animal NLRs, plant

2. Effector-triggered immunity and plant NLRs

NLRs are modular proteins that typically consist of three building blocks: an N-terminal domain, the central NB-ARC domain (named after nucleotide-binding adaptor shared with APAF-1, plant resistance proteins, and CED-4), and a C-terminal LRR (leucine-rich repeats) domain (Van der Biezen and Jones, 1998). The central domain of animal NLRs is also known as the NACHT domain (named after NAIP, CIITA, HET-E, and TP1) (Koonin and Aravind, 2000) which is structurally similar to the plant NB-ARC domain but distinctive of animal NLRs (van Ooijen et al., 2007; Takken et al., 2006). Despite their structural and functional similarities, plant and animal NLRs are likely the result of convergent evolution (Ausubel, 2005; Rairdan and Moffett, 2007; Staal and Dixelius, 2007). The presence of either a TOLL/interleukin 1 receptor (TIR) domain or a coiled-coil (CC) domain at the N-terminus is a plant-NLR-specific feature and defines two major types of plant NLRs termed the TIR-type NLRs (TNLs) and the CC-type NLRs (CNLs), respectively. Although the origins of TNLs and CNLs seem to date back to very early land plant lineages, TNLs are absent from monocots (Liu and Ekramoddoullah, 2007; Yue et al., 2012). The NLR family has massively expanded in several plant species. The massive expansions have rendered the NLR family one of the largest and most variable plant protein families (Clark et al., 2007; Ossowski et al., 2008). Expansion of the recognition repertoire and rapid evolution of the pathogens are likely the main forces which drive the NLR expansion and diversification in plants. This contrasts with the vertebrate NLR repertoires, typically comprising ca. 20 members (Lange et al., 2011; Meyers et al., 2003; Zhang et al., 2010; Zhou et al., 2004). Rapid evolution of the NLR repertoire by a rapid “birth and death” mechanism accounts for highly species-specific NLR repertoires in plants except for a few NLR families which follow different evolutionary dynamics and are conserved across several plant taxa (Jacob et al., 2013).

2.2. Function of the different NLR modules

NLRs are modular proteins consisting mainly of three modules: the N-terminal domain, the central NB-ARC domain and the C-terminal LRR. The “Rosetta Stone Hypothesis” proposes that when two proteins that are separate in some species are fused in another species, their fusion likely reflects a previously hidden interaction between the two seemingly non-related proteins (Marcotte et al., 1999). The Rosetta Stone Hypothesis might explain the plant NLRs evolutionary history. Indeed, co-expression of individual NLR domains (i.e., N-terminal, NB-ARC, and LRR domains) can often reconstitute the full-length protein function (Gutierrez et al., 2010; Leister et al., 2005; Moffett et al., 2002). This suggests that the NLR domains were

2. Effector-triggered immunity and plant NLRs

originally separated and have been assembled into a single multi-domain receptor during evolution. Thus, each domain represents a functional unit with assembly-dependent and assembly independent functions. The experimental data largely support such model.

The LRR domain is the most polymorphic domain and the main determinant for effector recognition or detection of effector-induced host modifications. However the other NLR domains also function in effector recognition in some cases (Qi and Innes, 2013). Recognition of the effector or modified self induces a conformational change which represents the first step in the switch process from the “off” to the signalling competent “on” state of the NLR receptor.

The central NB-ARC domain has an intramolecular regulatory function. Following detection of the effector or modified self by the LRR, an ADP to ATP exchange takes place which trigger further conformational changes leading to the signalling competent conformation. ATP binding depends on a functional P-loop which is a conserved motif within the NB-ARC domain. Therefore mutations in the P-loop motif usually lead to NLR inactivation. On the contrary, specific mutations in the MHD motif of the NB-ARC domain mimic ATP binding and lead to effector-independent activation of the NLR (Qi and Innes, 2013). Although no crystal structure of a full-length plant NLR is available yet, the first crystal structure of an animal NLR monomer (mouse NLRC4) in its inactive state was resolved (Hu et al., 2013) and contributed to support the auto-inhibition mechanism mediated by both LRR and NB-ARC domain. Experimental data from plant NLRs further support the model which was inferred from the mouse NLRC4 structure (Ade et al., 2007; Bendahmane et al., 2002; Hwang et al., 2000; Qi et al., 2012; Slootweg et al., 2013). In the case of RPS5 and Rx, the NB-ARC domain has an additional function in downstream signalling (Ade et al., 2007; Rairdan et al., 2008).

The N-terminal domain, which typically consists of either a CC domain or a TIR domain, has been associated in many cases with the NLR signalling function, and can also participate in effector/modified-self recognition and intramolecular regulatory interactions (Qi and Innes, 2013). Interestingly, both the CC domains of barley MLA, NRG1 and ADR1 from *A. thaliana*, NRG1 from *Nicotiana benthamiana*, ADR1 from potato, and the TIR domains of RPS4 and RPP1 from *A. thaliana*, L from flax, and N from tobacco can trigger an HR in an effector-independent manner (Bernoux et al., 2011; Collier et al., 2011; Frost et al., 2004; Krasileva et al., 2010; Maekawa et al., 2011b; Michael Weaver et al., 2006). This indicates that several TIR and CC domains from NLRs act as signalling modules sufficient for HR

2. Effector-triggered immunity and plant NLRs

activation. The crystal structure of MLA CC and L6 TIR domains revealed the presence of homodimers, and functional studies indicated that homodimerization is required for the signalling function (Bernoux et al., 2011; Maekawa et al., 2011b; Swiderski et al., 2009). These results contrast with the case of potato CNL Rx and the *A. thaliana* CNL RPS5, where the NB and the CC-NB part respectively is sufficient for triggering an HR (Ade et al., 2007; Rairdan et al., 2008). As suggested by the crystal structure of the MLA CC and L6 TIR homodimers, NLRs can form hetero- and homo-oligomers in either a constitutive or a inducible manner similarly to animal NLRs (Griebel et al., 2014).

2.3. Compartmentalization of NLRs and NLR functions

NLRs localize in various subcellular compartments (Wang and Balint-Kurti, 2015). For example the *A. thaliana* TNL RPS4 is partly associated to endomembranes and partly in the nucleus (Wirthmueller et al., 2007). This is similar to the barley CNL MLA described to be associated to membranes and in the nucleus (Bieri et al., 2004; Shen et al., 2007). The *A. thaliana* CNLs RPM1 and RPS2 are associated to the plasma membrane in both their active and their inactive states (Axtell and Staskawicz, 2003; Boyes et al., 1998; Gao et al., 2011). The flax TNL L6 is localized in the golgi apparatus (Takemoto et al., 2011). The localization of NLRs before activation reflects in most cases the site of effector recognition. NLR relocalization can occur after activation. For instance, the potato CNL R3a relocates from the cytoplasm to endosomal compartments (Engelhardt et al., 2012) whilst several other NLRs accumulate in the nucleus after activation (Caplan et al., 2008; Cheng et al., 2009; Shen et al., 2007; Wirthmueller et al., 2007). This indicates that NLRs initiate the ETI from distinct subcellular compartments, possibly via distinct mechanisms or pathways.

Furthermore, nuclear accumulation of several NLRs such as RPS4 and MLA is required for disease resistance (Heidrich et al., 2011; Shen et al., 2007) whilst cytosolic localization is required for disease resistance mediated by potato Rx (Slootweg et al., 2010).

Demonstration of compartment-specific functions for several NLRs indicates that a single NLR can activate distinct pathways in distinct subcellular compartments. For example, RPS4 nuclear pool is sufficient for disease resistance whereas the cytosolic pool is sufficient for HR (Heidrich et al., 2011). Similar functional properties were also shown for the barley CNL MLA (Bai et al., 2012; Shen et al., 2007).

2. Effector-triggered immunity and plant NLRs

2.4. Key components required for NLR function

Despite 20 years of intensive research in the field of plant NLR biology, the knowledge on signal transduction downstream of NLRs remains largely incomplete. This is particularly true for what regards the very first steps in the signal initiation downstream of NLRs. Several forward genetic screens have been conducted to identify genes involved in NLR functions but these identified only a limited number of genes, of which, only a small subset is involved in downstream signalling, indicative of a wide functional redundancy or requirement of the components for plant survival. On top of the signalling components described in the introductory section 1.3.1, a few general components downstream of NLRs have been identified. EDS1 was identified in *A. thaliana* in a screen for loss of ETI against avirulent *Hyaloperonospora parasitica* (Parker et al., 1996). EDS1, together with its interacting partner PAD4, is required for TNL-mediated ETI (Wiermer et al., 2005). Later on, EDS1 together with another interaction partner named SAG101 was found to form a distinct regulatory pair with immune functions partially overlapping these of the EDS1-PAD4 pair (Cui et al., 2015). The plasma membrane-anchored integrin-like protein NDR1 was identified in *A. thaliana* in a screen for loss of resistance against avirulent *Pseudomonas syringae* pv. *tomato* (Century et al., 1995) and is required for ETI mediated by a subset of CNLs (Day et al., 2006; Knepper et al., 2011). Both EDS1 and NDR1 are involved in resistance to virulent pathogens indicating that these components are also convergence points between PTI and ETI (Knepper et al., 2011; Wiermer et al., 2005). Contrary to EDS1 which seems to be present in nearly all angiosperms taxa, NDR1 is only found in eudicots, suggesting that NDR1 is a eudicot-specific immune regulator (Phytozome v11.0).

Several NLRs are required for the function of other NLRs. *A. thaliana* ADR1 (ACTIVATED DISEASE RESISTANCE 1) family, which comprises three paralogues in *A. thaliana* (ADR1, ADR1-like1, ADR1-like2), is exceptionally conserved among various plant species including monocotyledonous and eudicotyledonous plant species (Collier et al., 2011). Because of such a high degree of conservation, much attention has been paid to this family, which might represent a conserved and potentially ancestral function. ADR1 family members are also required for PTI and ETI mediated by a distinct set of NLRs, which are dependent on salicylic acid signalling for full immune response (Bonardi et al., 2011). Consistent with the immune responses conferred by those NLRs, the ADR1 family is involved in a feedback amplification loop of salicylic acid signalling and its biosynthesis, cooperating with EDS1 (Bonardi et al., 2011; Roberts et al., 2013). Another example for a helper function of NLRs is tomato NRC1.

2. Effector-triggered immunity and plant NLRs

NRC1 is required for the immunity conferred by Cf-4, a non-NLR R protein. Silencing of *NRC1* in *N. benthamiana* impairs the hypersensitive response mediated by several other R proteins including two NLRs, Rx, and Mi (Gabriëls et al., 2007). Because such “helper” NLRs are required for the function of other NLRs, they might be involved in relaying the signal downstream of the respective innate immune sensors besides a role in defence phytohormone pathways.

Forward genetic screens also lead to the identification of several components involved in the regulation of pre-activated NLR complexes. *RAR1* (*REQUIRED FOR MLA12 RESISTANCE 1*) was identified as a locus required for barley MLA12-mediated resistance to avirulent powdery mildew (Shirasu et al., 1999). RAR1 was found later to form, together with HSP90 (HEAT SHOCK PROTEIN 90) and SGT1 (SUPPRESSOR OF G-TWO ALLELE OF *SKP1*) a complex involved in NLR chaperoning (Kadota and Shirasu, 2012). The HSP90-RAR1-SGT1 complex is required for the stabilization of many NLRs, but not all (Kadota and Shirasu, 2012).

2.5. Conservation of the NLR signalling mechanisms across plant species

In a few cases, co-expression of an NLR, its cognate effector and the effector target in heterologous plant species induces an HR, indicating that the signalling mechanisms downstream of NLR might be conserved across diverse plant taxa (Wulff et al., 2011). However, these data are often based on transient gene expression with strong promoters and use host cell death as proxy for NLR activity. Since NLR-mediated host cell death responses can be uncoupled from NLR-mediated pathogen growth restriction in several cases (Coll et al., 2011; Maekawa et al., 2011a), it was unclear if plant NLRs also confer disease resistance in stable transgenic plants in phylogenetically distant species.

Recently, it was shown that a subset of plant NLRs confers disease resistance across different taxonomic classes (Maekawa et al., 2012; Narusaka et al., 2013). Our group demonstrated that a CNL named MLA1 (MILDEW A 1) from the monocotyledonous plant barley (*Hordeum vulgare*, Poaceae) functions in the eudicot plant thale cress (*A. thaliana*, Brassicaceae) against barley powdery mildew *Blumeria graminis* f. sp. *hordei* (*Bgh*) (Maekawa et al., 2012). These data suggest the existence of an evolutionarily conserved CNL-mediated immune mechanism. Similar to MLA1, co-acting *A. thaliana* TNL pair, RPS4 (RESISTANCE TO *PSEUDOMONAS SYRINGAE* 4) and RRS1 (RESISTANCE TO *RALSTONIA*

3. Case study on the ETI mediated by the barley MLA

SOLANACEARUM 1) also confers resistance in cucumber (Cucurbitaceae), *Nicotiana benthamiana*, and tomato (Solanaceae) (Narusaka et al., 2013). Additionally, the *A. thaliana* *RPW8.1* and *RPW8.2* encoding truncated CNL-like proteins, confer resistance to powdery mildews in *Nicotiana tabacum* and *Nicotiana benthamiana* like in *A. thaliana* (Xiao et al., 2003). These results strongly imply that a subset of plant NLRs, despite their evolutionary separation, can signal via an evolutionarily conserved mechanism. Again, the question arises about how such conserved mechanism can avoid interception by pathogen effectors. As previously mentioned, the robustness of signal transduction might be mediated by a complex network and the simultaneous connectivity to several entry nodes. One could also suspect that many key components of the immune network are heavily guarded by NLRs.

3. Case study on the ETI mediated by the barley MLA

The polymorphic barley *MLA* (mildew A) locus encodes functionally diversified CNLs which recognize isolate-specific effectors of the powdery mildew fungus, *Blumeria graminis* f. sp. *hordei* (*Bgh*) (Seeholzer et al., 2010). *MLA*-dependent recognition of avirulent *Bgh* triggers ETI accompanied by an HR.

MLA resistance alleles differentially require the three components of the heteromeric HSP90-RAR1-SGT1 complex for their function (Bieri et al., 2004; Halterman and Wise, 2004; Hein et al., 2005; Shen et al., 2003).

MLA1 and *MLA10* are localized in the cytosol and the nucleus including a membrane associated pool (Bieri et al., 2004; Shen et al., 2007). When excluded from the nucleus by fusion with a nuclear exclusion signal, immunity mediated by *MLA10* is compromised (Shen et al., 2007). On the contrary, confinement of *MLA10* in the nucleus by a nuclear localization signal abolishes its capacity to induce the HR (Bai et al., 2012). This implies compartment specific functions for *MLA*, with a nuclear pool required for disease resistance and a cytosolic pool required for the HR. The nuclear function of *MLA* was further investigated. Following up on the demonstration that barley *MLA10* interacts with the TFs *HvWRKY1* and *HvWRKY2*, negative regulators of immunity (Shen et al., 2007), Chang et al. (2013) elucidated the mechanism by which this interaction results in immunity. Their results indicate that the CC domain of barley *MLA10* interacts not only with the aforementioned repressors but also with the transcriptional factor *HvMYB6*, a positive regulator of immunity. Strikingly,

3. Case study on the ETI mediated by the barley MLA

only the active form of MLA10 is able to bind *HvMYB6*, which is sequestered by *HvWRKY1* in the absence of the activated MLA10. The interaction through the MLA CC domain prevents *HvWRKY1* from interacting with *HvMYB6*, thereby allowing *HvMYB6* binding to the corresponding *cis*-regulatory element. The MLA10-*HvMYB6* complex, in turn, greatly enhances transcription downstream of the *cis*-regulatory element compared to *HvMYB6* alone in a transient expression assay. This finding revealed at least part of the mechanism by which MLA transduces the immune signal to downstream signalling components in barley.

Since MLA belongs to a Triticeae-specific NLR clade, there is no MLA orthologue in *A. thaliana*. In order to test if the barley receptor MLA can function in *A. thaliana*, the MLA1-*Bgh* interaction was tested in *A. thaliana*. Since *A. thaliana* is resistant to *Bgh*, the partially immunocompromised *pen2 pad4 sag101 (pps)* *A. thaliana* mutant background was used which allows infection and growth of *Bgh*. In the *A. thaliana pps* mutant background, the MLA1-triggered immunity including host cell death response and disease resistance is fully retained (Maekawa et al., 2012). Furthermore, a similar analysis conducted in the *A. thaliana pen2 pad4 sag101 dde2 ein2 sid2 (ppsdes)* mutant suggested that MLA1-mediated immunity is also fully retained in *A. thaliana* mutant plants that are simultaneously impaired in the three major defence phytohormone pathways (ET, JA, and SA) (Maekawa et al., 2012). These data suggest the existence of an evolutionarily conserved and defence phytohormone-independent CNL-mediated immune mechanism. The known interaction between MLA10 and *HvWRKY1/2* and *HvMYB6* cannot explain the conserved function of MLA1 in *A. thaliana* since *HvMYB6* is a monocot-specific transcription factor (Chang et al., 2013). Therefore the underlying conserved immune signalling target is unknown. Since NLRs likely initiate downstream signalling via multiple signalling targets, the previous findings imply that at least one signalling target of MLA is conserved in *A. thaliana*.

Domain swap experiments between different MLA alleles which detect genetically diverse *Bgh* effectors, imply that recognition specificity is determined by the LRR domain (Shen et al., 2003). The N-terminal coiled-coil domain of MLA (MLA_{CC}) is largely invariant among the different MLA alleles (Seeholzer et al., 2010). MLA_{CC} forms a rod-shaped homodimer which defines the minimal functional unit required for triggering cell death in barley and *N. benthamiana* (Maekawa et al., 2011b). Since the MLA_{CC} triggers an effector-independent cell death in several species, the signalling mechanism leading to the cell death must be conserved in these species. MLA1 interacts with *HvWRKY1/2* and *HvMYB6* via its CC domain (Chang et al., 2013; Shen et al., 2007), therefore the MLA_{CC} might be involved in both cell death

4. The aim of this thesis

signalling and transcriptional regulation. Furthermore cytosolic MLA_{CC} can trigger cell death whereas nuclear MLA_{CC} cannot, suggesting that MLA_{CC} signalling function might follow the same subcellular compartmentalization as the full length MLA receptor (Bai et al., 2012).

4. The aim of this thesis

NLRs act as key intracellular immune sensors in plants by detecting invading pathogens. More than 20 years after the cloning of the first NLRs (Bent et al., 1994; Mindrinos et al., 1994; Whitham et al., 1994), the signalling mechanisms downstream of NLRs remain largely unknown. Understanding of this aspect of plant immunity would certainly contribute to the development of technologies to protect plants from pathogen attacks. Still, much has to be discovered about the signalling targets and the convergence points in the signalling network downstream of plant NLRs.

I addressed this question during my thesis work by using several complementary approaches which utilize classical techniques but also take advantage of recent technologies such as whole transcriptome shotgun sequencing (RNA-seq), protein complex identification by mass spectrometry and mapping by sequencing. The first step was to establish and validate a simplified system to study NLR-mediated signalling. The study was conducted in the model plant *A. thaliana* since it presents many advantages compared to other plant species, including high quality reference genome and annotation (*A. thaliana* genome initiative 2000, Lamesch et al., 2012), and diverse extensive mutant collections.

Since the barley CNL MLA can function in *A. thaliana* and the MLA_{CC} acts as a signalling module, the MLA_{CC} was used as a presumed effector-independent trigger for NLR-mediated responses. *A. thaliana* stable transgenic lines conditionally expressing MLA_{CC} were generated. These lines were characterized to determine whether MLA_{CC} induces responses similar to the ETI mediated by endogenous full-length NLRs in *A. thaliana*. The second step consisted in exploiting the conditional expression of MLA_{CC} in *A. thaliana* transgenic lines to study NLR-mediated signalling mechanisms and to unravel new components of the immune signalling network. Importantly, the system was designed to focus more specifically on the conserved signalling aspects, since the barley MLA_{CC} likely co-opts conserved signalling components present in *A. thaliana* for its function.

4. The aim of this thesis

Using a genetic approach, I assessed the requirement of defence phytohormones for the MLA_{CC} function. Common patterns in MLA_{CC}-mediated and other immune responses were defined by a comparative transcriptomic analysis. A forward genetic suppressor screening was conducted to identify mutations which suppress the MLA_{CC} mediated responses. Finally, identification of MLA_{CC} interacting partners was attempted using yeast-two-hybrid and affinity purification coupled with mass spectrometry.

Results

Chapter 1.

**Functional characterization of the MLA coiled-coil module
in *A. thaliana***

1.1. Introduction

Resistance (R) proteins sense the presence of effector molecules delivered by the pathogen into host cells to manipulate intracellular processes for successful pathogenesis. Upon pathogen sensing, R proteins become activated and trigger a rapid and intense immune response, termed effector-triggered immunity (ETI). In most cases ETI is accompanied by a so-called «hypersensitive response» (HR), which is a local and rapid cell death response at the sites of attempted infection.

Like many other R proteins, MLA belongs to the intracellular NLR family (nucleotide-binding leucine rich repeat containing protein). Barley (*Hordeum vulgare*) *MLA* confers isolate-specific recognition of *Blumeria graminis* f. sp. *hordei* (*Bgh*) isolates expressing a cognate effector gene, called *AVR_a*. Barley *MLA* orthologs are present in closely related plant species of the Triticeae such as wheat (Jordan et al., 2011), but not in dicotyledonous plants such as *Arabidopsis thaliana* (*A. thaliana*). The N-terminal coiled-coil (CC) domain of MLA (*MLA_{CC}*) has been reported as a minimal signalling module inducing cell death upon transient expression in barley and *Nicotiana benthamiana* (Maekawa et al., 2011b). *MLA_{CC}* homodimerization is required for its cell death-inducing activity since amino acid substitutions (e.g. I33E and L36E) that disrupt *MLA_{CC}* homodimer formation also abolish its cell death-inducing activity. Barley *MLA1* was recently shown to be functional in *A. thaliana* (Maekawa et al., 2012), i.e. transgenic expression of the immune receptor confers race-specific immunity only to a *Bgh* isolate expressing the cognate *AVR_a* effector. The wide range of genome-wide molecular and genetic tools available in the model plant *A. thaliana* enabled me to characterize molecular processes initiated by barley *MLA_{CC}* and to compare these with previously characterized innate immune responses in this dicotyledonous plant species. I established stable *A. thaliana* transgenic lines expressing barley *MLA_{CC}* to test whether the N-terminal CC module functions as an immune signalling module in *A. thaliana* that can initiate ETI-like responses. The transgenic lines were then used to characterize the underlying molecular mechanism. This chapter describes the characterization of transgenic *A. thaliana* lines conditionally expressing barley *MLA_{CC}*, genetic experiments aimed to examine the requirement of several key immune components for *MLA_{CC}* function and time-resolved RNA-seq experiments to compare barley *MLA_{CC}*-mediated transcriptional responses with those triggered by endogenous *A. thaliana* PRR or NLR-type immune receptors.

1.2. Expression of the MLA_{CC} module induces HR-like responses in *A. thaliana*

1.2.1. Growth phenotype of stable transgenic lines expressing MLA_{CC}

To explore a presumed MLA_{CC} activity in *A. thaliana*, I generated stable transgenic lines in ecotype Col-0 expressing MLA_{CC} (amino acids 1-160 of MLA10) with a C-terminal fusion to a monomeric yellow fluorescent protein (mYFP) under the control of a dexamethasone (DEX)-inducible promoter, enabling conditional and synchronous transgene expression. Hereafter, these lines are referred to as *DEXp:MLA_{CC}-mYFP* lines. I generated control transgenic *A. thaliana* lines expressing mYFP alone under the DEX-inducible promoter (*DEXp:mYFP*) to exclude the possibility that mYFP and/or the DEX-inducible transactivation system account for the phenotypes seen in the *DEXp:MLA_{CC}-mYFP* lines. I selected a total of eight independent *DEXp:MLA_{CC}-mYFP* transgenic lines that displayed a segregation of the selectable marker gene present in the transgene construct (hygromycin resistance) in the T₂ generation that is consistent with a single transgene insertion. The phenotype of homozygous T₃ progeny was examined at 14 days post germination (dpg) on MS agar medium in the absence or presence of 30 μM DEX. The seedlings of eight independent *DEXp:MLA_{CC}-mYFP* lines on medium supplemented with DEX displayed a range of phenotypes from slight to strong dwarfism (reduced shoot and root biomass) with an accompanying leaf chlorosis in comparison to the same genotype without DEX, the *DEXp:mYFP* transgenic line, or wild-type *A. thaliana* accession Col-0 (Figure 1-1). Although the transgenic *DEXp:MLA_{CC}-mYFP* lines showed in the absence of DEX a growth phenotype that was comparable to wild-type Col-0 plants, their root length appeared to be slightly shorter. Nevertheless, these observations indicate that neither the transactivation system nor the transgene insertion are responsible for the marked plant growth phenotype of *DEXp:MLA_{CC}-mYFP* expressing plants on medium supplemented with DEX.

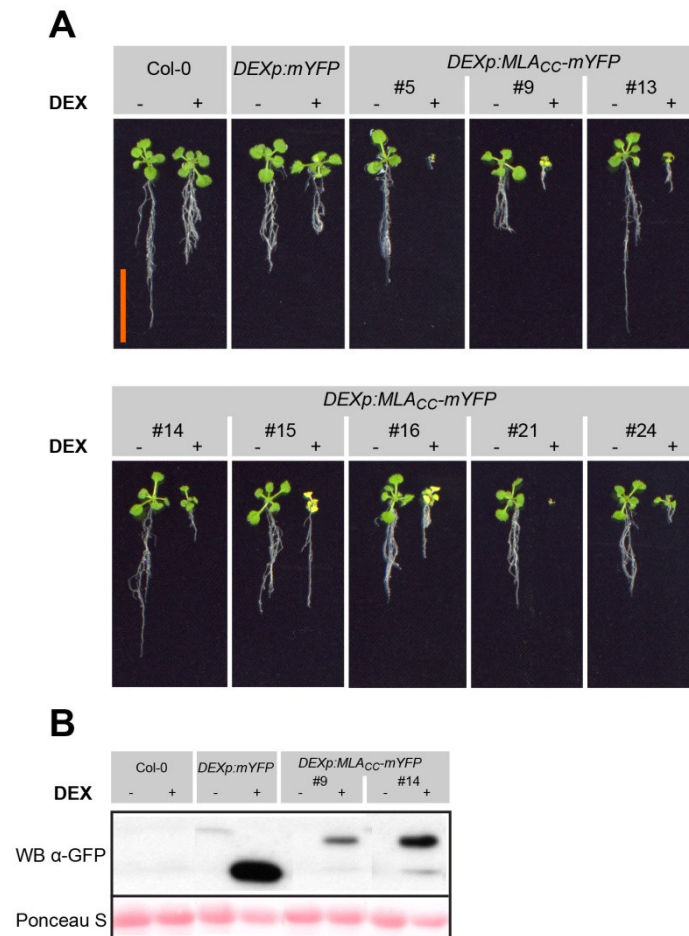


Figure 1-1: Plant growth phenotype and leaf chlorosis of *DEXp:MLA_{CC}-mYFP* expressing transgenic lines. **A**, Homozygous T₃ progeny at 14 days post germination, obtained from several independent *DEXp:MLA_{CC}-mYFP* T₁ transgenic lines, were grown on MS-agar plates containing 0 or 30 μM DEX. Scale bar: 2 cm. **B**, hygromycin-resistant T₂ seedlings grown on MS-agar plates were transferred 10 days after germination onto MS-agar plates containing 30 μM DEX. Proteins were extracted 24 h after transfer for immunoblotting with an anti-GFP antibody.

Immunoblotting analysis with a GFP antiserum confirmed the accumulation of the MLA_{CC}-mYFP fusion protein at the expected size of ~48 kDa (examples shown in Figure 1-1.B). Similar plant growth phenotypes have been reported for mutants displaying constitutively active defence responses such as *mekk1* (Ichimura et al., 2006), *chs2* (Huang et al., 2010) and for transgenic plants overexpressing the N-terminal TIR domain of the *A. thaliana* NLR RPS4 (Swiderski et al., 2009). This stimulated further experiments to clarify whether the growth phenotype and leaf chlorosis of *DEXp:MLA_{CC}-mYFP* lines is linked to constitutive MLA_{CC}-induced defence responses.

1.2.2. Selection and characterization of a *DEXp:MLACC-mYFP* line conferring stable transgene expression over multiple generations

I selected one T₃ progeny from *DEXp:MLACC-mYFP* line #5 (*DEXp:MLACC-mYFP* #5.1) for further characterization since the transgene expression was stable for four generations whilst the transgenes in the other lines were strongly affected by transgene silencing in successive generations. Furthermore, this line displayed a Col-0 wild-type-like phenotype in the absence of DEX, indicating that the transgene insertion and expression of the transactivation factor had no obvious effect in this line (Figure 1-1). Isolation of the transgene flanking regions by cloning and subsequent sequencing identified a single insertion locus at ~711,808 bp on *A. thaliana* chromosome 1. The insertion is located in an intergenic region downstream of *SPIRRIG* (*AT1G03060*) and upstream of *DWARF27* (*AT1G03055*) (Figure S1-1). A loss of function of either flanking gene should result in a clearly identifiable phenotype (e.g. distorted trichomes and secondary bud outgrowth, respectively) (Saedler et al., 2009; Waters et al., 2012). None of these phenotypes were observed in *DEXp:MLACC-mYFP* progeny plants of line #5.1, suggesting that the transgene insertion does not affect the function of these two flanking genes. Transcriptomic data obtained later and described in Results section 1.3.1 also indicates that *SPIRRIG* and *DWARF27* transcripts are detectable in leaves of the *DEXp:MLACC-mYFP* #5.1 line at 85% and 47% of the level seen in Col-0 wild-type, respectively. These results indicate that line *DEXp:MLACC-mYFP* #5.1 is suitable to conduct an in-depth characterization of *MLACC*-mediated responses. This line was employed for the experiments described in the following sections.

1.2.3. Conditional expression of *MLACC* induces a rapid cell death response and MAPK activation

The marked dwarfism and leaf chlorosis of *DEXp:MLACC-mYFP* expressing plants prompted me to examine a potential DEX-dependent leaf cell death response in these plants. To test this, I performed time-course experiments and quantified ion leakage from leaf discs, excised from six-week-old plants grown on soil, after immersion into a solution containing 10 μ M DEX or the corresponding control buffer (mock). Ion leakage is an early quantitative marker for cell death in plants (Demidchik et al., 2014). A rapid and marked increase in ion leakage after DEX treatment in *DEXp:MLACC-mYFP* leaves compared to mock treated and wild-type Col-0 samples indicated the onset of a *MLACC*-mediated cell death at ~eight hours post

induction (hpi) (Figure S1-2). DEX treatment alone did not induce any significant ion leakage.

Further characterization of this cell death was conducted under conditions closer to physiological conditions of intact plants by infiltrating 1 μ M DEX into leaves of four week-old *DEXp:MLACC-mYFP* or *DEXp:mYFP* plants. A similar DEX-inducible ion leakage with an onset between four to six hours after DEX infiltration was observed in this experimental system (Figure 1-2.A). *MLACC*-mediated cell death was confirmed by a trypan-blue vital staining assay in which I detected dye precipitate in leaf cells starting at 12 hpi that appears to increase over time at 24 and 48 hpi (Figure 1-2.B). Parallel immunoblot analysis of leaf protein extracts with a GFP antiserum revealed that *MLACC-mYFP* was clearly detectable at two hpi at low levels, accumulated to high levels at four hpi that did not change dramatically between six and eight hpi, but decreased markedly in abundance at 24 hpi (Figure 1-2.C). Thus, *MLACC* protein accumulation in leaves appears to slightly precede the onset of *MLACC*-dependent ion leakage. Chlorotic and necrotic leaf patches developed from 24 hpi to 72 hpi at the macroscopic level in *DEXp:MLACC-mYFP* expressing, but not in *DEXp:mYFP* plants (Figure 1-2.D). Mitogen-activated protein kinase (MAPK) activation can be used as a marker for both abiotic and biotic plant stress (Zhang et al., 2006). In *A. thaliana*, P/MAMP and effector sensing usually results in *AtMPK3/6* activation (Tsuda et al., 2009, 2013). MAPK activation was examined by immunoblotting using an anti-pT/pY MAPK antibody (Figure 1-2.E). Two immunoreactive bands were identified which correspond in size to *AtMPK3* and *AtMPK6*. Upon DEX infiltration, activated MAPKs were detected in *DEXp:MLACC-mYFP*-expressing plants starting from 4 hpi until at least 8 hpi, but not in *DEXp:mYFP* control plants. This finding indicates that *MLACC* induces a sustained *AtMPK3* and *AtMPK6* activation.

Sustained MAPK activation is a hallmark of NLR activation compared to transient (10-40 min) activation seen in response to plant treatment with P/MAMPs such as the flg22 peptide and subsequent activation of pattern-triggered immune responses (PTI) (Tsuda et al., 2009, 2013). MAPK activation upon conditional *MLACC* expression precedes or is concurrent with ion leakage (Figure 1-2.A, E), suggesting that MAPK activation is not a consequence of cell death but rather acts upstream or independently of the cell death response.

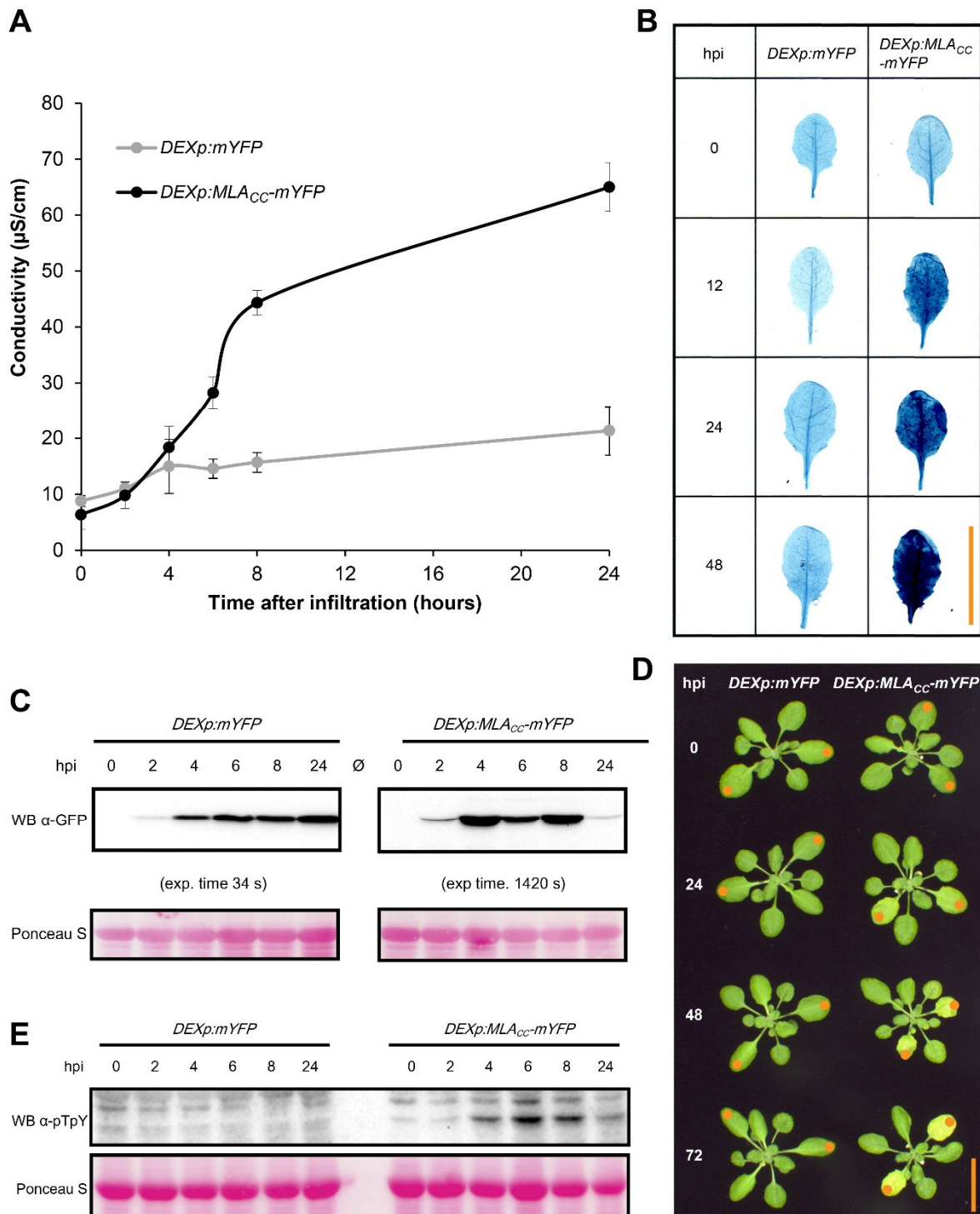


Figure 1-2: Timing of MLAcc-dependent activation of cell death and MAPKs in leaves. 4 week old leaves of the *DEXp:MLAcc-mYFP* or the *DEXp:mYFP* lines were infiltrated with 1 μ M DEX. **A**, ion leakage measurement. The error bars represent the standard deviation from three independent experiments. **B**, Detection of cell death by trypan staining of the DEX-infiltrated leaves. **C**, protein accumulation monitored by immunoblotting. **D**, macroscopic phenotype of the leaves infiltrated with DEX (orange dots). **E**, MAPK activation monitored by anti-pTpY immunoblot (WB). Ponceau S. staining indicates equal protein loading. hpi, hours post infiltration. exp. time, exposure time. Scale bar: 2 cm.

Taken together, my findings indicate that barley MLA_{CC} is capable to induce a rapid cell death response that might share features with the leaf-associated HR in race-specific immunity triggered by the barley $MLA1$ full-length receptor in transgenic *A. thaliana* plants following inoculation with a *Bgh* isolate containing AVR_{Ra1} (Maekawa et al., 2012).

Conditional expression of MLA_{CC} -mYFP enabled me also to examine the subcellular localization of the fusion protein by confocal imaging of the leaf epidermis of five week-old *DEXp:MLA_{CC}*-mYFP plants infiltrated with 10 μ M DEX. The MLA_{CC} -mYFP fusion protein was found to accumulate in both the cytoplasm and the nucleus (Figure 1-3), similar to full-length and transiently overexpressed $MLA10$ -YFP in barley leaf epidermal cells (Shen et al., 2007).

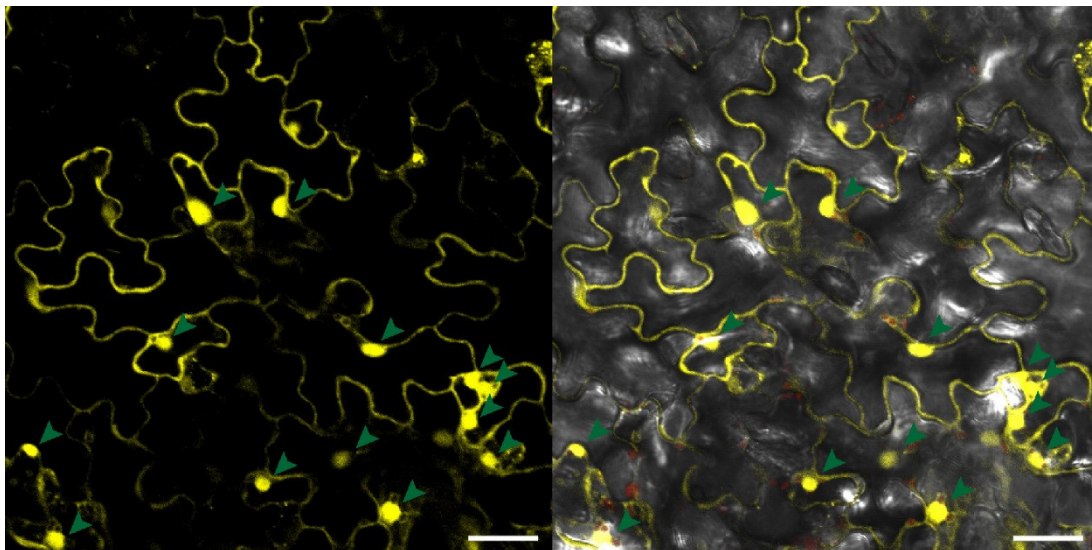


Figure 1-3: Subcellular localization of MLA_{CC} -mYFP fusion protein in *A. thaliana*. Confocal images of representative epidermal cells were taken 4 hours after DEX infiltration into leaves of five-week-old *DEXp:MLA_{CC}*-mYFP plants. Left panel shows detection of the mYFP signal. Right panel shows a merge of mYFP (yellow), chlorophyll (red) and transmitted light images (grey shades). Scale bar: 20 μ M. Green arrowheads indicate nuclei.

The mYFP-expressing cells were detectable as early as 2.5 hpi and evidence for cell death became microscopically visible as early as 3 hours after DEX infiltration by increased autofluorescence, lack of cytoplasmic streaming and vacuolization of epidermal cells. The mYFP signal in the nucleus almost completely disappeared at later time points (Figure 1-4). Whether this disappearance of the nuclear signal is due to disintegration of the nuclear envelope or specific elimination of the MLA_{CC} from the nucleus remains unclear. However, some nuclei showed altered morphologies (diffuse and/or distorted shape), suggesting that MLA_{CC}-mYFP-dependent cell death might lead to a loss of nucleus integrity in the leaf epidermis (Figure 1-4, red arrows).

A part of epitope-tagged functional barley MLA1, expressed under its native promoter in transgenic barley plants, has been reported to associate with the membrane fraction following leaf protein fractionation, whilst another part was found to be soluble (Bieri et al., 2004). In transient gene expression experiments, MLA_{CC}-dependent cell death activation in *N. benthamiana* leaves was shown to be dependent on the cytosolic MLA_{CC} pool (Bai et al., 2012). On the other hand, using transient single-cell gene expression experiments, the nuclear MLA10-YFP pool was shown to be required for effective race-specific disease resistance in barley (Shen et al., 2007) and the MLA_{CC} module was shown to interact directly with two antagonistically acting barley transcription factors, MYB6 and WRKY1 (Chang et al., 2013). Thus, accumulation of the MLA_{CC}-mYFP fusion protein in the nucleus and cytoplasm of transgenic *A. thaliana* plants might reflect associations with nuclear and cytosolic interacting proteins. I attempted to examine presumed subcellular-specific functions of MLA_{CC} by analysing DEX-inducible transgenic lines expressing the MLA_{CC} fused to either a nuclear localization signal (NLS) or to a nuclear export signal (NES) or to the respective inactive sequence variants. However, no conclusive data could be obtained due to high variation in the steady-state levels of MLA_{CC} in different transgenic lines and absence of clear qualitative differences between the different variants tested (data not shown).

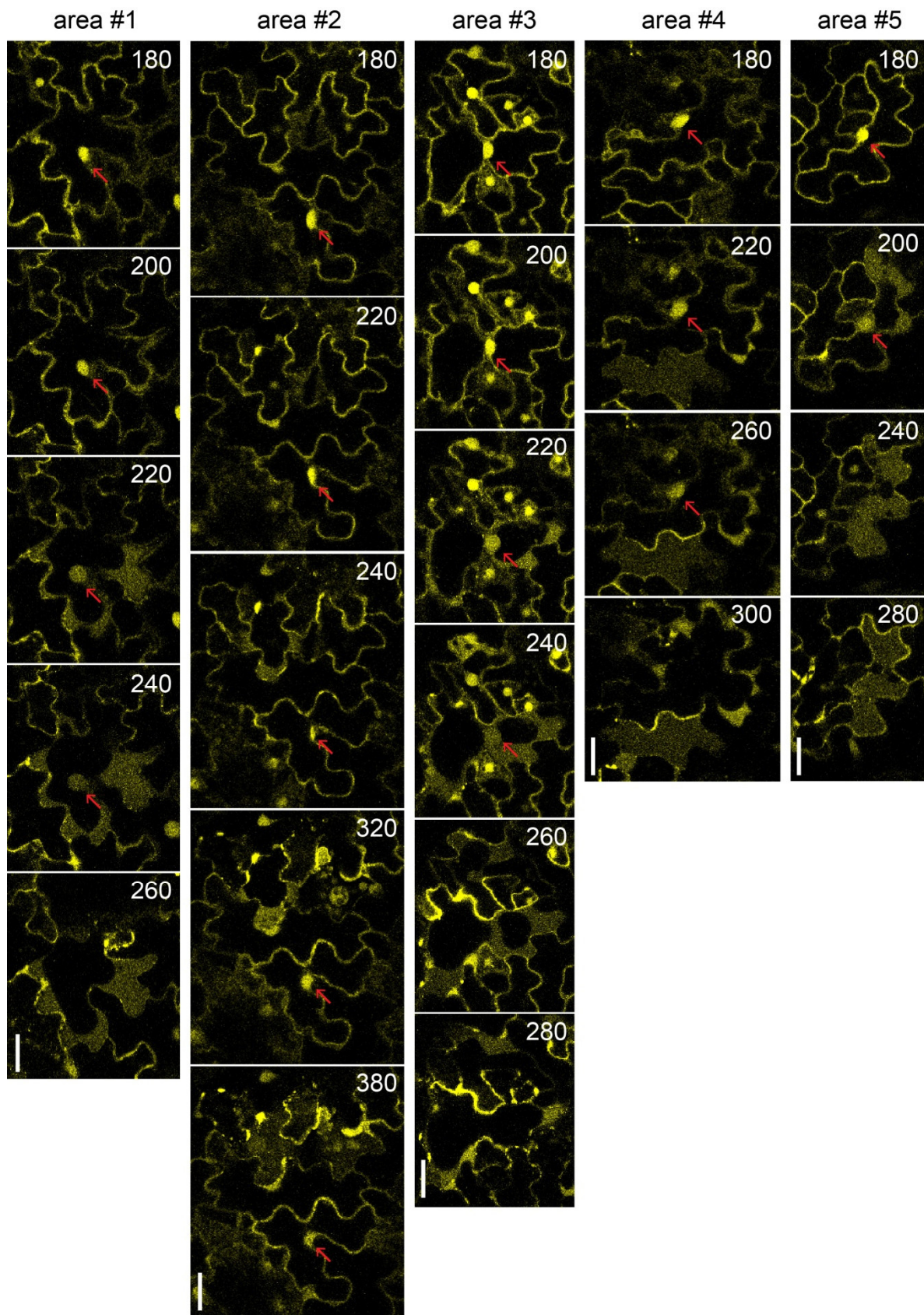


Figure 1-4: Time series of confocal images of epidermal cells expressing $MLACC$ -mYFP. Leaves of five-week-old *DEXp:MLACC-mYFP* plants were infiltrated with 10 μ M DEX. Leaf discs were imaged from 180 min after infiltration every 20 min for 5 hours maximum. Red arrows, nuclei. The numbers indicate the time after infiltration in minutes. Scale bar: 20 μ M

1.2.4. MLA_{CC}-mediated cell death requires extracellular calcium influx but not NADPH-dependent oxidase activity

To further test potential similarities between barley MLA_{CC}-mediated cell death in *A. thaliana* and the HR triggered by endogenous full-length *NLR* genes in this species, I examined the effect of lanthanum(III) chloride (LaCl₃). LaCl₃ is a calcium channel blocker reported to abolish the HR induced by the two *A. thaliana* CNLs RPM1 and RPS2 (Grant et al., 2000; Pike et al., 2005) on MLA_{CC}-mediated cell death. Application of LaCl₃ 20 min prior DEX treatment fully abolished leaf ion leakage induced by MLA_{CC}-mYFP expression (Figure 1-5.A) without significant effect on MLA_{CC}-mYFP accumulation (Figure 1-5.B). I also tested the effect of diphenylene iodonium (DPI), an inhibitor of the NADPH-dependent oxidase which is known to moderately affect leaf ion leakage upon RPM1 activation (Andersson et al., 2006). DPI treatment had neither a significant effect on MLA_{CC}-mediated cell death nor on MLA_{CC}-mYFP accumulation (Figure 1-5.B, C).

Altogether these results suggest that barley MLA_{CC} can induce in heterologous *A. thaliana* a cell death response which shares at least some features with the HR triggered by the tested endogenous full-length CNLs during authentic ETI responses.

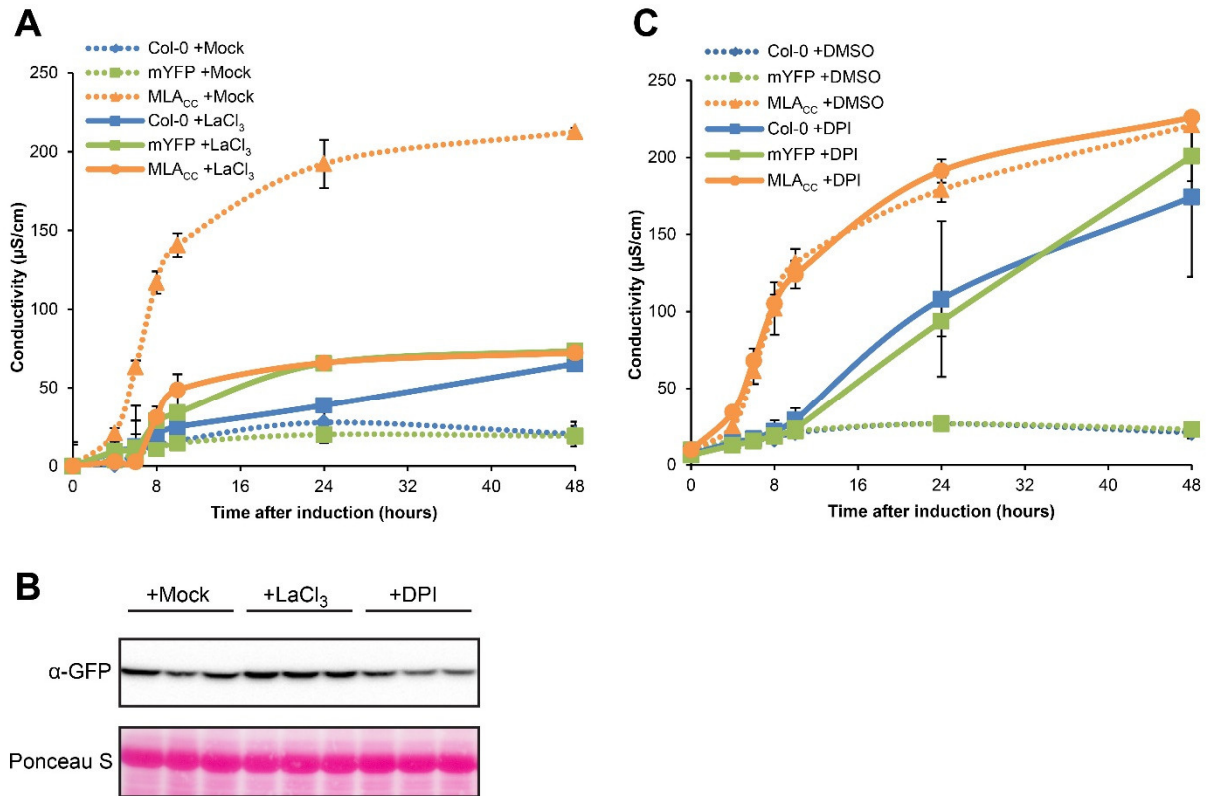


Figure 1-5: Effect of the calcium channel blocker LaCl₃ and the NADPH oxidase inhibitor DPI on MLA_{CC}-mediated cell death. Leaf discs of four week old *DEXp:MLA_{CC}-mYFP* plants were treated with DEX in combination with either mock solution, or 2 mM LaCl₃, or 7 μM DPI. **A** and **C**, ion leakage upon LaCl₃ (**A**) or DPI (**C**) treatment. The error bars represent the standard deviation from three biological replicates in one experiment. The experiment was reproduced at least three times with similar results. The conductivity values in the LaCl₃ treatment corresponds to the conductivity increase as compared to the 0 hour time point. **B**, Equal accumulation of the MLA_{CC}-mYFP protein at 6 hpi was verified in three biological replicates by immunoblot analysis. Equal sample loading was monitored by Ponceau S staining.

1.2.5. MLA_{CC}-mediated cell death is homodimer-dependent and similar to the HR induced by the autoactive full length MLA in *A. thaliana*

Maekawa et al. (2011) reported that MLA_{CC} homodimerization is required for disease resistance and cell death activation triggered by the full-length MLA10. Single amino acid substitutions impairing the MLA10_{CC} homodimerization such as I33E and L36E abolished both cell death induction and race-specific disease resistance (Maekawa et al., 2011b).

I tested whether the same amino acid substitutions also abolished cell death induction conditioned by the MLA10_{CC} in *A. thaliana*. Towards this end, I generated stable transgenic *A. thaliana* lines expressing MLA_{CC} variants carrying the two aforementioned substitutions under the DEX-inducible promoter. Electrolyte leakage measurement and detection of dead

cells by trypan blue staining indicate that both tested MLA_{CC} variants (denoted MLA_{CC}I33E and MLA_{CC}L36E) failed to activate a cell death response upon DEX treatment (Figure S1-3.A, B).

Moreover, the autoactive full-length MLA1(D502V) receptor variant (denoted MLA_{MHD}) induces cell death in transgenic *A. thaliana* leaves which resemble the MLA_{CC}-dependent cell death, whereas DEX-inducible expression of the functionally inactive P-loop MLA1(K207R) variant (denoted MLA_{P-loop}) failed to condition a cell death response (Figure S1-3.B).

Collectively, these results strongly suggest that cell death signalling initiated by the MLA_{CC} domain in *A. thaliana* is dependent on MLA_{CC} homodimer formation and is similar to the cell death response conditioned by the autoactive full-length MLA1_{MHD} receptor variant. This data is also consistent with previous reports obtained by transient expression of the corresponding transgenes in barley and *N. benthamiana* leaves (Maekawa et al., 2011b), further supporting the hypothesis that the MLA_{CC} dimer functions as cell death signalling moiety in the context of the full-length receptor and that signalling components needed for cell death execution might be conserved in barley, *N. benthamiana*, and *A. thaliana*.

1.2.6. The MLA_{CC} domain induces cell death but not MAPK activation in partially immunocompromised *pen2 pad4 sag101 dde2 ein2 sid2* sextuple mutant plants

A. thaliana wild-type (*col-0*) is fully resistant to the non-adapted *Bgh* fungal pathogen of barley, but on *pen2 pad4 sag101* (*pps*) mutant plants, the fungus can grow invasively and complete its life cycle due to impaired PEN2-dependent pre-invasive and PAD4- and SAG101-dependent post-invasive immune responses (Lipka et al., 2005). In plants lacking *PAD4* and *SAG101*, the activity of the key immune regulatory component EDS1 is abolished (Feys et al., 2005). In transgenic *A. thaliana* expressing MLA1, the barley *R* gene mediates race-specific disease resistance to *Bgh* accompanied by cell death in the partially immunocompromised *pps* background (Maekawa et al., 2012). Moreover, both MLA1-mediated race-specific disease resistance to *Bgh* and host cell death induction are retained in the *pen2 pad4 sag101 dde2 ein2 sid2* (*ppsdes*) sextuple mutant background, in which additionally all three major defence phytohormone pathways (jasmonate [JA], ethylene [ET], and salicylic acid [SA]) are depleted (Maekawa et al., 2012; Pieterse et al., 2012).

To test whether JA, ET, and SA are required for the MLA_{CC} -mediated responses, I generated and analysed transgenic lines expressing $DEXp:MLA_{CC}-mYFP$ in the *ppsdes* sextuple background. Cell death detection by ion leakage measurement and trypan blue staining indicates that MLA_{CC} induces cell death in *ppsdes* plants compared to non-transgenic *ppsdes* plants. However, the cell death appeared to be attenuated compared to the line expressing MLA_{CC} in the wild-type background Col-0 (Figure S1-3.A, B).

In contrast, MLA_{CC} -dependent MAPK activation was completely abolished in the *ppsdes* background (Figure 1-6.C). The absence of MAPK activation in the *ppsdes* background does not result from a general inability of this mutant to trigger MAPK activation since in several experiments, stress-induced MAPK activation was detected in the samples taken immediately after infiltration (data not shown).

Since the MLA_{CC} expression in terms of both protein and transcript steady state levels was substantially lower in the *ppsdes* background compared to the transgenic line in wild-type Col-0 background, it is not possible to conclude whether the partial suppression of MLA_{CC} -mediated cell death in the *ppsdes* background is due to the genetic background or due to the differences in MLA_{CC} abundance (Figure 1-6.A, B). The approximately eight fold difference in transcript accumulation of MLA_{CC} at 2 hpi in Col-0 compared to the *ppsdes* background might account for the attenuated cell death response. However the difference in transcript accumulation decreases over time down to ~two fold at 6 hpi, suggesting that qualitative and quantitative differences observed at later time points are less likely due to differential MLA_{CC} expression. Interestingly, whereas MLA_{CC} accumulation was substantially reduced at 24 hpi in the wild-type background, MLA_{CC} accumulation persisted in the *ppsdes* background (Figure 1-6.A). Whether this is due to a specific regulatory process or consequence of the massive cell death which occurs in the wild-type background is unclear.

Altogether, these results indicate that JA, ET, and SA are largely dispensable for MLA_{CC} -mediated cell death but not for MAPK activation. Therefore, MAPK activation appears to be dispensable for cell death induction by MLA_{CC} . The attenuated cell death in the *ppsdes* background could point to an amplification role of one or several of the corresponding wild-type immune components and/or lower MLA_{CC} expression. Since the key signalling pathways mediated by the three defence phytohormones SA, JA and ET are abolished in the *ppsdes* background, it is possible that MLA_{CC} is able to trigger a response in the leaf cells where it is sufficiently expressed independently of the phytohormones and EDS1, but that local and/or systemic spreading of this response is impaired in the *ppsdes* background.

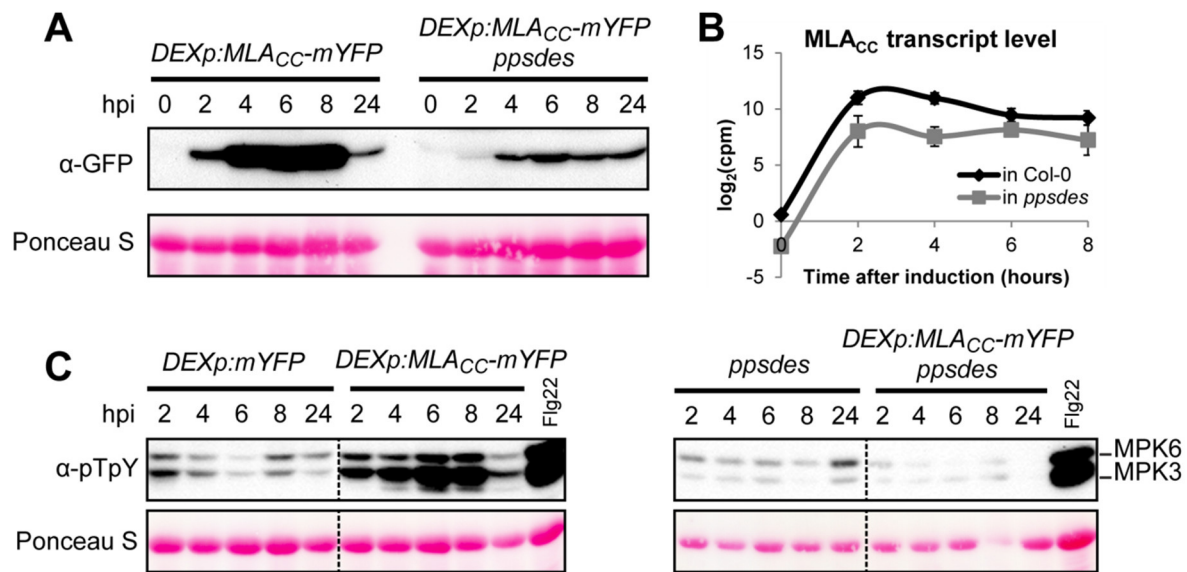


Figure 1-6: MLA_{CC}-mediated MAPK activation is abolished in the *ppsdes* mutant background. 4-week-old leaves of the indicated lines were infiltrated with 1 μ M DEX. **A**, MLA_{CC}-mYFP protein accumulation monitored by immunoblotting. **B**, MLA_{CC} transcript accumulation measured over time by RNA-seq as described in Results section 1.3.1. **C**, MAPK activation monitored by anti-pTpY immunoblot. A wild type leaf sample 15 min after infiltration with 1 μ M Flg22 was used as a positive control for MAPK activation. Ponceau S staining indicates equal protein loading. hpi, hours post infiltration.

1.3. Barley MLA_{CC} jump-starts an immune transcriptional program independent of MAPK activation and defence phytohormones in *A. thaliana*

1.3.1. MLA_{CC} rapidly induces a transcriptional reprogramming which does not require the major defence phytohormones and MAPK activation

Rapid and extensive transcriptional changes in response to effector perception is a general feature in ETI (Adams-Phillips et al., 2008; Caldo et al., 2004; Durrant et al., 2000; Eulgem et al., 2004; Moscou et al., 2011; Tao et al., 2003). Regulation of defence-related genes is required for disease resistance such as the production of antimicrobial compounds and activation of systemic acquired resistance (Caldo et al., 2004; Eulgem et al., 2004; Mao et al., 2011). However the mechanisms underlying NLR-mediated transcriptional regulation remain largely unknown. So far, several studies indicate that gene regulation mediated by NLRs differs quantitatively and temporally from PTI-related responses, but is not fundamentally different (Maleck et al., 2000; Navarro et al., 2004; Tao et al., 2003; Tsuda and Katagiri,

2010). Several lines of evidence prompted me to investigate the function of MLA_{CC} in gene regulation:

(i) In barley, nuclear MLA is required for disease resistance, and interacts with at least two classes of barley TFs which suggests that MLA can influence transcription by direct regulation of TF activity (Chang et al., 2013; Shen et al., 2007).

(ii) In *A. thaliana*, a fraction of MLA_{CC} localizes to the nucleus suggesting a possible role in transcription-related processes (Figure 1-3)

(iii) MLA_{CC}-dependent MAPK activation in *A. thaliana* indicates that MLA_{CC} might have an additional indirect role on transcription since MAPKs can regulate several transcription factors; including members of the WRKY family (Bethke et al., 2009; Djamei et al., 2007; Ishihama et al., 2011; Mao et al., 2011; Meng et al., 2013).

Whole transcriptome sequencing was employed to determine whether MLA_{CC} can influence the transcription in *A. thaliana*. Leaves of four week-old *DEXp:MLA_{CC}-mYFP* plants were infiltrated with 1 μ M DEX and samples collected at 0, 2, 4, 6 and 8 hpi for RNA extraction followed by RNA sequencing (RNA-seq). *DEXp:mYFP* plants were similarly treated and serve as control accounting for circadian variation in gene expression and potential stress effects of the leaf infiltration and the DEX-inducible expression system. In this experimental setup, the onset of ion leakage was detected at 4 to 6 hpi (Figures 1-2.A, S1-3.A). The transcriptome profiling was performed at early time points after induction to minimize interference with potential secondary inductive cues emanating from leaf cells destined to die or dead.

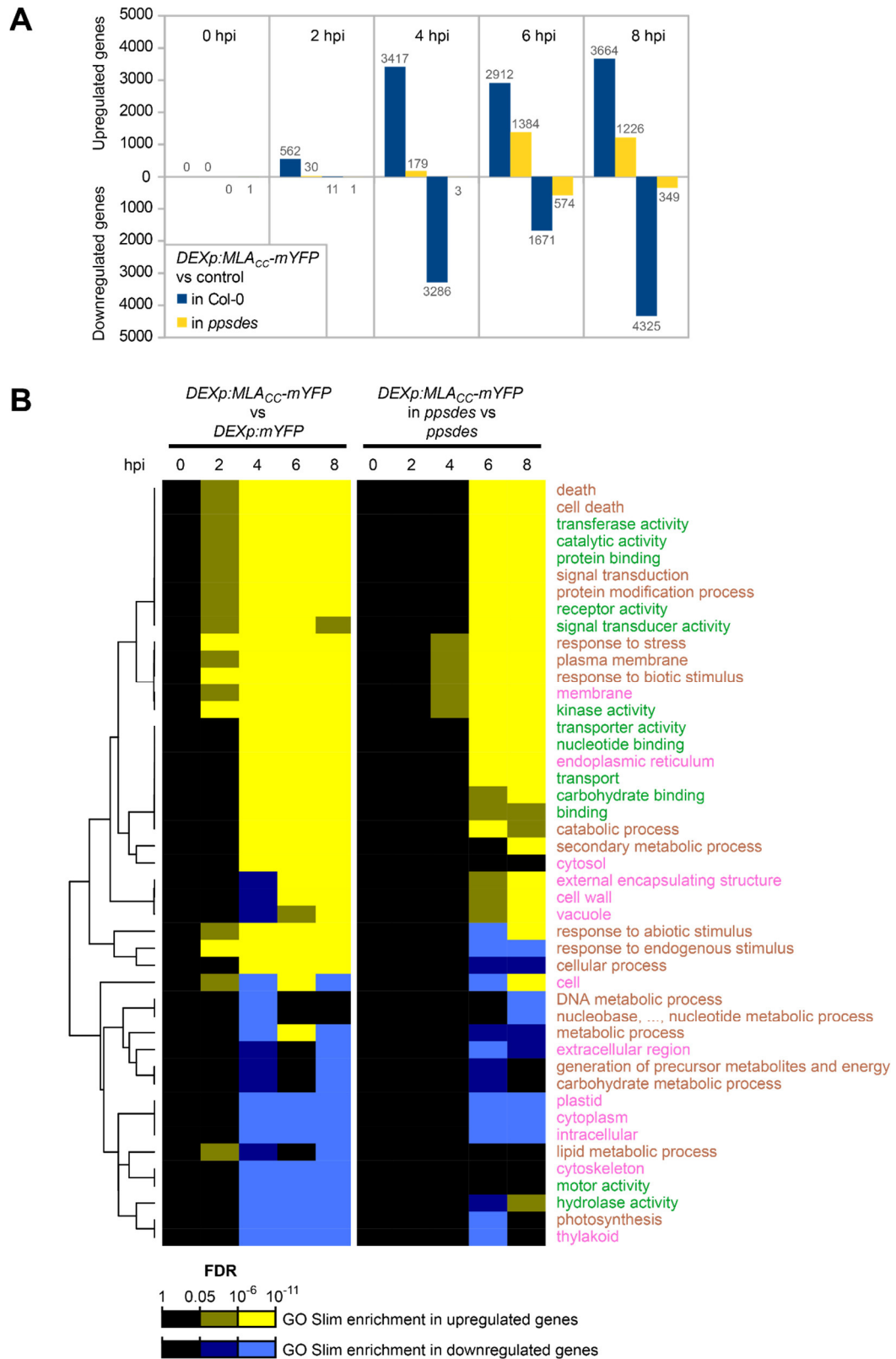
In the wild-type (Col-0) background, 12,742 genes were significantly (FDR < 0.01) differentially expressed in an MLA_{CC}-dependent manner over the time course compared to the *DEXp:mYFP* line. As shown in Figure 1-7.A, a large number of genes (573) were differentially regulated already two hours after induction. Almost all (562/573) of the differentially expressed genes (DEGs) at 2 hpi were upregulated indicating that transcriptional activation prevails during the early response. 4,336 genes were significantly (FDR < 0.01) differentially expressed in an MLA_{CC}-dependent manner over the time course compared to the *ppsd* mutant background. The response in the *ppsd* mutant background appears delayed and attenuated compared to the corresponding wild-type background (Figure 1-7.A-C).

To find out whether the transcriptional changes are qualitatively similar in wild-type compared to the *ppsd* mutant, I performed a gene ontology (GO) term enrichment analysis based on the upregulated and downregulated gene sets at each time point for each genotype.

To gain a general overview of the transcriptional changes, I used GO Slim terms instead of the more detailed GO regular terms. GO Slim terms with a highly significant enrichment ($FDR < 10^{-6}$) in at least one genotype and one time point were selected and their enrichment FDR plotted over time for the two different genotypes (Figure 1-7.B). The GO Slim enrichment pattern is highly similar in both genetic backgrounds though delayed in *ppsdes* plants compared to the wild-type background. This supports the hypothesis that MLA_{CC} induces a qualitatively similar response in wild-type Col-0 and *ppsdes* mutant backgrounds. The proportion and timing of GO term enrichment further supports the hypothesis that the MLA_{CC} -dependent early response is a rapid gene induction rather than downregulation. A detailed inspection of the enriched GO Slim terms suggests that plant defence responses (GO Slim term response to biotic stimulus, adjusted $p = 2.44 \cdot 10^{-9}$ at 2 hpi), cell death-related processes (GO Slim terms death and cell death; adjusted $p = 1.17 \cdot 10^{-5}$ and $1.17 \cdot 10^{-5}$ at 2 hpi respectively), and signalling/post-translational modification processes (GO Slim terms protein binding, signal transduction, protein modification process, receptor activity, signal transducer activity, and kinase activity; adjusted $p = 3.27 \cdot 10^{-5}$, $1.21 \cdot 10^{-4}$, $7.23 \cdot 10^{-4}$, $7.23 \cdot 10^{-4}$, $6.92 \cdot 10^{-6}$, and $6.20 \cdot 10^{-9}$ at 2 hpi respectively) are rapidly activated. On the other hand, at later time points (4 to 8 hpi), basal metabolism appeared to be downregulated (GO Slim terms metabolic process, generation of precursor metabolites and energy, and carbohydrate metabolic process) including photosynthesis (GO Slim terms plastid, photosynthesis, and thylakoid) and some nuclear processes (GO Slim terms DNA metabolic process, nucleoside [...] metabolic process). This may reflect a trade-off between an immune response and basal metabolism upon MLA_{CC} expression (Lozano-Duran and Zipfel 2015, Huot et al. 2014).

I further compared the responses mediated by MLA_{CC} in wild-type and *ppsdes* plants by plotting the \log_2FC in the two genotypes against each other at the tested time points (Figure 1-7.C). The linear correlation between both genotypes was particularly high except at the 2 hpi time point. This indicates that most genes behave similarly upon MLA_{CC} expression in wild-type and *ppsdes* backgrounds. Consistent with the previous observations, this data suggest a delay in onset and overall attenuation of the transcriptional response in the *ppsdes* mutant, but qualitatively the transcriptional outputs are highly similar in both genotypes.

Chapter 1. Functional characterization of the MLA coiled-coil module in *A. thaliana*



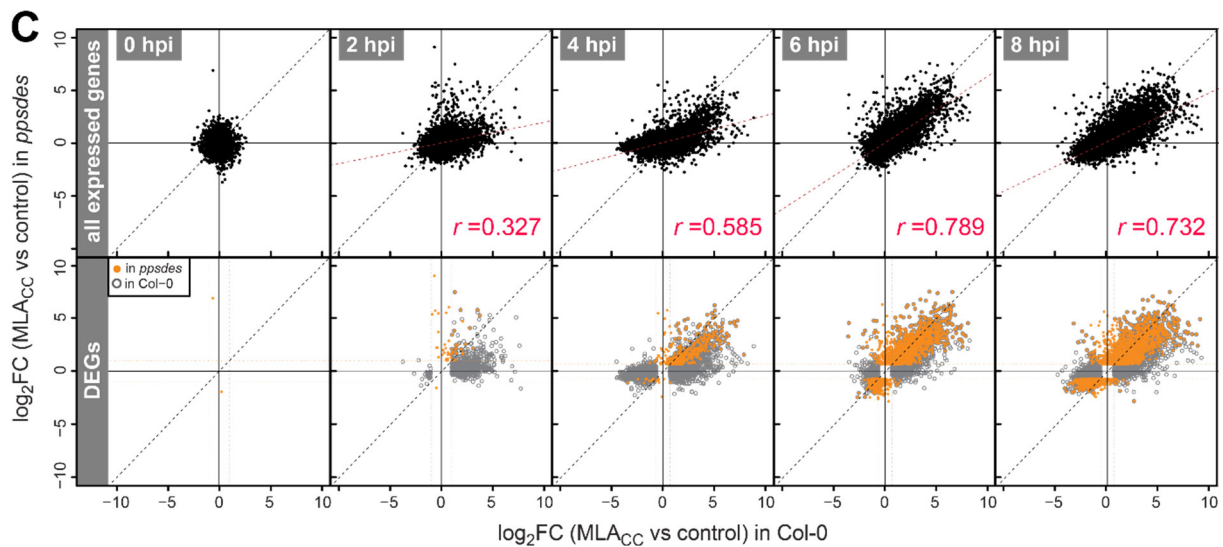


Figure 1-7: MLA_{CC} rapidly induces a similar transcriptional reprogramming in wild type *A. thaliana* (Col-0) and *ppsdes* mutant backgrounds. Leaves of the indicated genotypes were infiltrated with 1 μ M DEX and analysed at different time points by RNA-seq. **A**, number of differentially expressed genes (DEGs) in the *DEXp:MLA_{CC}-mYFP* lines as compared to the *DEXp:mYFP* or non-transgenic control line at the same time point, in wild-type and *ppsdes* mutant backgrounds respectively. DEGs are defined by FC > 2 and FDR < 0.01. **B**, Go Slim term enrichment analysis. The heatmap figures the enrichment pattern of the GO Slim terms enriched in at least one condition with FDR < 10⁻⁶. GO Slim terms related to biological processes, molecular functions and cellular components are indicated in brown, green, and pink respectively. **C**, Comparison of the MLA_{CC}-dependent transcriptional changes in wild-type (Col-0) and *ppsdes* mutant background. The log₂FC of all expressed genes (upper panel) or differentially expressed genes (DEGs, lower panel) at each time respective to the control at the same time point in Col-0 background was plotted against the corresponding log₂FC in *ppsdes* mutant background. The Pearson correlation coefficient (r) was calculated from the log₂FC of all expressed genes between both genotypes (red). hpi, hours post infiltration. FC, fold change.

Similar conclusions could be inferred from the inspection of the top 2,000 DEGs in wild-type and the top 2,000 DEGs in the *ppsdes* mutant. The intersection of both gene sets comprises 3,152 genes. The expression pattern of these 3,152 genes was represented on a heatmap (Figure S1-4.A). Hierarchical clustering was performed to identify gene clusters which follow similar expression patterns and the expression profile of each cluster was plotted over time (Figure S1-4.B). This further illustrates the quantitative similarity between MLA_{CC}-dependent gene regulation in wild-type and *ppsdes* backgrounds. Co-expression relationships among the genes within each cluster were analysed to identify genes which have the highest connectivity degree, i.e. the maximum number of neighbours (Figure S1-5.D). These genes are likely to represent regulatory nodes within the gene cluster. Some of them are characterized genes which are functionally linked to defence processes such as *EXO70B2*, *NHL3* and *PEN1*. Others have not been functionally characterized and define candidates for further functional study in the context of plant immunity.

Some marker genes for EDS1-, SA-, and ET-/JA-mediated responses are still induced in the *ppsdes* mutant upon MLA_{CC} expression, whereas some are not (Figure S1-5), suggesting either that the annotation of a subset of these “marker genes” is not correct or that their activation is a consequence of ectopic barley MLA_{CC} expression in *A. thaliana*.

Overall, this data indicates that MLA_{CC} induces a rapid and massive transcriptional reprogramming. GO term enrichment analysis suggests that this response is enriched in genes with defence-related functions. Furthermore, the transcriptional outputs are qualitatively similar between wild-type *ppsdes* mutant backgrounds, indicating that EDS1 and the phytohormones JA, ET and SA are dispensable for the transcriptional reprogramming although the overall transcriptional output in the *ppsdes* mutant is delayed and attenuated. As presented in Results section 1.2.6, MLA_{CC} transgene expression in the *ppsdes* background is delayed and weaker compared to the MLA_{CC} -expressing line in wild-type background. This makes it difficult to assign to the genes lacking in the *ppsdes* mutant a clear modulatory role regarding timing and amplitude of the observed transcriptional outputs. Importantly, cell death was neither detectable at 2 hpi by trypan blue staining nor by ion leakage assay (Figures 1-2.A and S1-3.A, B), strongly supporting the hypothesis that the observed transcriptional reprogramming is not a consequence of cell death but the result of an active process mediated by barley MLA_{CC} .

1.3.2. The MLA_{CC} -mediated transcriptional response is similar to several other NLR mediated- and P/MAMP-triggered early responses

According to the GO Slim term enrichment analysis presented in the previous section, MLA_{CC} can induce a transcriptional response, which might share common features with ETI, including rapid and preferential induction of defence- and cell death-related genes and a downregulation of genes encoding basal metabolic functions (Huot et al., 2014, Figure 1-7.B). Consistently with this, both conditional MLA_{CC} expression and the majority of tested *R* gene-conditioned ETI are accompanied by a cell death response. GO Slim term enrichment analysis within the distinct gene clusters defined in Figure S1-4.A also indicated an overrepresentation of defence-, stress-, and signalling-related terms in the upregulated clusters whilst basal metabolism-related terms dominate the downregulated clusters (Figure S1-4.C). Interestingly, the categories death and cell death are assigned to one specific cluster of upregulated genes

(cluster 1) whereas the stress- and defence- related categories are more broadly distributed among the upregulated gene clusters.

A more detailed insight into the functional categories over-represented over time in the upregulated and downregulated gene sets is presented in Figure S1-6. The two most significantly enriched categories were, in upregulated genes, “response to stimulus” and “response to stress” (adjusted $p=1.34 \times 10^{-57}$ and 8.13×10^{-49} at 8 and 4 hpi in wild-type background respectively), and in downregulated genes “photosynthesis” and “photosynthesis, light reaction” (adjusted $p=3.38 \times 10^{-58}$ and 1.97×10^{-36} at 8 hpi in wild-type background). Functional categories related to ETI such as “defence response”, “incompatible interaction” and “programmed cell death” were highly enriched in the upregulated genes of transgenic lines expressing MLA_{CC} in wild-type (adjusted $p < 10^{-6}$ at 2, 4, 6, and 8 hpi) or in *ppsdes* backgrounds (adjusted $p < 10^{-6}$ at 6 and 8 hpi). Therefore, the MLA_{CC}-mediated transcriptional response seems to share features with the ETI and with the hypersensitive response. On the other hand, the enriched GO term “response to chitin” indicates activation of responses related to PTI. This is consistent with the presence of many chitin-responsive genes in the main MLA1-dependent gene cluster in *A. thaliana* (Maekawa et al., 2012). Investigation of enriched GO terms in early-upregulated genes in wild-type (at 2 hpi) confirms that the MLA_{CC}-dependent response is tightly associated with defence gene activation (Figure 1-8). Thus, potential primary target genes of MLA_{CC}-mediated signalling are functionally associated with immunity but not a consequence of the MLA_{CC}-mediated cell death.



Figure 1-8: GO term enrichment analysis of MLA_{CC}-upregulated genes at 2 hours after induction. Each circle represents an enriched GO term compared to the whole genome after false discovery rate (FDR) correction. The size of each circle is proportional to the number of genes annotated to the node. The circle colour indicates the FDR-corrected enrichment p-value. Only the GO categories for biological processes with a p-value lower than 10^{-6} were represented. There were no GO categories enriched in the genes downregulated at 2 hpi.

To further assess the similarity between the MLA_{CC}-mediated transcriptional response and those during ETI and PTI, I conducted a comparative transcriptomic analysis using published and unpublished datasets (Table S1-1). I prioritized for the selection of datasets fulfilling at least one of the following criteria:

- (1) a fine time-resolution, at least at early time points after ETI or PTI induction
- (2) the use of a «pathogen-free» system for triggering ETI or PTI
- (3) the availability of genome-wide expression profiling data (RNA-seq or ATH1 22 K microarray)

Some datasets could be obtained from publicly available databases. However, many of the most relevant datasets are unpublished and were provided by collaborators. The group of

Kenichi Tsuda and the group of Jane Parker have to be acknowledged for sharing with me high quality transcriptomic datasets (Table S1-1). I obtained datasets related to pathogen-triggered NLR-mediated ETI, to P/MAMP treatments, and to temperature-shift-inducible RPS4-mediated ETI. Some datasets also allow examination of ETI-specific transcriptional regulation in defence phytohormone-depleted mutant backgrounds.

To allow comparison among the different datasets, the raw data was normalized and re-analysed with the same method. One method was used for all RNA-seq data and another one for all microarray data analysis (details in Methods section). Log₂FC expression values were calculated by comparing the induced samples to the negative controls at the same time point to highlight ETI- or PTI-specific gene regulation. For example, plants inoculated with a virulent pathogen (PTI-inducing treatment) were compared to mock-treated plants to highlight PTI-specific changes, and plants inoculated with avirulent pathogen (ETI-inducing treatment) were compared to plants inoculated with a virulent pathogen (PTI-inducing treatment) to highlight ETI-specific changes. To globally compare the different responses, the treatments and time points were analysed in a pairwise-manner by calculating the Pearson correlation coefficient (r) based on the log₂FC values of all commonly expressed genes. It should be noted that this coefficient quantifies the qualitative similarity/difference between two datasets but does account for quantitative differences in gene expression.

I first compared the responses triggered by MLA_{CC} and those triggered by several other NLRs (Figure 1-9.A). One dataset examined the temperature shift-dependent immune activation by the overexpressed TIR-type NLR (TNL) RPS4 (35S:RPS4) after shifting the plants from 28°C to lower temperature (19°C) (Heidrich et al., 2013). This is so far the only other dataset available allowing investigation of a synchronized full-length NLR-mediated transcriptional response in a pathogen-free system. The comparison with the MLA_{CC} is therefore particularly relevant and allows addressing a potential overlap between CC-type NLR- (CNL) and TNL-mediated responses under pathogen-free conditions. The use of a pathogen-free system to study NLR-mediated responses is particularly interesting since it allows dissection of the NLR-mediated response uncoupled from confounding effects mediated by pathogen effectors and P/MAMP responses.

For the other ETI-related datasets, the pathosystems used to trigger the ETI were as follows: *MLA1* and *RPS4* encode, respectively, a CNL and a TNL recognizing effectors of *Blumeria graminis* f. sp. *hordei* isolate K1 (*Bgh* K1) and *Pseudomonas syringae* pv. *tomato* DC3000 AvrRps4 (*Pst* AvrRps4). *MLA1* expressing plants have been generated in the partially

immunocompromised *pen2 pad4 sag101 (pps)* mutant background, which is susceptible to virulent *Bgh* strains whereas wild-type *A. thaliana* (Col-0) is resistant to both avirulent and virulent *Bgh* strains. *Pst* effectors AvrRpt2 and AvrRpm1 are recognized by the *A. thaliana* CNLs RPS2 and RPM1 respectively.

This analysis reveals a strong positive correlation between MLA_{CC}-mediated transcriptional changes between 4 and 8 hpi and those of 35S:RPS4 between 4 and 8 hpi ($0.74 < r < 0.83$, Figure 1-9.A). Therefore, the response induced by the overexpressed full-length TNL RPS4 after the temperature shift activating RPS4-conditioned ETI appears to be qualitatively very similar to that mediated by the constitutively active MLA_{CC}. This indicates that MLA_{CC} alone can trigger transcriptional changes similar to those mediated by a full length NLR.

To test whether MLA_{CC} and temperature-inducible RPS4 transcriptional outputs are similar to ETI triggered upon effector recognition during authentic plant-pathogen avirulent interactions, I calculated the correlation between the corresponding expression patterns. Both MLA_{CC} and temperature-inducible RPS4 transcriptional outputs shared a high positive correlation with the response mediated by MLA1 at 18 hpi ($0.42 < r < 0.60$). MLA1-dependent transcriptional reprogramming was detected in avirulent *Bgh*-challenged leaves at 18 hpi, but not at other tested time points (6, 12, and 24 hpi) (Maekawa et al., 2012). This shows a substantial difference in the timing of chemically-/temperature-inducible and NLR-mediated transcriptional outputs upon *Bgh* challenge, likely reflecting a long time period (~15 h) needed until fungal AvrA1 effector is delivered into plant cells. An even stronger correlation was observed between MLA_{CC} and temperature-inducible RPS4 transcriptional outputs, and ETI triggered by avirulent *Pst* AvrRpt2 and *Pst* AvrRpm1 at 4-6 hpi ($0.57 < r < 0.86$ and $0.48 < r < 0.79$ respectively). ETI-specific transcriptional outputs upon avirulent *Pst* inoculation start to be detected at 4 hpi (first tested time points with >100 DEGs [FC>2 and FDR<0.01], 384 and 1012 DEGs at 4 hpi upon *Pst* AvrRpm1 and *Pst* AvrRpt2 inoculation respectively). A similar pattern was observed upon inoculation with *Pst* AvrRps4 where the highest correlation was observed at 6 hpi ($0.38 < r < 0.54$).

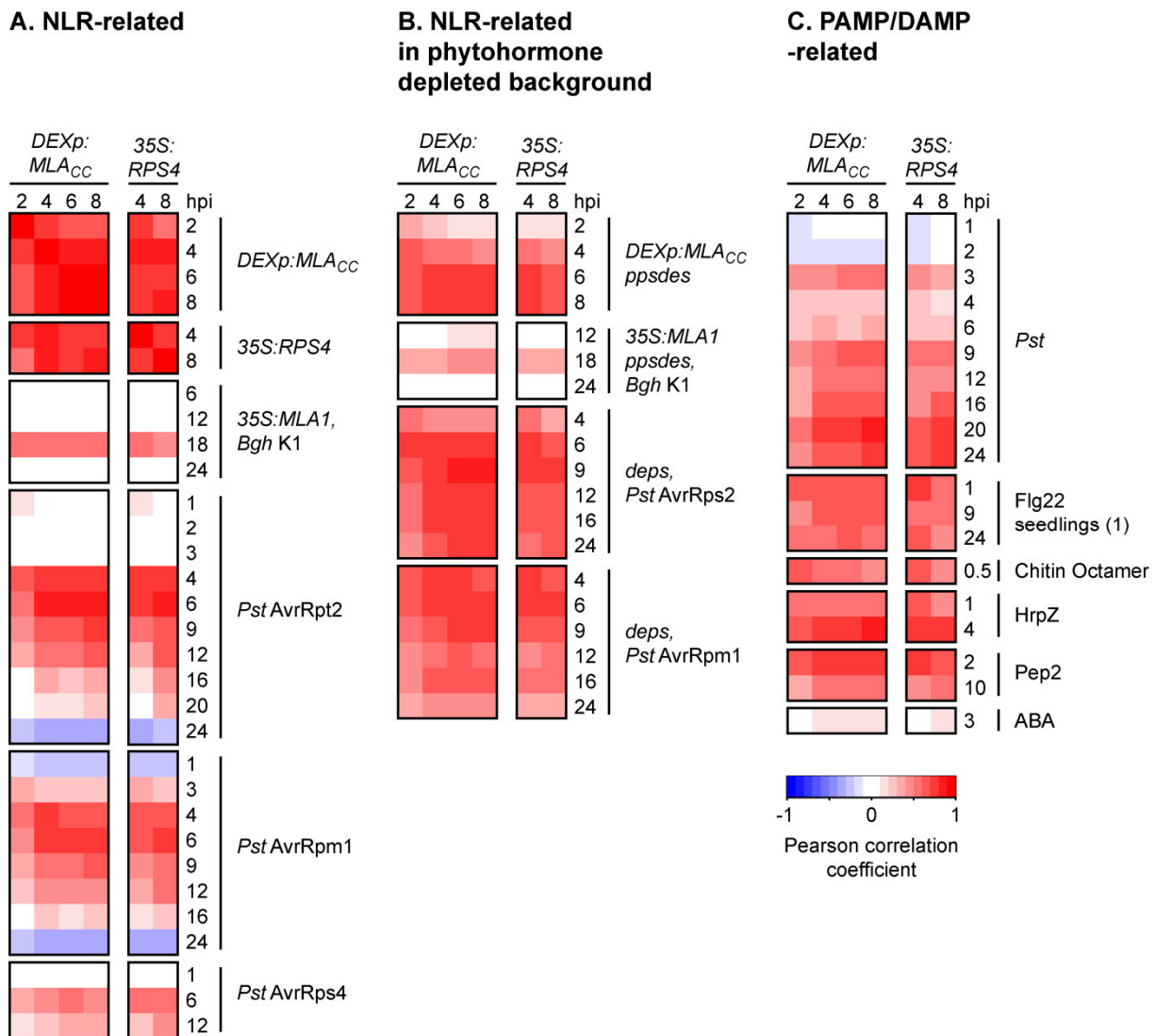


Figure 1-9: Transcriptome-wide correlation analysis among MLA_{CC} -, ETI- and PTI-associated gene expression patterns. Relative expression ($\log_2FC(\text{treatment/control})$) of all commonly expressed genes were used to calculate the Pearson correlation coefficient between two different treatments at a given time point. A, Comparison of ETI-related responses. MLA and $RPS4$ encode a CNL and a TNL recognizing effectors of *Blumeria graminis* f. sp. *hordei* isolate K1 (*Bgh K1*) and *Pseudomonas syringae* pv. *tomato* DC3000 AvrRps4 (*Pst AvrRps4*) respectively. AvrRpt2 and AvrRpm1 effectors are recognized by the CNLs RPS2 and RPM1 respectively in *A. thaliana*. B, Comparison of ETI-related responses in phytohormone depleted mutant backgrounds. The *ppsd* mutant is partially immunocompromised and deficient in multiple phytohormone signalling pathways (SA, ET and JA) whereas the *deps* mutant is compromised in the signalling pathways mediated by SA, ET and JA phytohormones, with a simultaneous impairment in both synthesis of, and sensitivity to SA. C, Comparison of ETI-like responses mediated by MLA_{CC} and $RPS4$ with PTI-related responses triggered by inoculation with a virulent pathogen (*Pst*) or by treatment with purified P/MAMPs (Flg22, chitin, HrpZ) or DAMP (Pep2). ABA treatment was also included as a control figuring an abiotic stress response.

Overall, these results indicate that, in terms of transcriptional profiles, the MLA_{CC} -dependent transcriptional profiles are very similar to those upon temperature shift-induced $RPS4$ activation, and these outputs, in turn, also largely similar to pathogen-induced ETI mediated by either type of NLRs (CNLs or TNLs) at early time points after pathogen inoculation.

Therefore, MLA_{CC} and 35S:RPS4 activities appear to converge on the same transcriptional machinery that is activated during authentic ETI typically occurring upon interaction with avirulent bacteria and fungi. Since 35S:RPS4 does not induce cell death at 4 or 8 hpi (Heidrich et al., 2013), it is very unlikely that the strong correlation observed between the inducible MLA_{CC} and RPS4 transcriptional outputs and those stimulated during authentic pathogen-triggered ETI are confounded by secondary cues emanating from dying plant cells.

The fact that both MLA-mediated immunity to *Bgh* and MLA_{CC} cell death-inducing activity are not compromised in the *ppsdes* mutant background (Maekawa et al. 2012, Results section 1.3.1) prompted me to test whether early ETI-related transcriptional reprogramming is dependent on hormone-mediated signalling. The *ppsdes* mutant is partially immunocompromised and deficient in multiple phytohormone signalling pathways (SA, ET and JA, Maekawa et al. 2012) whereas the *deps* (*dde2 ein2 pad4 sid2*) mutant is compromised in the signalling pathways mediated by SA, ET and JA phytohormones, with a simultaneous impairment in both synthesis of and sensitivity to SA (Tsuda et al., 2009). I analysed the similarity between MLA_{CC}-dependent transcriptional outputs in the *ppsdes* mutant, or ETI-specific responses in the *deps* or the *ppsdes* mutant, and the inducible MLA_{CC}- or RPS4-dependent transcriptional outputs in wild-type background (Figure 1-9.B). In the case of *MLA1 ppsdes* plants inoculated with *Bgh*, total RNA was obtained from leaf lower epidermal peels. This allowed enriching for leaf cells directly challenged by *Bgh* spores, and thus, to detect the MLA1-dependent transcriptional outputs, which were undetectable in whole leaves. A high positive correlation was observed for all tested comparisons and the temporal correlation pattern was overall very similar to the one observed for the same responses in wild-type (Figure 1-9.A, B). However, the responses in the defence phytohormone-depleted mutants appeared slightly delayed and the correlation to the inducible MLA_{CC} and RPS4 transcriptional outputs was slightly lower than in the wild-type background, indicative of slight temporal and qualitative differences. The highest correlation coefficients between the MLA_{CC}-dependent transcriptional outputs in wild-type background, and the MLA_{CC}-dependent and ETI responses in wild-type and hormone-depleted mutant backgrounds are, respectively: 1 and 0.79 (*DEXp:MLA_{CC}*), 0.84 and 0.82 (*Pst AvrRpt2*), 0.79 and 0.80 (*Pst AvrRpm1*), 0.57 and 0.43 (*Bgh K1*). Therefore, the transcriptional outputs are qualitatively similar in the wild-type and hormone-depleted backgrounds. In this comparison, the correlation differences observed for MLA_{CC}- and MLA1- dependent transcriptional outputs might be partly due to the different MLA_{CC} steady state levels in the transgenic lines compared and the use of a different tissue (whole leaf versus leaf epidermis) respectively.

Overall, these results indicate that the inducible MLA_{CC}- and RPS4-mediated as well as three tested pathogen-stimulated ETI transcriptional outputs are largely robust against simultaneous impairment of SA, JA, and ET defence phytohormone signalling.

The above described similarity of the transcriptional profiles was assessed in more detail by plotting the expression pattern of selected gene sets over time in the different datasets (Figure S1-7). For this, I selected five gene sets shown to be i) regulated in an MLA1-dependent manner in *A. thaliana* (Maekawa et al., 2012), ii) the conserved immune regulon described by Humphry et al. (2010), iii) the 562 genes rapidly induced by MLA_{CC}, iv) the major gene cluster upregulated by MLA_{CC}, and v) the major gene cluster downregulated by MLA_{CC} (Figure S1-4.A, D). Similar expression patterns were observed across all the datasets analysed, with the four upregulated gene sets being consistently upregulated, and the downregulated one being consistently downregulated across all tested datasets (Figure S1-7). This further supports the existence of common patterns of transcriptional changes upon MLA_{CC} expression, pathogen-induced ETI activation by CNLs or TNLs, and PTI.

I then aimed at comparing the inducible MLA_{CC} and RPS4 transcriptional outputs with other biotic stresses. PTI was triggered by inoculation with a virulent pathogen (*Pst*) or by treatment with purified P/MAMPs (flg22, chitin, HrpZ) or DAMP (damage-associated molecular pattern: Pep2). ABA treatment was also included as a representative of abiotic stress responses. Remarkably, this comparison revealed that PTI-associated transcriptional responses are also highly positively correlated (Figure 1-9.C). The highest correlation coefficients were 0.81 (inoculation of virulent *Pst* at 20 hpi), 0.72 (flg22 treatment at 1h), 0.70 (chitin treatment at 30 min), 0.81 (HrpZ treatment at 4h), and 0.78 (Pep2 treatment at 2h). In contrast, the highest correlation coefficient upon ABA treatment was only 0.19. This indicates that early P/MAMP- and DAMP-induced gene regulation largely overlap with those of inducible MLA_{CC}- and RPS4-mediated responses and during pathogen-stimulated ETI. This is consistent with models proposed by previous reports (Navarro et al., 2004; Tao et al., 2003; Tsuda and Katagiri, 2010) where most of the differences in gene expression between ETI and PTI are quantitative. It has been proposed that ETI might amplify the signal initiated by PTI. However, the data presented here instead indicate that ETI-associated gene regulation can be activated in the absence of P/MAMPs and therefore independently of PTI. Since in a typical avirulent interaction the plant is simultaneously exposed to elicitors of PTI and ETI, the nature of the interaction (e.g. additive, synergistic, or antagonistic) between both processes on gene regulation remains to be determined.

1.3.3. Investigation of the 562 genes rapidly induced by MLA_{CC} and identification of immediate early immune response genes

The data presented in the previous section strongly supports the hypothesis that MLA_{CC} triggers an ETI- and P/MAMP-like transcriptional response. The *DEXp:MLA_{CC}-mYFP* lines are particularly appropriate for conducting time-resolved transcript profiling of the MLA_{CC}-mediated response: the proportion of leaf cells synchronously expressing MLA_{CC} upon DEX infiltration is likely much higher than in leaf tissue challenged with an avirulent pathogen. Thus, the chemically-inducible MLA_{CC} expression system is better suited to examine with high signal to noise ratio and temporal resolution the onset of transcriptional changes and to separate those from subsequent local and systemic transcriptional regulation mechanisms. Moreover, the conditional MLA_{CC} expression is induced in the absence of potentially confounding effectors and P/MAMPs.

The first major MLA_{CC}-dependent transcriptional changes can be detected at 2 hpi. At this time point, 562 genes are significantly upregulated whereas only 11 genes are significantly downregulated ($|\log_2FC| > 1$ and $FDR < 0.01$, Results section 1.3.1). Based on this observation, I hypothesized that the MLA_{CC}-mediated primary transcriptional response consists almost exclusively of a gene activation mechanism and that at least a subset of the 562 rapidly upregulated genes might represent primary gene targets of MLA_{CC}-mediated signalling. Most of these genes appeared to be also induced by MLA_{CC} in the *ppsdes* mutant. A detailed analysis indicated that the gene induction was mostly similar at 6 hpi upon expression of MLA_{CC} in *ppsdes* plants. At this time point, 49% of the genes were significantly upregulated ($FC > 2$ and $FDR < 0.01$). Moreover, when examining the FC alone (no FDR cut-off), 78% were induced ($FC > 2$) at 6 hpi and 81% were induced ($FC > 2$) at least at one time point between 2 hpi and 8 hpi. This indicates that SA, ET and JA are not required for activation of the majority of the genes in the early MLA_{CC}-induced cluster.

I then aimed at comparing the expression pattern of the 562 genes in this cluster with those of the early response upon various biotic, abiotic, hormone and chemical treatments. Suitable RNA-seq- or microarray-derived transcriptomic data were collected as described in Table S1-1. The comparison was performed as in Results section 1.3.2. Because a large part of the data originated from ATH1 22K microarray analyses, the analysis was restricted to 478 of the 562 early MLA_{CC}-induced genes identified by RNA-seq, which are non-ambiguously represented on the ATH1 22K microarray. The $\log_2FC(\text{treatment/control})$ for all 478 genes was calculated

and plotted onto a heatmap across all experiments and all relevant time points (Figure S1-8). From this analysis, I selected a subset of the data according to the following criteria (Figure 1-10):

- (i) When several equivalent treatments were available, representative examples were chosen.
- (ii) When several time points were available, the early time point with the most upregulated genes was selected. In some cases, when almost no upregulation was observed at early time points, later time points were also shown to support the overall absence of gene induction.

Analysis of the expression pattern upon inducible MLA_{CC} and RPS4 transcriptional outputs in either wild-type or defence phytohormone-depleted backgrounds indicates that most of the 478 genes displayed a similar induction pattern (Figure 1-10). Therefore, these genes might be common primary targets downstream of MLA_{CC} and RPS4.

The gene induction pattern was also very similar in several early ETI-associated responses (Figure 1-10). 76% of all commonly detected genes were upregulated in at least one ETI-associated response (percentage calculated from the complete dataset shown in Figure S1-8). Consistent with the transcriptome-wide analysis conducted in Results section 1.3.2, this suggests that chemically- or temperature-inducible MLA_{CC} and RPS4 induce a transcriptional response similar to ETI. Therefore, the early MLA_{CC}-induced genes might be common primary targets downstream of the tested full-length NLRs activated during ETI, and ET, SA, and JA are dispensable for rapid induction of these genes.

A similar induction pattern was observed upon P/MAMP and DAMP treatments where 79% of the commonly detected genes were induced by at least one P/MAMP or DAMP treatment and, to a lesser extent, upon abiotic stresses where 70% of the genes were induced in at least one condition. Similar numbers of conditions were tested for both types of response (16 conditions from 6 different treatments and 15 conditions from 7 different treatments for P/MAMP and DAMP treatments and abiotic stresses respectively, Figure 1-10). Importantly, no clear pattern of gene induction was observed upon inoculation with virulent *Pst* at two early time points (3 and 4 hpi), although a response similar to a P/MAMP treatment is conceivable. It is tempting to speculate that PTI is in this case inhibited by bacterial effectors injected into plant cells.

In contrast, phytohormone treatments were not effective in rapidly triggering induction of the early MLA_{CC}-induced genes (Figure 1-10). Despite the large number of data related to

phytohormone treatments (24 conditions from 9 different treatments), only 34% of the commonly detected genes were induced in at least one condition. Even the defence-related phytohormone SA did not clearly activate the early MLA_{CC} -induced cluster. This supports the hypothesis that induction of the early MLA_{CC} -induced genes does not require phytohormone signalling.

Cell death inducing treatments at early and late time points did not generally induce the early MLA_{CC} -induced genes (Figure 1-10). Only 30% of all commonly detected genes were induced in at least one condition. Thus, the early MLA_{CC} -induced cluster is not generally activated in response to different plant cell death-inducing agents.

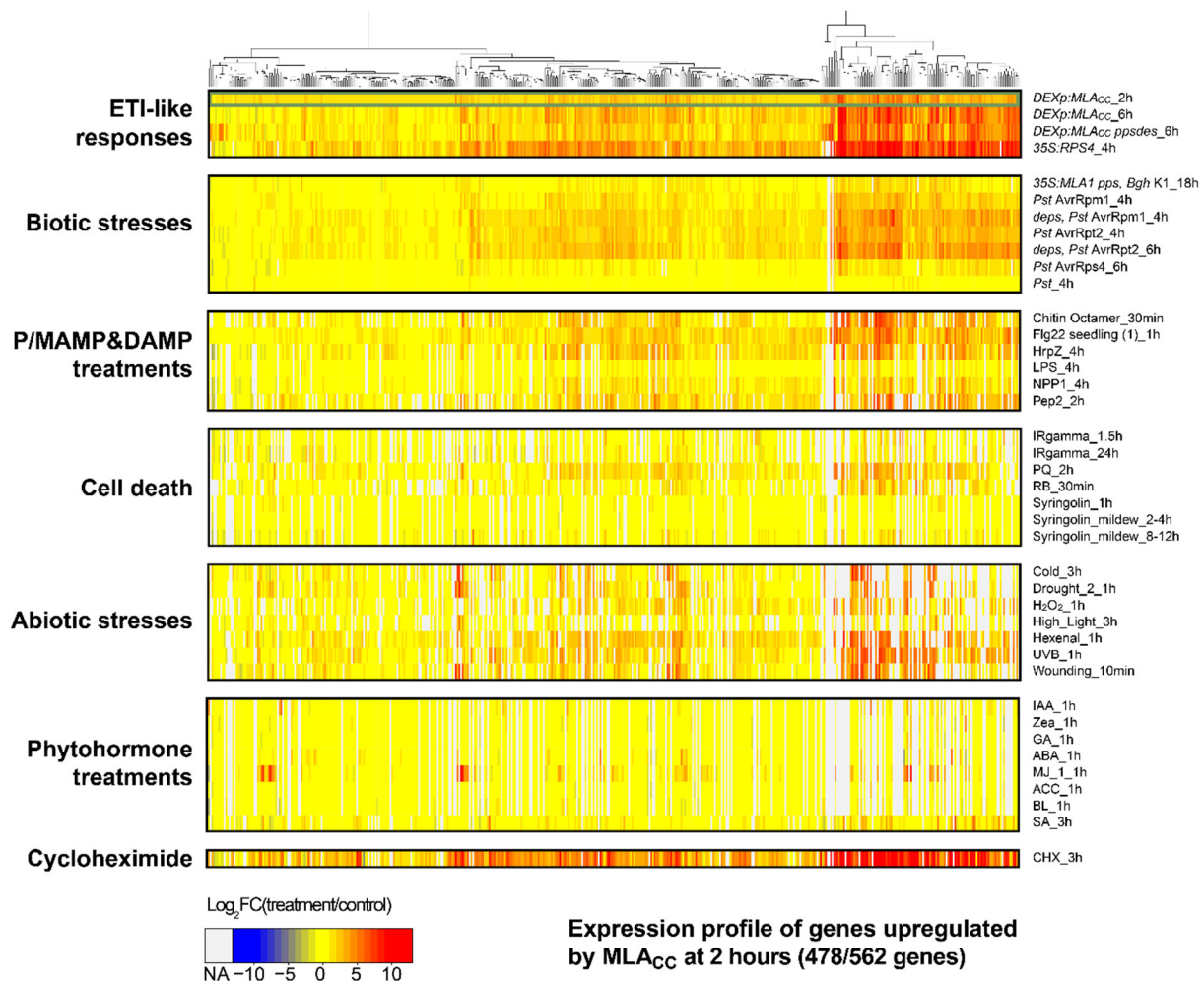


Figure 1-10: Expression profile of the genes rapidly induced upon MLA_{CC} expression in the early response to diverse biotic, abiotic, hormone and chemical treatments. The $\log_2FC(\text{treatment/control})$ for 478 genes out of 562 rapidly MLA_{CC} -induced genes was plotted on a heatmap. Hierarchical clustering was performed on the x-axis. NA, not available (expression not detected). The data represented here represent a selected subset of the extended dataset shown in Figure S1-8. For a description of the datasets used, see Table S1-1.









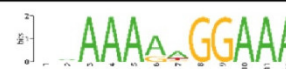
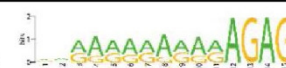
Overall, these results suggest the existence of a common set of potential primary target genes convergently induced by both TNL- and CNL-type NLRs and PRRs during PTI. This finding further suggests that ETI and PTI might engage a common transcriptional machinery for immune response activation.

Many genes are commonly and rapidly induced by MLACC and various other treatments and stresses. I hypothesized that these genes might be controlled by one or several regulators present in non-stimulated plants and whose activity or stability is rapidly altered in order to achieve the observed rapid gene induction. This (these) pre-formed regulator(s) can have either a positive or a negative regulatory function on transcription. Treatment with cycloheximide (CHX), an inhibitor of protein synthesis, can induce rapid and massive transcriptional changes (Goda et al., 2008; William et al., 2004). The CHX-mediated response is thought to result from the disappearance of short-lived transcriptional repressors. Most of the early MLACC-induced genes (>74.7%) are also induced by CHX treatment (Figure 1-10). I analysed two independent and publicly available transcriptomic datasets describing the effects of CHX on gene expression at early time points in *A. thaliana* compared to a mock treatment (at 3 h and 4 h after CHX treatment, Table S1-1). 3,888 genes were upregulated in at least one dataset and 1,837 genes were commonly upregulated (FC>2 and FDR<0.05). Differences in the used plant tissue, or plant age, or sampling time might partly account for the differences between the two experiments.

I investigated the regulation of the 562 early MLACC-regulated genes in these two independent CHX treatments. The global expression pattern of the early MLACC-induced genes in both datasets is represented in Figure S1-8. Expression of 456 out of 562 genes was detected in at least one of the two datasets. Out of these 456 detected genes, 348 genes (76.3% and 61.9% of the 456 and the 562 upregulated genes respectively) were upregulated in both experiments and 420 genes (92.1% and 74.7% of the 456 and the 562 upregulated genes respectively) were upregulated in at least one of them (FC>2 and FDR<0.05). Thus, at least 74.7% of the early MLACC-induced genes appear to be immediate early response genes since their induction does not depend on *de novo* protein synthesis, and were designated plant immediate early genes. This observation suggests that these genes are activated by the removal of short-lived repressors. Interestingly, the transcriptional induction by two independent CHX treatments was globally stronger than that of all other responses analysed (Figure 1-10 and Figure S1-8). Navarro et al., (2004) have reported that a large proportion of the early flg22-induced genes is also induced by CHX and have therefore proposed that

defence genes are under the control of a repression mechanism. Our data indicates that rapid de-repression by removal of short-lived negative regulators might be a common mechanism for various biotic and abiotic stresses. Because the genes rapidly induced by MLA_{CC} represent only a small fraction of all CHX-induced genes (420/3,888), there are likely several short-lived negative regulators involved in regulating unrelated plant-specific biological processes.

Table 1-1: Overrepresentation of cis-regulatory sequences in the promoter of the 562 MLA_{CC} early-induced genes

Motif	Sequence	Logo	Genome	MLA _{CC} cluster
RSRE, CAMTA (1)	vCGCGb		% 11.60% FDR	29.20% 1.34E-28
CAMTA (2)	vCGyGb		% 47.20% FDR	66.40% 5.97E-19
CAMTA (3)	vCGyGT		% 31.60% FDR	56.20% 8.09E-33
G-box (ABRE)	CACGTGb		% 9.10% FDR	16.20% 1.59E-06
ABRE-CE	mACGCGb		% 6.70% FDR	22.20% 6.05E-32
W-box	TTGACy		% 45.60% FDR	57.10% 6.655E-07
WRKY60	GGTCAA		% 20.70% FDR	29.40% 2.23E-05
HSE	GAA _n TTC		% 18.10% FDR	31.10% 1.05E-12
PI	AAA _n GGAAA		% 7.50% FDR	11% 0.04983
unknown	rrrrrrrrAGAGA		% 9.50% FDR	14.20% 0.006105

% Percentage of genes containing the indicated motifs. The enrichment false discovery rate (FDR) was calculated by using the cumulative hypergeometric distribution with correction for multiple testing.

To identify transcription factors regulating the expression of the early MLA_{CC}-induced gene cluster, I performed a *cis*-regulatory element analysis in the 5' regulatory regions of the 562 early MLA_{CC}-induced genes. Several algorithms were used for *de novo* motif discovery and for analysis of known regulatory motifs (for details, see material and methods). I selected motifs consistently identified by several independent methods and calculated their frequency in the early MLA_{CC}-induced genes using RSAT pattern matching tool (Table 1-1). The motif frequency was tested against a hypergeometric distribution to determine whether it is significantly higher in the early MLA_{CC}-induced genes compared to all promoters in the

genome. Strikingly, half of the identified motifs are derived from the GCyG core motif bound by the CAMTA (calmodulin-binding transcriptional activator) family and are very similar to the RSRE (rapid stress response element, CGCGTT, (Walley et al., 2007)). These include three motifs which were found to be bound by CAMTAs (the vCGCGb motif, the relaxed vCGyGb motif and its vCGyGT derivative which was identified in this study as the most significantly enriched motif), and two longer motifs which share the same GCyG core sequence: the CACGTGb motif, also known as G-box, and part of the ABRE (ABA-responsive element), and the mACGCGb motif known as the ABRE-CE motif (Hobo et al., 1999; Narusaka et al., 2003; Shen and Ho, 1995). The vCGCGb and the mACGCGb motifs displayed the highest enrichment (~3 fold) among all identified motifs. The mACGCGb motif together with the vCGyGT motif had the most statistically significant enrichments. The relaxed consensus vCGyGb was present in 5' regulatory regions of 66% of the early MLACC-induced genes, indicating that up to 2/3 of the genes in early MLACC-induced cluster might be controlled by the same regulatory sequence and the same group of cognate transcription factors. According to the sequence of the motifs identified, the CAMTA TF family might have a critical role in regulating the early MLACC-induced gene cluster including the pIE genes.

The five other motifs identified were not sequence-related to the one presented above. Two of them were known motifs bound by the WRKY family (W-boxes). However, the enrichment and its statistical significance were not as high as for the RSRE-like motifs. Therefore, WRKY transcription factors might also contribute to a lesser extent to the regulation of the early MLACC-induced cluster.

An 8-bp palindromic motif (GAAnnTTC) was found in 31% of the genes with a highly significant overrepresentation. This was reported as a heat shock element (HSE) regulated by heat shock factors. Interestingly, a role for some heat shock factors in defence regulation has been recently identified (Bechtold et al., 2013; Pick et al., 2012) as well as a possible regulation by MAPK6 (Evrard et al., 2013).

Finally, two other motifs consist in a long G/A rich stretch which is somewhat reminiscent of the stress-related motif identified in the conserved immune regulon identified by Humphry et al. 2010. Though significantly overrepresented, these motifs were found at low frequency (11% and 14%). One of them is similar to the sequence bound by the floral homeotic MADS transcription factor PISTILLATA (PI), indicating that this motif might be bound by some MADS TFs. In total, 510 genes contain in their 5' regulatory region at least one of the three

most frequent motifs (vCGyGb, TTGACy, GAAnnTTC). I analysed the correlation between the occurrences of these three motifs in the promoters of the 562 early MLA_{CC}-induced genes. However, there was no obvious correlation in the occurrence of the three motifs tested (data not shown). A similar motif enrichment analysis was performed on separate clusters of the MLA_{CC}-induced gene set as defined by hierarchical clustering. Similar motifs were identified but no striking cluster-specific enrichment for these motifs was detected.

Since the vCGyGb-related motifs are the most frequently occurring and most enriched motifs, I analysed the distribution of the vCGyGb and the vCGCGb motifs in the promoter of the 562 early MLA_{CC}-induced genes (Figure 1-11). Most of the motifs were found in the first 500 bp upstream of the transcription start site (TSS) with a very pronounced peak located in the 100 bp upstream of the TSS. Therefore the spatial distribution of these two motifs in the promoter region of the 562 genes does not seem to be random, supporting their presumed relevance for the rapid gene induction.

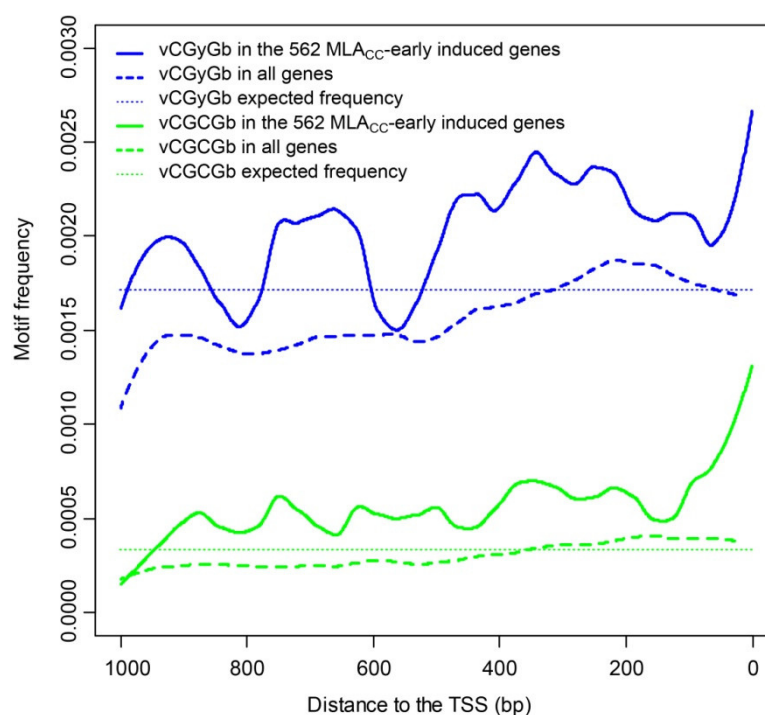


Figure 1-11: Analysis of CAMTA binding motif frequency and distribution in 5' cis-regulatory sequences. Frequency of the indicated motif was computed based on pattern matching results produced by RSAT. The frequency was calculated for the 5' cis-regulatory sequences from the transcription start site (TSS) up to 1,000 bp upstream. The analysis was performed for all *A. thaliana* genes annotated in TAIR10 (33,602 genes) and for the 562 genes rapidly induced by MLA_{CC}. The expected frequency was calculated for each motif following the same method, and based on nucleotide sequences randomly generated according to the average nucleotide frequency of found in the corresponding 5' cis-regulatory sequences.

In conclusion, these results indicate that the transcriptional reprogramming induced by MLA_{CC} is qualitatively very similar to the early transcriptional response to temperature-inducible RPS4 and pathogen-triggered early ETI mediated by either CNLs or TNLs and during PTI. Therefore, MLA_{CC} acts as a signalling module sufficient for transcriptional activation of an early immune response gene cluster common to the early response during ETI and PTI. Thus, ETI-associated transcriptional reprogramming is not merely a sustained/amplified PTI-associated transcriptional reprogramming. But both branches of the plant innate immune system independently converge on common early immune response genes, most of which are pIE genes. I found that defence phytohormones are largely dispensable for induction of the identified early immune response genes. The earliest gene set regulated by MLA_{CC} is similarly regulated at early time points in other biotic responses. This supports the existence of a common transcriptional machinery for a core set of early immune response genes. CAMTA-, WRKY-, and HSF-binding motifs are overrepresented in the promoters of the 562 early MLA_{CC}-induced genes. A subset of transcription factors of the CAMTA and/or WRKY and/or HSF families might be common factors involved in the regulation of the primary nuclear targets of both ETI and PTI.

1.4. Robustness of the MLA_{CC}-triggered signalling mechanism

1.4.1. *RAR1* is dispensable for MLA_{CC}-mediated responses

Previous mutational studies in several plant species have identified genetic components required for plant NLR function. The heteromeric protein complex involving the chaperone HSP90 and two associated co-chaperones SGT1 and RAR1, is required for stabilization of a subset of pre-activated NLR complexes (Kadota and Shirasu, 2012). Interestingly, MLA requirement for RAR1 and SGT1 in barley differs for different MLA recognition specificities (Azevedo et al., 2002; Hein et al., 2005; Jørgensen, 1988; Torp and Jørgensen, 1986). SGT1 and HSP90 but not RAR1 are required for MLA_{CC}-mediated cell death in *Nicotiana benthamiana* (Bai et al., 2012). NDR1 is a regulatory component required for the function of multiple CNLs (Aarts et al., 1998; Century et al., 1995; Day et al., 2006; Knepper et al., 2011; Selote et al., 2014).

To test a potential MLA_{CC} requirement for *RAR1* in *A. thaliana*, I crossed the *DEXp:MLA_{CC}-mYFP* with the *rar1* mutant. Ion leakage was monitored upon DEX treatment of the

homozygous F₃ progeny. Ion leakage was induced to a lower level in the *DEXp:MLA_{CC}-mYFP rar1* lines compared to the *DEXp:MLA_{CC}-mYFP* line in wild-type Col-0 background (Figure 1-12.A). The MLA_{CC} protein accumulation was lower in the *rar1* compared to wild-type background (Figure 1-12.B). This result indicates that *RAR1* is dispensable for MLA_{CC}-mediated cell death induction. Since MLA_{CC} accumulated at a lower level in the *rar1* background, no clear conclusion can be drawn regarding a possible partial suppression of cell death in the *rar1* background. A similar analysis was undertaken in the *sgt1b* and *ndr1* single mutant backgrounds. However, in the generated homozygous F₃ progeny in *sgt1b* and *ndr1* backgrounds, the MLA_{CC} protein was not detectable, suggesting a decrease of MLA_{CC} steady-state levels. Therefore, these lines were not appropriate for monitoring the MLA_{CC}-dependent ion leakage. The observed decrease in MLA_{CC} steady-state levels might be due to the single mutation introduced or gene silencing. Since the MLA_{CC} steady-state levels were decreased irrespective of the three tested mutant backgrounds (*sgt1b*, *rar1*, and *ndr1*), this decrease might result from transgene silencing rather than a specific alteration of the MLA_{CC} turnover in the three tested mutant backgrounds, including *rar1*. Measuring the MLA_{CC} transcript levels in the above-mentioned lines would be required to confirm the transgene silencing. Overall, this data suggests that *RAR1* is largely dispensable for MLA_{CC}-mediated cell death induction.

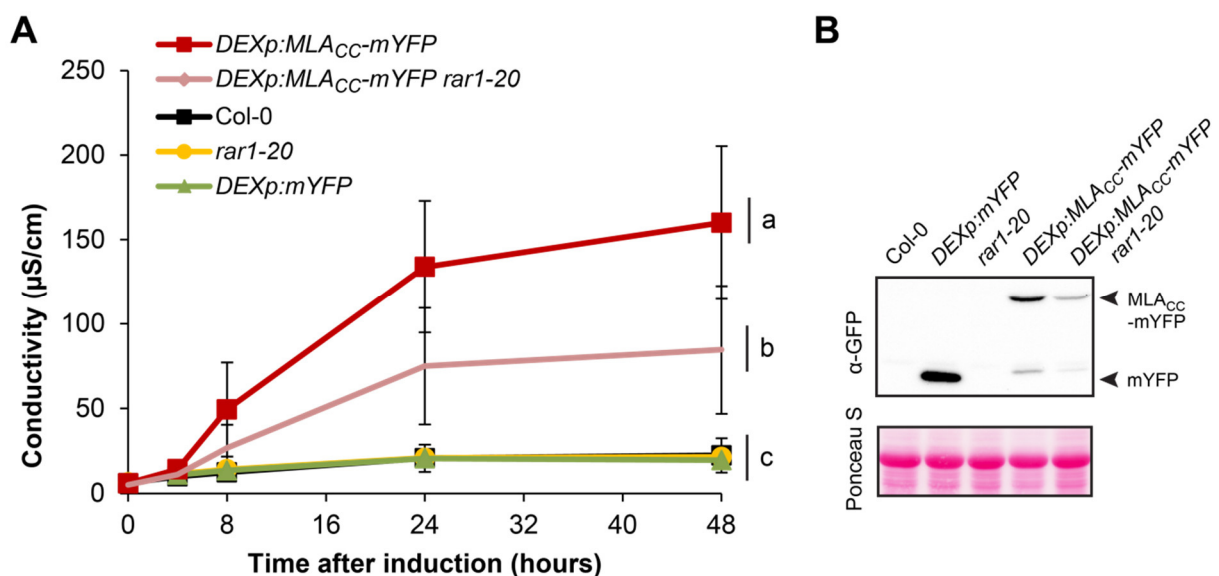


Figure 1-12: *RAR1* is dispensable for MLA_{CC} function. B, MLA_{CC} triggers cell death in *rar1-20*. Ion leakage was measured in leaf discs after immersion into 10 μM DEX + 0.001% Silwet L-77. Error bars indicate standard deviation from three independent experiments. The letters on the right side indicate statistical groups defined by one way Anova followed by posthoc Tukey HSD based on the p-value <0.001 and three biological replicates for each of the three independent experiments. C, Transgene expression was detected by immunoblotting for the lines shown in B. at 6 hours after induction. Equal sample loading was monitored by Ponceau S staining.

1.4.2. Robustness of MLA_{CC}-triggered responses in diverse environmental conditions

To gain further insight into the parameters or components required for MLA_{CC} function in *A. thaliana*, the effect of diverse environmental parameters were studied.

In this study, the standard plant growth substrate used *in vitro* was MS agar supplemented with a low sucrose concentration (0.5%). Sucrose not only represents a carbon source for the plant but also can act as a signalling molecule which can regulate defence responses (Moghaddam and Ende, 2012; Morkunas and Ratajczak, 2014). The effect of sucrose supply was studied. The growth of *DEXp:MLA_{CC}-mYFP* plants on MS agar medium supplemented with 0.5 or 2% sucrose and 0 or 30 μ M DEX was analysed. Sucrose concentration did not affect the MLA_{CC}-induced growth phenotype of plants on DEX-containing medium (Figure S1-9).

The effect of day length was also studied. *DEXp:MLA_{CC}-mYFP* plants were grown on MS agar medium containing 0 or 30 μ M DEX under a photoperiod of 8 or 16 h. The photoperiod did not affect the MLA_{CC}-induced growth phenotype (Figure S1-9).

The growth phenotype induced by constitutively active or overexpressed CNL SUMM2 and TNLs RPP4, RPS4, and SNC1 can be suppressed at elevated growth temperature (Heidrich et al., 2013; Huang et al., 2010; Ichimura et al., 2006; Yang and Hua, 2004). Experimental data supports a model where the plant prioritizes ETI at lower temperature (10~23°C) and PTI at higher temperature (23~32°C) (Cheng et al., 2013). Therefore, I examined whether ambient temperature can affect the MLA_{CC}-mediated growth phenotype. Towards this end, I generated stable *A. thaliana* transgenic lines expressing the MLA_{CC}-mYFP under the strong constitutive CaMV 35S promoter (*p35S:MLA_{CC}-mYFP*). The corresponding T₁ transgenics were grown under high temperature (28°C) and high humidity. I selected two independent T₂ progeny displaying detectable levels of MLA_{CC}-mYFP protein.

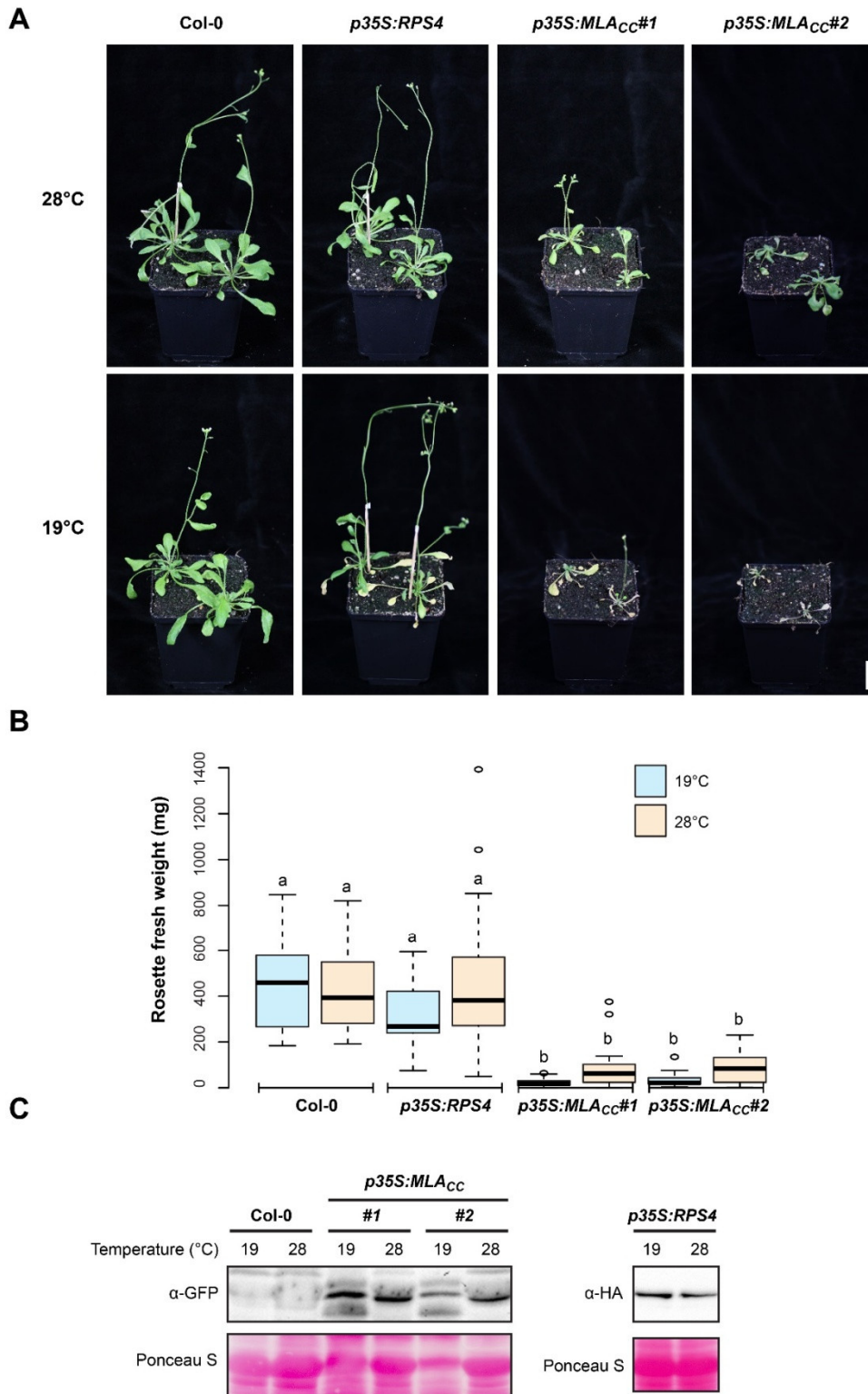


Figure 1-13: MLAcc-mediated growth phenotype is only partially temperature sensitive. Two independent lines expressing *p35S:MLAcc-mYFP* were initially grown for four weeks at 28°C before shifting them to 19°C. The analysis was performed one week after the shift. Wild-type Col-0 and *p35S:RPS4-HS* plants were used as controls. A, MLAcc expression induces dwarfism and temperature dependant leaf yellowing. Scale bar: 3 cm. B, rosette fresh weight reduction is observed for the *p35S:MLAcc-mYFP* plants at both temperatures. Fresh weight from at least 17 plants in each condition was represented on a boxplot. Dark horizontal lines represent the mean, with the box representing the 25th and 75th percentiles, the whiskers the 5th and 95th percentiles, and outliers represented by dots. Letters indicate significant differences (p -value<0.01) determined by one-way anova with post hoc Tukey HSD. C, Expression of the MLAcc-mYFP protein monitored by immunoblotting. Equal sample loading was monitored with Ponceau staining.

The T₂ progeny plants were grown for four weeks at 28°C under high humidity and transferred for one week at 19°C under high humidity. In this system, one week after the temperature shift, macroscopically visible growth phenotypes of the temperature-shifted plants were compared to those of plants grown continuously at 28°C. A dramatic MLA_{CC}-dependent growth impairment was observed at both temperatures (Figure 1-13.A, B), indicating that MLA_{CC}-induced responses are retained at 28°C and 19°C. However, the chlorosis symptoms were enhanced after the switch to lower temperature (Figure 1-13.A) suggesting a partial suppression of MLA_{CC}-mediated responses at higher temperature. The partial suppression at 28°C is not due to lower expression of the MLA_{CC}-mYFP as indicated by immunoblotting anti-GFP (Figure 1-13.C).

The phenotype is reminiscent of the temperature sensitivity reported for the NLRs cited above, even though RPS4-, SNC1- and RPP4-mediated growth phenotypes can all be completely suppressed at elevated temperature. In contrast, the phenotype dependent on SUMM2 activation is only partially suppressed at elevated temperature (Ichimura et al., 2006). This variation in temperature sensitivity of NLR responses might reflect a functional difference between CNLs and TNLs, although too few NLRs have been tested to generalize this hypothesis.

In conclusion, the three major defence phytohormones SA, ET, and JA (Results section 1.2.6), and the NLR and ETI regulatory component *RARI*, are largely dispensable for the MLA_{CC}-dependent HR-like response in *A. thaliana*. Additionally, this response seems largely unaffected by variations in several environmental parameters such as temperature, day length, or nutritional supply. Overall, these results indicate the existence of a robust and undescribed HR-like signalling mechanism activated by barley MLA_{CC}.

Chapter 2.

A genetic suppressor screen to unravel evolutionarily conserved signalling components required for the MLACC-triggered immune responses in *A. thaliana*

2.1. Introduction

In *Arabidopsis thaliana* (*A. thaliana*) transgenic lines, conditional expression of the coiled coil domain of barley MLA (MLACC) under a dexamethasone (DEX)-inducible promoter (*DEXp:MLACC-mYFP*) triggers effector-triggered immunity (ETI)-like responses upon DEX treatment (Chapter 1). Transgenic lines with a high MLACC steady state level after DEX treatment display a growth arrest when sown directly on DEX-containing medium (Figure 2-1).

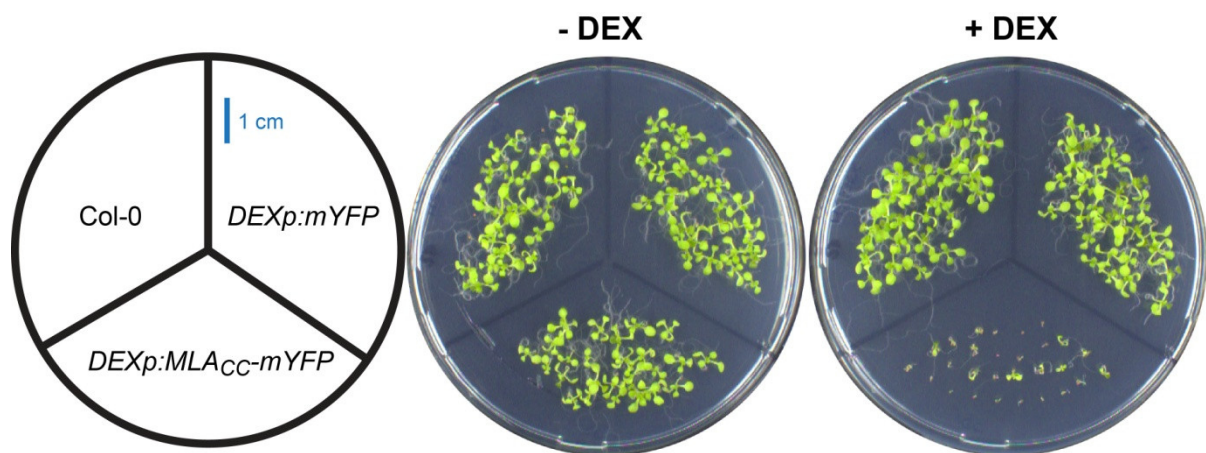


Figure 2-1: DEX-inducible expression of *MLACC-mYFP* leads to growth arrest. Wild-type *A. thaliana* Col-0, *DEXp:mYFP* and *DEXp:MLACC-mYFP* #1.5.1 plants were grown as indicated (left). The pictures were taken at 14 days after sowing on medium without DEX (- DEX, middle) or with 30 μ M DEX (+ DEX, right).

To identify genetic components required for MLACC function, I took advantage of this phenotype by conducting a forward genetic suppressor screen of the MLACC-induced growth arrest. A mutant population was generated by chemical mutagenesis of the *DEXp:MLACC-mYFP* transgenic line and screened for mutant candidates which do not display the MLACC-dependent growth arrest. The phenotype of the identified candidates was further analysed using additional assays (here called secondary and parallel screens) and confirmed by growth assay on DEX-containing medium using the corresponding progeny. Subsequently, whole-genome sequencing of individual mutants was performed to identify the causal mutation(s) (Figure 2-2).

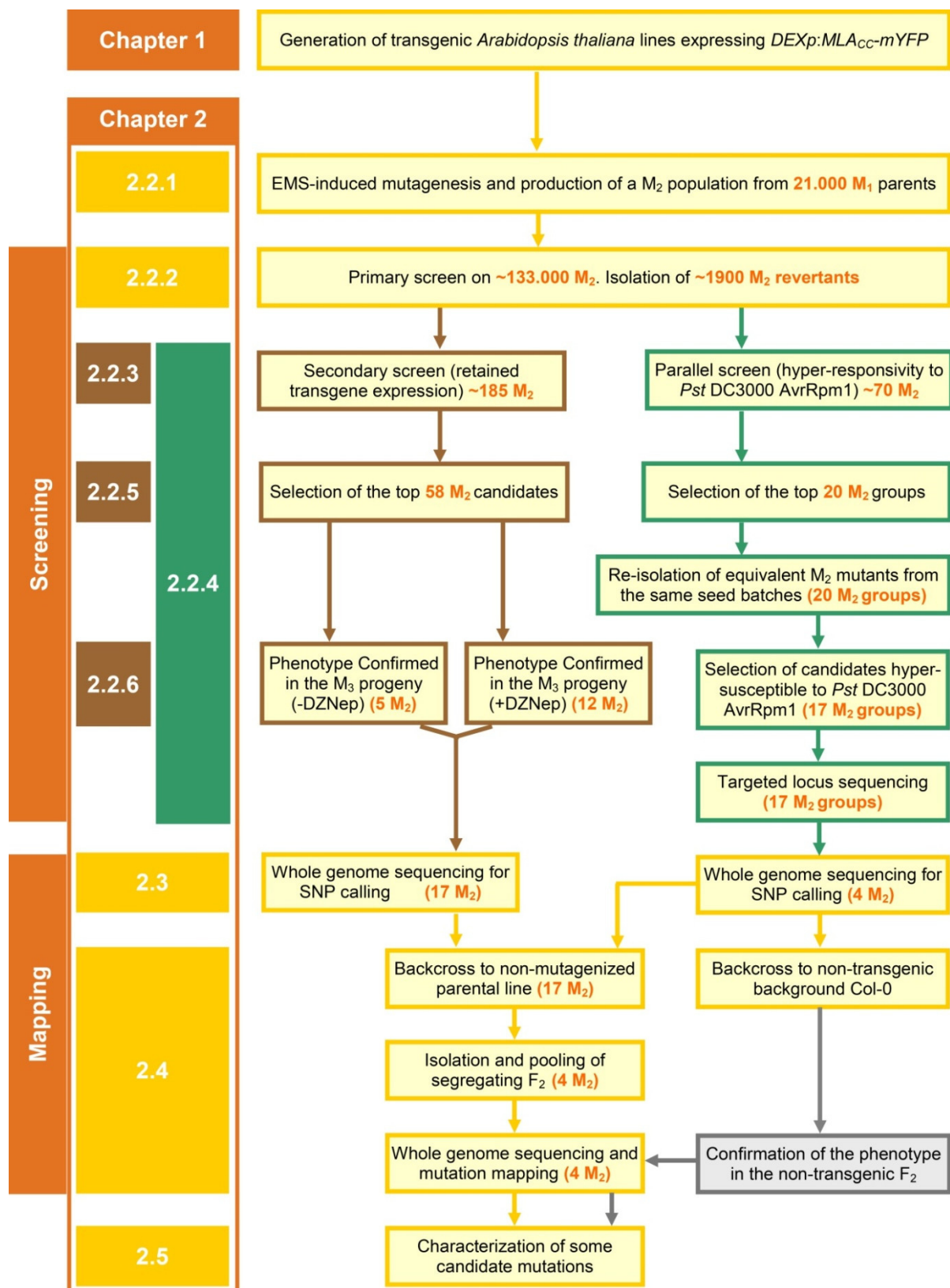


Figure 2-2: Flowchart of the genetic suppressor screen for MLAcc-dependent growth arrest. The sections of Chapter 2 corresponding to the different steps are indicated to the left side of the flowchart. Generic steps performed for all candidates are indicated with yellow boxes and arrows whereas brown and green colors identify two independent screening pathways. Grey color indicates steps that have not been performed yet. EMS, ethyl methanesulfonate. *Pst*, *Pseudomonas syringae* pv. *tomato*. DZNep, 3-Deazaneplanocin A. SNP, single nucleotide polymorphism.

The screening procedure includes several advantageous features. A genetic mutant screen could be unsuccessful when functionally redundant components are involved in the pathway of interest. Such a feature may apply to NLR-mediated signalling pathway(s) given that the previous mutant screens failed to identify downstream components (see below). However, the barley MLA_{CC} expressed in a heterologous system such as *A. thaliana* might recruit fewer signalling components, such as the subset of signalling components conserved between barley and *A. thaliana*. This potentially increases the probability to identify evolutionarily conserved signalling components by forward genetic screens.

Previous genetic screens for suppressors of the response mediated by full-length NLRs preferentially identified components regulating NLR pre-activation/activation/folding (e.g. chaperonins and co-chaperonins such as SGT1b, RAR1 and HSP90) (Bao et al., 2014; Parker et al., 1996; Shirasu et al., 1999; Yu et al., 1998). Since the autoactive MLA_{CC} module is autonomously structured, it unlikely requires (co-)chaperonins for its folding and stabilization (Maekawa et al., 2011b). Therefore, my screen might preferentially identify downstream signalling components for MLA.

False positive mutants can occur from the lack of MLA_{CC} expression which can result from intragenic mutations or transgene silencing. Multiple tandem copies of the *DEXp:MLA_{CC}-mYFP* construct in the genome of the transgenic line prevents the unfavorable recovery of false positives since the likelihood of mutations impairing all the copies at the same time is very low. In addition, the mYFP translational fusion to the MLA_{CC} allows direct and high-throughput monitoring of the MLA_{CC} steady state level under a fluorescence microscope. Many false positives resulting from a loss of transgene expression were indeed efficiently identified by this mean.

2.2. The screening procedure: from primary screening to confirmed candidate suppressors

2.2.1. Mutagenesis and generation of the M₂ seed batches

The homozygous *DEXp:MLA_{CC}-mYFP* transgenic line #1.5.1 (T₃ generation) exhibits a severe growth retardation on DEX-containing medium (Figure 2-1). Three T₄ sister progeny derived from the *DEXp:MLA_{CC}-mYFP* line #1.5.1, designated as FJM1, FJM2 and FJM3, together

totalizing ~25,000 seeds, were mutagenized by treatment with ethyl methanesulfonate (EMS) which typically induces G→A and C→T random transitions in the genomic DNA. The first generation after mutagenesis (M_1) was self-fertilized to produce the M_2 . In *A. thaliana*, recessive EMS-induced mutants segregate in a 7:1 ratio in the M_2 population (Page and Grossniklaus, 2002). Approximately 21,000 M_1 individuals completed their life cycle after mutagenesis. The M_2 progeny were collected either individually (1,409 seed batches containing single progeny of the FJM1 M_1 plants) or in mini pools of ~15 progeny (584 and 690 seed batches containing pooled progeny of the FJM2 and the FJM3 M_1 plants respectively). This pooling strategy offers the advantage that, even if certain M_2 progeny undergo silencing of the transgene, only a limited number of pools are affected and can be removed from the analysis. In addition, my pooling strategy allows re-isolating mutant candidates of interest in the same generation from the respective seed batch when progeny are collected individually. The nomenclature for the plant generations used in the screen is summarized in Figure 2-3.

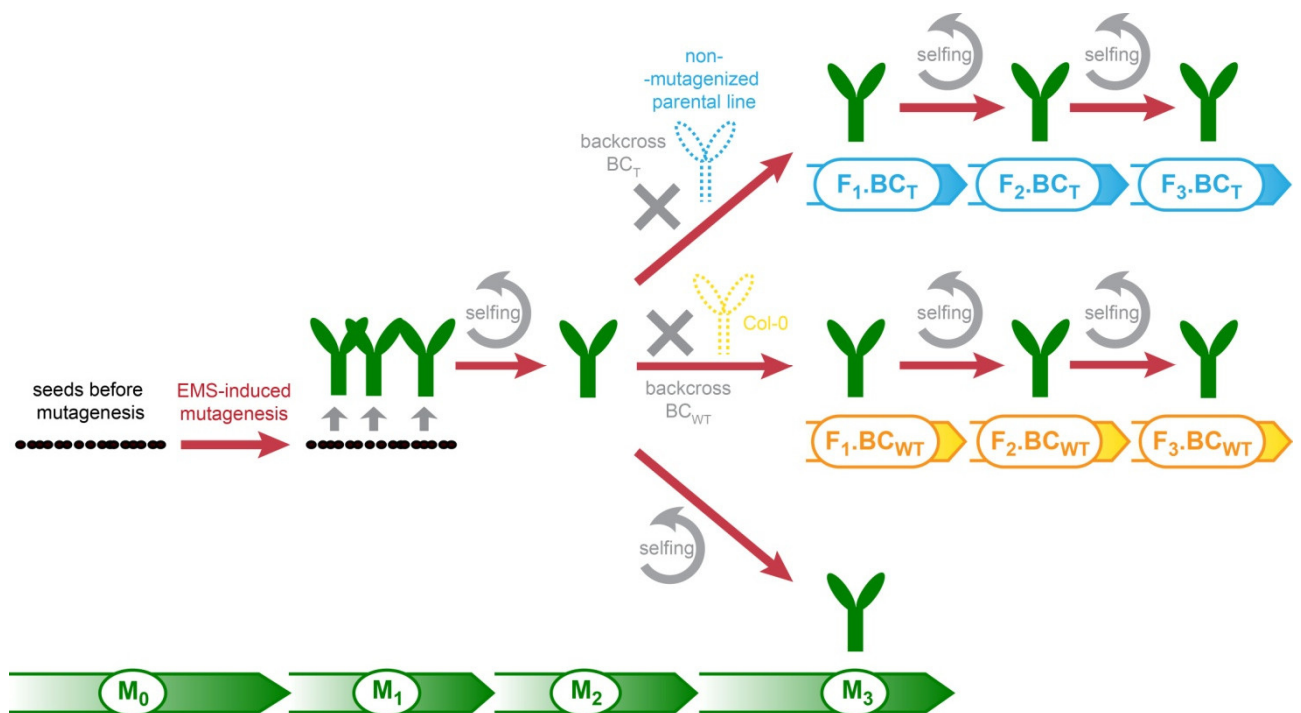


Figure 2-3: Nomenclature used in this chapter to identify each analysed generation and lineage. Identification names were assigned to the distinct plant populations analysed in this chapter (labels below the flowchart branches). The starting mutagenized population (M_1) was self-fertilized to produce the population used for the primary and secondary screenings (M_2). Distinct plant lines obtained by self-fertilization (selfing) of the M_2 individuals or by back-crossing of the M_2 individuals to either wild-type Col-0 (BC_{WT}) or to the non-mutagenized parental transgenic lines *DEXp:MLA_{CC}-mYFP* #1.5.1 (BC_T) were used for subsequent validation and mapping of the candidate mutants identified.

2.2.2. Primary suppressor screening of the M₂ population

2.2.2.1. Primary screening on MS plates

To identify mutations suppressing the MLA_{CC}-mediated growth arrest, I screened the EMS-induced M₂ mutant population on DEX-containing agar plates as described in Section 2.2.1. Approximately 1,100 M₂ plants showing a loss of MLA_{CC}-dependent growth retardation were isolated out of ~100,000 M₂ individuals (examples of M₂ suppressor mutants shown in Figure S2-1).

2.2.2.2. Primary screening on soil

I also examined whether the growth arrest is observed when seeds of the *DEXp:MLA_{CC}-mYFP* line are sown on soil. The transgenic seeds coated with DEX-containing agar (0.01% agar + 30 μM DEX) were directly sown on soil, and the seedlings were sprayed with DEX solution (30 μM DEX + 0.01% Silwet L-77) at five and seven days post germination (dpg).

A pilot experiment was conducted to analyse the growth phenotype of wild-type Col-0, *DEXp:mYFP*, and *DEXp:MLA_{CC}-mYFP* plants on soil along with plants from ten independent M₂ batches (Figure S2-2). At 10 dpg, wild-type Col-0 and *DEXp:mYFP* plants showed a germination rate of nearly 100% whereas those of the *DEXp:MLA_{CC}-mYFP* line was reduced to 0%. Three candidate suppressor mutants showing a loss of MLA_{CC}-dependent growth retardation were identified from the tested M₂ seeds. The frequency of mutant recovery is similar to that of the screen conducted on MS agar plates. I employed this technique to further screen 690 seed batches of the FJM3 M₂ progeny. Approximately 800 M₂ suppressor mutants were isolated by this mean out of ~34,000 M₂ individuals screened.

2.2.3. Secondary screening of the ~1,900 primary M₂ suppressor mutants

M₂ plants might show a suppressor phenotype due to the loss of MLA_{CC}-mYFP expression. To eliminate such plants, I systematically examined MLA_{CC}-mYFP protein accumulation in the ~1,900 suppressor candidates using fluorescence microscopy. The vast majority of mutant candidates exhibited a level of YFP signal lower than the parental lines. This indicates that the transgene expression decreased over two generations. Approximately 10% of the suppressor mutants (184) retained a level of YFP signal comparable to the parental lines.

2.2.4. Parallel screening of the ~1,900 M₂ suppressor candidates for hyper-responsivity to *Pst* DC3000 AvrRpm1

The resistance protein RPM1 (RESISTANCE TO *P. SYRINGAE* PV. *MACULICOLA* 1) confers resistance to *Pseudomonas syringae* pv. *tomato* (*Pst*) DC3000 AvrRpm1 by indirect recognition of AvrRpm1 effector in *A. thaliana* (Mackey et al., 2002). Like MLA, RPM1 belongs to the CNL type of NLRs which is characterized by an N-terminal CC domain as opposed to the NLRs with a N-terminal TIR domain (TNLs). Notably, RPM1 CC domain shares a high structural similarity with MLA_{CC} (Maekawa et al., 2011b). To test whether RPM1-mediated disease resistance is compromised in the candidate mutants, ~1900 M₂ candidate mutants were spray-inoculated with *Pst* DC3000 carrying AvrRpm1. Approximately 70 M₂ suppressor candidates, originating from 57 independent seed batches, displayed enhanced macroscopic symptoms, indicative of hyper-responsiveness to *Pst* DC3000 AvrRpm1 (examples shown in Figure 2-4). Out of these 57 independent groups (a group refers to plants originating from a single M₂ seed batch), I selected 20 groups for further characterization based on the symptoms severity and the phenotypic data obtained in the secondary screen (Section 2.2.3). Hyper-responsive candidates failed to produce seeds after spray with *Pst* DC3000 AvrRpm1. Therefore, I re-isolated candidate suppressors from the same seed batches (101 individuals from 20 groups). Although the re-isolated candidates might not carry identical mutations than the mutants previously isolated, such event is rather unlikely since the candidates were re-isolated from the same seed batch and showed the same phenotype.



Figure 2-4: Examples of M₂ candidates displaying enhanced symptoms after inoculation with *Pst* DC3000 AvrRpm1. Pictures were taken before (0 dpi) and 6 days after spray-inoculation (6 dpi). A representative subset of the candidates is shown here as an example. Scale bar=2 cm

To clarify if the hyper-responsiveness is a consequence of hyper-susceptibility to the pathogen, the susceptibility of these 101 candidates to *Pst* DC3000 AvrRpm1 was quantitatively assayed by dipping detached leaf into a solution containing *Pst* DC3000 AvrRpm1 followed by quantification of the bacterial density two days after dipping. Seventeen independent groups showed enhanced susceptibility to *Pst* DC3000 AvrRpm1 (data not shown). I extracted the gDNA from 25 hyper-susceptible candidates (1-3 individuals for each of the 17 hyper-susceptible groups) and sequentially sequenced the three major loci previously shown to be required for RPM1-mediated resistance to *Pst* DC3000 AvrRpm1 (Bisgrove et al., 1994; Century et al., 1995; Tornero et al., 2002a), namely *RPM1*, *RAR1* and *NDRI*. Three independent mutations were identified in the *RPM1* locus (resulting in G9R, L344F and R519K substitutions) in three groups out of the 17 tested and no mutations were found in the *RAR1* or *NDRI* loci. Since the three mutations in the *RPM1* locus correlate with the hyper-susceptibility of the plants to *Pst* DC3000 AvrRpm1, these mutations most likely affect RPM1 function. The L344F substitution was reported as a loss of function mutation (Tornero et al., 2002b), whereas the G9R and the R519K mutations have not yet been described. Both residues 344 and 519 are located in the NB-ARC domain whereas residue 9 is located in the CC domain (Figure 2-5).

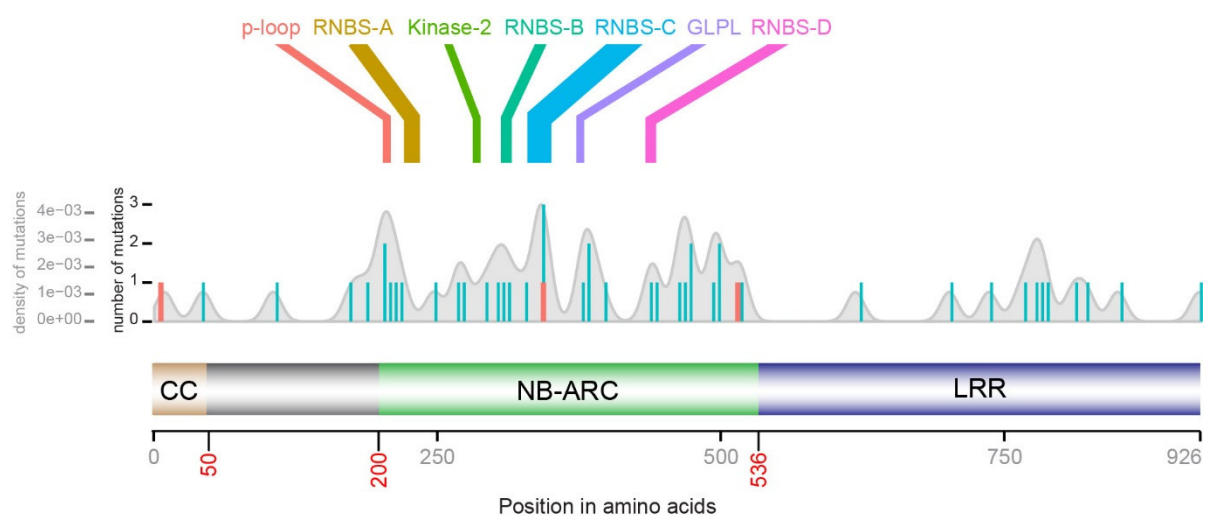


Figure 2-5: Position of the confirmed and putative loss of function mutations identified in RPM1. The density graph (grey) indicates the density of mutations identified by Tornero et al. (2002) and Grant et al. (1995). The turquoise bars on the density graph represent the number of previously identified mutations on a sliding window of 5 amino acids. The orange bars indicate the position of the mutations identified in this study. Above the graph: position of the conserved motifs in the NB-ARC domain. Below the graph: RPM1 domain structure.

Based on the above analysis, I selected for further analysis six mutant groups which exhibited the highest susceptibility to *Pst* DC3000 AvrRpm1 and carry no mutation in *RPM1*, *RARI* and *NDR1* loci. A single M₂ individual was chosen as representative of each group (FJM2.552.3b, FJM2.586.1b, FJM3.109.1b, FJM3.125.3b, FJM3.683.2b, FJM3.686.1b).

2.2.5. Integration of the different screening data and selection of 58 candidates for further characterization

Since a large number of candidate suppressors was identified by the primary and secondary screens, I decided to rank the ~1,900 candidate suppressors according to a global score (S_G) which integrates the different assayed phenotypic characteristics. These characteristics include the transgene expression level, the microscopic phenotype, the hyper-responsivity to *Pst* DC3000 AvrRpm1, and the frequency of the mutant phenotype in the M₂ mini pool/progeny. The S_G calculation method is described in Table 2-1. The ranking method chosen strongly disfavors potential false positives resulting from transgene silencing over all other characteristics. After evaluation of the score distribution among the suppressor candidates (Figure S2-3), I chose a cut-off score of 3.5, which places 131 candidates (~7%) above this cut-off. However, this number of candidates has further decreased to 58 candidates (~3%), since gDNA samples and/or M₃ seed progeny were not available for several candidates among the 131 selected.

Table 2-1: Calculation method for the candidate mutant score

Score for transgene expression level = S_T	
+	+1
++	+2
+++	+3
++++	+4
Score for microscopic phenotypes = S_M	
Change in MLACC-mYFP subcellular localization	+0.5
Autofluorescence +	-0.25
Autofluorescence ++	-0.5
Autofluorescence +++	-0.75
No autofluorescence and transgene expression > ++	+0.5
Score for hyper-responsivity to Pst DC3000 AvrRpm1= S_P	
Hyper-responsivity (+)	+0.25
Hyper-responsivity +	+0.5
Hyper-responsivity ++	+1
Score for mutant phenotype frequency = S_F	
Number (n) of candidates isolated from the same batch	+0.5 x n
Global Score = S_G	
$S_G = S_T + S_M + S_P + S_F$	

2.2.6. Validation of the 58 mutant candidates by analysis of their M_3 progeny phenotype

Phenotypic suppression resulting from a homozygous mutation at a single recessive locus in an M_2 candidate implies that the suppressor phenotype is transmitted to 100% of its progeny. To determine whether the 58 M_2 candidates carry a single recessive causal mutation, the respective progeny produced by self-fertilization, termed M_3 (Figure 2-3), were screened according to the same procedures used for the primary and secondary screens. Progeny derived from 35 M_2 candidates (60.3%) were able to grow on DEX-containing medium whereas the 23 other were not. Out of these 35 progeny, 5 (progeny of M_2 candidates FJM1.1083.3, FJM2.354.1, FJM2.131.1, FJM3.682.1, and FJM3.137.2) exhibited reduced but still detectable transgene expression (at least 20 % of YFP-positive cells in average).

These results indicate that the mutant phenotype of five candidates was confirmed in the M_3 generation. Therefore these five candidates were chosen for further characterization and were named 1A, 1B, 1C, 1D and 1E, respectively (Table 2-2).

Apart from the five candidates expressing the transgene up to their M₃ progeny, progeny of 30 M₂ candidates displayed a marked loss of MLACC expression likely due to the transgene silencing. However, it is possible that some of them carry mutations responsible for the suppressor phenotype. I thought that some more mutants could be confirmed if re-analysed under conditions where the transgene expression is re-activated. Thus I tested two chemical inhibitors, 3-Deazaneplanocin A (DZNep) and zebularine (Zeb) that are known to restore silenced gene expression by inhibiting histone and cytosine methylation, respectively (Baubec et al., 2009, 2010; Miranda et al., 2009).

Table 2-2: Description of the 21 M₂ mutant candidates selected for characterization

Original candidate ID	ID after validation	Phenotype
FJM1.1083.3	1A	
FJM2.354.1	1B	
FJM2.131.1	1C	• Suppressor phenotype and transgene expression retained in the M ₃ progeny
FJM3.682.1	1D	
FJM3.137.2	1E	
FJM3.251.3	2A	
FJM3.666.1	2B	
FJM3.208.2	2C	
FJM1.96.2b	2D	
FJM1.1405.2	2E	• Suppressor phenotype confirmed in the M ₃ progeny
FJM2.24.1	2F	• Reduced transgene expression
FJM2.552.1**	2G	
FJM2.586.1**	2H	• Suppressor phenotype retained in the presence of DZNep
FJM2.476.2#	2I	
FJM3.182.2	2J	
FJM3.671.3	2K	
FJM3.454.1	2L	
FJM3.109.1b	3A	
FJM3.125.3b	3B	• Hyper-susceptibility to <i>Pst</i> DC3000 AvrRpm1
FJM3.683.2b	3C	
FJM3.686.1b	3D	

*Putative hyper-susceptibility to *Pst* DC3000 AvrRpm1. The mutant displays enhanced disease symptoms upon *Pst* DC3000 AvrRpm1 inoculation

#Hyper-susceptibility was observed in at least one mutant isolated from the same M₁ seed batch.

As a pilot experiment, I tested whether either chemicals could restore the expression of the transgene in a sister line (FJM5) of the line used for mutagenesis (FJM1/2/3). In the FJM5 line, the MLACC transgene expression was strongly reduced compared to the parent, likely due to transgene silencing. I used the MLACC-induced growth arrest as an indication for restored MLACC expression. As shown in Figure S2-4, application of 2 μ M DZNep restored a growth arrest similar to that of the non-silenced FJM3 line, whilst 10 μ M Zeb had weak effects. Importantly, both 2 μ M DZNep and 10 μ M Zeb had minor effects on the plant growth in absence of DEX. Therefore only DZNep appears to efficiently reactivate the transgene expression under the tested conditions.

I examined the phenotype of the 58 M₃ progeny on plates containing both 10 μ M DEX and 2 μ M DZNep at 13-14 dpg. A partial suppression of the phenotype was observed for 13 progeny although the frequency of phenotype suppression in all M₃ progeny was below 100% (ranging from 46% to 83%). The combined application of DEX and DZNep might possibly have an additive negative effect on plant growth in some of the M₃ progeny. Twelve progeny exhibited a suppressor phenotype on both media containing either DEX alone or DEX and DZNep together. Therefore, I selected these 12 candidates for further characterization and named them 2A, 2B, 2C ..., and 2L, respectively (Table 2-2).

2.3. Preliminary mutation mapping based on the whole genome sequences of the M₂ mutant population

2.3.1. Introduction

Due to the rapid development of the next generation sequencing technologies, genome sequencing has become a standard approach to identify mutations in forward genetic screens. Such genome re-sequencing-based approaches are collectively named “mapping by sequencing” (Abe et al., 2012; Schneeberger et al., 2009). These can be easily applied to *A. thaliana* Col-0 due to its high quality reference genome. Classical mapping by sequencing relies on bulk segregant analysis which usually requires a F₂ population, which is obtained by crossing a mutant with a wild-type. Such mapping population is necessary to enrich the causal mutation over the other background mutations (e.g. other EMS-induced mutations). Indeed, direct sequencing of a mutant obtained by random mutagenesis will likely reveal a complex profile of sequence changes that does not allow direct mapping of the causal mutation. So far,

such direct mapping approach has been employed in *C. elegans* and but lead only to the identification of a relatively narrow candidate interval (Sarin et al., 2008).

I aimed at identifying the causal mutations in the M₂ candidates by analyzing their genome-wide SNP profile. Two independent approaches were undertaken in parallel: i) a targeted analysis of 377 loci known to be required for, or associated with, resistance gene-mediated immune responses and ii) an untargeted approach to identify allelic mutations present in multiple mutant candidates. The latter strategy consists in detecting loci whose mutation frequency is significantly higher than expected under a random distribution in the mutant candidate population. At the time I initiated this project, there was no published report regarding the latter strategy even though it had been already conceptually proposed by Schneeberger and Weigel (Schneeberger and Weigel, 2011). At the time this thesis is written, the concept has been implemented successfully by at least two groups (Nordström et al., 2013, JD. Jones, personal communication).

2.3.2. Determination of the SNP profile of 21 M₂ candidates using whole genome resequencing

To identify causal mutations in the selected M₂ candidates, SNP mapping was performed using whole genome sequencing. This approach was applied to 17 M₂ candidates identified from the screening for the loss of MLACC-induced growth arrest and to four mutants hyper-susceptible to *Pst* DC3000 AvrRpm1 (FJM3.109.1b, FJM3.125.3b, FJM3.683.2b and FJM3.686.1b) (Results section 2.2.4). The latter four lines were named 3A, 3B, 3C and 3D respectively (Table 2-2). Out of the six hyper-susceptible candidates originally selected, two (FJM2.552.3b and FJM2.586.1b) were not included for the analysis since they were likely redundant with the candidates 2G and 2H which were isolated from the same seed batch and displayed similar phenotypes. Additionally, one non-candidate M₂ individual (FJM2.52.1) was sequenced as a control.

The overall number of homozygous SNPs was relatively similar among the mutant candidates and in the control (only candidate 1D falls out the 95% confidence interval [954, 1837] calculated from mean \pm 1.96 x standard deviation) (Figure 2-6). This suggests that the EMS-induced mutation rate was uniform in the initial M₀ individuals. There was no correlation between the SNP discovery rate and the sequencing depth indicating that the sequencing depth was sufficient for saturating SNP identification (data not shown).

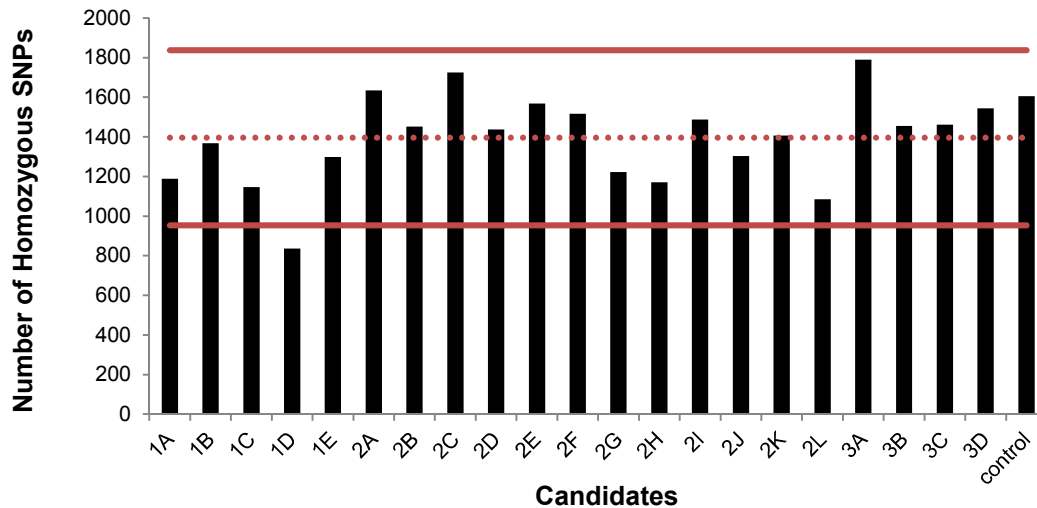


Figure 2-6: Number of homozygous SNPs identified in each of the 22 M₂ plants. The red plain lines indicate the limits of the 95% confidence interval [954, 837] calculated from mean $\pm 1.96 \times$ standard deviation, and the dotted red line the mean.

I focused on the homozygous SNPs which potentially have a significant impact on the protein function (e.g. non synonymous SNP and non-sense mutation).

However, since the SNP-calling pipeline relies on the published reference Col-0 genome information, it also detects SNPs which exist in the used parental lines prior to the mutagenesis (i.e. due to natural variation in Col-0 ecotype). In addition, the pipeline was also affected by mis-aligned reads and reference genome errors. Thus, I conducted a semi-manual curation of the SNPs: each locus presenting at least three independent SNPs was manually inspected in the IGV Browser. Out of the 262 loci inspected, 41 loci appear to harbor homozygous SNPs independent of the background noise. The 221 loci carrying background SNPs were removed from the subsequent analysis (Figure 2-7.A). Comparison of the SNPs before and after curation indicates that the curation results in a marked enrichment for typical EMS-induced SNPs (Figure 2-7.B). As expected, most of the background SNPs are clustered at chromosomal regions where the mapping quality is low such as centromeric regions enriched with repeated sequences (Figure 2-7.C).

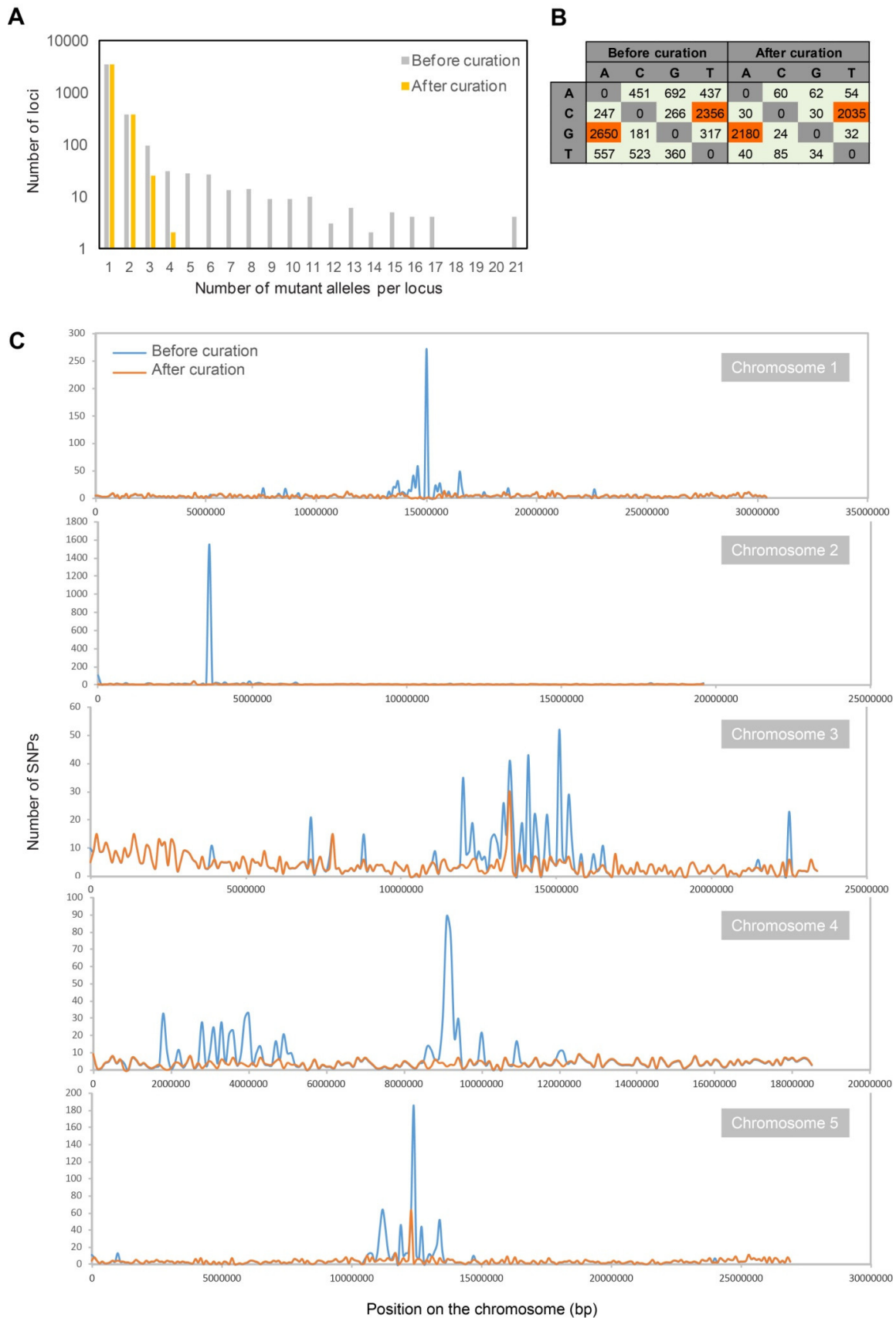
Chapter 2. A genetic suppressor screen [...] for the ML_{Acc}-triggered immune responses

Figure 2-7: Overall SNP analysis before and after curation for background SNPs. **A**, Distribution of the number of alleles identified per locus. **B**, Distribution of the type of substitutions. G→A and C→T are the substitutions typically induced by EMS (highlighted in orange). **C**, Distribution of the SNPs per window of 100,000 bp on the five *A. thaliana* chromosomes.

Table 2-3: Analysis of the SNPs number and their effects in the 21 M₂ candidate mutants

	Total number/percentage	Average per individual
Homozygous SNPs in gene body	4622	220.1
Total Effects	8708	414.7
INTRAGENIC	0.9%	3.6
INTRON	29.0%	120.4
NON_SYNONYMOUS_CODING	57.1%	236.8
SPLICE_SITE_ACCEPTOR	0.9%	3.8
SPLICE_SITE_DONOR	0.5%	2.1
SPLICE_SITE_REGION	3.4%	14.0
START_GAINED	0.3%	1.2
START_LOST	0.02%	0.1
STOP_GAINED	2.9%	12.0
STOP_LOST	0.2%	0.7
UTR_3_PRIME	2.7%	11.3
UTR_5_PRIME	2.1%	8.8

Overall, this data indicates that the curation was able to efficiently remove a large number of background SNPs. Additional details about the number of SNPs identified and their predicted effects is summarized in Table 2-3. I used this SNP information to look for causal mutations as described in the two following sections.

2.3.3. Targeted analysis of prospective suppressor loci

Using the aforementioned SNP information, I first investigated 377 loci that are known or supposed to be involved in plant immunity or cell death response. These loci are categorized in four classes: 61 loci required for R-gene function, 113 loci encoding transcription factors (TFs) potentially involved in R-gene-mediated transcriptional reprogramming, all CNL-encoding loci (57) and all TNL-encoding loci (146) (Table S2-1). Information for presence/absence (translated as 1/0) of SNPs in these loci was retrieved using a bioinformatics pipeline from the curated SNPs list for each candidate mutant. In order to confirm the presence/absence of SNPs at the 61 loci required for R-gene function, each locus was manually inspected with the IGV Browser, based on the information from uniquely mapped reads. For the insufficiently covered loci, I used information from non-uniquely mapped reads. This verification is necessary for genes belonging to multigenic families such as the HSP90 family.

Among the loci required for R gene function, I found two alleles for *SGT1a* (both are low impact SNPs: one at the 5'-UTR and one intronic), two alleles for *PAD4* (one at the 5'-UTR and one nonsense mutation), one allele for *SGT1b* (resulting in E121K substitution), one allele for *SID2* (intronic mutation), and one allele for *NPR4* (resulting in A434T substitution). The E121K substitution in *SGT1b* induces a charge exchange at a conserved amino acid. The A434T substitution in *NPR4* results in the exchange of a conserved hydrophobic amino acid by a polar amino acid at the NPR1/NIM1-like, C-terminal domain. Even though both mutations affect conserved residues, their impact on *SGT1b* and *NPR4* function cannot be predicted with high confidence, and mutations at these positions have not been previously reported. Since the MLACC-mediated growth retardation is detectable in a *sgt1b* mutant background and MLACC-induced responses are not fully suppressed by the loss of SA-mediated signalling (Chapter 1, Figures S1-3 and 1-13), *SGT1b* and *NPR4* are likely dispensable for the MLACC functions.

Regarding the loci belonging to the TF and NLR classes, the highest number of mutant alleles was three, which was found in the TF-encoding locus *bZIP69*. However, the three SNPs had presumably a low impact as they occur either in introns or at the 5'-UTR (Table S2-2.B).

In conclusion, the absence of significant allelic mutations in the candidate genes suggests that the suppressor mutations of the MLACC-mediated growth arrest might be located at loci that have not yet been implicated in NLR signalling or plant disease resistance.

2.3.4. Genome-wide analysis of the mutant allele frequencies

I hypothesized that my mutant collection might contain allelic mutants, each harboring mutations within the same locus. Thus, I examined the number of allelic mutations in the 21 genomes of the mutant candidates. The SNP-calling found two loci with four alleles, 25 loci with three alleles, 382 loci with two alleles and ~4,000 loci with one allele only (Figure 2-7.A). I focused on the loci with an allele frequency of three or four (Table S2-2.B). None of these loci has been implicated in R-gene functions. Noteworthy, the occurrence of four allelic mutations in a given locus out of 21 genomes is not statistically different from what can occur under a random SNP distribution (p -value=0.574). Therefore I could not infer whether these loci with a higher allele frequency carry the causal mutations.

2.4. Mapping of the causal mutations by classical “mapping by sequencing”

2.4.1. Generation and analysis of the segregating F₂ populations

Since the sequence analysis of the 21 M₂ candidates did not identify unequivocally the causal mutations, a bulk segregant mapping strategy was envisaged. For this, I backcrossed the mutant candidates to the non-mutagenized transgenic parental line. The resulting F₁ population, termed F₁.BC_T, was self-fertilized to produce the F₂.BC_T segregating population (Figure 2-2). The phenotype of the F₂.BC_T populations was analysed to confirm the 3:1 segregation ratio expected for a single recessive mutation and to isolate suppressor mutants for mapping. I obtained F₁.BC_T populations for 16 out of 21 candidates. Crossing between mutant and parental line was validated by genotyping based on SNP markers identified in the M₂ whole genome re-sequencing data. F₁.BC_T plants were not obtained for candidates 3A, 3C, and 3D. For candidates 3A and 3D, F₂.BC_{WT} populations were obtained instead, which can be used for mapping based on the susceptibility phenotype to *Pst* DC3000 AvrRpm1.

I found that the transgene expression in the F₂.BC_T plants was generally weaker compared to the parental non-mutagenized line. One possible explanation is that the non-silenced transgenic epiallele could be trans-inactivated via a dominant epigenetic silencing effect from its silenced sister allele, a phenomenon also termed paramutation (Matzke and Mosher, 2014; Pecinka et al., 2013).

The phenotype of 25 F₂.BC_T from six independent candidate mutants was analysed on DEX-containing agar plates (Figure S2-5). The majority of F₂.BC_T (23/25 F₂.BC_T) were affected by transgene silencing. However, two F₂.BC_T progeny from candidate 1E displayed a segregation ratio close to 3:1 as expected for a single recessive mutation.

Analysis of the other F₂.BC_T populations was conducted on growth medium containing both DEX and DZNep as described in Results section 2.2.6. These included 69 F₂.BC_T progeny from 16 candidates (n>100, Figure 2-8). The phenotype was rather variable among sister progeny. This, together with the gradient of growth observed, rendered the segregation analysis difficult. Overall, 25 progeny related to candidates 1A, 1B, 1D, 1E, 2A, 2B, 2E, 2H, 2J and 3B displayed a segregation ratio close to 3:1. Thus, the latter F₂.BC_T progeny are suitable to isolate positive segregant bulks for mapping. Each individual among a given positive segregant bulk should carry the identical homozygous causal mutation. To isolate F₂.BC_T individuals carrying the homozygous causal mutation, I selected among the progeny

Chapter 2. A genetic suppressor screen [...] for the MLACC-triggered immune responses

the individuals exhibiting both loss of MLACC-dependent growth retardation, and microscopically detectable mYFP signal (minimum 40% of fluorescent epidermal cells). This additional criterion was chosen to limit unfavorable recovery of false positives due to the transgene silencing. The three progeny 1E F₂.BC_T_3, 2B F₂.BC_T_2 and 2H F₂.BC_T_2 displayed a YFP signal above the threshold at frequency 63%, 34%, and 18%, respectively. The genomic DNA of 46, 49 and 35 positive F₂.BC_T individuals were isolated for 1E, 2B and 2H respectively. These were pooled together and used for the subsequent mapping.

In addition to the above three F₂.BC_T, the segregation phenotype of candidate 1A was clear and consistent in two independent F₂.BC_T progeny (F₂.BC_T_2 and F₂.BC_T_3) (Figure 2-8, Figure S2-5). Although no clear YFP signal was detected, I decided to analyse a bulk of 65 F₂.BC_T suppressor mutants from this candidate.

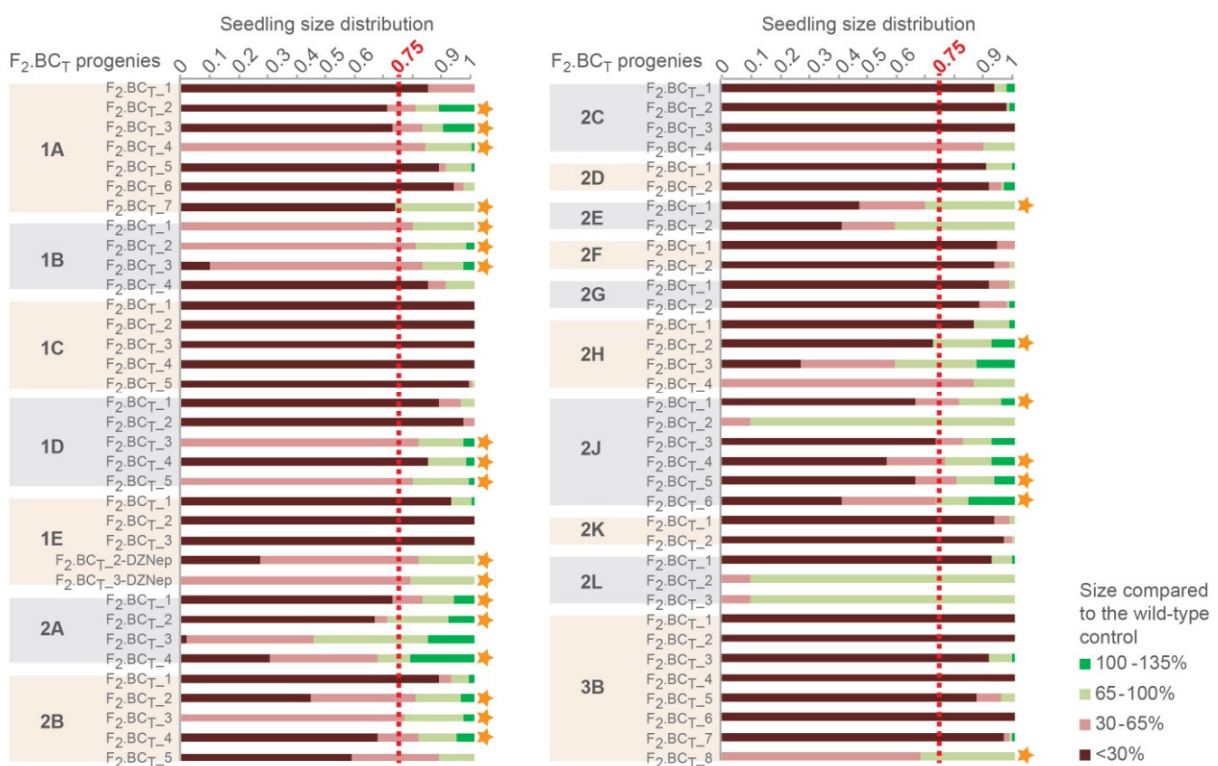


Figure 2-8: Segregation ratio of the F₂.BC_T progeny of the candidate mutants. F₂.BC_T progeny were grown for 14-16 days on medium containing 10 μM DEX and 2 μM DZNep unless otherwise mentioned in the x-axis label and the phenotypic segregation determined based on the seedling size with respect to the wild-type control *DEXp:mYFP* or Col-0 grown under the same conditions (n > 100). Orange stars indicate F₂.BC_T progeny with a segregation close to 3:1 (75% non-revertants, indicated by a red dashed line) as expected for a single recessive mutation.

2.4.2. Mapping by sequencing applied to candidates 1A, 1E, 2B and 2H

The positive segregant bulk gDNA obtained from the candidates 1A, 1E, 2B, or 2H was sequenced. The sequence data was used to evaluate the SNP frequency in the segregant bulks. Surprisingly, no EMS-induced mutation was found in the 1E segregant bulk, indicating that this population was the product of self-fertilization of the non-mutagenized parental line used for crossing, although genotyping of the respective F_1 .BC_T indicated successful crossing. Possibly, a partially penetrant transgene silencing resulted in a 3:1 segregation ratio in the F_2 .BC_T of candidate 1E. Thus, the sequence data from candidate 1E was excluded from the subsequent analysis.

The SNP profiles in the segregant bulk of candidates 1A, 2B and 2H were analysed to identify genomic regions segregating with a higher allele frequency compared to the rest of the chromosome (Figure 2-9). Several candidate intervals were identified (Figure 2-9, highlighted in yellow). The highest SNP frequency was 79%, 75% and 68% for 1A, 2B and 2H respectively. If all bulked progeny carry the same homozygous mutation, the SNP frequency is typically 100% in a chromosomal interval encompassing the causal mutation. The observed lower SNP frequency indicates that each positive segregant bulk still contains false positives despite the stringent selection criteria applied.

I examined the list of candidate mutations and selected a subset of the candidate mutations based on frequency, type (e.g. nonsense mutation and non-synonymous substitution), gene annotation, and expression profile. I retrieved 12, 30 and 22 SNPs for 1A, 2B and 2H respectively (Table S2-3). The candidate SNPs mapped to two different chromosomal regions for each of the three mutant candidates.

To further refine the mapping, a complementary approach was undertaken, which uses the SNP profiles of bulked segregants which retain MLACC-dependent cell death activation, termed “negative segregant bulk” contrary to the “positive segregant bulk” analysed earlier (Results section 2.4.1). For this, I selected among the F_2 .BC_T progeny the individuals exhibiting macroscopic cell death symptoms upon infiltration of DEX into the leaves. The genomic DNA of 45 and 36 negative F_2 .BC_T individuals were isolated for 2B and 2H respectively. These were pooled together and used for subsequent sequencing and mapping. A *p*-value was computed for each SNP based on the SNP frequency in the positive and the negative segregant bulks (unpublished pipeline developed by Xiangchao Gan). This approach allows correcting for linkage disequilibrium compared to the initial mapping analysis. Upon

manual inspection of the 50 best SNP hits for each candidate, 17 and 19 SNPs were confirmed for candidates 2B and 2H respectively. Among either confirmed SNP list, nearly all SNPs were present on chromosome 1, suggesting that chromosome 1 carries most of the SNPs with a significant enrichment. Therefore I focused the analysis on the SNPs present on chromosome 1.

The analysis revealed ten and eight candidate SNPs with significant impact on genes for candidates 2B and 2H respectively (Figure 2-10, Table 2-4). Among the candidate SNPs for mutant 2B, the SNPs in *AT1G71980* and *AT1G73670* were heterozygous in the M₂ plant originally isolated. Since the segregation of the mutant phenotype of candidate 2B indicates a recessive mutation, it is unlikely that the SNPs in *AT1G71980* and *AT1G73670* are the suppressor mutations. Therefore eight candidate SNPs remain for the candidate mutant 2B. Candidate 2H displayed only three SNPs which were homozygous in the M₂ parent. These were located in *AT1G32640*, *AT1G60380*, and in *AT1G63170*. *AT1G32640* is unlikely to carry the suppressor mutation since it does not belong to the chromosomal region where most candidate SNPs are clustered. *AT1G32640* encodes MYC2, a transcription factor involved in jasmonic acid-dependent functions. One could hypothesize that due to its potential partial suppressor effect. This mutation might partially contribute to the suppressor phenotype, and might therefore partially co-segregate with the main suppressor mutation. In case of a recessive mutation, the expected frequency in the negative segregant bulk should be 1/3 (1/3 of WT plants, and 2/3 of heterozygous plants). In several cases, the SNP frequency observed in the negative segregant bulk was lower than 1/3 (Table 2-4.A). This can result from several phenomena dependent or not on the causal mutation. If related to the causal mutation, a lower frequency of heterozygous plants in the negative segregant bulk suggests a semi-dominant effect of the causal mutation. This hypothesis is particularly relevant for candidate 2H whose top four candidate SNPs have a low frequency in the negative bulk and are heterozygous in the M₂ suppressor mutant.

Chapter 2. A genetic suppressor screen [...] for the MLAcc-triggered immune responses

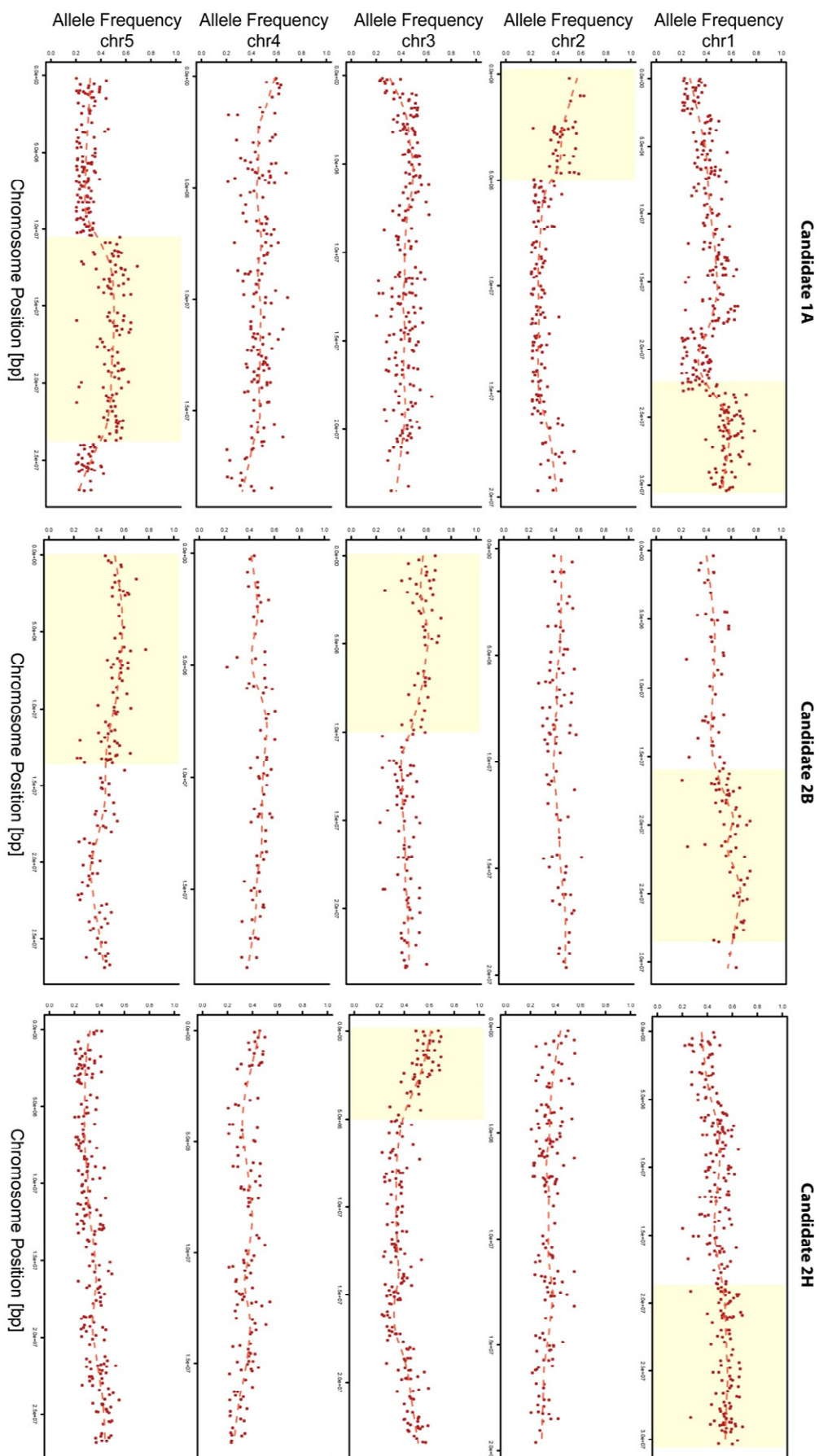


Figure 2-9: Allele frequencies identified by sequencing of segregant bulks for the candidate mutants 1A, 2B and 2H. The frequency of the alleles found by segregant bulk sequencing for the candidates 1A, 2B and 2H is plotted along the chromosome length (red dots). Regression lines have been added to figure the tendency of allele frequencies evolution along the chromosome (red dashed lines). The candidate intervals are highlighted in yellow. Chr, chromosome.

I inspected the genome sequences of the 19 other sequenced M₂ candidates to identify alleles of the candidate suppressors of candidates 2B and 2H. Another allele was found for *AT1G68060* (in 2J, T437I amino acid exchange), and two more for *AT1G66950* (in 2A, downstream; in 3A, E268K amino acid exchange).

Further work will be required to pin point the suppressor mutations. Nevertheless, with a candidate list narrowed down to less than ten genes per candidate, a more detailed analysis on each candidate mutation has become feasible.

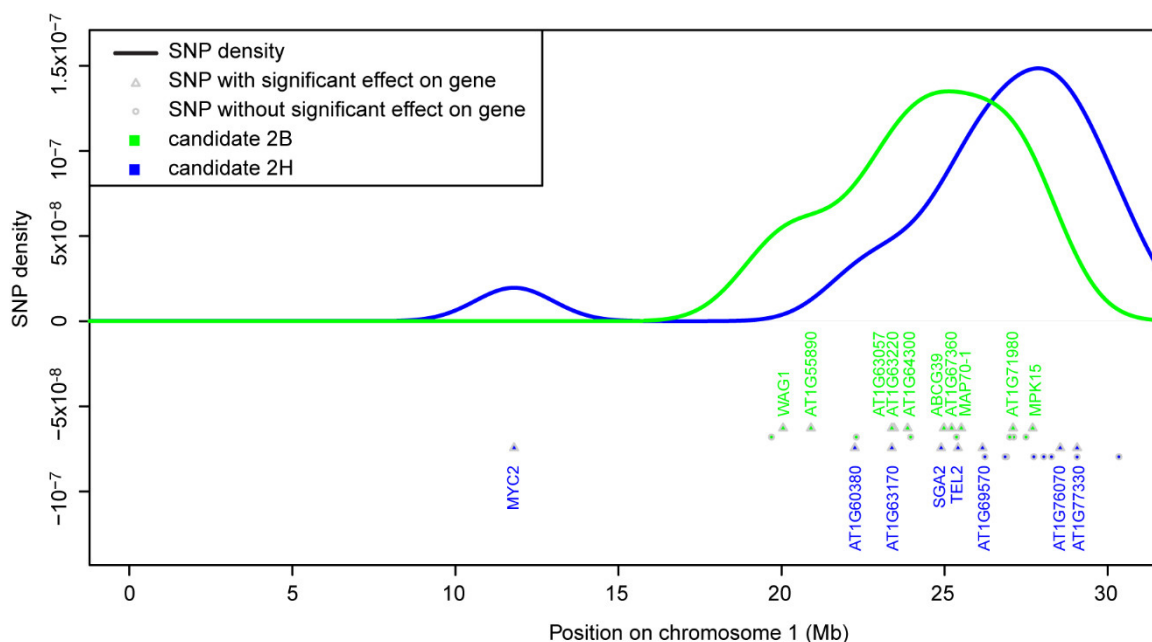


Figure 2-10: Candidate SNPs identified on chromosome 1 by analysis of positive and negative segregant bulks of the mutant candidates 2B and 2H. The candidate SNPs of the candidates 2B and 2H are plotted along the chromosome 1 length. Genes significantly affected by some candidate SNPs are named by their name or AGI code.

Table 2-4: Candidate SNPs with significant impact on genes identified on chromosome 1 of candidate mutants 2B and 2H. A, SNP description. B, gene description

A	Gene	Candidate	P-value	%P	%N	Type	Effect	Status	Other alleles
	AT1G71980	2B	99.03	67	13	Nonsyn	L65F	HZ	
	AT1G64300	2B	77.86	74	25	Nonsyn	G385D	HOM	
	AT1G67360	2B	64.43	67	24	~TSS		HOM	
	AT1G68060	2B	61.44	71	33	Nonsyn	S99F	HOM	T437I (2J)
	AT1G66950	2B	57.17	65	22	Nonsyn	R27K	HOM	down (2A), E268K (3A)
	AT1G53700	2B	55.01	65	28	Nonsyn	D3N	HOM	
	AT1G63220	2B	47.32	59	19	Nonsyn	D37N	HOM	
	AT1G55890	2B	47.17	60	24	Nonsyn	G229E	HOM	
	AT1G63057	2B	42.71	75	32	Nonsyn	M1I	HOM	
	AT1G73670	2B	42.24	70	36	Nonsyn	A226V	HZ	
	AT1G76070	2H	59.59	60	18	Nonsyn	G29E	HZ	
	AT1G77330	2H	55.55	64	15	Nonsyn	P278S	HZ	
	AT1G69570	2H	54.7	66	16	Nonsyn	S51F	HZ	
	AT1G67770	2H	46.45	58	14	Intronic		HZ	
	AT1G66740	2H	43.73	65	27	Nonsyn	R145K	HZ	
	AT1G32640	2H	41.92	57	21	Nonsyn	A529V	HOM	
	AT1G63170	2H	36.2	62	24	Nonsyn	R282Q	HOM	
	AT1G60380	2H	35.79	57	24	Stop gain	Q266*	HOM	

HZ, heterozygous in the M₂ mutant

HOM, homozygous in the M₂ mutant

%P, SNP frequency in the positive segregant bulk

%N, SNP frequency in the negative segregant bulk

Nonsyn, non synonymous, TSS, transcription start site, Down, downstream

B	Gene	Symbol	Candidate	Description
	AT1G71980		2B	protease-associated and C3HC4-type RING finger
	AT1G64300		2B	protein kinase-like protein
	AT1G67360		2B	Rubber elongation factor protein
	AT1G68060	MAP70-1	2B	microtubule-associated proteins 70-1
	AT1G66950	ABCG39	2B	ABC transporter G family member 39
	AT1G53700	WAG1	2B	protein WAG1
	AT1G63220		2B	calcium-dependent lipid-binding domain
	AT1G55890		2B	pentatricopeptide repeat-containing protein
	AT1G63057		2B	uncharacterized protein
	AT1G73670	MPK15	2B	mitogen-activated protein kinase 15
	AT1G76070		2H	uncharacterized protein
	AT1G77330		2H	aminocyclopropanecarboxylate oxidase
	AT1G69570		2H	Dof zinc finger protein DOF1.10
	AT1G67770	TEL2	2H	terminal EAR1-like 2 protein
	AT1G66740	SGA2	2H	histone chaperone ASF1
	AT1G32640	MYC2	2H	transcription factor MYC2
	AT1G63170		2H	E3 ubiquitin-protein ligase
	AT1G60380		2H	No Apical Meristem domain-containing protein

2.5. Characterization of *AT3G02840*, a candidate gene encoding an ARM-containing protein sharing high similarity with *AtCMPG1/PUB20* and *AtPUB21*

A V289I substitution in *AT3G02840* has been identified as a candidate suppressor mutation of ML_{Acc}-mediated growth arrest in the candidate mutant 2H by the SHOREmap analysis described in Results section 2.4.2. Although several other candidate mutations were present in the same interval, this particular mutation was of interest since the V289I affects a conserved residue, and since *AT3G02840* is related to a protein family known to regulate immunity (see details below).

AT3G02840 has not been functionally characterized so far. *AT3G02840* encodes a short protein of 379 amino acids (Figure 2-11). The only domain predicted is an armadillo-type fold (ARM, INTERPRO accession G3DSA:1.25.10.10, InterPro, <http://www.ebi.ac.uk/interpro>) which encompasses 78% of the protein sequence.

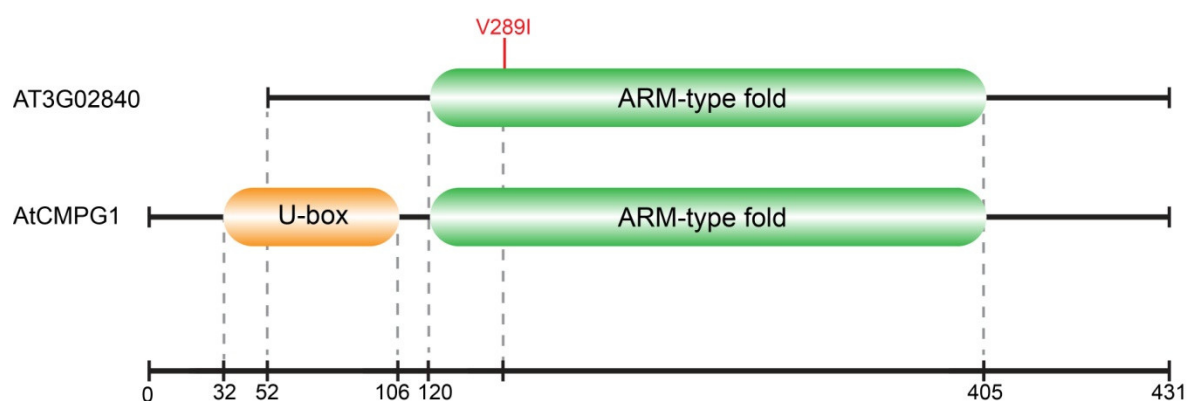


Figure 2-11: Comparison of *AT3G02840* and *AtCMPG1* protein structure and domain composition. The identified EMS-induced mutation is indicated in red.

Chapter 2. A genetic suppressor screen [...] for the ML_{ACC}-triggered immune responses

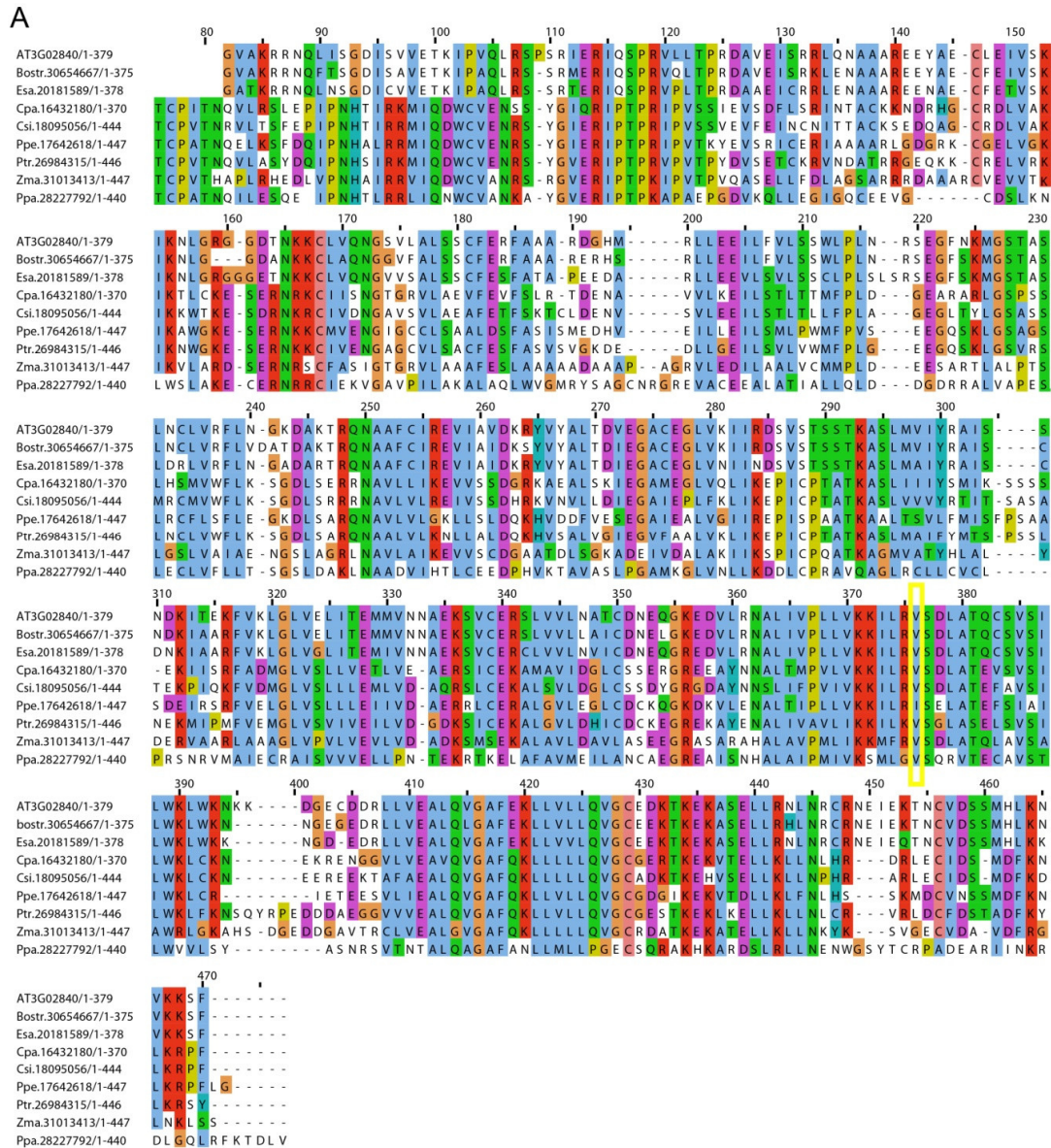


Figure 2-12: AT3G02840 sequence analysis. **A**, protein sequence alignment of AT3G02840 and its orthologues in *Boechera stricta* (Bostr), *Eutrema salsugineum* (Esa), *Carica papaya* (Cpa), *Citrus sinensis* (Csi), *Prunus persica* (Ppe), *Populus trichocarpa* (Ptr), *Zea mays* (Zma) and *Physcomitrella patens* (Ppa). The position of the EMS-induced mutation that putatively suppresses ML_{ACC}-mediated growth arrest is framed in yellow. **B**, Promoter sequence of AT3G02840. The W-boxes are underlined. Sequences of the E17 and F elements identified in *PsCMPG1* and *AtCMPG1* promoters are aligned and concordant base pairs are indicated in green, red, transcribed region. Uppercase, translated region.

An orthologue search in Phytozome v10.3 detected 783 putative orthologues for AT3G02840 throughout the Viridiplantae. These orthologues mainly match the ARM domain (family 58431214). This indicates a high conservation of this ARM domain in the Viridiplantae taxa.

The best pblast hits for AT3G02840 were two *A. thaliana* CMPG proteins, AT1G66160 (*AtCMPG1/PUB20*) and AT5G37490 (*PUB21*), with 42% and 40% identity respectively. The ARM domain of AT3G02840 is highly similar to the C-terminal ARM domain of the CMPG family (Figure 2-12.A). The CMPG family forms a subgroup of the PUB (plant U-box proteins) family and is defined by a common domain with four conserved amino acid residues [Cys, Met, Pro, and Gly (CMPG)]. Homologs of *AtCMPG1* in tobacco, tomato, potato, and *Haynaldia villosa* are involved in defence and cell death responses triggered by various pathogens (Bos et al., 2010; González-Lamothe et al., 2006; Zhu et al., 2015). This indicates a conserved defence-related function of the *CMPG1* genes in both monocots and dicots. In many cases *CMPG1* genes are rapidly induced upon pathogen challenge or elicitor treatment (González-Lamothe et al., 2006; Heise et al., 2002; Kirsch et al., 2001; Zhu et al., 2015). This transcriptional regulation has been associated with the presence of W-box -containing, elicitor-responsive *cis*-elements: the E17 *cis*-element in *PcCMPG1* promoter and the F *cis*-element in *AtCMPG1* promoter (Heise et al., 2002; Kirsch et al., 2001).

In contrast to *CMPG1* proteins, AT3G02840 lacks the U-box domain and therefore, corresponds to a N-terminally truncated form of *CMPG1*. Despite this N-terminal truncation, the *AT3G02840* promoter contains a *cis*-regulatory element similar to E17 and F (Heise et al., 2002; Kirsch et al., 2001) (Figure 2-12.B), suggesting that it follows similar regulations as the *CMPG1* genes. To test this hypothesis, I analysed the co-expression pattern of *AT3G02840* and *AtCMPG1/AtPUB21*. *AT3G02840* and *AtCMPG1* have a mutual ranking (MR) of 27.9, whereas *AT3G02840* and *AtPUB21* MR score is 159.3 (CoexVersion vc4.1, www.atted.jp). This indicates that *AT3G02840* is tightly co-expressed with *AtCMPG1* and to a lesser extent with *AtPUB21*. *AT3G02840* has been reported as a H₂O₂-responsive gene (Inzé et al., 2012) and is induced by multiple biotic and abiotic stresses as well. The RNA-seq data produced in this study (Result section 1.3), confirmed by qRT-PCR analysis also indicates that *AT3G02840* is rapidly and sustainably induced upon MLACC expression in *A. thaliana* (Figure 2-13).

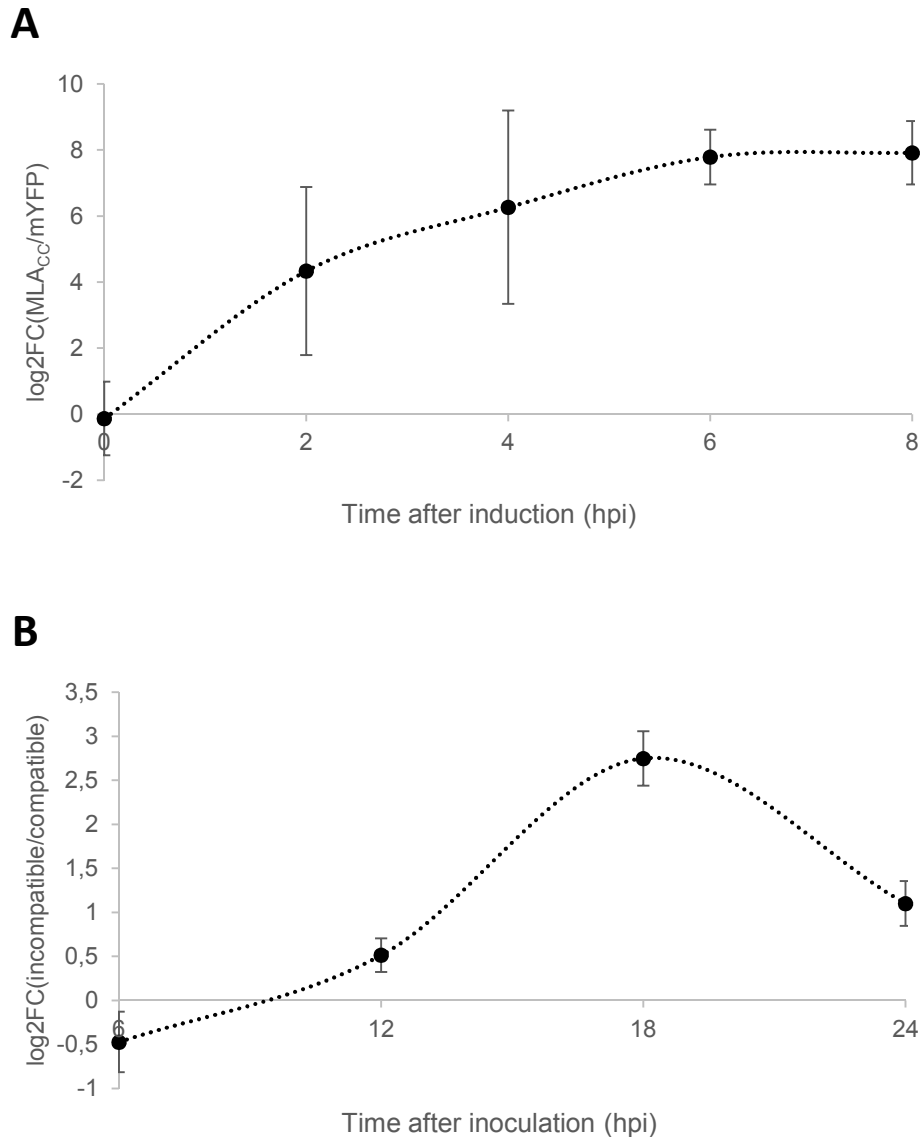


Figure 2-13: Analysis of *AT3G02840* expression in *A. thaliana* upon MLA_{CC} expression or MLA1 activation. Expression of *AT3G02840* was monitored by RNA-seq over time upon MLA_{CC} expression or MLA1 activation in the after inoculation with MLA1 cognate pathogen. **A**, relative expression of *AT3G02840* in the *DEXp:MLA_{CC}-mYFP* line as compared to the *DEXp:mYFP* line after DEX treatment. **B**, Relative expression of *AT3G02840* in a partially immunocompromised *A. thaliana pen2 pad4 sag101* expressing MLA1 line inoculated with MLA1 cognate pathogen *Blumeria graminis* f. sp. (*Bgh*) strain K1 (activation of MLA1, incompatible interaction) as compared to the same line inoculated with the non-recognized *Bgh* strain A6, and to the non MLA1-expressing *A. thaliana pen2 pad4 sag101* line inoculated with either *Bgh* K1 or *Bgh* A6 (no activation of MLA1, compatible interactions). The RNA-seq data are those published in Maekawa et al. 2013. The relative expression is expressed as a log₂-transformed cpm fold change (log₂FC).

AT3G02840 is localized in the cytosol and the nucleus with an increased accumulation in the nucleolus when transiently expressed in *Nicotiana benthamiana* (Inzé et al., 2012).

Orthologues of this truncated were found in *Arabidopsis lyrata*, *Boechera stricta*, *Capsella grandiflora*, *Brassica rapa* and *Eutrema salsugineum* but not in species outside of the

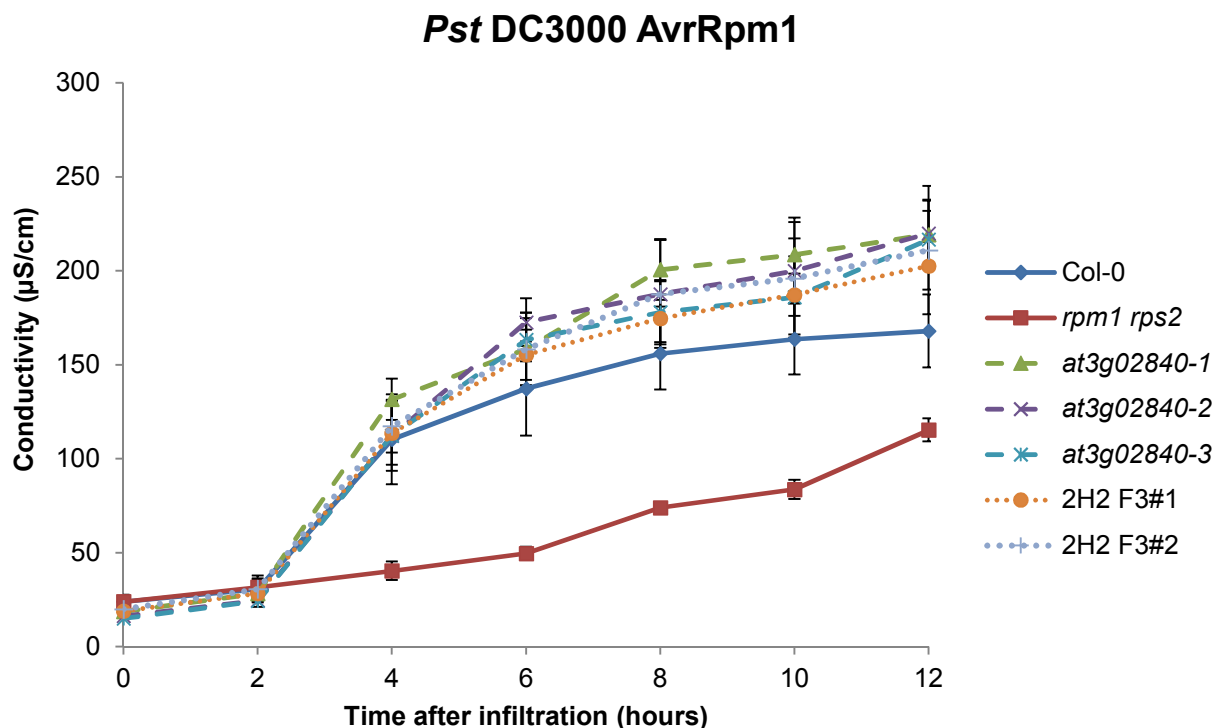
Brassicacea family (Phytozome v10.3). Therefore this gene represents a Brassicacea-specific innovation.

The mutation identified in this study is a typical EMS-induced mutation and results in a V→I substitution at the position 289 located in a highly conserved region of the ARM-type fold (Figure 2-12.A).

To examine the role of AT3G02840 in the MLA_{CC}-mediated cell death, I transiently co-expressed either AT3G02840 or AT3G02840(V289I) together with MLA_{CC} in *N. benthamiana*. Transient co-expression of AT3G02840 WT or V289I together with MLA_{CC} in *N. benthamiana* did not alter MLA_{CC}-mediated cell death response (data not shown).

Analysis of three independent *A. thaliana* T-DNA insertion lines for AT3G02840 suggest that AT3G02840 is a negative regulator of HR cell death induced upon *Pst* DC3000 AvrRpm1 inoculation (Figure 2-14.A).

A



B

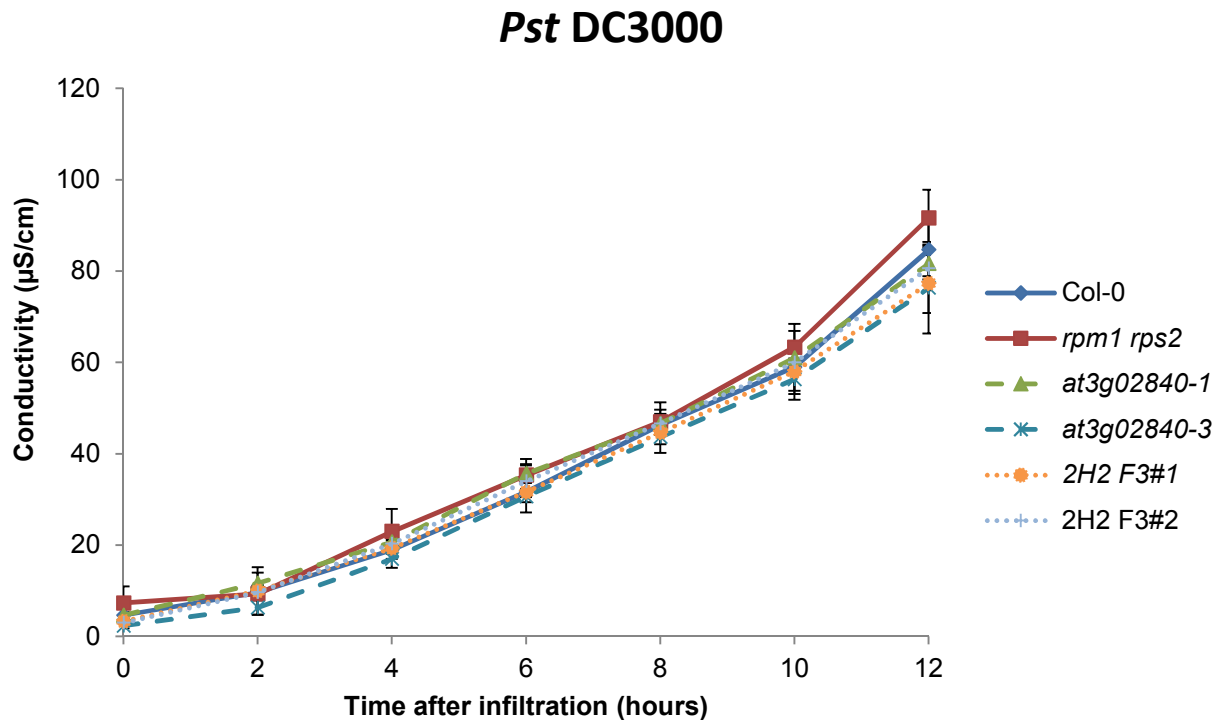


Figure 2-14: Effect of AT3G02840 deficiency on HR cell death triggered by RPM1. Ion leakage assay of 4-5 week-old Col-0 WT, *rpm1 rps2* double mutant (susceptible control), three independent T-DNA insertion lines for AT3G02840 (*at3g02840-1*, *at3g02840-2* and *at3g02840-3*) and two independent F₃.BCT progeny of candidate 2H carrying the homozygous V289I mutation in AT3G02840 (2H2 F3#1 and 2H2 F3#2) after leaf-infiltration with *Pst* DC3000 AvrRpm1 (A) or *Pst* DC3000 (B). Means and standard deviation were calculated from four leaf discs with three replicates within an experiment. The experiment presented in A. was repeated three times with similar tendencies. The data presented in B. corresponds to a single experiment.

To determine the effect of the V289I mutation on AT3G02840 function, I isolated two independent progeny (F₃.BCT, Figure 2-3) of a F₂.BCT segregant from candidate mutant 2H which were homozygous for the V289I mutation. The two independent F₃.BCT progeny displayed a cell death response similar to the *AT3G02840* T-DNA insertion lines, suggesting that the V289I mutation results in a loss of AT3G02840 function (Figure 2-14.A).

The cell death induced upon *Pst* DC3000 inoculation was identical between the *AT3G02840* T-DNA insertion lines, the mutant F₃.BCT progeny and the WT line indicating that AT3G02840 negative regulation of cell death is specific to RPM1-mediated cell death and does not occur during a compatible interaction with the same pathogen (Figure 2-14.B).

The ARM-type fold is predicted to mediate protein-protein interactions. Thus, AT3G02840 might act as a dominant negative regulator by competing with other proteins for the interaction with their cellular targets or as a bridging protein to form higher order protein complexes. A similar dominant negative function has already been demonstrated for the ARM

domain of *AtPUB13* in the context of *AtFLS2-AtPUB13* interaction (Zhou et al., 2015). In order to identify *AT3G02840* interaction partners, we conducted a Y2H screen using *AT3G02840* as a bait against an *A. thaliana* cDNA library. We identified 28 candidates with at least three independent clones among the 231 sequenced (Table 2-5). The 28 candidate interactors represent a very heterogeneous group of proteins with various subcellular localizations (cytoplasmic, chloroplastic, mitochondrial, peroxisomal, transmembrane and secreted) and various molecular functions (e.g. transcription factors, elongation factors, chaperonins, ATP synthases and kinases).

In conclusion, I identified a gene, *AT3G02840*, involved in negative regulation of RPM1-mediated cell death. This data contrasts with the initially presumed positive regulatory function of *AT3G02840* in MLA_{CC}-mediated cell death. However further mapping data obtained by genotyping of the negative segregant bulk of the candidate mutant 2H (section 2.4.2) suggests that the suppressor mutation of MLA_{CC}-mediated growth arrest does not co-segregate with *AT3G02840*. Thus, MLA_{CC} might function independently of *AT3G02840*. Further investigation will be required to confirm this hypothesis and to determine the molecular function of *AT3G02840* in cell death regulation. I generated crosses between the *DEXp:MLA_{CC}-mYFP* lines and the *AT3G02840* T-DNA insertion lines. This material can be used in the future to further examine the role of *AT3G02840* in MLA_{CC}-mediated cell death and growth arrest.

Chapter 2. A genetic suppressor screen [...] for the MLAcc-triggered immune responses

Table 2-5: AT3G02840 candidate interactors identified by Y2H. Only the candidates identified by at least 3 independent clones out of the 231 sequenced are indicated.

Gene ID	Clones number	Name	Description
AT1G62750	17	SNOWY COTYLEDON 1 (SCO1)	Nuclear encoded protein consists of the five domains conserved in EF-G proteins, with two GTP-binding sites in the first domain, and an additional transit peptide at the N-terminus. Localized in chloroplasts.
AT1G75690	11	LOW QUANTUM YIELD OF PHOTOSYSTEM II 1 (LQY1)	DnaJ/Hsp40 cysteine-rich domain superfamily protein
ATCG00480	10	ATP SYNTHASE SUBUNIT BETA (PB)	chloroplast-encoded gene for beta subunit of ATP synthase
AT3G25910	9		FUNCTIONS IN: zinc ion binding (DUF1644)
AT1G15730	7		Cobalamin biosynthesis CobW-like protein;
AT4G38550	7		Arabidopsis phospholipase-like protein (PEARLI 4) family; LOCATED IN: chloroplast
AT5G10450	7	G-BOX REGULATING FACTOR 6 (GRF6)	Member of the 14-3-3 gene family. Interacts with APX3 (ascorbate peroxidase) and AKR2, suggesting a role in mediating oxidative metabolism in stress response. Colocalize and interact with SERK1 by which it is phosphorylated. Interact with the phosphorylated form of the BZR1 transcription factor involved in brassinosteroid signaling. Interacts with JAZ10.4
AT5G45050	7	TOLERANT TO TOBACCO RINGSPOT NEPOVIRUS 1 (TTR1); WRKY16	Encodes a member of the WRKY Transcription Factor (Group II-e) family.
AT3G11630	6		Encodes a 2-Cys peroxiredoxin (2-Cys PrxA) that contains two catalytic Cys residues.
AT1G71730	5		unknown protein
AT1G73060	5	LOW PSII ACCUMULATION 3 (LPA3)	Low PSII Accumulation 3 (LPA3)
AT3G44200	5	NIMA (NEVER IN MITOSIS, GENE A)-RELATED 6 (NEK6)	Encodes AtNek5, a member of the NIMA-related serine/threonine Kinases (Neks) that have been linked to cell-cycle regulation in fungi and mammals. Plant Neks might be involved in plant development processes
AT3G52370	5	FASCICLIN-LIKE ARABINOGALACTAN PROTEIN 15 PRECURSOR (FLA15)	FASCICLIN-like arabinogalactan protein 15 precursor (FLA15); INVOLVED IN: cell adhesion
AT3G62250	5	UBIQUITIN 5 (UBQ5)	ubiquitin 5 (UBQ5)
AT5G51110	5		Transcriptional coactivator/pterin dehydratase; FUNCTIONS IN: 4-alpha-hydroxytetrahydrobiopterin dehydratase activity; INVOLVED IN: tetrahydrobiopterin biosynthetic process; LOCATED IN: chloroplast;
AT1G23310	4	GLUTAMATE:GLYOXYLATE AMINOTRANSFERASE (GGT1)	Identified by cloning the gene that corresponded to a purified protein having glyoxylate aminotransferase activity. Localized to the peroxisome and thought to be involved in photorespiration/ metabolic salvage pathway.
AT1G45976	4	S-RIBONUCLEASE BINDING PROTEIN 1 (SBP1)	
AT4G37925	4	NADH DEHYDROGENASE-LIKE COMPLEX M (NdhM)	Encodes subunit NDH-M of NAD(P)H:plastoquinone dehydrogenase complex (Ndh complex) present in the thylakoid membrane of chloroplasts.
AT1G29900	3	CARBAMOYL PHOSPHATE SYNTHETASE B (CARB)	Encodes carbamoyl phosphate synthetase (CPS) large subunit (CARB), also named as VEN3.
AT1G66660	3		Protein with RING/U-box and TRAF-like domains
AT2G05840	3	20S PROTEASOME SUBUNIT PAA2 (PAA2)	Encodes 20S proteasome subunit PAA2 (PAA2).
AT2G22770	3	NAI1	regulates the development of ER bodies. also involves in response to the endophytic fungus <i>Piriformospora indica</i> .
AT2G35635	3	UBIQUITIN 7 (UBQ7)	
AT3G18240	3		Ribosomal protein S24/S35, mitochondrial
AT4G27490	3	RRP41 LIKE (RRP41L)	3'-5'-exoribonuclease family protein
AT5G14740	3	CARBONIC ANHYDRASE 2 (CA2)	Encodes a beta carbonic anhydrase likely to be localized in the cytoplasm.
AT5G19330	3	ARM REPEAT PROTEIN INTERACTING WITH ABF2 (ARIA)	Encodes an armadillo repeat protein involved in the abscisic acid response. The protein interacts with a transcription factor, ABF2, which controls ABA-dependent gene expression via the G-box-type ABA-responsive elements.
ATCG00470	3	ATP SYNTHASE EPSILON CHAIN (ATPE)	

Chapter 3.

**Identification of the MLA_{CC}-associated signalling partners
in *A. thaliana***

3.1. Introduction

The barley resistance protein MLA belongs to the nucleotide-binding domain and leucine rich repeats-containing protein (NLR) family and confers race-specific resistance upon interfamily transfer to *Arabidopsis thaliana* (Maekawa et al., 2012). This finding implies that, upon activation, MLA transduces the immune signal to some yet unknown *A. thaliana* signalling component(s). The N-terminal coiled-coil (CC) domain of MLA (MLA_{CC}) acts as a minimal signalling module triggering cell death upon transient expression in barley and *Nicotiana benthamiana*. MLA_{CC} cell death signalling activity is dependent on MLA_{CC} homodimerization since mutations (e.g. I33E and L36E) that disrupt the MLA_{CC} homodimer formation also abolish its cell death-inducing activity (Maekawa et al. 2011). In order to identify the signalling target(s) of MLA in *A. thaliana*, I conducted two independent biochemical approaches: i) a yeast two hybrid (Y2H) screen against nearly all *A. thaliana* transcriptional regulators and ii) the purification and characterization of MLA_{CC}-associated protein complexes in *A. thaliana*. Both approaches involved the MLA_{CC} as a bait to minimize the complexity of the protein interactions and to focus on the components associated with the signalling module.

3.2. Screening for physical interaction between MLA_{CC} and *A. thaliana* transcriptional regulators by yeast two hybrid

Accumulating reports indicate that NLRs can interact with transcription factors (TFs) (Ando et al., 2014; Chang et al., 2013; Inoue et al., 2013; Jacob et al., 2013; Padmanabhan and Dinesh-Kumar, 2014; Padmanabhan et al., 2013; Qi and Innes, 2013; Xu et al., 2014). This data supports a signalling model where at least a subset of NLRs can regulate transcriptional reprogramming by direct physical interaction with TFs (Jacob et al., 2013). In barley, MLA receptor interacts with the TFs *HvWRKY1/2* and *HvMYB6* via its N-terminal CC domain (MLA_{CC}) and the interactions appear to be important for immunity (Chang et al., 2013; Shen et al., 2007). The barley MLA is fully functional in *A. thaliana* (Maekawa et al., 2012) although no clear *HvMYB6* homolog was found in this species, suggesting that another TF compensates for the *HvMYB6* function in *A. thaliana*.

Furthermore, considering all the reported NLR-TF interactions, there is yet no evidence for TFs being commonly recruited by multiple NLRs even though such scenario appears intuitively as most biologically relevant. Therefore, many questions remain open concerning this aspect of the NLR function.

MLA_{CC} can induce transcriptional changes in *A. thaliana* similar to the full length MLA in the same species (chapter 1). I hypothesized that MLA_{CC} interacts with some *A. thaliana* TFs, or chromatin regulators, or mediator components whom I altogether refer to as transcriptional regulators (TRs).

The interactions between MLA_{CC} and *A. thaliana* TRs were tested using a yeast two-hybrid (Y2H) system. The Y2H system, hereafter called “AIST system” was described in Mitsuda et al., (2010). The AIST system-based screening is rather low-throughput but highly sensitive in detecting binary interactions due to the binary interaction screening method employed. The TRs prey library encompasses at least 50% of *A. thaliana* TRs. The bait and prey libraries used are described in Table 3-1. Two different MLA_{CC} bait constructs were used: MLA10_{CC1-225} which was reported to interact with *HvMYB6* and *HvWRKY1/2* (Chang et al., 2013; Shen et al., 2007), and MLA10_{CC1-160} which represents the minimal unit required for cell death induction (Maekawa et al., 2011b) and sufficient to mediate transcriptional reprogramming in *A. thaliana* (chapter 1). The number of MLA_{CC} candidate interactors is largely different depending on the bait protein (Table 3-2). A total of 31 candidate interactors were identified (Table 3-3).

Table 3-1: Description of the clone libraries used for yeast two hybrid screening.

Clones	Description	Cloning
Baits	MLA10 _{CC1-225}	Cloning to pDEST-BTM116
	MLA10 _{CC1-160}	
Preys	TOTAL: 2	Not required, clones already available in pDEST-GAD424 (Mitsuda et al. 2010)
	1500 TFs	
	20 chromatin remodelers 19 mediator components	
TOTAL: 1539		

Table 3-2: Number of candidate interactions identified by Y2H.

System	Bait	Number of interactions
AIST	MLA10 _{CC1-225}	29
	MLA10 _{CC1-160}	3

Table 3-3: Description of the ML_{ACC} candidate interactors identified by Y2H.

Protein ID	CC 1-225	CC 1-160	Family	Name	GO term biological process
AT1G28300	X		B3	LEC2	somatic embryogenesis, seed maturation, positive regulation of transcription, embryo development, positive regulation of auxin biosynthetic process, seed oilbody biogenesis
AT2G22770	X		bHLH	NAI1	endoplasmic reticulum organization
AT5G54680	X		bHLH	ILR3	
AT5G42520	X		BPC	BPC6	response to ethylene
AT1G06070	X		bZIP	bZIP69	
AT1G43700		X	bZIP	VIP1	cellular response to sulfate starvation, negative regulation of cell differentiation, sulfate transport, nuclear import, osmosensory signalling pathway
AT5G38800	X		bZIP	bZIP43	
AT1G47870	X		E2F	E2F2	negative regulation of cell division, cell morphogenesis, cell division, DNA endoreplication
AT1G53910	X		ERF/AP2	RAP2.12	detection of hypoxia, ethylene-activated signalling pathway, response to hypoxia
AT2G40340	X		ERF/AP2	DREB2C	response to abscisic acid, heat acclimation
AT3G14230	X		ERF/AP2	RAP2.2	response to hypoxia, regulation of gene expression, ethylene-activated signalling pathway
AT3G16770	X		ERF/AP2	EBP	response to other organism/jasmonic acid/cytokinin/ethylene, cell death, ethylene-activated signalling pathway, heat acclimation
AT4G18450	X		ERF/AP2		ethylene-activated signalling pathway, response to chitin
AT5G64750	X		ERF/AP2	ABR1	negative regulation of abscisic acid-activated signalling pathway, defence response to fungus, response to abscisic acid/glucose/osmotic stress, ethylene-activated signalling pathway, abscisic, acid-activated signalling pathway
AT5G44190	X		GARP	GLK2	negative regulation of leaf senescence, chloroplast organization, regulation of chlorophyll biosynthetic process, negative regulation of flower development
AT4G34680	X		GATA	GATA3	regulation of transcription from RNA polymerase II promoter, cell differentiation, circadian rhythm
AT2G18550	X		HD	HB21	
AT4G36740	X		HD	HB40	response to auxin
AT4G11660	X		HSF	HSFB2B	response to chitin
AT1G48150	X		MADS		
AT5G26950	X		MADS	AGL93	
AT1G74660	X		MIF	MIF1	response to gibberellin/abscisic acid/auxin/cytokinin/brassinosteroid, regulation of meristem development, photomorphogenesis, multicellular organismal development
AT2G47460	X		MYB	MYB12	response to auxin, flavonoid biosynthetic process, response to ethylene
AT1G32640	X		MYC	MYC2	response to abscisic acid/jasmonic acid/wounding/chitin/dessication/oxidative stress/insect, root development, indole glucosinolate biosynthetic process, indole glucosinolate biosynthetic process, tryptophan metabolic process, jasmonic acid mediated signalling pathway
AT3G15170	X		NAC	CUC1	lateral root development, gynoecium development, meristem initiation, secondary shoot formation, flower development, meristem initiation, primary shoot apical meristem specification, embryo development, flower development, negative regulation of cell division, formation of organ boundary
AT5G07680	X		NAC	NAC080	multicellular organismal development
AT5G18270	X		NAC	ANAC087	multicellular organismal development
AT5G53950	X		NAC	CUC2	multicellular organism development, secondary shoot formation, leaf development, leaf morphogenesis, primary shoot apical meristem specification, regulation of timing of organ formation, formation of organ boundary
AT1G54060		X	Trihelix	ASIL1	seed maturation, regulation of seed germination, response to auxin, regulation of shoot system development, embryo development ending in seed dormancy
AT1G76870	X		Trihelix		
AT3G11100	X	X	Trihelix		

These 31 candidates belong to diverse TF families (B3, BPC, bHLH, BPC, bZIP, E2F, ERF/AP2, GARP, GATA, HD, HSF, MADS, MIF, MYB, MYC, NAC and trihelix, Table 3-3). The TF families most represented among the candidate interactors were ERF/AP2, NAC, bZIP and Trihelix with six, four, three, and three members respectively (Table 3-4). Most interactions were obtained with the MLA10_{CC1-225} bait. The screen did not identify any WRKY transcription factor, despite the reported interaction between MLA_{CC} and *Hv*WRKY1/2 (Shen et al., 2007). Similarly, there was no MYB transcription factor closely related to *Hv*MYB6 among the candidate interactors identified. This suggests that interactions between MLA_{CC} and *At*WRKYs or *At*MYBs are not conserved in *A. thaliana*, or that the Y2H screen employed failed in detecting the potential interactions in *A. thaliana*.

In order to determine the biological significance of the candidate interactors identified, I performed a GO-term enrichment analysis. Apart from “transcription regulation”, no other enriched biological process was found for the list of candidates identified.

Altogether, these results suggest that MLA_{CC} interacts with various TFs in *A. thaliana*.

Table 3-4: TF family representation in the 31 MLA_{CC} candidate interactors

TF family	Number of candidates
ERF/AP2	6
NAC	4
bZIP	3
Trihelix	3
bHLH	2
HD	2
MADS	2
B3	1
BPC	1
E2F	1
GARP	1
GATA	1
HSF	1
MIF	1
MYB	1
MYC	1

3.3. Isolation and characterization of MLA_{CC}-associated protein complexes in *A. thaliana*

3.3.1. Design of the experimental setup and material preparation

3.3.1.1. Aims of the approach and experimental setup

As a complement to the aforementioned Y2H approach, I employed affinity purification of protein complexes coupled with mass spectrometry (MS) analysis to isolate and identify MLA_{CC}-associated protein complexes.

Affinity purification of protein complexes followed by MS characterization constitutes one of the available strategies to identify unknown protein partners associated with a given protein (bait) within a functional complex *in vivo*. Numerous reports have contributed to develop this method, and technological progress in mass spectrometry constantly pushes forward the detection limits rendering the analysis of minute amounts of biological material possible.

Even though several standard protocols have been developed, the protein complex isolation often requires a careful choice of the protocol and fine-tuning related to the peculiarities of the system and the protein complex of interest. In that sense, this technique remains highly empirical.

To purify and characterize *in vivo* MLA_{CC}-associated protein complexes, I developed a suitable affinity purification protocol. Since the MLA_{CC} induces cell death upon expression, an inducible promoter was favoured to express the bait protein. Additionally, since the MLA_{CC}-dependent cell collapse prevents the accumulation of the bait protein, an efficient purification method was needed to efficiently enrich for a low amount of bait protein over background. Due to the availability of a robust inducible system, namely the estradiol (ER) inducible promoter based on the pMDC7 vector (Curtis and Grossniklaus, 2003), I generated stable *A. thaliana* transgenic lines that conditionally express MLA_{CC} bait constructs.

I employed a tandem affinity purification (TAP) rather than single step affinity purification. Trade-offs and recent developments for both systems have been reviewed in (Pflieger et al., 2011) and (Dedecker et al., 2015). TAP was considered more suitable in this study because it has a higher purification efficiency compared to single step affinity purification.

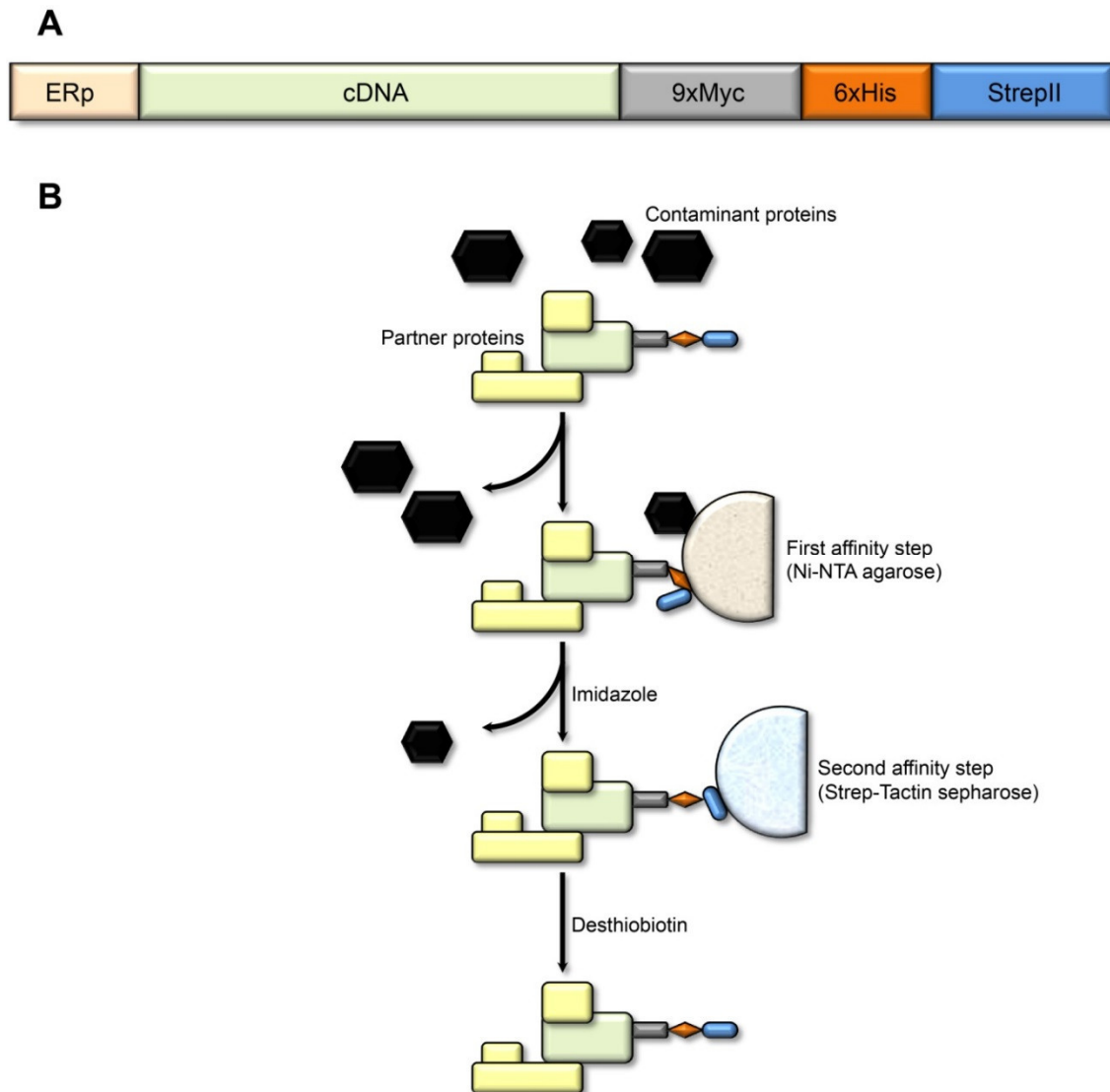


Figure 3-1: Overview of the TAP strategy and the construct used. Modified from Bigeard et al. 2014 (A) Structure of the TAP PC2 cassette figuring the bait in fusion with the various tags and expressed under the estradiol-inducible promoter (ERp). (B) Overview of the TAP strategy. Yellow boxes represent partner proteins of the TAP-tagged bait protein and black boxes represent contaminant proteins; the green box and the three small grey, orange and blue boxes correspond to the TAP-tagged bait protein.

The affinity tag is critical in determining the TAP efficiency. The PC2 tag consists of nine Myc repeats (EQKLISEEDL), a stretch of eight histidine residues (8xHis) and a C-terminal StrepII tag (WSHPQFEK). This tag has been successfully employed at the URGV for mitogen activated protein kinase-associated complex isolation (Bigeard et al. unpublished results) and does not require any protease cleavage for bait elution. The corresponding protocol has already been published (Bigeard et al., 2014). Thus, I used the PC2 tag for TAP of MLACC-associated protein complexes. The TAP involves a first purification step based on the 8xHis affinity onto a Ni-NTA (nickel-nitrilotriacetic acid) matrix followed by a second

step based on the StrepII affinity for a Strep-Tactin matrix (Figure 3-1). The Myc tags are not directly involved in the purification and can be employed for bait protein immunodetection with anti-myc antiserum (Figure 3-1).

To efficiently remove the background from the list of proteins identified, a set of control lines was generated (Figure 3-2.A). Additional baits and controls were prepared but not included in the analysis, and kept for potential future analysis in addition to the first tested lines if necessary (Figure 3-2.B).

		ACTIVITY	SEQUENCE SIMILARITY	DIMER
A				
Sample	MLA _{CC1-160} -PC2	+		+
Standard control	mYFP-PC2	--	--	-
Inactive MLA _{CC}	MLA _{CC1-160} L36E-PC2	--	+++	-
MLA _{CC} (no TAP)	MLA _{CC1-160} -mYFP	+	+++	+
B				
Sample	MLA _{CC1-160} -NLS-PC2	+	+++	+
Sample	MLA _{CC1-160} -NES-PC2	+	+++	+
Inactive MLA _{CC}	MLA _{CC1-160} I33E-PC2	--	+++	-
Other CC _{EDVIV}	RPM1 _{CC1-155} -PC2	--	++	+
CC _R	ADR1-L2 _{CC1-153} -PC2	+	-	?

Figure 3-2: Bait constructs expressed in the *A. thaliana* transgenic lines for the TAP analysis. A, primary set of samples and controls. B, secondary set of samples and controls.

3.3.1.2. Generation and characterization of the transgenic plant material

Eight bait constructs in fusion with the PC2 tag had to be produced and cloned into a vector suitable for inducible expression. Given this number and for facilitating other future experimental developments, I engineered a gateway-compatible binary vector for expression of the construct in frame with the PC2 tag (C-terminal fusion) under an estradiol-inducible promoter (*ERp*) based on the pMDC7-GW vector (Curtis and Grossniklaus, 2003) and hereafter referred to as pMDC7-GW-PC2 (Figure S3-1).

The constructs described in Figure 3-2 (apart from the previously described *DEXp:MLA_{CC}-mYFP* construct, Chapter 1) were cloned into pMDC7-GW-PC2 and the resulting constructs were transformed into *A. thaliana* wild-type (Col-0). Homozygous T₃ lines with single transgene insertions and similar transgene expression levels were selected for further characterization.

I assayed cell death induction mediated by MLA_{CC}-PC2 and ADR1-L2_{CC}-PC2 after estradiol (ER) treatment. As shown in Figure 3-3, both constructs were able to significantly induce ion leakage and tissue collapse, both indicative of cell death, as compared to Col-0 and the lines expressing inactive PC2-tagged constructs. I concluded that the C-terminal fusion to the PC2 tag does not qualitatively alter the bait function.

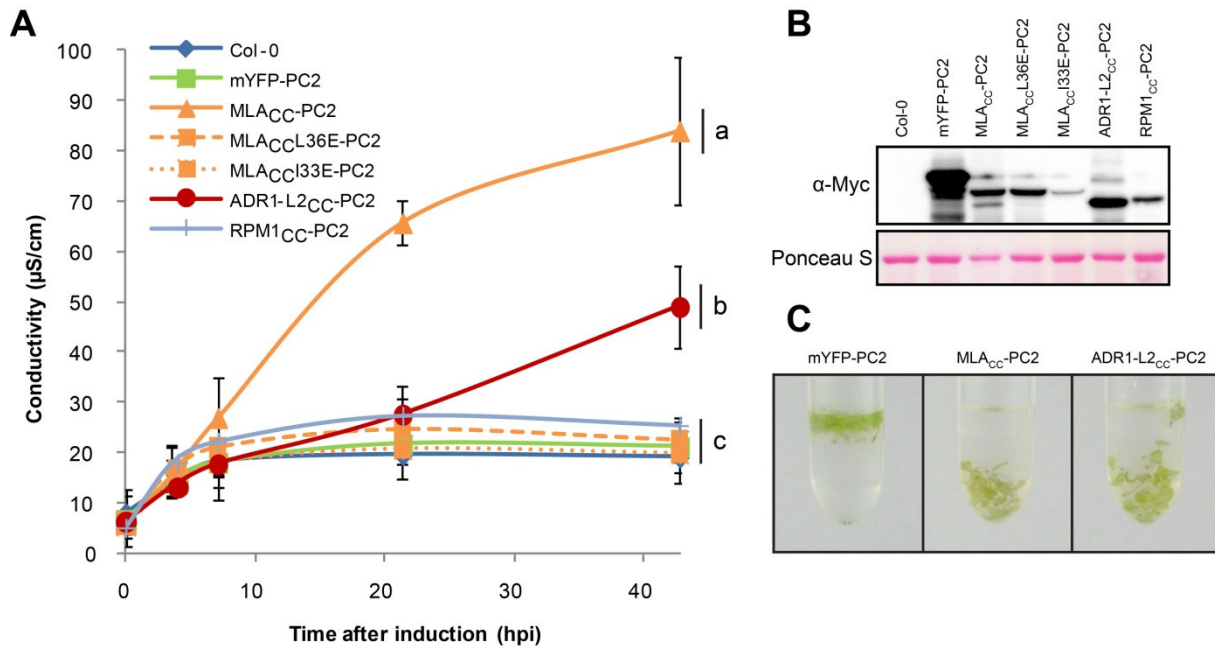


Figure 3-3: Characterization of the bait-PC2 constructs used for TAP. 10 day-old seedlings were immersed into 10 μ M ER + 0.001% Silwet L-77.A, cell death measured by ion leakage. The letters on the right side indicate statistical groups defined by one way Anova followed by posthoc Tukey HSD based on a p -value <0.001 and at least three independent experiments with three biological replicates each. B, protein accumulation at 16 hpi visualized by immunoblotting anti-myc. C, macroscopic phenotype of eight seedlings immersed in the induction solution at 48 hpi. Tissue collapse results in seedling drowning in the lines expressing either *MLA_{CC}-PC2* or *ADR1-L2_{CC}-PC2* but not *mYFP-PC2*.

3.3.2. Optimization of the tandem affinity purification protocol

3.3.2.1. Optimization of the affinity purification procedure

I conducted pilot experiments using the *ERp:MLA_{CC}-PC2* and the *ERp:mYFP-PC2* lines following a protocol essentially similar to what was published by Bigeard et al. (2014). The amount of bait protein recovered by this protocol was not sufficient for the subsequent MS analysis. Further pilot experiments were performed to optimize four major TAP/MS steps to circumvent this issue: i) the conditions used for plant growth and estradiol (ER) induction, ii) the protein extraction, iii) the final elution and iv) the protein precipitation following purification.

I analysed the bait expression in plants grown as described in Bigeard et al. (2014). Three week old plants grown in liquid medium were induced by adding 10 μ M ER + 0.001% Silwet L-77 into the culture medium. Protein accumulation was analysed 16 hours after induction. The *MLA_{CC}-PC2* protein was at the lower detection limit by immunoblotting suggesting that

the amount of bait protein was very low (data not shown). A significant improvement of the expression level was observed when the plants were grown on soil for the same duration, their aerial part sampled and incubated for 16 hours in 10 μ M ER + 0.001% Silwet L-77.

Monitoring of the bait extraction efficiency by immunoblotting indicated that the MLA_{CC}-PC2 protein, contrary to the mYFP-PC2 protein, was not efficiently extracted by the standard extraction procedure (Figure S3-2.A). A similar tendency was observed with the MLA_{CC}-mYFP and ADR1-L2_{CC}-PC2 proteins (Figure S3-2.A, B), indicating that both CC baits are poorly soluble and that this property is independent of the epitope tag. Such low solubility might be explained by the association to an insoluble compartment (e.g. membranes) or the formation of insoluble aggregates. Biéri et al. (2004) reported the presence of a membrane-associated and salt-sensitive MLA1 pool in barley. However the solubility of the MLA_{CC}-PC2 was not improved when extracted with a buffer containing either 50 mM or 250 mM NaCl (data not shown). Similarly, various non-denaturing detergents (NP-40, Tween 20, CHAPS, DDM, triton and digitonin) at concentration 0.1% or 1% did not improve the extraction efficiency (examples in Figure S3-2.C). In contrast, addition of 0.1% but not 0.01% SDS significantly increased the extraction efficiency (Figure S3-2.C-D). These observations may suggest an aggregation behaviour rather than an association to membranes. Thus, I used 0.1% SDS in the extraction buffer.

To improve the efficiency of the final elution step, the elution efficiency of the standard desthiobiotin-containing buffer was compared to that of the same buffer containing 2% SDS. The amount of bait protein obtained after elution with 2% SDS was higher than with desthiobiotin. However, MS analysis of the elution fractions revealed that the signal-to-noise ratio of the SDS-eluted sample was lower than that of the desthiobiotin-eluted sample. Thus, I selected the standard desthiobiotin-containing elution buffer to conduct the TAP.

To reduce the loss of material caused by the protein precipitation step following the final elution, the eluates were directly used for the subsequent steps (reduction, alkylation, digestion and MS) without precipitation.

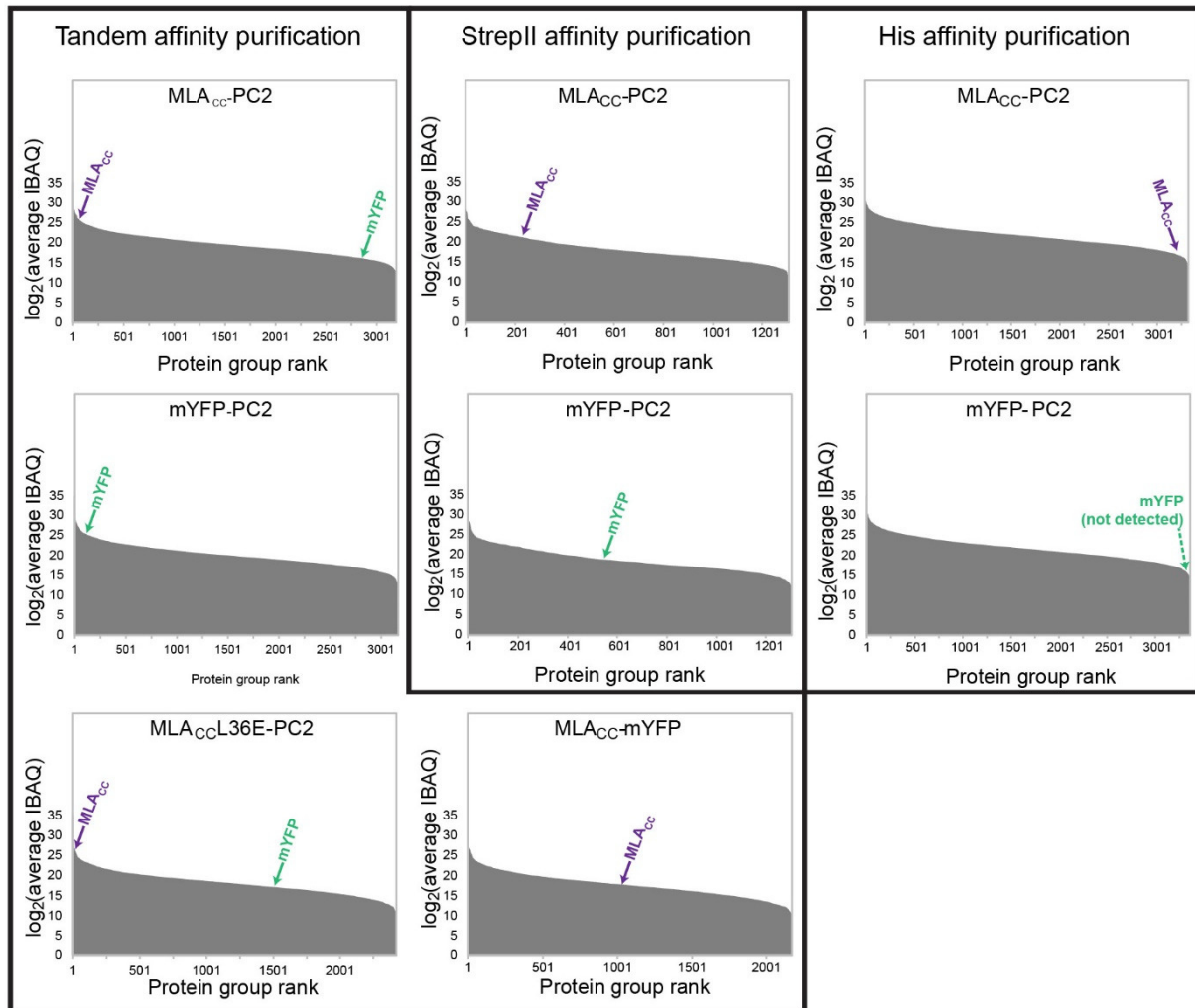


Figure 3-4: Abundance-based ranking of the proteins identified in the different pull downs. The proteins identified in tandem affinity, StrepII and histidine (His) pull downs are ranked according to their average iBAQ (intensity-based absolute quantification). The ranks of the pulled down proteins are indicated by arrows. One biological replicate was performed for the His pull downs and at least three independent biological replicates for all the other pull downs.

Finally, I also tested single step purifications with either of the 8xHis or the StrepII tag following a protocol similar to the TAP and down-scaling the procedure for 2 g (FW) of starting material. The analysis of three replicates obtained by purification based on the StrepII tag and using the mYFP-PC2 bait as a control did not yield any candidate interactor (data not shown). Overall, MS analysis of the resulting eluates showed a signal-to-noise ratio largely below that of the TAP, indicating that the TAP is more efficient than single step affinity purifications (Figure 3-4).

3.3.2.2. Processing of the TAP samples

The modified TAP protocol (described in Section 3.3.2.1) was employed to prepare at least three independent biological replicates for each bait (Table 3-5).

Table 3-5: Summary of the samples processed by TAP and analysed by MS.

Bait	Type	Replicates	
		Performed	Included in the final analysis
MLACC-PC2	sample	6	5
mYFP-PC2	control	4	3
MLACCL36E-PC2	control	3	1
MLACC-mYFP	control	3	1
Total		16	10

Due to time constraints, only the sample and control lines from the primary set of transgenic lines were used for the TAP analysis (described in Figure 3-2.A). This includes the lines expressing the MLACC-PC2 bait (sample) along with three control lines. A first control line expressing the mYFP-PC2 was used to identify the proteins which are non-specifically purified by the TAP procedure. A second control line expressing the MLACCL36E-PC2, a non-functional MLACC variant due to the loss of homodimer formation (Maekawa et al., 2011b), was used to remove the interactors co-purified with the MLACC but whose association does not correlate with the MLACC homodimerization. Finally, the third control line included expresses the MLACC-mYFP without TAP tag. As MLACC-mYFP induces a cell death response similar to MLACC-PC2, this control was used to subtract unspecific proteins which are co-purified in a cell-death-dependent manner.

Detection of the bait protein by immunoblot analysis suggested that the TAP procedure consistently enriched the three bait proteins (MLACC-PC2, mYFP-PC2, and MLACCL36E-PC2) (Figure 3-5). Thus, by comparing the MLACC sample to these controls across multiple TAP replications, proteins enriched in the MLACC-PC2 pull downs should be considered as high-confidence candidates.

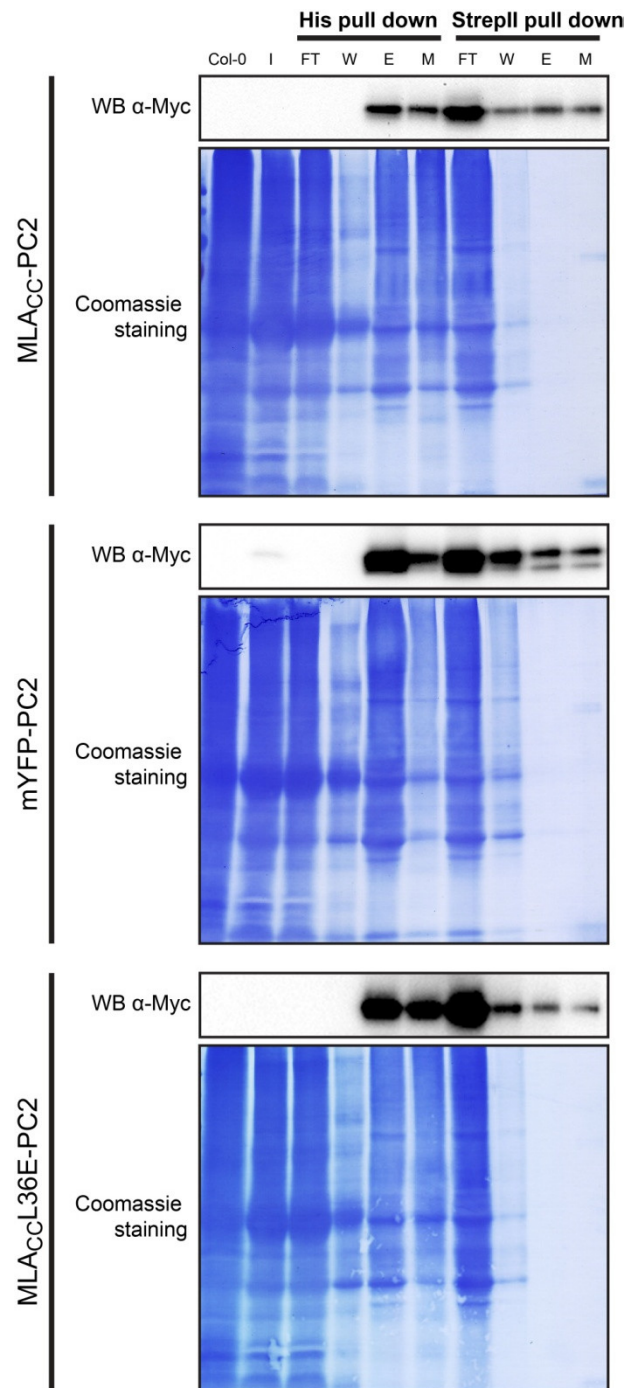


Figure 3-5: Immunoblot analyses of tandem affinity-purified plant extracts expressing MLAcc-PC2, mYFP-PC2 and MLAccL36E-PC2. I, input; FT, flow through; W, wash; E, eluate; M, matrix.

3.3.2.3. Analysis of the pull down input fractions for quality control and investigation of the proteome-wide MLACC-dependent responses

To examine the global protein expression patterns of the input materials, a shotgun MS analysis was performed. In total, ~4,300 protein groups were identified in the 16 input samples.

To assess the overall variability in protein abundance among input samples, I performed a clustering analysis based on the abundance (measured as label free quantification [LFQ] intensities) of all protein groups identified in the input samples (Figure S3-3.A). This analysis indicates a high variation among samples as well as among replicates. A batch effect appeared to account to a large extent for the observed variation, since replicates prepared and analysed at the same time tend to cluster together (Figure S3-3.A-B).

Pairwise comparison of the input samples also indicates that a batch effect would account for the variation (highlighted in yellow, Figure S3-4.A-B).

This proteomic data was further analysed to identify the proteins differentially regulated upon MLACC-PC2 expression. For this, I compared the input samples of MLACC-PC2 pull down with the input samples of mYFP-PC2 pull down. To minimize the batch effects, the analysis was limited to the 4 pairs of MLACC-PC2/mYFP-PC2 samples which were processed together. Analysis of the LFQ intensities between the MLACC-PC2 and the mYFP-PC2 inputs identified 747 differentially expressed protein groups (DEPGs) (average fold change >2). 491 and 256 DEPGs were enriched, respectively depleted, in the MLACC-PC2 line compared to the mYFP-PC2 line. Gene ontology (GO) term enrichment analysis did not identify any GO term significantly enriched in either sets of proteins upregulated or downregulated (AgriGO, <http://bioinfo.cau.edu.cn/agriGO/>). Based on a volcano plot representing the LFQ fold change (FC) *p*-value against the average LFQ FC for each protein group, I selected the top four downregulated DEPGs and the top twelve upregulated DEPGs in the MLACC-PC2 line compared to the mYFP-PC2 line (Figure 3-6, Table S3-1). Among the top 12 protein groups upregulated in the MLACC-PC2 line, several proteins are induced upon pathogen challenge (e.g. AT1G33960 [AIG1] and AT2G28830 [PUB12]).

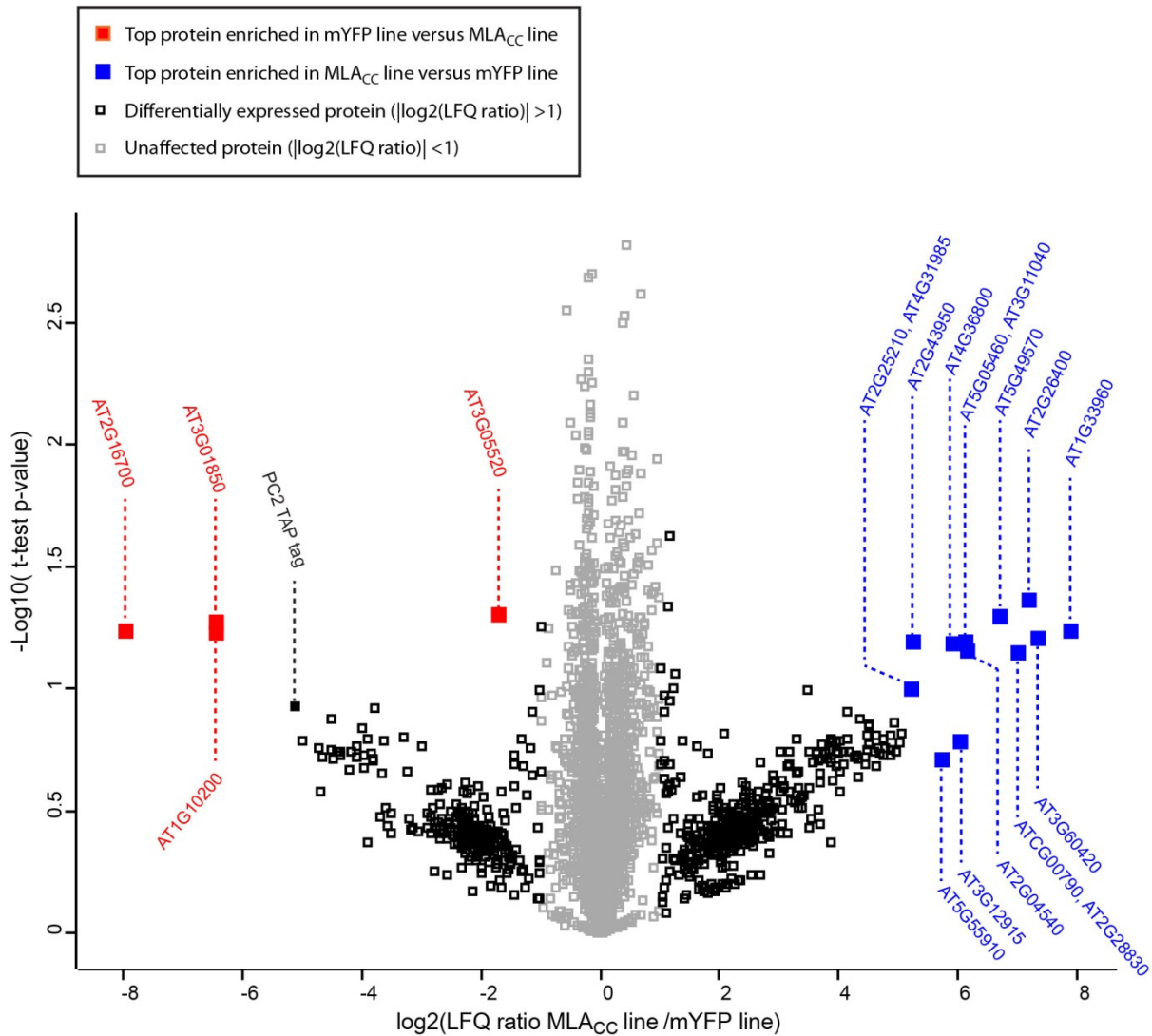


Figure 3-6: Volcano plot of the protein groups identified in the TAP input samples of the MLA_{CC} line and the mYFP line. The average LFQ ratio of the MLA_{CC} line against the control mYFP line for each protein group is plotted against the t-test p -value of the same ratio. NaN values were replaced by 14.

I compared this data to the transcriptome analysis performed on the *DEXp:MLA_{CC}-mYFP* line (Results section 1.3.1). This comparison is somewhat limited due to the use of a different system at different time points. A tight correlation between proteomic data and transcriptome data can not be expected as a result of posttranscriptional regulation. Such assumption has been already confirmed by comparing RNA-seq data to proteomic data in various organisms. However such comparative analysis can still be very informative to study the protein output in a given response and highlight possible post-transcriptional regulations (Payne, 2015). Considering the low number of DEPGs compared to the high number of differentially expressed genes (DEGs) identified by transcriptome analysis, there are at least large quantitative differences between the two data sets. 2D plots of the two datasets indicated no

significant correlation between transcriptomic data and proteomic data (data not shown). Out of the 747 DEPGs identified, 148 show a similar regulation at the transcript level in the transcriptomic analysis of the *DEXp:MLA_{CC}-mYFP* line (at least two fold increase or decrease compared to the mYFP control line, based on the average FC at 2, 4, 6 and 8 hpi, examples shown in Table S3-2).

3.3.3. Quantitative MS data analysis of the pull downs leads to the identification of a MLA_{CC} candidate interactor list

3.3.3.1. Quantitative MS data analysis and identification of MLA_{CC} interactor candidates

TAP eluate fractions from all the pull downs were analysed by MS. Approximately 3,200 protein groups were identified in total. The first replicate pair of MLA_{CC}-PC2 / mYFP-PC2 pull down was largely different from all the other replicates and was therefore not included in the final analysis (Table 3-5, Figure S3-3.C and Figure 3-7.A).

The MLA_{CC} or the mYFP bait proteins were identified as one of the most abundant proteins in the respective samples confirming the efficiency of the pull down (Figure 3-4). Moreover the bait proteins were not identified or only in trace amounts in the samples where they were not expressed or not pulled down, which rules out the possibility of significant cross-contamination among samples and indicates that the false discovery rate was low.

Similarly to the input fractions, the TAP samples were clustered by time of preparation, indicating that most of the variation among samples was due to batch effects (Figure S3-3.B-C).

Ten protein groups were identified in the MLA_{CC}-PC2 pull down but not in the negative controls (Figure 3-7.B and Table 3-6). However, these were detected in two replicates out of five, indicating that they were not reproducibly enriched throughout the five MLA_{CC}-PC2 pull down replicates. It is noteworthy that two protein groups have been reported as recurrent pull down false positive (De Jaeger et al. personal communication).

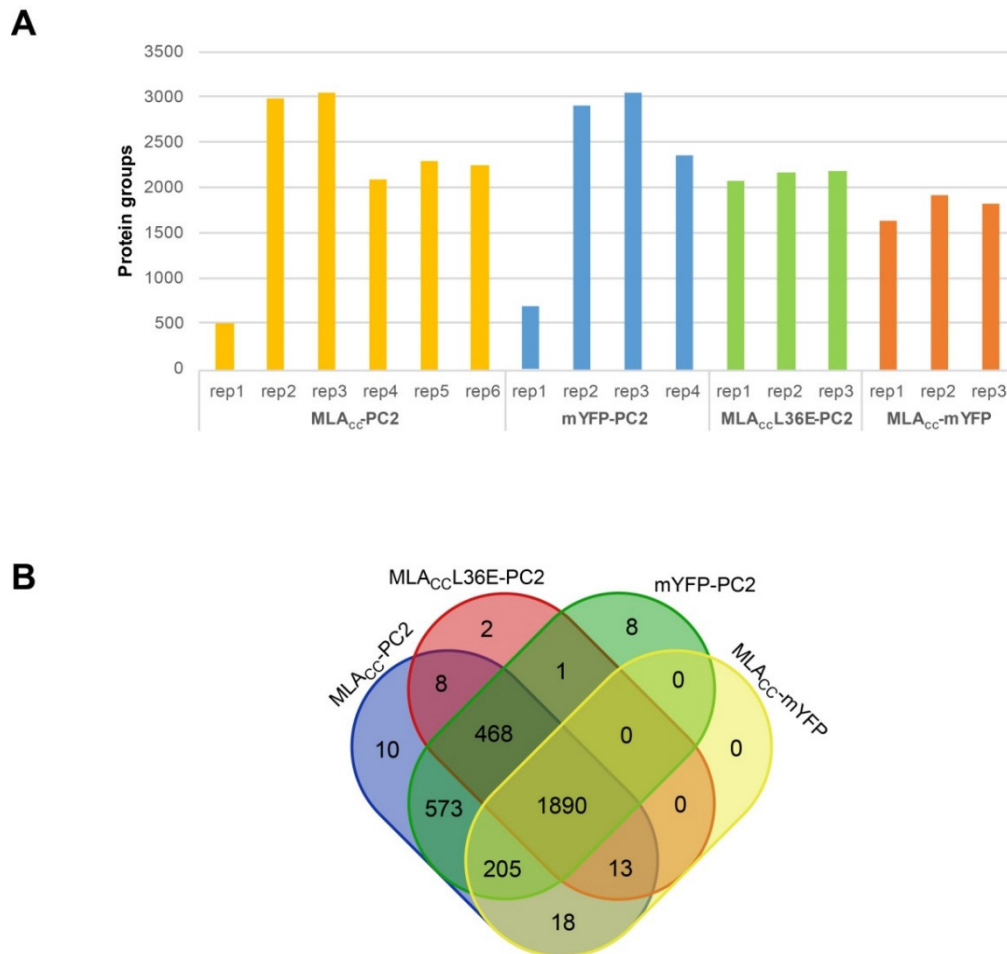
Chapter 3. Identification of the MLA_{cc}-associated signalling partners in *A. thaliana*

Figure 3-7: Overview of the protein groups identified by MS analysis in the TAP samples. A, number of protein groups identified in each sample. rep, replicate. B, four-set Venn diagram comparing the protein groups identified in each pull down.

Table 3-6: Protein groups identified by MS analysis exclusively in the MLA_{cc}-PC2 pull down fractions but not in the pull down controls.

ID	Pept.	Cov. (%)	Number of identifications in 5 MLA _{cc} pull down replicates	Description
AT3G53130	1	3.7	2	LUT1, CYP97C1, Cytochrome P450 superfamily
AT1G60850#	1	4.3	2	ATRPAC42, DNA-directed RNA polymerase family
AT3G26520	1	7.1	2	TIP2, SITIP, tonoplast intrinsic protein 2
AT3G09150	1	3.6	2	HY2, phytochromobilin:ferredoxin oxidoreductase
AT3G54150	4	10.8	2	S-adenosyl-L-methionine-dep. methyltransferases
AT3G12680	1	2.5	2	HUA1, floral homeotic protein (HUA1)
AT3G55400	1	2.4	2	OVA1, methionyl-tRNA synthetase
AT1G09770	1	1.9	2	ATCDC5, CDC5, ATMYBCDC5, cell division cycle 5
AT5G13030#	2	4.1	2	unknown protein
AT1G06060	1	7	2	LisH and RanBPM domains containing protein

#, identified as recurrent false positive by De Jaeger et al. (personal communication)

Pept., number of matching peptides

Cov., protein coverage

I performed a quantitative analysis based on LFQ intensities to identify protein groups significantly enriched in MLACC-PC2 pull down compared to the control pull downs. To limit the batch effects, I performed a pairwise analysis of the MLACC-PC2 and the control pull downs processed side by side. Five pairs of sample/control pull downs were used for the downstream analysis (Table 3-5, Figure S3-3.B-C). These include three MLACC-PC2/mYFP-PC2 pull down pairs, one MLACC-PC2/MLACC-mYFP pull down pairs and one MLACC-PC2/MLACCL36E-PC2 pull down pair.

Nine protein groups with a high fold enrichment (>2) and a high fold enrichment *p*-value segregate from the majority of proteins identified (Figure 3-8, Table 3-7, Table S3-3). Thus, these nine protein groups constitute the top MLACC candidate interactors. Eight protein groups matched each a unique protein whilst the protein group containing AT5G54640 ambiguously matched eight proteins of the histone family (Table 3-7). The fold enrichment of the candidate interactors was clearly lower than the fold enrichment of the pulled down MLACC-PC2 protein (Figure 3-8). Therefore I could not conclude about the stoichiometry of the candidate interactions between MLACC and the nine candidate interactors identified and this suggests that the potential interactions identified are weak.

Table 3-7: MLACC candidate interactors identified by MS analysis of MLACC pull down. The candidate interactors were isolated based on their fold enrichment in the MLACC pull down versus control pull downs and on the statistical significance of the fold enrichment (t-test *p*-value). The fold enrichment was also normalized to the fold enrichment measured in the pull down input fractions (input-corrected average log₂ (LFQ ratio MLACC-PC2/controls)).

Protein group ID	Pept.	Cov. (%)	-Log ₁₀ (p-value)	Average log ₂ (LFQ ratio)		Other Proteins and Description
				Raw	Input-corrected	
AT1G79600	1	1.8	1.78	3.97	N.D	Protein kinase AT4G27230; AT3G20670; AT1G51060; AT1G54690; AT1G08880; AT5G59870; AT5G27670; H2A.1, H2A.2, H2A.13, H2A.10, H2A.X, H2A.XA, H2A.6, H2A.7;
AT5G54640#	2	17.7	1.15	3.93	N.A	histones
AT5G11420#	6	13.9	1.07	3.53	3.70	Putative transmembrane protein, DUF642
AT5G45190	7	18.7	1.01	3.11	N.D	Cyclin family protein
AT2G22400	3	4.8	1.00	2.83	2.36	S-adenosyl-L-methionine-dependent methyltransferase
AT5G51750	7	14	1.08	1.90	2.04	SBT1.3; subtilase 1.3
AT2G26560	11	36.1	1.61	1.28	0.83	PLA2A; phospholipase A2 A
AT3G48090	10	18	1.30	1.10	0.25	EDS1; enhanced disease susceptibility
AT2G19800	6	22.4	1.27	1.06	0.61	MIOX2; myo-inositol oxygenase 2

#, identified as recurrent false positive by De Jaeger et al. (personal communication)

Pept., number of matching peptides.

Cov., protein coverage

N.D, not detected in the input fraction

N.A, not available due to identification of partially dissimilar protein groups in the input fraction

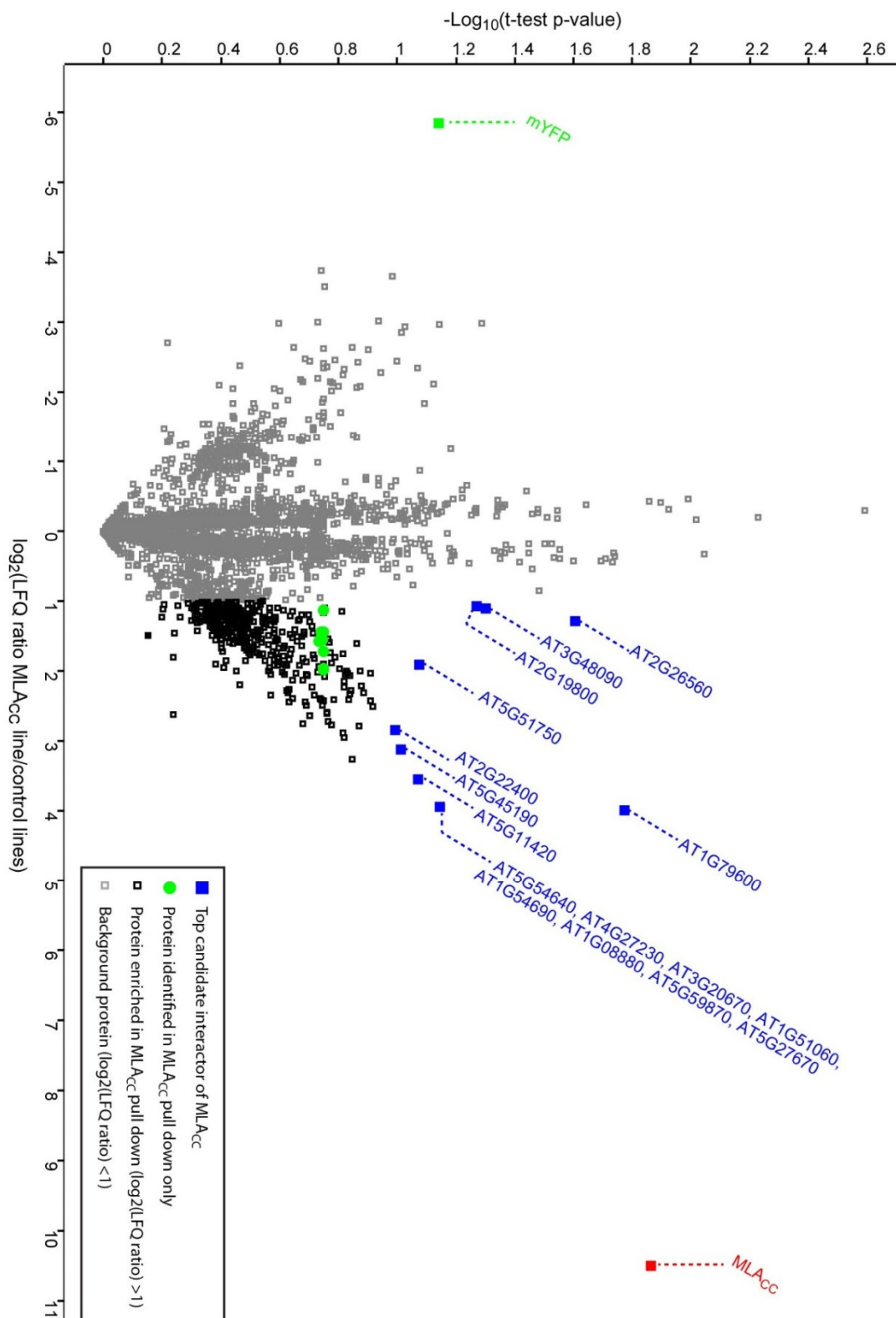


Figure 3-8: Volcano plot of the protein groups identified by MS analysis in MLAcc-PC2 pull down versus the control pull downs. The fold enrichment p -value of each protein group is plotted against the average fold enrichment (LFQ ratio) of the MLAcc pull down against the control pull downs. NaN values were replaced by 14.

Since the protein abundance in the input material might influence the abundance in the pull down fraction, I normalized, when possible, the fold difference observed in the pull down samples by the fold difference in the input fractions (input-corrected average \log_2 [LFQ ratio MLACC-PC2/controls], Table 3-7). After normalization, the fold enrichment of AT2G26560, AT3G48090 and AT2G19800 fell below two whereas it remained globally unchanged for AT5G11420, AT2G22400 and AT5G51750. AT1G79600 and AT5G54190 were not detectable in the input fractions. Thus, this analysis supports the identification of five candidates out of nine.

Abundance-based ranking of the protein groups detected in the pull downs indicates that seven MLACC candidate interactors have an increased relative abundance in the MLACC pull down compared to the control pull downs whilst two candidates (AT5G11420 and AT5G45190) don't (Figure 3-9). Several candidates were detected in the pull down fractions at a low abundance indicating that they are close to the detection limit. Under such conditions, the risk of false positive identification might also be increased due to a possible stochastic detection rate among samples. This observation is particularly relevant for candidates AT1G79600, AT5G45190 and AT2G22400 (Figure 3-9, Table S3-3) which were close to the detection limit in the pull down fractions.

I looked into the online databases whether some functional correlation exists between the nine candidates identified, as a hint for proteins belonging to the same complex or the same pathway. I did not find evidence for direct physical interaction between the candidates identified. Co-expression analysis by EdgeAnnotation (atted.jp) indicates that the MLACC candidate interactors are not strongly co-expressed (Table S3-4).

As a conclusion, this analysis identified nine MLACC candidate interactors with various levels of confidence. These might interact directly with the MLACC or be co-purified within a complex associated to the MLACC. At this level, the candidates still need to be validated by orthogonal methods such as co-immunoprecipitation, yeast two hybrid, or bimolecular fluorescence complementation.

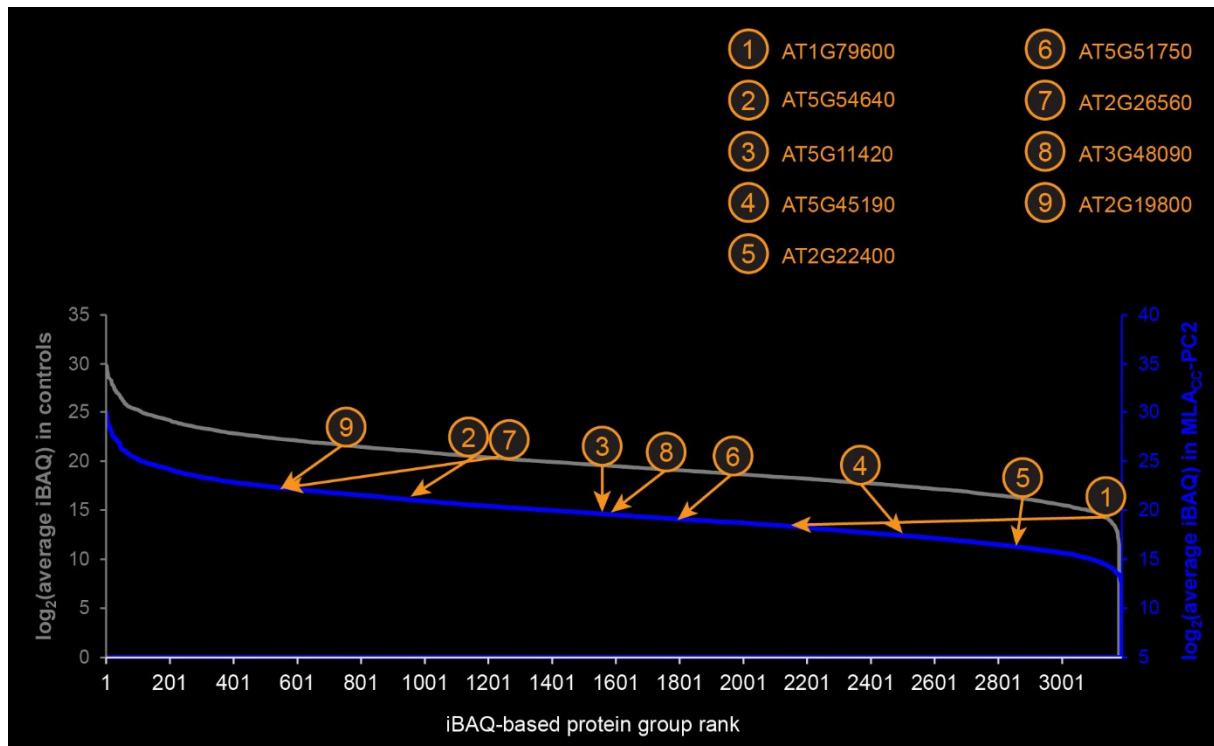


Figure 3-9: Abundance-based ranking of the protein groups confirms the enrichment of several candidate interactors in the MLACC pull down compared to the control pull downs. Protein groups identified by MS analysis of MLACC and control pull downs were ranked based on their average abundance (iBAQ). Ranks of the identified candidate MLACC interactors are indicated by orange arrows (rank in control pull downs: arrow tail; rank in MLACC pull down: arrow head).

3.3.3.2. Assessment of the biological relevance of the MLACC candidate interactors by data mining

The TAP analysis resulted in the identification of nine protein groups as candidate MLACC-interactors. In order to identify which candidates are the most biologically relevant, data mining was performed to gather evidence about a possible functional link between the candidates and the regulation of immunity or cell death. Five candidate interactors have been functionally characterized (AT1G79600, AT5G54640 group, AT2G26560, AT3G48090 and AT2G19800). Two of them (PLA2A, AT2G26560 and EDS1, AT3G48090) are involved in defence or cell death regulation. EDS1 is a regulatory hub involved in basal and NLR-mediated immunity (Wiermer et al., 2005). PLA2A is a pathogen-inducible cytoplasmic lipid acyl hydrolase belonging to the patatin-like family and has been shown to positively contribute to cell death induced by paraquat or avirulent *Pseudomonas syringae* pv. *tomato*

(*Pst*) AvrRpt2, as well as to susceptibility to the necrotrophic fungus *Botrytis cinerea* and to avirulent *Pst* AvrRpt2, and final, to resistance to the *Cucumber mosaic virus* (Camera et al., 2009; La Camera et al., 2005). PLA2A also positively regulates necrotic symptoms of the lesion-mimic mutant *vad1* and lipid-induced cell death in trichomes (La Camera et al 2009, Reina-Pinto 2009).

To gain insights into the function of the four uncharacterized candidate interactors, online databases were screened for functional annotations (Thalmine), physical interactions (BioGRID, Intact) and co-expression data (atted.jp, Ath-m.c4-1). I did not find any relevant protein-protein interaction. Then, I examined the five most co-expressed genes for each candidate. Co-expression data indicates that AT2G22400 is co-expressed with powdery mildew resistant 5 (At5g58600).

The transcriptional regulation of the candidates identified was also examined in the context of the MLA_{CC} expression in *A. thaliana* Col-0 (Result section 1.3.1, Figure 3-10). AT2G26560 (PLA2A) and AT3G48090 (EDS1) were particularly strongly and early induced upon MLA_{CC} expression, suggesting a possible role in the MLA_{CC}-mediated response. AT1G79600 was induced at later time points whereas AT5G11420 and AT5G51750 were downregulated at later time points.

The presence of orthologues in species outside of the Brassicaceae was used to narrow down the candidate list since the MLA function is conserved in different plant genera. This implies that MLA_{CC} interacts with evolutionarily conserved signalling components. I searched for orthologues of the nine candidates outside of the Brassicaceae family. Orthologue search in Phytozome v10.3 identified possible orthologues/paralogues for all of the nine candidates (Table S3-5).

Integration of all these data highlights AT1G79600 and AT2G26560 as the two best candidates for further analysis.

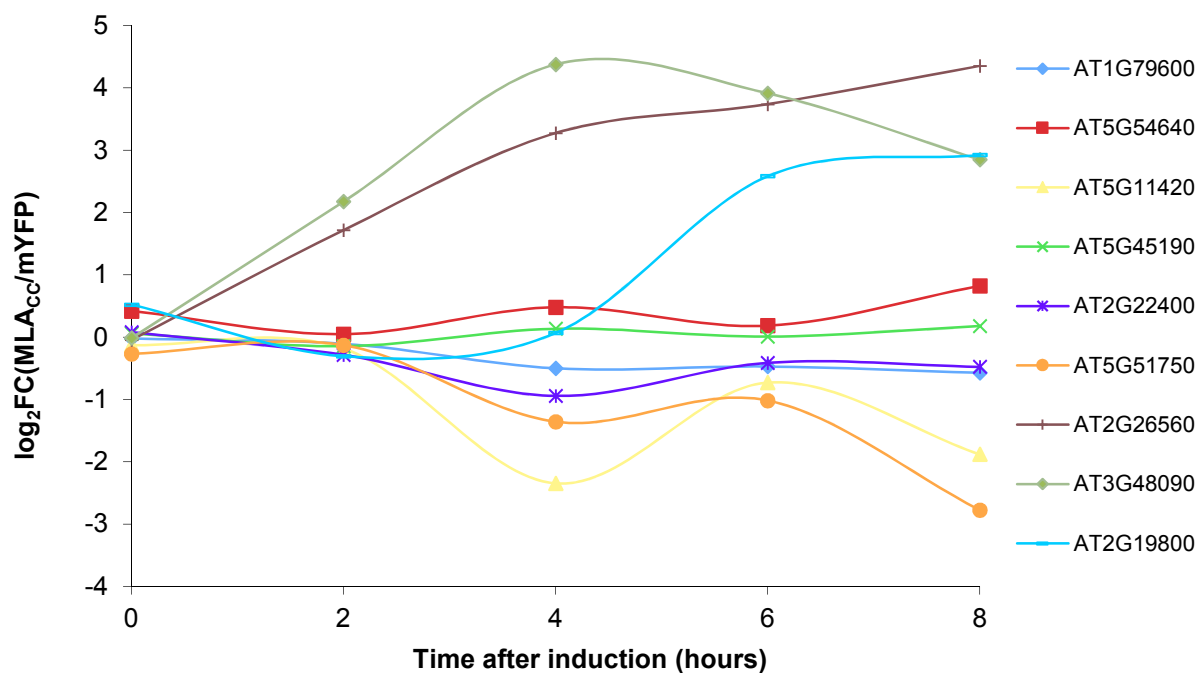


Figure 3-10: Expression profile of the MLACC candidate interactors in *A. thaliana* upon MLACC expression. The gene expression was monitored by RNA-seq over a time course upon MLACC expression after DEX treatment. The relative expression of the *DEXp:MLACC-mYFP* line as compared to the *DEXp:mYFP* line is expressed as a \log_2 -transformed cpm fold change (\log_2FC).

3.3.3.3. Preliminary data for the functional characterization of PLA2A

Phospholipase A2 A (PLA2A, AT2G26560) has been identified as one of the best candidate MLACC interactors. I investigated the role of PLA2A in MLACC-mediated cell death in *A. thaliana*. I used aristolochic acid (ARA) and bromoenol lactone (BEL) to inhibit PLA2A activity and examined the impact on MLACC-mediated ion leakage in *A. thaliana*. These two chemical have been shown to inhibit lipid-induced cell death in trichomes (Reina-Pinto et al., 2009). A *DEXp:MLACC-mYFP* line (Chapter 1) was used for this analysis. No significant difference in MLACC-mediated ion leakage was observed in presence of either ARA or BEL compared to the mock control (Figure 3-11). The slight increase with BEL and ARA treatment is likely due to an MLACC-independent effect because controls treated with BEL and ARA in absence of MLACC expression display a similar increase compared to the untreated control. This result suggests that PLA2A phospholipase activity is dispensable for MLACC-induced ion leakage. However, a role of PLA2A in cell death-independent MLACC-mediated response cannot be excluded. Further analysis is required to determine whether the chemical treatment applied in the conditions tested effectively inhibits the PLA2A activity.

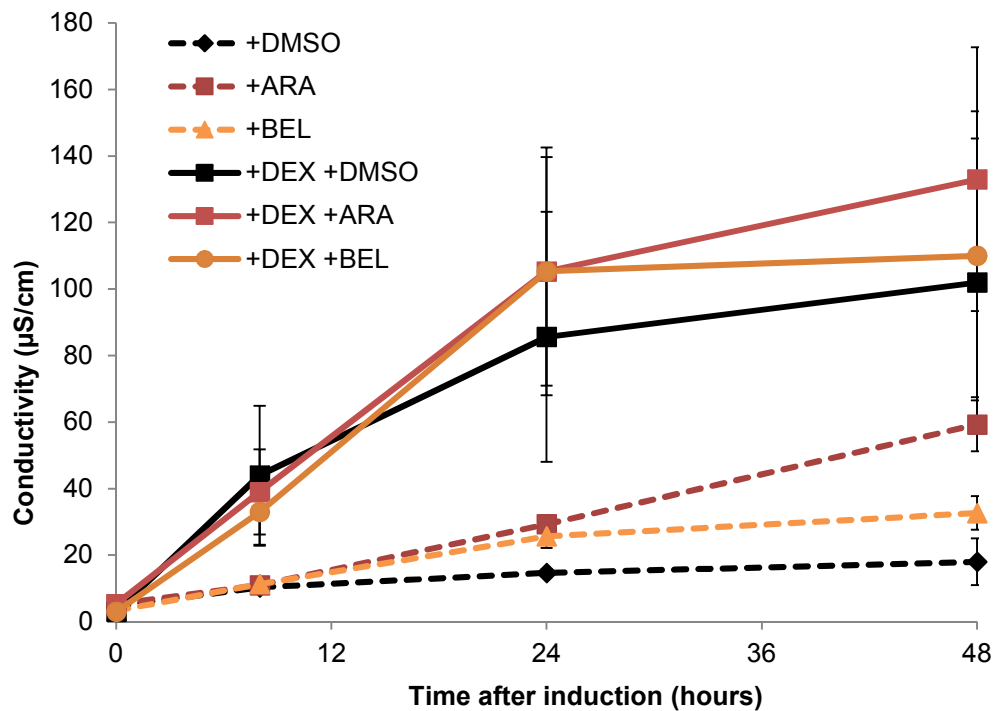


Figure 3-11: Effects of PLA2A inhibitors on MLACC-mediated cell death. Cell death was monitored by ion leakage measurement in *A. thaliana* stable transgenic lines expressing *DEXp:MLACC-mYFP* under treatment with dexamethasone and either of the two PLA2A inhibitors aristolochic acid (ARA) and bromoenol lactone (BEL) at 0, 8, 24 and 48 hpi. The results presented here correspond to one experiment. The experiment was repeated two times with similar results. Error bars indicate standard deviation of the three biological replicates measured in one experiment.

3.3.4. MLACC might reside within large SDS-resistant protein polymers

By analogy to the inflammasomes formed by NLRs in animals, plant NLRs might assemble into large higher order molecular complexes. Recently, Hu et al., (2013) provided molecular insights into the self-propagation properties of the NAIP-NLRC4 inflammasome. In their model, following nucleation by NAIP, a NLRC4 complex is formed which can self-propagate in a manner similar to prion proteins. This finding, and the fact that non-denaturing detergents are failing to solubilize the MLACC, prompted me to test whether MLACC associates into prion-like complexes in *A. thaliana*. Semi-denaturing detergent agarose gel electrophoresis (SDD-AGE), a technique commonly used to detect large SDS-resistant protein polymers, suggested that MLACC was predominantly present in SDS-resistant high molecular weight complexes contrary to the mYFP control (Figure 3-12). So far, the nature of this aggregate remains unknown.

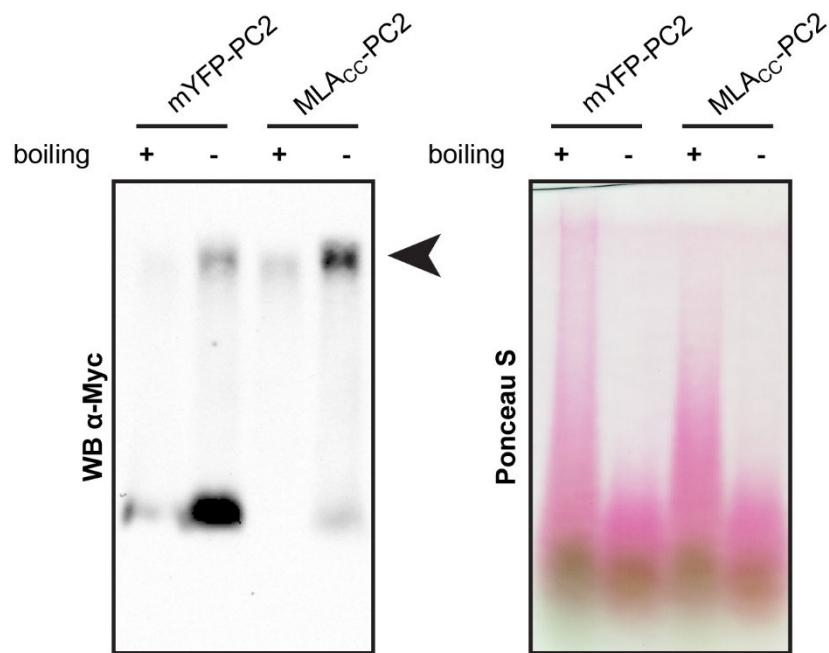


Figure 3-12: MLACC predominantly resides in large SDS-resistant protein complexes. SDD-AGE was performed on plant material identical to the one used for affinity purification. Left panel, immuno-detection of the protein blot with an antibody α -Myc. Right panel, proteins staining with Ponceau S. Arrowhead, MLACC high molecular weight complex. The picture shown is representative from three independent experiments.

Discussion

1. MLA_{CC} induces effector-triggered immunity-like responses in *A. thaliana*

In this study, I report that the coiled-coil domain of the barley NLR MLA, denoted MLA_{CC} , triggers a rapid cell death, MAPK activation, and immune transcriptional reprogramming in stable *A. thaliana* transgenic lines. These findings all support the hypothesis that MLA_{CC} is a signalling module sufficient to trigger effector-triggered immunity (ETI)-like responses. Since the transcriptional reprogramming can be detected prior to cell death and a similar transcriptional profile is induced during the temperature-dependent RPS4-mediated response in the absence of cell death (Heidrich et al., 2013), the early transcriptional reprogramming occurs upstream or independently of cell death. Two reports indicate that *de novo* protein synthesis is required for Fumonisin B-1- and H_2O_2 -mediated cell death in *A. thaliana* and soybean, respectively (Asai et al., 2000; Solomon et al., 1999). Thus, a subset of the cell death responses might be transcriptionally controlled. Interestingly, the cytoplasmic pool of MLA_{CC} is required for cell death induction (Bai et al., 2012). This result suggests that MLA_{CC} -mediated cell death signalling might be initiated in the cytosol, but does not exclude the possibility that MLA_{CC} -mediated cell death is transcriptionally controlled, since the signal initiated in the cytosol might be transduced to the nucleus. The only straight-forward approach to test whether MLA_{CC} -mediated cell death requires specific gene regulation is to inhibit *de novo* protein synthesis using chemicals such as cycloheximide (CHX). Since CHX would inhibit the expression of the *DEXp:MLA_{CC}* transgene, this approach is unsuitable with the DEX-inducible transgenic lines generated in this study. NLR-mediated host cell death responses can be uncoupled from NLR-mediated pathogen growth restriction (Bai et al., 2012; Bendahmane et al., 1999; Chang et al., 2013; Coll et al., 2010; Yu et al., 1998, 2000). Therefore, disease resistance and cell death are controlled by independent pathways. This functional property has been demonstrated in the case of full-length MLA, whose nuclear pool is required for disease resistance whilst the cytosolic pool is required for cell death induction (Bai et al., 2012; Shen et al., 2007). Whether MLA_{CC} also initiates a similar bifurcated signalling mechanism remains to be determined.

Chang et al. (2013) have shown that MLA_{CC} antagonizes *HvWRKY1* repression of *HvMYB6*, thereby promoting *HvMYB6*-mediated transcriptional activation by transient expression in *A. thaliana* protoplasts. *In vitro* and *in planta* analyses further showed that *HvWRKY1* induces

HvMYB6 dissociation from DNA and that the MLA_{CC} domain competes with *HvWRKY1* for the interaction with *HvMYB6* (Chang et al., 2013). These findings imply that MLA_{CC} regulates gene expression by interacting with some TFs. Consistently with the proposed function of the MLA_{CC} in transcription regulation, my results confirmed in a stable expression system in *A. thaliana* that MLA_{CC} regulates gene expression, and suggest that MLA_{CC} interacts with 31 *A. thaliana* TFs in yeast two-hybrid. Importantly, my results does not provide clues about the functional relevance of the above-mentioned MLA_{CC} -TF direct interactions since there is no *HvMYB6* homologue in *A. thaliana*, and the motifs enriched in the 5' regulatory sequences of the potential direct target genes of MLA_{CC} -mediated signalling are not related with the 31 *A. thaliana* TFs interacting with MLA_{CC} in yeast two-hybrid or MYB TFs. Instead, my data suggest that Ca^{2+} /CAMTA-mediated signalling plays a central role in the MLA_{CC} -mediated immediate early transcriptional response. However, one can hypothesize that MLA_{CC} initiates a bifurcated signalling and that direct interaction with TFs represents only one of the signalling mechanisms initiated in parallel. In *A. thaliana*, the interaction with an *HvMYB6* homolog does not occur but other interacting TFs could account for part of the MLA_{CC} -mediated transcriptional regulation.

Some other aspects of the MLA_{CC} -mediated responses are similar to the ETI. $LaCl_3$, a calcium channel blocker, fully abolishes cell death mediated by RPM1 and RPS2 (Grant et al., 2000; Pike et al., 2005). Similarly, MLA_{CC} -mediated cell death is completely suppressed by $LaCl_3$ treatment. This suggests that extracellular calcium influx is required for the HR induced by MLA_{CC} and several other CNLs. DPI, a NADPH oxidase inhibitor, affects moderately or not at all the HR induced by the CNL RPM1 or some HR elicitors (Andersson et al., 2006; Binet et al., 2001; Wei Ning, 2004). Similarly, MLA_{CC} -mediated cell death is not suppressed by DPI. Thus, NADPH oxidase-mediated ROS production is not required for the HR mediated by MLA_{CC} , RPM1, and several HR elicitors. However, I observed that, even at low concentration, DPI has a toxic effect on plant cells and such effect has been reported before in tobacco cells (Binet et al., 2001). Another common feature between MLA_{CC} -mediated responses and ETI is their robustness. The MLA_{CC} -mediated response was not influenced by changes in sucrose supply or day length. *PEN2*, *PAD4*, *SAG101*, *DDE2*, *EIN2*, and *SID2* are together at least partially dispensable for MLA_{CC} activity. The same genetic dispensability has been shown for full-length *MLA1* in *A. thaliana* (Maekawa et al., 2012).

The MLA_{CC}-mediated response was partially suppressed at higher growth temperature (28°C) compared to 19°C (weaker leaf chlorosis). The response induced by the constitutively active TNLs RPP4(S389P), 35S:RPS4, and SNC1 in *bon1-1* plants are fully suppressed at higher temperature (Heidrich et al., 2013; Huang et al., 2010; Yang and Hua, 2004). On the contrary, the response triggered by the constitutively active CNL SUMM2 in *mekk1* plants is only partially suppressed at higher temperature (Ichimura et al., 2006; Zhang et al., 2012). Therefore, temperature sensitivity is a common feature between NLR-mediated responses and MLA_{CC}-mediated responses.

MLA_{CC} signalling activity appears to require the same amino acid residues which are critical for the function of full-length MLA. Several substitutions predicted to disrupt the MLA_{CC} homodimer, such as I33E and L36E, impair resistance and cell death mediated by full-length MLA10 (Maekawa et al., 2011b). The same mutations also impair MLA_{CC} cell death-inducing activity in transient gene expression assays (Bai et al., 2012; Maekawa et al., 2011b). Here I show in a stable expression system in *A. thaliana* that the I33E and L36E substitutions also impair MLA_{CC} cell death activity. Therefore, homodimer formation is likely required for MLA_{CC} cell death inducing activity in *A. thaliana*. It will be interesting to test whether the same substitutions impair MLA_{CC}-mediated transcriptional regulation by transcriptome profiling of the response induced by the corresponding MLA_{CC} substitution variants in *A. thaliana*. The cell death responses induced by the autoactive full-length MLA_{MHD} and MLA_{CC} in *A. thaliana* are very similar to each other. The transcriptional response mediated by MLA_{MHD} in *A. thaliana* will be investigated in future experimentation to determine possible differences compared to the MLA_{CC}-mediated response.

Different *MLA* resistance alleles have different requirements for the three components of the heteromeric HSP90-RAR1-SGT1 complex (Bieri et al., 2004; Halterman and Wise, 2004; Hein et al., 2005; Shen et al., 2003). I aimed at investigating the genetic requirement of MLA_{CC} for the components of the HSP90 complex. Such genetic analysis in *A. thaliana* is challenging. There are four *A. thaliana* genes encoding partially redundant cytosolic HSP90s and multiple mutants are lethal. Thus, I could not analyse MLA_{CC} function in the context of a loss of HSP90 function. In *rar1* mutant plants, MLA_{CC}-mediated cell death is still detectable indicating that *RAR1* is at least partially dispensable for MLA_{CC} function. There are two copies of *AtSGT1*: SGT1A and SGT1B, and the *sgt1a sgt1b* double mutant is embryo lethal (Azevedo et al., 2002). However the *sgt1b* single mutation does suppress resistance and/or cell death mediated by a subset of NLRs such as RPP2 and RPP7 (Tör et al., 2002).

Therefore, I aimed at testing whether the *sgt1b* mutation impairs MLA_{CC}-mediated responses. However, lines expressing MLA_{CC} at detectable levels in *sgt1b* background could not be obtained.

The three major defence phytohormones (ET, JA, and SA) are dispensable for isolate-specific MLA1-specified disease resistance to *Bgh* isolates expressing *AVR_{AI}* in *A. thaliana* (Maekawa et al., 2012). In this study, I show that, similarly, transcriptional reprogramming and cell death mediated by the MLA_{CC} can occur in absence of ET, JA, and SA signalling in *A. thaliana*.

Mostly quantitative differences were observed in the response induced by MLA_{CC} in the wild-type background compared to the response in the defence phytohormone-depleted mutant (*ppsdes*) background. Since the MLA_{CC} protein accumulation was lower in the *ppsdes* mutant compared to wild-type, it is not possible to conclude whether the MLA_{CC} response is partially suppressed in the absence of SA, JA and ET. One of the most striking differences was the absence of MPK3 and MPK6 activation in *ppsdes* mutant plants. This implies that MPK3/6 activation is overall dispensable for cell death and transcriptional reprogramming mediated by MLA_{CC}.

The data presented in this thesis suggest that MLA_{CC} triggers a authentic ETI response. Other NLR domains such as the TIR domain of RPS4 and the NB domain of Rx similarly induce an HR-like response (Rairdan et al., 2008; Swiderski et al., 2009). Moreover, it is known that NLRs can form heteromeric complexes with other NLRs (Griebel et al., 2014). It has been proposed that, some parts of NLRs, when expressed alone, might interact with endogenous NLRs thereby triggering their activation resulting in an HR. In this scenario, the separate NLR parts which induce an HR would not have a signalling function *per se* and would activate endogenous NLRs. This hypothesis could explain the observed MLA_{CC} responses, and is difficult to fully refute. However, although I used several independent approaches to identify components involved in MLA_{CC}-mediated responses, no NLRs were identified either in the suppressor screen (Chapter 2) or as direct interaction partner (Chapter 3). Moreover, since *RARI* is dispensable for MLA_{CC}-mediated cell death in *A. thaliana*, MLA_{CC} activity does not seem to require *RARI*-dependent endogenous NLRs. On the other hand, an indirect mechanism for barley MLA_{CC}-induced immune responses through activation of *A. thaliana* full-length NLRs could be biologically relevant. An alternative model could be that, upon pathogen recognition, an activated NLR activates other NLRs by direct interaction and this interaction is part of a signal relay or amplification mechanism. In this scenario, activation of

NLRs by interaction with specific NLR domains such as the MLA_{CC} module might reflect a biologically relevant and evolutionarily conserved mechanism.

2. The early transcriptional responses during PTI, ETI and those mediated by MLA_{CC} and temperature-dependent RPS4 are largely overlapping

I showed by RNA-seq analysis that MLA_{CC} can induce a rapid transcriptional response in *A. thaliana* and that this response correlates with activation of defence-related genes. This is, to my knowledge, the first time-resolved transcriptomic analysis addressing a NLR-dependent early transcriptional response. Heidrich et al., (2013) reported the transcriptomic analysis of the temperature-conditioned response mediated by 35S:RPS4. However, in the absence of a wild-type control, the 35S:RPS4-specific changes cannot clearly be addressed.

An obvious question is whether MLA_{CC} can trigger gene expression changes like during ETI. To answer this, I compared the time-resolved MLA_{CC}-dependent transcriptional profiles with those of other immune-related responses in *A. thaliana*.

A qualitative comparison was first performed on a transcriptome-wide scale. The transcriptional profiles of MLA_{CC}-expressing plants are strongly correlated with those in temperature shift-induced RPS4-expressing plants. This was unexpected since RPS4 and MLA belong to two different NLR classes (TNL and CNL respectively). The transcriptional profiles of both MLA_{CC} and RPS4 inducible responses were strongly correlated with those of the early ETI responses mediated by MLA (CNL), RPM1 (CNL), RPS2 (CNL), and RPS4 (TNL) after activation by avirulent pathogens. This suggests that the transcriptional responses mediated by MLA_{CC} and 35S:RPS4 are very similar to those induced during the ETI. The expression pattern of several gene clusters differentially regulated during ETI or upon MLA_{CC} expression was similar in all tested ETI responses and upon MLA_{CC} expression, further confirming this hypothesis. On the other hand, it was unexpected to observe that the transcriptional responses triggered by MLA_{CC} and 35S:RPS4 were equally similar to the ETI triggered by CNLs and TNLs suggesting that the early transcriptional response mediated by CNLs and TNLs is not qualitatively different. It was also surprising to observe a high correlation between MLA_{CC}-mediated and RPM1- mediated responses since MLA_{CC} partly localizes in the nucleus and has been shown to regulate transcription by direct interaction with

transcription factors (Chang et al., 2013) whereas RPM1 is retained at the plasma membrane (Gao et al., 2011). This fact also questions the role of the direct TF-MLA_{CC} interaction in transcriptional reprogramming. The nuclear action of NLRs remains an enigma due to contradicting data. Another contradicting piece of data is that the CNLs Rx and I-2 seemingly bind directly to DNA (Fenyk et al., 2015, 2016). TNL- and CNL-mediated signalling have been shown to converge at the later stages (Eulgem et al., 2004), however my data suggest that this convergence also occurs at the early stages of the response, likely upstream of the transcriptional reprogramming.

A high correlation was also observed between the transcriptional profiles of MLA_{CC}- and temperature-induced 35S:RPS4-expressing plants in wild-type and RPM1- and RPS2-mediated responses in a background impaired for defence phytohormone signalling. This indicates that RPM1- and RPS2-mediated early transcriptional responses do not require the three major defence phytohormones similarly to the MLA_{CC}. Comparison with the early transcriptional profiles after P/MAMP or DAMP treatment indicates large qualitative similarities at early time points between ETI, ETI-like responses and PTI, implicating overlapping signalling mechanisms in ETI and PTI. Such overlap has been observed previously (Maleck et al., 2000; Navarro et al., 2004; Tao et al., 2003) but my results provide stronger evidence for convergence since I analysed the whole transcriptome at early time points in a dataset including several pathogen-free ETI-like responses. This study also allows me to conclude that transcriptional reprogramming in the ETI can occur in the absence of PTI, and therefore ETI does not rely on an amplification of the response initiated by PTI (Cui et al., 2015; Day and He, 2010; Garcia and Hirt, 2014; Vidhyasekaran, 2014). Furthermore, this excludes the possibility that the resemblance between PTI and ETI is due to the P/MAMP carried by both virulent and avirulent pathogens since both MLA_{CC}- and temperature-induced RPS4-mediated ETI-like responses occur in a pathogen-free context.

The qualitative comparison conducted here does not account for quantitative differences among the datasets. Despite the fact that they are qualitatively very similar to each other in terms of transcriptional regulation, the responses might differ in a quantitative or temporal manner and this could result in significant differences in the defence output and define the response specificity. Such hypothesis has been already proposed to explain the differences between PTI and ETI outputs (Jones and Dangl, 2006; Maleck et al., 2000; Navarro et al., 2004; Tao et al., 2003; Tsuda and Katagiri, 2010).

Since I conducted a time-resolved transcriptomic analysis of the MLA_{CC}-mediated response, I could analyse the expression changes at early time points after DEX-mediated transgene activation. A substantial number of DEGs can be detected at 2 hpi, most of which (562/573) are upregulated. The transcriptional response is initiated around 2 hpi since marker genes show highly variable expression patterns at 1 hpi (preliminary data not shown). This set of rapidly MLA_{CC}-induced genes is of particular interest since it potentially reflects the first transcriptional events in the response and thus, the primary gene targets downstream of MLA_{CC} and, by inference, of NLR activation. The comparative transcriptomic analysis which I conducted indicates that the 562 early MLA_{CC}-induced genes show a similar rapid upregulation in ETI-like responses, ETI and PTI, even in the absence of ET, JA, and SA signalling. Therefore, most of these 562 genes can be considered as rapid immune response genes and their upregulation does not require ET, JA, SA, and sustained MAPK activation. Consistently with the idea that these genes are general immune response genes, none of them is specifically induced in ETI since their rapid activation is also observed during PTI. Therefore, there seem to be no early marker gene for the ETI. The gene set expression pattern was to a lower degree similar during various responses to abiotic stresses, indicating that a subset of the 562 genes is also rapidly induced by abiotic stresses. An overall low similarity could be observed with the cell death-inducing treatments, confirming that these 562 genes are likely not upregulated by the MLA_{CC}-mediated cell death. The induction of the 562 genes is retained in the phytohormone deficient mutant background, implying that ET, JA, and SA signalling pathways are not required for their induction.

Whilst the 562 early MLA_{CC}-induced genes represent a group of rapid immune response genes, a subset of the genes is also rapidly induced by abiotic stresses. Still, this gene set is largely enriched in defence-related components as indicated by GO term enrichment analysis. Thus, a subset of the 562 genes appears to be immune specific whilst another subset is responsive to a broader range of stresses. In plants, various stresses can result in the rapid and transient induction of a set of genes thought to prime the plant for later stress-specific responses (Bjornson et al., 2016; Walley and Dehesh, 2010). Such rapid and transient gene regulation is termed as the general stress response (GSR). Thus MLA_{CC} early response shares common features with the GSR. It was previously reported that abiotic stresses can increase the resistance to biotic stresses and *vice versa* (Perez and Brown, 2014). This implies the existence of a cross-talk between biotic and abiotic stress responses. In line with this, my results suggest an overlap of the early transcriptional responses downstream of biotic and abiotic stresses.

A large portion of the 562 early MLA_{CC}-induced genes was upregulated by cycloheximide treatment, suggesting that these genes are under control (direct or indirect) of a short-lived negative regulator of gene expression and that their rapid upregulation does not require *de novo* protein synthesis. Similarly, two studies reported that early upregulation in PTI or ETI does not require *de novo* protein synthesis (Durrant et al., 2000; Navarro et al., 2004). Immediate early response (IE) genes have been defined in mammalian systems as genes rapidly induced upon environmental stimulation without requirement for *de novo* protein synthesis (Fowler et al., 2011; Galbraith and Espinosa, 2011; O'Donnell et al., 2012; Saha and Dudek, 2013). In that respect, at least a subset of the genes rapidly induced in ETI-like responses, ETI, and PTI can be considered as plant IE (pIE) genes. It was shown that mammalian IE genes display characteristic features such as a low expression under resting conditions, a constitutively open chromatin context, CpG rich promoters, short transcripts with no or few introns, and a large proportion of loci encoding TFs (Fowler et al., 2011; Galbraith and Espinosa, 2011; O'Donnell et al., 2012; Saha and Dudek, 2013). Moreover, some insight have been gained on the regulation of mammalian IE genes indicating a role of protein kinases, mediator components and chromatin remodelers in the regulation of chromatin context and RNA polymerase II stalling at the IE genes promoters (Fowler et al., 2011; Galbraith and Espinosa, 2011; O'Donnell et al., 2012; Saha and Dudek, 2013). Therefore, it will be interesting to study whether pIE genes share common features and regulatory mechanisms with mammalian IE genes. Noteworthy, only 63 TFs are found among the 562 early MLA_{CC}-induced genes (http://plntfdb.bio.uni-potsdam.de/v3.0/PlnTFDB_tf_1826091934.txt). This number is not indicative of a significant enrichment for TF-encoding genes among the early MLA_{CC}-induced genes. In contrast, kinase activity appears to be the most enriched molecular function in this gene set (59/562 genes).

Investigation of the 5' -regulatory sequences of the 562 early MLA_{CC}-induced genes revealed the over-representation of several motifs including CAMTA/Ca²⁺-related motifs, W-boxes and heat shock elements (HSE). This analysis was performed by combining the results of five different algorithms and a high reliability was achieved by considering only the motifs consistently identified by several independent algorithms.

CAMTA/Ca²⁺-related motifs are the most enriched motifs and are found in up to 66.40% of the 5' -regulatory sequences of the 562 early MLA_{CC}-induced genes ($p=6.0 \times 10^{-19}$). CAMTA or other Ca²⁺-regulated TFs might thus regulate the expression of a large part of these genes. Several reports indicate that CAMTA3 regulates plant defence (Poovaiah et al., 2013). Zhang

et al. (2014) showed that CAMTA3 is rapidly degraded by the proteasome following virulent or avirulent *Pst* inoculation. Knock-out of the E3 substrate adaptor protein required for pathogen-inducible CAMTA3 degradation leads to elevated CAMTA3 levels and higher susceptibility to virulent *Pst*. In light of these results, CAMTA3 seems to act as a negative regulator of defence which is degraded upon defence activation. My data indicate that CAMTA3 or other Ca²⁺-regulated TFs might regulate a large part of the immediate early immune response genes, thereby linking Ca²⁺-mediated signalling to the immediate early immune transcriptional reprogramming. Both ETI and PTI are dependent on Ca²⁺-mediated signalling and can be inhibited by the calcium channel blocker LaCl₃ (Grant et al., 2000; Lecourieux et al., 2006; Pike et al., 2005; Segonzac et al., 2011; Tavernier et al., 1995). Of note, the mechanism by which biotic stresses activate calcium fluxes is still unknown. It will be interesting to investigate further the role of CAMTA3 in the regulation of the early immune response. For this, CAMTA3 steady-state levels upon MLA_{CC} expression could be monitored to test whether MLA_{CC} induces CAMTA3 degradation. Since P/MAMP treatments such as flg22 induce the same set of early genes as MLA, It would also be interesting to monitor CAMTA3 steady-state levels after flg22 treatment to test whether flg22 triggers CAMTA3 degradation. The final challenge would be to genetically dissect the role of CAMTA3 in immunity since CAMTA3 functions partly redundantly with CAMTA1 and CAMTA2, and since *camta3* knock-out activates ETI mediated by two TNLs, suggesting that CAMTA3 is guarded by at least two NLRs (Greeff, 2014). In such context, the characterization of the *camta3* knock-out mutant can only be informative if performed in a genetic background where all the guarding NLRs are inactive. A dominant negative CAMTA3 might uncouple loss of CAMTA3 function and ETI activation, thereby providing an interesting tool to study CAMTA3 function (Nie et al., 2012). Since in the published literature, a large part of the functional characterization of CAMTA3 was performed using the *camta3* mutant, the results obtained might be misleading. To confirm the role of extracellular Ca²⁺ influx in the regulation of the early MLA_{CC}-induced genes, the expression of marker genes could be monitored upon MLA_{CC} expression in presence of LaCl₃, a calcium channel blocker.

Another family of enriched motifs relates to the sequence bound by WKRY transcription factors (W-box). This family of TFs has important functions in plant immunity (Tsuda and Somssich, 2015). The canonical W-box is found in 57.1% of the 562 early MLA_{CC}-induced genes ($p=6.7 \times 10^{-7}$). Therefore, some WRKY TFs might contribute to the regulation of a subset of the early MLA_{CC}-induced genes.

The heat shock element (HSE) was detected in 31.1% of the 562 MLA_{CC}-induced genes, which represents a highly significant enrichment ($p=1.1 \times 10^{-12}$). The HSE is bound by heat-shock factors (Hsf) which have been originally identified as proteins accumulating in response to abiotic stresses such as heat stress. Recent reports suggest that a subset of Hsfs is involved in the response to biotic stresses. For example, *AtHsfA1b* induces defence-related genes leading to increased resistance to pathogen (Bechtold et al., 2013), *AtHsfB1* and *AtHsfB2b* negatively regulate the ET/JA pathways and thereby resistance to necrotrophs (Kumar et al., 2009), and *AtHsfB1* is required for systemic acquired resistance and for SA- and P/MAMP-mediated induction of defence (Pajerowska-Mukhtar et al., 2012; Pick et al., 2012). Evrard et al., (2013) showed that, upon activation by heat stress, *AtMPK6* can phosphorylate *AtHsfA2*. Since *AtMPK6* is induced by biotic stresses, *AtMPK6* constitute a potential link between biotic stresses and Hsf regulation. However, my data show that in the *ppsdes* mutant, most of the early MLA_{CC}-induced genes are still upregulated in the absence of *AtMPK3/6* activation. Therefore, activation of *AtMPK3/6* does not account for the induction of the early MLA_{CC}-induced genes in the *ppsdes* mutant background. Altogether, this data suggest that early transcriptional regulations in biotic and abiotic stress responses are operated by a common molecular mechanism.

3. Early transcriptional reprogramming jump-started by NLRs in the absence of ET, JA, SA, and EDS1

Since both cell death and transcriptional responses induced by MLA_{CC} are qualitatively similar in wild-type and *ppsdes* mutant background, NLRs might induce responses even in the absence of the ET, JA, SA and EDS1 signalling sectors. Therefore, a core set of the early transcriptional response appears not to require signalling from the ET, JA, SA and EDS1 sectors. In an effort to explain the robustness of the NLR signalling, Tsuda et al. (2013) have proposed that NLRs can by-pass the SA-mediated response by a prolonged MPK3/6 activation. Such by-pass is unlikely to occur in the MLA_{CC}-mediated signalling since MPK3/6 activation is abolished in the *ppsdes* mutant background. Thus, sustained MPK3/6 activation cannot explain the robustness of the MLA_{CC}-mediated response in the *ppsdes* mutant. Analysis of the *cis*-regulatory elements of the 562 early MLA_{CC}-induced genes suggests that

calcium-mediated signalling might be a key player in the regulation of the early transcriptional response.

Tsuda et al., (2009) reported that ETI-mediated resistance is largely impaired in an *A. thaliana* mutant where ET, JA and SA sectors are simultaneously impaired. This suggests that despite the qualitative similarity in the early response mediated by MLA_{CC} or other NLRs in wild-type compared to the defence phytohormone-depleted mutant backgrounds, hormone-signalling impairment does result in clear differences in the defence outputs. First, one can expect that the phytohormone signalling depletion would impact the later stages rather than the early stages of the response since the defence phytohormones, as mobile signals, are likely involved in the spatial propagation of the response. Second, subtle temporal and quantitative differences during the immune response might account for significant differences in the defence outputs as shown by the comparison of PTI and ETI (Jones and Dangl, 2006; Maleck et al., 2000; Navarro et al., 2004; Tao et al., 2003; Tsuda and Katagiri, 2010). Altogether, defence phytohormones might be dispensable in the signal initiation while playing a critical role in signal amplification and/or spatial propagation and/or temporal regulation.

In this study, the contribution of other phytohormones such as abscisic acid, gibberellins, auxin, and cytokinins was not addressed. These hormones were shown to contribute to the immune response regulation though to a lower extent than ET, JA, and SA (Pieterse et al., 2012). It would be interesting to examine whether these signalling sectors are involved in the early transcriptional reprogramming in PTI and ETI.

4. Forward suppressor screening of MLA_{CC} -mediated responses: outcome and conclusions

To identify genetic components required for MLA_{CC} functions, I conducted a forward genetic screen by mutagenizing the *DEXp:MLA_{CC}-mYFP* transgenic line. Many screens for loss of NLR-mediated responses have been conducted in the past to identify components downstream of NLRs. However, most of them yielded mutations either in NLR loci themselves or in loci encoding components regulating the NLR pre-activation complex (Bao et al., 2014; Bisgrove et al., 1994; Century et al., 1995; Eulgem et al., 2007; Parker et al., 1996; Salmeron et al., 1996; Shirasu et al., 1999; Tornero et al., 2002a, 2002b; Yu et al., 1998). In my screen, the

use of a constitutively active and self-structured signalling module would allow to identify loci responsible for downstream signalling of MLA_{CC}. The difficulty in identifying downstream components by forward genetics can be due to functional redundancy or lethality of the suppressor mutations. To overcome this issue, I performed an extensive mutant screening which was near to saturating conditions (~130,000 M₂ plants screened) to allow identification of rare mutations such as gain of function alleles exerting dominant effects on other functionally redundant components, and partial loss of function mutations which impair MLA_{CC} function but still allow plant survival. Although NLRs are proposed to initiate downstream signalling through multiple but distinctive downstream components (Maekawa et al., 2012), I hypothesized that MLA and MLA_{CC} in distantly related plant species might engage a reduced number of signalling pathways compared to barley, since all downstream components may not be conserved between *A. thaliana* and barley. Thus, I speculated that the complexity and redundancy of the immune signalling mechanism are lowered downstream of MLA_{CC} in *A. thaliana*. If this were the case, my screen could potentially identify downstream components for ETI which have not been identified by previous screens.

My mutant screen yielded 21 candidate mutants. Genome re-sequencing was used to identify the SNPs of each candidate. I tested whether a new approach, based on the identification of multiple independent alleles among the 21 suppressor candidates can pinpoint the causal mutations. This approach was however not successful for the tested 21 mutants. Since the power of this technique increases with the number of independent candidates jointly analysed, more independent mutants would increase the likelihood to robustly identify some causal mutations. Nevertheless, the resulting SNP information strongly suggests that none of the reported immune-related loci carry mutations responsible for the suppressor phenotype (377 immune-related loci inspected, Table S2-1). Therefore the suppressor mutations are located in loci encoding not yet-described immune components. In addition, allelic mutations at a single NLR locus were not identified. This suggests that MLA_{CC} function is not dependent on a single NLR. This does not exclude the possibility that multiple NLRs are involved redundantly in MLA_{CC}-mediated response. I initiated the mapping of three independent mutants using mapping by sequencing. This first mapping approach was not sufficient to accurately define the candidate intervals. I hypothesized that some mis-phenotyping occurred during the selection of the mapping population or that some complex genetic phenomenon, possibly involving multiple genes, is responsible for the observed phenotype suppression. A novel and complementary mapping-by-sequencing pipeline (Gan et al. unpublished) was further used to refine the mapping of two mutants. This pipeline narrowed down the candidate

interval to ~10 genes. This new approach has several advantages: i) phenotyping of the negative segregant bulk is more accurate than that of the positive segregant bulk when a phenotype suppression is mediated by transgene silencing and ii) it can correct for linkage disequilibrium. Fine-mapping will be performed on separate individuals to further narrow down the candidate list. The frequency of suppressor mutants in the mutagenized population was very low (21 out of ~130,000 M₂ plants). This is consistent with my initial hypothesis that the screen is unlikely to identify simple loss-of-function mutations. Therefore, one should expect that the mutants identified carry suppressor mutations with rare effects or multiple causal mutations.

The mapping process and the analysis of the mutation dominance/recessivity were strongly impeded by heterogeneous levels of transgene expression, despite all the precautions taken to avoid and overcome this issue. The transgene silencing process was likely exacerbated by the presence of tandem repeats of the transgene. For this reason and due to technical constraints, I did not perform allelic tests among the 21 mutants although this might have helped defining the complementation groups.

As a by-product of my search for loss of RPM1-mediated immunity, I identified three *rpm1* alleles (G9R, L344F, and R519K). The extensive screening for the loss of RPM1-mediated immunity conducted by Tornero et al (2002a) also identified loss-of-function mutations in RPM1 at the residue 344 (*rpm1-32*), and the residue 515 (*rpm1-9*) close to the residue 519 (Figure 2-5). Both residues at positions 344 and 519 are located in the NB-ARC domain whilst the glycine residue at position 9 is located at the very start of the CC domain. In the screen published by Tornero et al. (2002a), only few loss of function mutations were identified in the N-terminal CC domain of RPM1 and the G9R mutation is not located in proximity to any of them (Figure 2-5). In that respect, the G9R and R519K mutations are novel and highlight the importance of these residues for RPM1 function. The genome-wide mutation rate ($p=0.007857$) inferred from the M₂ sequence information described in the Results section 2.3.3 was used to determine if the frequency of *rpm1* mutants isolated among the MLA_{CC} suppressors is significantly higher than expected under a random distribution. In the case of a random mutation distribution, the probability to identify three *rpm1* alleles can be approximated by a binomial distribution of parameter (1900, p) of Esperance $1900p=14.93$. Testing for the null hypothesis with $p=0.007857$ returns a *p*-value of 0.99996. Therefore, there seems to be no significant mutation enrichment at the *RPM1* locus. However, this calculation method does not take in account that only a subset of the possible EMS-induced

mutation would cause a loss of *RPM1* function. Provided that all the possible EMS-induced loss of function mutations were identified by the extensive screen in Tornero et al. (2002a), only 67 out of 1157 C or G nucleotides can produce a loss of function in *RPM1* gene. Under this extreme assumption, the corrected p for *RPM1* is $0.007857/1157 \times 67 = 0.000455$ and the *p*-value for the null hypothesis is 0.0572. Even under an extreme *p* adjustment, the observed frequency is not significantly different from that of a random mutation distribution. This suggests that the *RPM1* locus is genetically not associated with *MLA_{CC}* function.

From careful inspection of the large candidate gene list obtained after the first mapping step, I became interested in *AT3G02840*. *AT3G02840* carries a mutation at a highly conserved residue (V289I) and was found as candidate causal mutation for the phenotype of mutant 2H. *AT3G02840* shares high sequence similarity to the CMPG1 family of PUB proteins which has a conserved function in plant defence (Bos et al., 2010; González-Lamothe et al., 2006; Zhu et al., 2015), and *AT3G02840* transcripts rapidly accumulates upon *MLA* activation or *MLA_{CC}* expression in *A. thaliana*. I expected *AT3G02840(V289I)* to have a dominant negative effect on *MLA_{CC}*-mediated phenotype but this hypothesis was not confirmed by transient co-expression experiments in *Nicotiana benthamiana*. Analysis of T-DNA insertion lines in *A. thaliana* together with *at3g02840(V289I)* mutant and wild-type plants suggests that the V289I mutation induces a loss of function in *AT3G02840* and that *AT3G02840* is a negative regulator of *RPM1*-mediated HR. Therefore, *at3g02840(V289I)* is unlikely the suppressor of *MLA_{CC}* but is a negative regulator of the HR. In Y2H experiments, *AT3G02840* yielded an unusually high number of interactions which will need further confirmation and characterization.

5. Identification of candidate *MLA_{CC}* interaction partners

To identify *MLA_{CC}* signalling targets, I used two different approaches: yeast two-hybrid (Y2H) and tandem affinity purification of protein complexes followed by mass spectrometry. Both approaches identified distinct candidate *MLA_{CC}* interaction partners. A Y2H screen was used to probe interactions between *MLA_{CC}* and *A. thaliana* transcriptional regulators. 31 TFs were found to interact with *MLA_{CC}*. This suggests that *MLA_{CC}* can interact with multiple TFs in *A. thaliana*. The AP2/ERF TF family predominantly interacts with *MLA_{CC}* in Y2H. Interestingly, the AP2/ERF family has been associated to plant immunity (Tsuda and

Somssich, 2015). Although MLA_{CC} was found to interact with *Hv*WRKY1/2 and *Hv*MYB6 (Chang et al., 2013; Shen et al., 2007), the Y2H screen did not identify WRKY or MYB TF related to *Hv*MYB6. I hypothesized that either MLA_{CC} interacts with some *Hv*WRKY1/2- and *Hv*MYB6-related TFs in *A. thaliana* but these interactions were not detected in our Y2H or that the MLA_{CC}-*Hv*WRKY1/2/*Hv*MYB6 interaction is not conserved in *A. thaliana*. In the latter case, other conserved signalling targets must exist, which support MLA_{CC} function in *A. thaliana*. Few overlap exists between the binding motifs of the 31 identified TFs and the motifs enriched in the 562 early MLA_{CC}-induced genes. MYC2 can bind to the G-box and the Z-box which are similar to some CAMTA binding motifs presented in Table 1-1 (Boter et al., 2004; Dombrecht et al., 2007; Yadav et al., 2005). The G-box can be bound by some TFs from the bZIP family and also represents a specific type of E-box (CANNTG) which can be bound by TFs of the bHLH family (Ferré-D'Amaré and Burley, 1995). Three bZIPs and two bHLHs were found to interact with the MLA_{CC} by Y2H in this study. Although most of the TFs found by Y2H belong to the AP2/ERF family which binds to GCC-boxes (Ohme-Takagi and Shinshi, 1995), none of the motifs enriched in the 562 early MLA_{CC}-induced genes is similar to the GCC-box. Therefore the TFs identified by Y2H does not provide obvious candidates for the regulation of the 562 early MLA_{CC}-induced genes. Nonetheless, the sensitivity of the Y2H technique is very low and the risk of false positive implies a need for validation of the observed interactions by an orthogonal approach. The candidate interactors were also not identified in the complexes associated to MLA_{CC}. This observation is not surprising since Y2H preferentially identifies binary interactions whereas affinity purification isolates proteins which belong to a stable complex. To increase the probability to identify interaction with TFs by affinity purification, nuclei purification would be required whilst the method I used was based on whole cell extracts.

The analysis of MLA_{CC}-associated complexes (Results section 3.3) somewhat suffered from a lack of reproducibility. Some candidate interactors could however be identified by refining the quantitative analysis. The two best candidates are AT1G79600 and AT2G26560. AT1G79600 has been described as a chloroplast-localized kinase and has not been associated to immunity yet. An interaction between MLA_{CC} and a chloroplast-localized protein is rather unlikely due to the MLA_{CC} nucleo-cytoplasmic localization, suggesting that AT1G79600 might be a false positive. Alternatively, an AT1G79600 pool might reside outside of the chloroplast. In any case, further work will be needed to confirm and define the biological relevance of this interaction. AT2G26560 (PLA2A) has been associated to cell death regulation (Camera et al., 2009; La Camera et al., 2005; Reina-Pinto et al., 2009). A

preliminary analysis indicated that the phospholipase activity of PLA2A is not required for MLA_{CC}-mediated cell death. Therefore the functional relevance of the interaction between MLA_{CC} and PLA2A remains unknown.

Overall, the analysis suggested that, under the conditions tested, MLA_{CC} does not form stable soluble complexes in *A. thaliana* and might function via transient interaction with its signalling target(s). Whether this holds true in its authentic physiological context in barley remains unknown. A fair assumption could also be that this observation results from the experimental conditions used. For example, the use of 0.1% SDS during extraction, as well as a long multi-step purification protocol might contribute to destabilize protein complexes or weak interactions. A faster one-step affinity protocol performed in the absence of SDS might yield better results: However, the pilot experiments conducted in this study suggested that the enrichment efficiency is not sufficient. The time of sampling after estradiol induction might also be a critical parameter. It would be useful to test other earlier and later time points to find out whether some complexes are detectable only at certain time points.

Moreover, in the context of a heterologous expression system such as *A. thaliana*, MLA_{CC} might still be able to interact with conserved protein partners but the interactions might be less stable, though sufficient to support MLA_{CC} function. Alternatively, the MLA_{CC}-associated complexes might have inherent properties which make their purification technically challenging. Although accumulating evidence indicate that plant NLRs do form higher order complexes, so far, successful isolation of plant NLR-associated protein complexes was only reported for the tomato CNL Prf and the *A. thaliana* CNL RPS2 (Bonardi and Dangl, 2012; Gutierrez et al., 2010; Qi and Katagiri, 2009; Qi et al., 2011). MLA itself has been shown to form higher molecular order complexes *in planta* (Maekawa et al., 2011b). In both cases, the isolation was conducted in conditions where the NLR is inactive whereas I used a bait in its signalling competent state. A subset of mammalian NLRs can assemble into higher order molecular complexes called inflammasomes (Maekawa et al., 2011a). It remains to be demonstrated whether plant NLRs might similarly assemble into large higher order molecular complexes. Such hypothesis might explain the difficulties encountered for biochemical purification of the NLR-associated complexes in plants. Semi-denaturing detergent agarose gel electrophoresis suggested that MLA_{CC} is predominantly present in SDS-resistant high molecular weight complexes (Figure 3-12). Future biochemical characterization studies will be required to identify the nature and the potential biological relevance of these large SDS-resistant polymers.

Conclusion and Perspectives

This thesis revealed the N-terminal coiled-coil domain of the barley NLR MLA (MLA_{CC}) as suitable model to study NLR-mediated initiation of transcription-dependent immune responses and ensuing cell death in heterologous *A. thaliana*. Here, I have shown that these two MLA_{CC}-mediated responses phenocopy ETI mediated by the endogenous *A. thaliana* NLRs RPM1, RPS2, and RPS4. Thus, conditional MLA_{CC} expression recapitulates in a pathogen- and effector-free system immune signalling activated by CC- or TIR-type NLRs. Whether MLA_{CC} functions as direct immune signalling module or indirectly induce defence responses by activating other endogenous NLRs still needs to be clarified. However, since the MLA_{CC} domain directly regulates *HvWRKY1/2* and *HvMYB2* TFs in barley (Chang et al., 2013), an indirect immune response activation through endogenous *A. thaliana* NLRs appears less likely.

The MLA_{CC} signalling function is either not or only partially suppressed when EDS1 (which acts through PAD4 and SAG101)-, ET-, JA-, and SA-mediated defence pathways are simultaneously depleted. This suggests that the core mechanism for the initiation of NLR-mediated and transcription-dependent immunity does not require these defence phytohormones and key immune regulator(s). Similarly, *RARI* appears at least partially dispensable for MLA_{CC}-mediated signalling.

Comparison of genome-wide gene expression changes in PTI and ETI with those stimulated by MLA_{CC} or autoactive RPS4 revealed remarkably similar profiles, irrespective of the type of NLR involved. A key conclusion of this work is that initiation of rapid transcriptional responses mediated by the autoactive full-length RPS4 or the MLA_{CC} signalling module can occur independently of PRR-triggered immune signalling. This challenges a widespread model in which ETI is believed to converge on and amplify P/MAMP-triggered transcriptional outputs (Cui et al., 2015; Day and He, 2010; Garcia and Hirt, 2014; Vidhyasekaran, 2014). However, my findings are not inconsistent with earlier studies suggesting that in plant-pathogen interactions quantitative and temporal rather than qualitative differences define PTI and ETI transcriptional outputs and response specificity (Jones and

Dangl, 2006; Maleck et al., 2000; Navarro et al., 2004; Tao et al., 2003; Tsuda and Katagiri, 2010).

Most of the 562 genes rapidly induced by conditional MLA_{CC} expression are also rapidly induced upon P/MAMP perception and during authentic avirulent plant-pathogen interactions, when ETI and/or PTI are active, and can be considered immediate early response genes. Defence phytohormones, EDS1 (PAD4 and SAG101), and sustained MAPK activation are dispensable for the activation of this large set of immediate early immune response genes. These findings strongly suggest convergence of NLR- and PRR-triggered signalling pathways, independently of each other, on the same transcriptional machinery for the initiation of immune response gene activation. I identified several *cis*-acting elements enriched in the 5' regulatory regions of these 562 genes, including Ca^{2+} /CAMTA-related motifs, heat stress elements and W-boxes. Since this gene set likely contains primary gene targets of immune receptor-triggered signalling, the identification of cognate TFs involved in their regulation will be key to understanding the initiation of transcription-dependent immunity. It is reasonable to assume that these TFs are potential targets of pathogen effectors for immune suppression and thus, guarded by NLRs. Indeed, the TF CAMTA3 is guarded by at least two NLRs (Greeff, 2014). Since the immediate early immune response likely involves the rapid removal of negative regulators, engagement of ubiquitin-mediated and proteasome-dependent protein degradation serves as one plausible molecular mechanism underlying the initiation of transcription-dependent immunity.

I conducted several approaches to identify MLA_{CC} interacting partners and downstream components including a forward suppressor screen, a yeast two-hybrid screen and MS-based characterization of protein complexes. The latter two approaches identified several candidates which still need to be confirmed by orthogonal assays. Most of the candidates identified were not previously associated with NLR functions. Validation and characterization of these candidates might reveal new components engaged in NLR-mediated immunity.

Materials and methods

1. Material

1.1. Plant materials

1.1.1. *Arabidopsis thaliana*

All experiments were performed using *Arabidopsis thaliana* (*A. thaliana*) wild-type, mutant, and transgenic lines in the ecotype Columbia-0 (Col-0) background (J. L. Dangl, UNC, Chapel Hill, USA).

Mutant *A. thaliana* lines used in this study

Mutant allele	Accession	Mutagen	Reference/Source
<i>at3g02840-1</i>	Col-0	T-DNA	SALK_113770C
<i>at3g02840-2</i>	Col-0	T-DNA	SALK_040843 (Q) (AE)
<i>at3g02840-3</i>	Col-0	T-DNA	SALK_007906C
<i>rpm1-3 rps2-101C</i>	Col-0/gl1	EMS/diepoxybutane	Mackey et al., 2003
<i>pen2-1 pad4-1 sag101-2 dde2-2 ein2-1 sid2-2</i>	Col-0	EMS/T-DNA	Maekawa et al., 2013
<i>dde2-2 ein2-1 pad4-1 sid2-2</i>	Col-0	EMS/T-DNA	Tsuda et al., 2009
<i>sgt1b/eta3</i>	Col-0	EMS	Gray et al., 2003
<i>ndr1-1</i>	Col-0	Fast neutron	Century et al., 1995
<i>rar1-20/pbs2-1</i>	Col-0	EMS	Tornero et al., 2002

Transgenic *A. thaliana* lines used in this study

Name	Accession	Construct	Reference/Source
<i>DEXp:MLA_{CC}-mYFP</i>	Col-0	p35S:GVG, 6xUAS:p35S(-46,+1):MLA10 _{CC1-160} -mYFP	This study
<i>DEXp:mYFP</i>	Col-0	p35S:GVG, 6xUAS:p35S(-46,+1):mYFP	This study
<i>DEXp:MLA_{CC}I33E-mYFP</i>	Col-0	p35S:GVG, 6xUAS:p35S(-46,+1):MLA10 _{CC1-160} I33E-mYFP	This study
<i>DEXp:MLA_{CC}L36E-mYFP</i>	Col-0	p35S:GVG, 6xUAS:p35S(-46,+1):MLA10 _{CC1-160} L36E-mYFP	This study
<i>MLA1 in pps</i>	<i>pen2 pad4 sag101</i>	p35S:MLA1-HA	Maekawa et al., 2012
<i>MLA1 in ppsdes</i>	<i>ppsdes*</i>	p35S:MLA1-HA	Maekawa et al., 2012
<i>DEXp:MLA1_{D502V}</i>	Col-0	p35S:GVG, 6xUAS:p35S(-46,+1):MLA1 _{D502V} -TY1	Takaki Maekawa
<i>DEXp:MLA1_{K207R}</i>	Col-0	p35S:GVG, 6xUAS:p35S(-46,+1):MLA1 _{K207R} -TY1	Takaki Maekawa
<i>ERp:MLA_{CC}-PC2</i>	Col-0	p _{G10-90} :XVE, O _{LexA} :p35S(-46,+1):MLA10 _{CC1-160} -PC2	This study
<i>ERp:mYFP-PC2</i>	Col-0	p _{G10-90} :XVE, O _{LexA} :p35S(-46,+1):mYFP-PC2	This study
<i>ERp:MLA_{CC}L36E-PC2</i>	Col-0	p _{G10-90} :XVE, O _{LexA} :p35S(-46,+1):MLA10 _{CC1-160} L36E-PC2	This study
<i>ERp:MLA_{CC}I33E-PC2</i>	Col-0	p _{G10-90} :XVE, O _{LexA} :p35S(-46,+1):MLA10 _{CC1-160} I33E-PC2	This study

<i>ERp:RPM1_{CC}-PC2</i>	Col-0	p _{G10-90} :XVE, O _{LexA} :p35S(-46,+1):RPM1 _{CC1-155} -PC2	This study
<i>ERp:ADR1-L2_{CC}-PC2</i>	Col-0	p _{G10-90} :XVE, O _{LexA} :p35S(-46,+1):ADR1-L2 _{CC1-153} -PC2	This study
<i>p35S:MLA_{CC}-mYFP</i>	Col-0	p35S:MLA10 _{CC1-160} -mYFP	This study
<i>p35S:RPS4-HS</i>	Col-0	p35S:RPS4-HS	Heindrich et al., 2013
<i>p35S:MLA_{CC}-HA in sgt1b</i>	<i>sgt1b</i>	p35S:MLA10 _{CC1-160} -3xHA	This study
<i>p35S:MLA_{CC}-mYFP sgt1b</i>	<i>sgt1b</i>	p35S:MLA10 _{CC1-160} -mYFP	This study
<i>DEXp:MLA_{CC}-mYFP rar1</i>	<i>rar1-20</i>	p35S:GVG, 6xUAS:p35S(-46,+1):MLA10 _{CC1-160} -mYFP	This study
<i>DEXp:MLA_{CC}-mYFP ndr1</i>	<i>ndr1-1</i>	p35S:GVG, 6xUAS:p35S(-46,+1):MLA10 _{CC1-160} -mYFP	This study
<i>DEXp:MLA_{CC}-mYFP sgt1b</i>	<i>sgt1b</i>	p35S:GVG, 6xUAS:p35S(-46,+1):MLA10 _{CC1-160} -mYFP	This study
<i>DEXp:MLA_{CC}-mYFP ppsdes</i>	<i>ppsdes</i>	p35S:GVG, 6xUAS:p35S(-46,+1):MLA10 _{CC1-160} -mYFP	This study

**ppsdes*: *pen2-1 pad4-1 sag101-2 dde2-2 ein2-1 sid2-2*

1.1.2. *Nicotiana benthamiana*

Nicotiana benthamiana (310A) plants were obtained from T. Romeis (MPIPZ) and used for transient *Agrobacterium*-mediated transformation of leaf tissue.

1.2. Bacterial strains

Agrobacterium tumefaciens

Strain	Purpose	Source
GV3101 +pMP90 RK	<i>A. thaliana</i> transformation, transient expression in <i>N. benthamiana</i>	Koncz and Schell, 1986
GV3101 +pMP90 RG	<i>A. thaliana</i> transformation, transient expression in <i>N. benthamiana</i> , same as above but the kanamycin resistance gene was deleted from the pMP90 helper plasmid	Koncz and Schell, 1986

Pseudomonas syringae pv. *tomato* (*Pst*)

Strain	Purpose	Source
<i>Pst</i> DC3000 AvrRpm1-HA	Inoculation of <i>A. thaliana</i>	R. Innes (Indiana University, Bloomington, USA)
<i>Pst</i> DC3000 AvrRpt2-HA	Inoculation of <i>A. thaliana</i>	R. Innes (Indiana University, Bloomington, USA)
<i>Pst</i> DC3000	Inoculation of <i>A. thaliana</i>	R. Innes (Indiana University, Bloomington, USA)

Escherichia coli

Strain	Purpose	Source
DH5α	Plasmid amplification	Invitrogen™ (Karlsruhe, Germany)

1.3. Vectors

Vectors used or generated in this study

Vector	Description	Source
pXCSG-3HA	Binary Gateway® destination vector for expression of proteins under the 35S promoter with a C-terminal fusion to the 3xHA tag in plants	derived from pAMPAT-MCS GenBank accession no. AY436765
pXCSG-MLA _{cc} -3HA	Binary Gateway® destination vector for expression of MLA10CC ₁₋₁₆₀ -3HA under the 35S promoter in plants	This study
pXCSG-mYFP	Binary Gateway® destination vector for expression of proteins under the 35S promoter with a C-terminal fusion to the mYFP in plants, also used for subcloning of the mYFP	derived from pAMPAT-MCS GenBank accession no. AY436765
pXCSG-MLA _{cc} -mYFP	Binary Gateway® destination vector for expression of MLA10CC ₁₋₁₆₀ -mYFP under the 35S promoter in plants, also used for sub-cloning of the MLA _{cc} -mYFP fusion	This study
pXCSG-MLA _{cc} l33E-mYFP	Binary Gateway® destination vector for expression of MLA10CC ₁₋₁₆₀ l33E-mYFP under the 35S promoter in plants, also used for sub-cloning of the MLA _{cc} l33E-mYFP fusion	This study
pXCSG-MLA _{cc} L36E-mYFP	Binary Gateway® destination vector for expression of MLA10CC ₁₋₁₆₀ L36E-mYFP under the 35S promoter in plants, also used for sub-cloning of the MLA _{cc} L36E-mYFP fusion	This study
pTA7002 ^a	Binary Gateway® destination vector for dexamethasone-inducible expression of a protein in plant	Aoyama and Chua, 1997
pTA7002-mYFP	Binary Gateway® destination vector for dexamethasone-inducible expression of mYFP in plant	This study
pTA7002-MLA _{cc} -mYFP	Binary Gateway® destination vector for dexamethasone-inducible expression of MLA10CC ₁₋₁₆₀ -mYFP in plant	This study
pTA7002-MLA _{cc} l33E-mYFP	Binary Gateway® destination vector for dexamethasone-inducible expression of MLA10CC ₁₋₁₆₀ l33E-mYFP in plant	This study
pTA7002-MLA _{cc} L36E-mYFP	Binary Gateway® destination vector for dexamethasone-inducible expression of MLA10CC ₁₋₁₆₀ L36E-mYFP in plant	Takaki Maekawa
pTA7002-MLA1D502V-TY1	Binary Gateway® destination vector for dexamethasone-inducible expression of MLA1D502V-TY1 in plant	Takaki Maekawa
pTA7002-MLA1K207R-TY1	Binary Gateway® destination vector for dexamethasone-inducible expression of MLA1K207R-TY1 in plant	Takaki Maekawa
pGB42AD	Binary Gateway® destination vector for expression of a prey protein in yeast two hybrid	Shen et al., 2007
pLexA	Binary Gateway® destination vector for expression of a bait protein in yeast two hybrid	Shen et al., 2007

pLexA-AT3G02840	Binary Gateway® destination vector for expression of LexA(BD)-AT3G02840 in yeast two hybrid	This study
pDEST-BTM116	Binary Gateway® destination vector for expression of a bait protein in yeast two hybrid	Mitsuda et al., 2010
pDEST-BTM116-MLACC ₁₋₁₆₀	Binary Gateway® destination vector for expression of the MLACC ₁₋₁₆₀ bait protein in yeast two hybrid	This study
pDEST-BTM116-MLACC ₁₋₂₂₅	Binary Gateway® destination vector for expression of the MLACC ₁₋₂₂₅ bait protein in yeast two hybrid	This study
pDEST-GAD424	Binary Gateway® destination vector for expression of a prey protein in yeast two hybrid	Mitsuda et al., 2010
pENTR/D-TOPO	Gateway® entry vector for TOPO cloning	Invitrogen™ (Karlsruhe, Germany)
pENTR-MLACC ₍₁₋₁₆₀₎	pENTR/D-TOPO Gateway® entry vector that contains MLA10CC ₁₋₁₆₀ with or without stop codon	Maekawa et al., 2011
pENTR-MLACC ₍₁₋₂₂₅₎	pENTR/D-TOPO Gateway® entry vector that contains MLA10CC ₁₋₂₂₅ with or stop codon	Maekawa et al., 2011
pENTR-MLACC _{I33E}	pENTR/D-TOPO Gateway® entry vector that contains MLA10CC ₁₋₁₆₀ I33E without stop codon	Maekawa et al., 2011
pENTR-MLACC _{L36E}	pENTR/D-TOPO Gateway® entry vector that contains MLA10CC ₁₋₁₆₀ L36E without stop codon	Maekawa et al., 2011
pENTR-MLA1D502V-TY1	pENTR/D-TOPO Gateway® entry vector that contains MLA1D502V-TY1 with stop codon	Takaki Maekawa
pENTR-MLA1K207R-TY1	pENTR/D-TOPO Gateway® entry vector that contains MLA1K207R-TY1 with stop codon	Takaki Maekawa
pENTR-MLACC-mYFP	pENTR/D-TOPO Gateway® entry vector that contains MLA10CC ₁₋₁₆₀ -mYFP with stop codon	This study
pENTR-MLACC _{I33E} -mYFP	pENTR/D-TOPO Gateway® entry vector that contains MLA10CC ₁₋₁₆₀ I33E-mYFP with stop codon	This study
pENTR-MLACC _{L36E} -mYFP	pENTR/D-TOPO Gateway® entry vector that contains MLA10CC ₁₋₁₆₀ L36E-mYFP with stop codon	This study
pENTR-mYFP	pENTR/D-TOPO Gateway® entry vector that contains mYFP without stop codon	This study
pENTR-mYFP-stop	pENTR/D-TOPO Gateway® entry vector that contains mYFP with stop codon	This study
pENTR-RPM1 _{cc}	pENTR/D-TOPO Gateway® entry vector that contains RPM1CC ₁₋₁₅₅ without stop codon	This study
pENTR-ADR1-L2 _{cc}	pENTR/D-TOPO Gateway® entry vector that contains ADR1-L2CC ₁₋₁₅₃ without stop codon	This study
pENTR-MLACC-NLS/NES	pENTR/D-TOPO Gateway® entry vector that contains MLA10CC ₁₋₁₆₀ carrying a localization signal without stop codon	This study
pENTR-AT3G02840	pENTR/D-TOPO Gateway® entry vector that contains AT3G02840 with stop codon	This study
pGEMTeasy-Nsil-PC2-Nsil	T vector containing the PC2 TAP tag used as PCR template for producing the pacl-PC2-Pacl fragment cloned into pMDC7	Jean Colcombet

pMDC7	Binary Gateway® destination vector for estradiol-inducible expression of a protein in plant	Curtis and Grossniklaus, 2003
pMDC7-PC2 ^b	Binary Gateway® destination vector for estradiol-inducible expression of a fusion protein with a C-terminal PC2 TAP tag in plant	This study
pMDC7-MLA _{CC} -PC2	Binary Gateway® destination vector for estradiol-inducible expression of the MLA10CC ₁₋₁₆₀ -PC2 protein with a C-terminal PC2 TAP tag in plant	This study
pMDC7-MLA _{CC} I33E-PC2	Binary Gateway® destination vector for estradiol-inducible expression of the MLA10CC ₁₋₁₆₀ I33E-PC2 protein with a C-terminal PC2 TAP tag in plant	This study
pMDC7-MLA _{CC} L36-PC2	Binary Gateway® destination vector for estradiol-inducible expression of the MLA10CC ₁₋₁₆₀ L36E-PC2 protein with a C-terminal PC2 TAP tag in plant	This study
pMDC7-mYFP-PC2	Binary Gateway® destination vector for estradiol-inducible expression of the mYFP-PC2 protein with a C-terminal PC2 TAP tag in plant	This study
pMDC7-RPM1 _{CC} -PC2	Binary Gateway® destination vector for estradiol-inducible expression of the RPM10CC ₁₋₁₅₅ -PC2 protein with a C-terminal PC2 TAP tag in plant	This study
pMDC7-ADR1-L2 _{CC} -PC2	Binary Gateway® destination vector for estradiol-inducible expression of the ADR1-L2CC ₁₋₁₅₃ -PC2 protein with a C-terminal PC2 TAP tag in plant	This study
pMDC7-MLA _{CC} -NLS/NES-PC2	Binary Gateway® destination vector for estradiol-inducible expression of the MLA10CC ₁₋₁₆₀ -NLS/NES protein with a C-terminal PC2 TAP tag in plant	This study

^apTA7002-GW is derivative of pTA7002 vector by insertion of the gateway cassette into pTA7002 using XhoI and SpeI restriction sites

^bcloning described below

The pMDC7-PC2 vector used in this study was produced by PacI restriction of pMDC7 vector and of PC2 fragment flanked by PacI restriction sites, followed by blunt ligation of both restriction products. In-frame ligation products were selected by sequencing of the ligation borders. A map of both original and derived vector is shown in Figure S3-1.

1.4. Oligonucleotides

Oligonucleotides used in this study were purchased from Sigma-Aldrich (Deisenhofen, Germany), Metabion (Martinsried, Germany), or Invitrogen (Karlsruhe, Germany). Lyophilised primers were resuspended in TE 10:1 pH 8 to a final concentration of 100 µM. Working solutions were diluted in ddH₂O to 10 µM.

Oligonucleotides used in this study		
Name	Purpose	Sequence 5'→3'
Cloning		
D-TOPO_MLA10-f	D-TOPO cloning of MLA10	CACCATGGATATTGTCACCGGTGCCATT
MLA _{cc} -NLS-r	Adding NLS after MLA10 _{cc} (1-160) without STOP codon	AGGGTCCTCAACCTTACGCTTCTTTTTAGGC AAAGCTCGAAGGCAAGGGTCAAT
MLA _{cc} -NES-r	Adding NES after MLA10 _{cc} (1-160) without STOP codon	CTTGTTAATATCAAGTCCAGCCAACCTAAGA GCAAGCTCGTTCAAAGCTCGAAGGCAAGGG TCAAT
D-TOPO_mYFP-f	TOPO Cloning of mYFP	CACCATGGTGAGCAAGGGCGAGGAGCTGTT
mYFP-r	Cloning of mYFP with stop codon	TTACTTGTACAGCTCGTCCATGCCG
mYFP Δ stop-r	Cloning of mYFP without stop codon	CTTGACAGCTCGTCCATGCCGTGAG
AT3G02840-Fw1	TOPO cloning of AT3G02840	CACCATGGTGTTACCTTGGAGATCAAGAGGA GGAGT
AT3G02840-Rv1	TOPO cloning of AT3G02841 without STOP	AAATGATTTCTTCACATTCTTCAAATGCA
AT3G02840-Rv2	TOPO cloning of AT3G02841 with STOP	CTAAAATGATTTCTTCACATTCTTCAAATGCA
D-TOPO_ADR1-L2-f	TOPO cloning of ADR1-L2	CACCATGGCAGATATAATCGGCGGCGAAGT TGT
D-TOPO_RPM1-f	TOPO cloning of RPM1 _{cc} (1-155)	CACCATGGCTTCGGCTACTGTTGATTTTGGG ATC
RPM1(1-155)-r	TOPO cloning of RPM1 _{cc} (1-155)	CTTGCATCGCCATCATCAATAGGCGGTAA
PacI-PC2-f	Amplification PC2 Tap tag cloned into pMDC7	CCTTAATTAAGTCCAGCTTCTTGTACAAAGT GGTGAT
PacI-PC2-r	Amplification PC2 Tap tag cloned into pMDC7	GGTTAATTAATCACTTCTCGAACTGAGGATG AGACCA
Sequencing		
pTA7002insert-r	Sequencing of the inserts in pTA7002	GGGCGATGAATTCTCAACAAGC
pTA7002insert-f	Sequencing of the inserts in pTA7002 or pMDC7	CATTTGGAGAGGACACGCTGAAGC
pMDC7insert-r	Sequencing of the inserts in pMDC7	GGATTCTGGTGTGTGGGCAATGAAACT
RPM1-f	Amplification of <i>RPM1</i> locus for sequencing	CCCTTTCAGTTTCAGGTAACGAATGA
RPM1-r	Amplification of <i>RPM1</i> locus for sequencing	TTGACTTTCAAAGACAACACATGACAAT
RPM1-f2	Sequencing of <i>RPM1</i> locus	CAGGTAACGAATGACGAAAACAACA
RPM1-f3	Sequencing of <i>RPM1</i> locus	GCG TGC GTT TCA TTT CCC GAG GTA T
RPM1-f4	Sequencing of <i>RPM1</i> locus	GGTGAAAAACTTGTGGAGTATTT

RPM1-f5	Sequencing of <i>RPM1</i> locus	CAATGATTTGCCATACCCGCTTAAA
RPM1-f6	Sequencing of <i>RPM1</i> locus	CTCTCCATCAGCAAGTTACCAGATT
RPM1-r2	Sequencing of <i>RPM1</i> locus	CAC ATG ACA ATC AAT CTG TTT GGT A
NDR1-f4	Amplification and sequencing of <i>NDR1</i> locus	CCCTCGTTAATTCTTGTGTTTGGTTCTT
NDR1-r3	Amplification and sequencing of <i>NDR1</i> locus	GGGACGGTTTCAATTCTGTGATAGAGTA
NDR1-r	Sequencing of <i>NDR1</i> locus	TATAAGTTTCTTTTCCCCATTTGAAC
RAR1-f	Amplification of <i>RAR1</i> locus for sequencing	GTTGTTACTCATTGTTAGTTTGAGATA
RAR1-r	Amplification of <i>RAR1</i> locus for sequencing	GCCTTGAATTACTCCACGGAGAGGTAC
RAR1-f2	Sequencing of <i>RAR1</i> locus	TACGGGCAAATCTTAATGTGAGATTTT
RAR1-f3	Sequencing of <i>RAR1</i> locus	CCAAGCCCCTCTGCATGGTATTAT
RAR1-f4	Sequencing of <i>RAR1</i> locus	GGTTTTGGATTAGCTGATTGATTAC
RAR1-f5	Sequencing of <i>RAR1</i> locus	GCACTGACTACTGGTTTTTGTTC
RAR1-r2	Sequencing of <i>RAR1</i> locus	TGATCCAAAACACAGAAGATGAGCATT
Genotyping		
MLA10seq-f	Genotyping of lines with MLA _{cc} -mYFP	CCTGATTCCCAAGTTGGGGGAGC
mYFPseq-r	Genotyping of lines with MLA _{cc} -mYFP	CTCGACCAGGATGGGCACCACCC
dde2-2-f	CAPS (BstUI) genotyping of <i>dde2-2</i>	GACACGAACCGGATCCAAAG
dde2-2-r	CAPS (BstUI) genotyping of <i>dde2-2</i>	GCCGAAATCCGCTTCCCTTTA
rar1-20-Fw	Genotyping of <i>rar1-20</i>	GAAGTAGGAGCCGCAACAGGATG
rar1-20-Rv	Genotyping of <i>rar1-21</i>	ACGACGGAATGAAAGAGTGGAG
dCAPS-AT3G02840-Fw	dCAPS (BstBI) AT3G02840 with AT3G02840-Rv1	GAAGATGTTCTTAGAAACGCTTTGATCGTTCCTCTTCTGGTGAAGAAGATTCTT <u>CGA</u>
sgt1b-Fw	dCAPS (Ddel) genotyping of <i>sgt1b (eta3)</i>	CTAATGAGATTTTCTCTCGGGTGGTTcTT
sgt1b-Rv	dCAPS (Ddel) genotyping of <i>sgt1b (eta3)</i>	TCTTGAGCTCCATGCCATCT
ndr1-1-Rv	Genotyping of <i>ndr1-1</i>	GGGACGGTTTCAATTCTGTGATAG
ndr1-1-Fw	Genotyping of <i>ndr1-1</i>	CGAGATTGCTCATTGCCATTGG

NDR1-WT-Fw	Genotyping of <i>ndr1-1</i>	TTTTCCACCATCAACACGA
NDR1-WT-Rv	Genotyping of <i>ndr1-1</i>	GCTCCAACCTCAACCCATA
Mq_1A-Fw1	CAPS (MnII) Genotyping of mutant candidate 1A	GGACCTACCTTTCACAGCATTCTTT
Mq_1A-Rv1	CAPS (MnII) Genotyping of mutant candidate 1A	TCGGAGGATAAGCCGGGAAAA
Mq_1B-Fw1	CAPS (MbolI) Genotyping of mutant candidate 1B	GATGTAGAGATTAAGAATTATGCTGACTCAA
Mq_1B-Rv1	CAPS (MbolI) Genotyping of mutant candidate 1B	TAGATCAATGCCCAAGACCCTGTAAAT
Mq_1C-Fw1	CAPS (EarI) Genotyping of mutant candidate 1C	GTTGCACCGAATGAACCAAAGTTT
Mq_1C-Rv1	CAPS (EarI) Genotyping of mutant candidate 1C	TGGTAGAACTCGTGCCTGTTGAGCAAT
Mq_1D-Fw1	CAPS (AluI) Genotyping of mutant candidate 1D	CCTGAACACAAGTCGCATAAAA
Mq_1D-Rv1	CAPS (AluI) Genotyping of mutant candidate 1D	GCTCCTTCGCCATCGATTGACTAA
Mq_1E-Fw1	CAPS (NdeI) Genotyping of mutant candidate 1E	GGGGCAATTCGTCCCTCCAGCAA
Mq_1E-Rv1	CAPS (NdeI) Genotyping of mutant candidate 1E	GCATTTTCATATCCTACCCCTAAA
Mq_2A-Fw1	CAPS (DraI) Genotyping of mutant candidate 2A	ACACAAAATGTTTCATCTGTAAATAAACTT
Mq_2A-Rv1	CAPS (DraI) Genotyping of mutant candidate 2A	CCTACTTTCGTCAAACCTCATGATCGCAA
Mq_2B-Fw1	dCAPS (SfaNI) Genotyping of mutant candidate 2B (AT1G11510)	GGTCGGGAGATCATGGCAGCTCCGTTTTTG GACGAGATCATCGCGTCTTAATGAAATTGAG CA
Mq_2B-Rv1	dCAPS (SfaNI) Genotyping of mutant candidate 2B (AT1G11510)	TTTTGATAATTTAGGGTTTTGCCCTTTT
Mq_2B-Fw2	dCAPS (BspCNI) Genotyping of mutant candidate 2B (PDR11)	GAGTGGGAGAGTGAGTTTGGCCTCCACCAG TCTCA
Mq_2B-Rv2	dCAPS (BspCNI) Genotyping of mutant candidate 2B (PDR11)	CAAGCTCAATCTTCCCGTTAGCCGACGTTT
Mq_2C-Fw1	dCAPS (Bsu36I) Genotyping of mutant candidate 2C	CCTTTTCTTAAAGAACCAACTTGCTTAGAAAT GAAGACAACAACCACAAAAGGCCCTAAG
Mq_2C-Rv1	dCAPS (Bsu36I) Genotyping of mutant candidate 2C	GGTACTAAGAAATGGACTGGTATTAATGACT
Mq_2D-Fw1	CAPS (Hpy166II) Genotyping of mutant candidate 2D	TACCAAGTATTAACGATCTCAGGAT
Mq_2D-Rv1	CAPS (Hpy166II) Genotyping of mutant candidate 2D	ATCAGGTCCACAGTTATTTTTATAA
Mq_2E-Fw1	CAPS (PsiI) Genotyping of mutant candidate 2E	CAAACATGGCATAACAATCTTACACTGACAGA T
Mq_2E-Rv1	CAPS (PsiI) Genotyping of mutant candidate 2E	ATTGATCCAAAACGCGCCAAGAGGTATT

Mq_2F-Fw1	dCAPS (BsmBI) Genotyping of mutant candidate 2F (CPK6)	GATTATGCATCATTTAGCTGGTCACAA
Mq_2F-Rv1	dCAPS (BsmBI) Genotyping of mutant candidate 2F (CPK6)	ACGCCTCAACAACACCGACAATGATCTTGGT CAACTCAGCAGCTTTTCGTCT
Mq_2F-Fw2	dCAPS (SfaNI) Genotyping of mutant candidate 2F (AGD1)	ATCAAAGTTGATGCAGATCAGACCGAT
Mq_2F-Rv2	dCAPS (SfaNI) Genotyping of mutant candidate 2F (AGD1)	CATCAATAAGATTTAAAAAATTCTGGTCATTC GGGGATGATGGAAGAGAGCA
Mq_2G-Fw1	CAPS (BbvI) Genotyping of mutant candidate 2G	GTACATACCTTAATTTATCATCTTGATAGT
Mq_2G-Rv1	CAPS (BbvI) Genotyping of mutant candidate 2G	ATTGTGTTATCGTGCGAGCCCATTGATGT
Mq_2H-Fw1	CAPS (Bfal) Genotyping of mutant candidate 2H	CTAGATTCAACTCTAATCATTGCGTCCCAA
Mq_2H-Rv1	CAPS (Bfal) Genotyping of mutant candidate 2H	AGAAGTAGCAGTAGAGAAACGTCCAAAGAAA CGAGGAA
Mq_2I-Fw1	CAPS (Sau96I) Genotyping of mutant candidate 2I	AAATACCGTTGGATTGGGACACAA
Mq_2I-Rv1	CAPS (Sau96I) Genotyping of mutant candidate 2I	ACCCAAGTTACTAGATTCTGTTCAT
Mq_2J-Fw1	dCAPS (Sau96I) Genotyping of mutant candidate 2J	GGAGACGAATGAGTTACCTTTTGATTTT
Mq_2J-Rv1	dCAPS (Sau96I) Genotyping of mutant candidate 2J	TCACTACTCTCTTTTCTCGCCTCATCCAACCA CTCTTTTGCTTGCTCAAGCTTGCC
Mq_2K-Fw1	dCAPS (PstI) Genotyping of mutant candidate 2K	GAGCAGAGGCCGTGGCAGATGCGAACAAA
Mq_2K-Rv1	dCAPS (PstI) Genotyping of mutant candidate 2K	CAAAAACCAACCATGAACAATGGAAGTAAT AGCTTGACAGATATATACCACATCTGCA
Mq_2L-Fw1	CAPS (AluI) Genotyping of mutant candidate 2L	AGCTAATACTACAGTGAGGAAAATCTTCT
Mq_2L-Rv1	CAPS (AluI) Genotyping of mutant candidate 2L	TATCTGCATCAATCTCTTCTTGTTTAGA
Mq_3A-Fw1	dCAPS (HindIII) Genotyping of mutant candidate 3A	GGAAAGAGAACAAACCAGGCCGTGT
Mq_3A-Rv1	dCAPS (HindIII) Genotyping of mutant candidate 3A	GCAATTAATGAGCTTTGCAGATGTATAA ATCTATCAGTGCAAGGTTCTGTAAGCT
Mq_3A-Fw2	CAPS (SfaNI) Genotyping of mutant candidate 3A	AAATCTTGATGACTGTAGAGCTCTTTGAT
Mq_3A-Rv2	CAPS (SfaNI) Genotyping of mutant candidate 3A	GCTCGAGCCTGTACAAGGCACAACCATCAC A
Mq_3A-Fw3	CAPS (MbolI) Genotyping of mutant candidate 3A	GAAGAAAGTCGCAAACCTTACCCAAAA
Mq_3A-Rv3	CAPS (MbolI) Genotyping of mutant candidate 3A	TGAAGAAGCCGCTACAGAACCAGTAAACGTC ACCGTTGCTT
Mq_3B-Fw1	dCAPS (Bfal) Genotyping of mutant candidate 3B	CAGTTGGGCTTTGCAAGTGCCCAATGGGCTT CGACAGTTTTTGAGGCGGTTACT
Mq_3B-Rv1	dCAPS (Bfal) Genotyping of mutant candidate 3B	GGCTCAATCTTCGTGATAATTTGAAGGATGA A
Mq_3C-Fw1	dCAPS (XbaI) Genotyping of mutant candidate 3C	CGACTACAGACTTGGACTAAGGACCCATTTCT T

Mq_3C-Rv1	dCAPS (XbaI) Genotyping of mutant candidate 3C	AGACTGTGCTAATGTCCAATTTAGTAAGTTACTAG
Mq_3D-Fw1	dCAPS (XhoI) Genotyping of mutant candidate 3D	CCCCTGCTTCTGGTATTCGACGATGCGTTAGGGTTTTATAAGAATTGAATTTGGGTTGAGCTC
Mq_3D-Rv1	dCAPS (XhoI) Genotyping of mutant candidate 3D	GTAATTCATAAGAGAAGATCAAAGGCCCTT
LBb1.3_long	Genotyping of SALK lines	TATAAGGGATTTTGCCGATTTCCGGAAC
RP_AT3G02840-Fw	Genotyping of SALK lines SALK_040843, SALK_007906C, SALK_113770C	GGTAAAGGGGAAACACGCGTAATCT
LP_AT3G02840-Rv	Genotyping of SALK lines SALK_040843, SALK_007906C, SALK_113770C	TTTTAGCGTCCTTACCGTTCAAGAACCG
Genome Walking		
LB-GSP1	Genome walking from Left Border of pTA7002	AAAAACGTCGCAATGTGTTATTAAGTTGTCTAA
LB-GSP2	Genome walking from Left Border of pTA7002	AGCGTCAATTTGTTTACACCACAATATATCCTG
RB-GSP2	Genome walking from Right Border of pTA7002	CAGTGTGGACAGGATATATTGGCGGGTAAA
LB-GSP4	Genome walking from Left Border of pTA7002	GTCCTCGGCCCAAAGCATCAGCTCAT
RB-GSP4	Genome walking from Right Border of pTA7002	TAAGTAAGAAAGGAACTAACAGTGTGATATTAA

1.5. Enzymes

1.5.1. Restriction endonucleases

Restriction enzymes were purchased from New England Biolabs (Frankfurt, Germany). Enzymes were supplied with 10x reaction buffer which was used for restriction digests according to the manufacturer instructions.

1.5.2. Nucleic acid modifying enzymes

Standard PCR reactions were performed using homemade *Taq* DNA polymerase. For higher accuracy in generating PCR products for cloning, *Pfx* polymerase was used. Enzymes and suppliers are listed below:

Taq DNA polymerase	homemade
AccuPrime™ <i>Pfx</i> DNA polymerase	ThermoFischer (Darmstadt, Germany)
pENTR™ /D-TOPO® Vector-topoisomerase I	Invitrogen (Darmstadt, Germany)
Gateway® LR Clonase® II Enzyme mix	Invitrogen (Darmstadt, Germany)

1.6. Chemicals

Laboratory grade chemicals and reagents were purchased from Sigma-Aldrich (Deisenhofen, Germany), Roth (Karlsruhe, Germany), Merck (Darmstadt, Germany), Invitrogen™ (Darmstadt, Germany), and Difco™ (Heidelberg, Germany) unless otherwise stated. A few critical chemicals are listed below:

Dexamethasone (DEX) (Sigma-Aldrich, D1756-1G): Stock 30 mM in 100% ethanol
 Estradiol (ER) (Sigma-Aldrich, E2758-1G): Stock 30 mM in 100% ethanol
 3-deazaneplanocin A (DZNep) (Millipore, 252790-2mg): Stock 2 mM in DMSO
 Zebullarine (Zeb) (Sigma-Aldrich, Z4775-25mg): Stock 11 mM in DMSO
 Lanthanum(III) chloride (LaCl₃) (Sigma-Aldrich, 203521-25G): Stock 100 mM in ddH₂O
 Diphenyleneiodonium (DPI) (Sigma-Aldrich, 43088-5G): Stock 700 μM in DMSO

1.7. Antibiotics

Ampicillin (Amp)	100 mg/ml in ddH ₂ O
Carbenicillin (Carb)	50 mg/ml in ddH ₂ O
Claforan (Cla)	200 mg/ml in ddH ₂ O
Gentamycin (Gent)	25 mg/ml in ddH ₂ O
Kanamycin (Kan)	50 mg/ml in ddH ₂ O
Rifampicin (Rif)	100 mg/ml in DMSO
Spectinomycin (Spe)	50 mg/ml in ddH ₂ O

Stock solutions (1000x) stored at -20°C. Aqueous solutions were sterile filtrated.

1.8. Media

Media were sterilised by autoclaving at 121°C for 20 min. Antibiotics and thermo-labile compounds were added into the media after cooling down to 55°C.

<i>Escherichia coli</i> media	Luria-Bertani (LB) broth or agar plates; SOC
<i>Pseudomonas syringae</i> media	NYG broth or agar plates
<i>Agrobacterium tumefaciens</i> media	YEB broth or agar plates
<i>Arabidopsis thaliana</i> media	Murashige and Skoog (MS) agar plates
<i>Saccharomyces cerevisiae</i> media	YPD broth or agar plates

1.9. Antibodies

Antibodies used for immunoblot analyses are listed below.

Primary antibodies used in this study

Antibody	Source	Dilution	Reference
α -GFP	mouse monoclonal	1:5000	JL-8, Clontech (Mountain View, USA)
α -pTpY	rabbit polyclonal	1:3000	9101, Cell Signaling (Danvers, USA)
α -Myc	goat polyclonal	1:5000	ab9132, Abcam (Cambridge, UK)
α -HA	rat monoclonal	1:5000	3F10, Roche (Penzberg, Germany)

Secondary antibodies used in this study

Antibody	Feature	Dilution	Source
goat α -mouse IgG-HRP	HRP-conjugated	1:10,000	Santa Cruz (Santa Cruz, USA)
goat α -rabbit IgG-HRP	HRP-conjugated	1:10,000	Santa Cruz (Santa Cruz, USA)
rabbit α -goat IgG-HRP	HRP-conjugated	1:10,000	Santa Cruz (Santa Cruz, USA)
goat α -rat IgG-HRP	HRP-conjugated	1:10,000	Santa Cruz (Santa Cruz, USA)

1.10. Buffers and solutions

Buffers and solutions are listed either below or in the corresponding method section. Buffers and solutions were prepared with ddH₂O water and either autoclaved or sterile-filtered when possible.

DNA gel loading dye (6x)	Tris	10 mM
	EDTA	60 mM
	Glycerol	60 ml
	Bromophenol blue	30 mg
	Xylene cyanol FF	30 mg
	ddH ₂ O to 100 ml	
	pH 7.5	
PCR reaction buffer (10x)	Tris	100 mM
	KCl	500 mM
	MgCl ₂	15 mM
	Triton X-100	1%
	pH 9.0	
Ponceau S	Ponceau S working solution was prepared by dilution of ATX Ponceau S concentrate (Sigma-Aldrich) 1:5 in ddH ₂ O	
SDS Running buffer (10x)	Tris	30.2 g
	Glycine	188 g
	SDS 10%	100 ml
	ddH ₂ O to 1 L	

SDS Sample buffer (2x)	Tris	0.125 M
	SDS	4%
	Glycerol	20%
	Bromophenol blue	0.02%
	Dithiothreitol (DTT)	0.2 M
	pH 6.8	
SDS Sample buffer (6x)	Tris	60 mM
	Glycerol	4.7 mL
	SDS	1.2 g
	Bromophenol	6 mg
	DTT (if necessary)	0.93 g
	ddH ₂ O to 10 ml	
	pH 6.8	
TAE buffer (50x)	Tris	242 g
	EDTA	18.6 g
	Glacial acetic acid	57.1 ml
	ddH ₂ O to 1 L	
	pH 8.5	
TBS-T buffer	Tris	1.21 g
	NaCl	8.76 g
	Tween	0.1%
	ddH ₂ O to 500 ml	
	pH 7.5	
TE buffer	Tris	10 mM
	EDTA	1 mM
	pH 8.0	
Transfer buffer	Tris	3 g
	Glycine	14.4 g
	SDS 10%	1 ml
	Methanol	200 ml
	ddH ₂ O to 1 L	

2. Methods

2.1. Maintenance and cultivation of *A. thaliana* plants

Unless otherwise specified, sterilised seeds were sown onto ½ MS 0.8% agar plates containing claforan. The seeds were stratified 3 days at 4°C in the dark. Afterwards, the plates were transferred to a plant growth cabinet under short day conditions (10 h photoperiod, 22°C). After 10-14 days of growth on plates, the seedlings were transferred to 7x7 cm pots containing moist compost treated with BioMükk (Biofa, Münsingen, Germany) and grown under short day conditions (10 h photoperiod, 22/21°C, 65/60% humidity (d/n)). The pots were covered with propagation lids until two weeks after transfer. To obtain progeny, six week old plants were transferred to long day conditions (16 h photoperiod) and allowed to flower. To collect seeds, aerial tissue was enveloped with a paper bag and sealed with tape at its base until siliques were ripe.

2.2. Generation of *A. thaliana* F₁, F₂, and F₃ progeny

Male flower organs were removed with fine tweezers. Flowers with a well-developed stigma and immature stamens were used for crossing to prevent self-pollination. Fresh pollen from three independent donor flowers was dabbed onto each stigma. F₁ seeds were harvested from mature siliques and allowed to dry. F₁ seeds were grown as described above, genotyped using resistance or genetic markers, and allowed to self-pollinate. Produced F₂ seeds were collected, genotyped, stored, and/or propagated to produce the F₃ seeds similarly to the F₂.

2.3. *Agrobacterium*-mediated stable transformation of *A. thaliana* (floral dip)

The method for *Agrobacterium*-mediated stable transformation of *A. thaliana* was adapted from Clough and Bent, 1998. When plants had a maximum of young flower heads, plants were used for transformation. Already formed siliques were cut off. *Agrobacterium* was grown in YEB broth containing the proper antibiotics at 28°C overnight. The bacteria were pelleted and resuspended in 5% sucrose 0.06% Silwet L-77 (Lehle seeds, USA) to OD₆₀₀ 0.8. Inflorescences to transform were inverted and submerged into the cell suspension for 10 seconds. The inflorescences were allowed to dry for a few minutes and covered with plastic bags. The plants were kept one day away from direct light. Afterwards the bags were removed and the plants moved to direct light and let to set seeds.

2.4. *A. thaliana* seed surface sterilization

2.4.1. Standard seed surface sterilization

Unless otherwise specified, seeds were sterilized according to the method described here. Seed sterilization was applied prior to *in vitro* sowing of *A. thaliana* seeds. Seeds were distributed into 1.5 ml microcentrifuge tubes, incubated in 70% EtOH + 0.05% Tween20 for 5 min (1 min for *ppsdes* mutant), briefly washed in 95% EtOH and allowed to dry on sterile Whatman paper in a sterile hood.

2.4.2. Vapor phase seed surface sterilization

This method was used for high throughput sterilization of the M₂ seeds prior sowing onto plates for screening (see Results section 2.2.2.1). Batches of about 50 seeds were transferred into small glass vials let open and racked. The racks were placed into a desiccator jar. A beaker containing 80 ml of 12% NaOCl was placed into the jar. The jar was quickly closed after adding 2.5 ml concentrated HCl into the beaker. Sterilization by chlorine fumes was allowed for five hours.

2.5. *Pseudomonas syringae* pv. *tomato* inoculation

Pst cultures of the denoted strains were started from bacteria grown on NYG agar plates younger than one week. One day before infection, bacterial strains were grown in NYG broth medium containing the appropriate antibiotics and incubated ON at 28°C. Afterwards, bacteria were pelleted and resuspended at the appropriate concentration in the appropriate solution.

2.5.1. *Pst* spray-infection

Concentration of *Pst* AvrRpm1 bacteria was adjusted to OD₆₀₀ 0.2 (10⁸ CFU/ml) in 10 mM MgCl₂ + 0.02% Silwet L-77 (Lehle seeds, USA). Five week old M₂ plants grown under short day conditions were watered and covered with a lid to allow opening of stomata for four hours. Afterwards, the plants were sprayed with the bacterial solution using a dispenser, returned to a growth chamber under short day conditions and kept under cover for two more days.

2.5.2. *Pst* detached leaf dipping

Concentration of *Pst* AvrRpm1 bacteria was adjusted to OD₆₀₀ 0.2 (10⁸ CFU/ml) in 10 mM MgCl₂ + 0.02% Silwet L-77 (Lehle seeds, USA). Four week old M₂ plants grown under short

day conditions were watered and covered with a lid to allow opening of stomata for four hours. Afterwards several leaves for each individual plant were cut, dipped for 10 s into the bacterial solution and incubated on 1% agar plates containing 25 $\mu\text{g/ml}$ Kan. After two days, the leaves were surface sterilized with 70% ethanol for 30 s, briefly rinsed with ddH₂O, and dried on paper. Five leaf discs (5 mm diameter) were sampled with a biopsy punch, ground in 100 μL MgCl₂, incubated 1h with shaking, and the volume was adjusted to 1 ml. Dilution series were plated onto YEB containing the appropriate antibiotics. The plates were incubated for two days at 28°C before scoring colonies.

2.5.3. *Pst* infiltration assay for ion leakage measurement

Concentration of *Pst* bacteria was adjusted to OD₆₀₀ 0.4 ($2 \cdot 10^8$ CFU/ml) in 10 mM MgCl₂. Two to three leaves from four to five week old plants grown under short day conditions were syringe-infiltrated. Twenty min after infiltration, 3x4 leaf discs (5 mm diameter) were sampled with a biopsy punch, rinsed briefly in ddH₂O, dried on paper, and transferred to three wells of a 24-well plate containing each 1 ml ddH₂O + 0.001% Silwet (Lehle seeds, USA). The conductivity was measured every two hours using a LAQUAtwin COND (Horiba).

2.5.4. *Pst* infiltration assay for RNA-seq

Concentration of *Pst* bacteria was adjusted to OD₆₀₀ 0.001 ($5 \cdot 10^5$ CFU/ml) in ddH₂O. Leaves from 4.5 week old plants grown under short day conditions were syringe-infiltrated. Samples were taken at the appropriate time points for RNA extraction.

2.6. Temperature shift

2.6.1. Temperature shift for analysis of the phenotype of the *p35S:MLACC-mYFP* lines

Seeds were sown onto $\frac{1}{2}$ MS agar plates, vernalized for three days, and transferred to a growth chamber at 28°C under short day conditions. Ten-day old seedlings were transferred to pots (2 seedlings per pot) and further grown at 28°C covered by a lid under short day conditions. Four weeks after germination, half of the pots were kept in the same chamber whilst the other half was transferred to 19°C and short day conditions for one week. One week after transfer, pictures were taken, 30 mg FW were extracted with 80 μL of 2x SDS Sample buffer and 20 μL were used for western blot analysis, and the fresh weight of each plant was measured. The experiment was repeated three times apart from the weight quantification which was performed for two independent experiments.

2.6.2. Temperature shift for RNA-seq

The experiment was essentially performed as described in Heidrich et al., (2013). Seeds were sown directly onto pots (10 seeds-pot) covered with a lid, vernalized three days at 4°C and subsequently transferred to 28°C under short days conditions. The lid was removed one week after germination. 3.5 weeks after germination, the plants were transferred to 19°C and sampled at the appropriate time points after shift. The temperature shift was conducted at different times in the day to obtain synchronised harvests between 4 pm and 5 pm for all time points. Leaf material from 4-6 individual plants was pooled for each sample and used subsequently for RNA extraction and RNA-seq. The experiment was repeated independently three times.

2.7. EMS-induced mutagenesis

Batches of 100-200 mg seeds were imbibed ON at 4°C in 12.5 mL ddH₂O. Afterwards, 12.5 mL of 0.6% (v/v) ethyl methanesulfonate (EMS, prepared fresh, Sigma-Aldrich M0880) was added and the resulting mixture was incubated for 8-9 h with shaking at room temperature. After incubation, the seeds were extensively washed with ddH₂O and kept three days at 4°C in water until sowing.

2.8. Yeast two-hybrid (Y2H) screening

2.8.1. Y2H screening for AT3G02840 interaction partners

The *A. thaliana* cDNA library in pB42AD was generated by van der Biezen et al., (2000). The pB42AD vectors were transformed in YM4271 (MAT α) using the LiAc method (Gietz and Woods, 2002).

The pLexA-AT3G02840 was obtained from LR reaction between the pLexA-GW and the pENTR-AT3G02840 vector, and transformed into the yeast strain EGY48 (MAT α) using the LiAc method.

The yeast two hybrid screening was performed with a method modified from Kolonin et al., (2000). An overnight culture of the bait strain or control strain was prepared in SD -His -Ura liquid medium and resuspended in ddH₂O at the concentration 10⁹ CFU/mL. The library strain (YM4271 (MAT α)) was combined with the bait strain (EGY48 (MAT α)) or control strain. 2.10⁸ CFU of the bait strain or control strain were combined with 10⁸ CFU of the library strain, transferred to 200 μ L YPD medium, plated on YPD plates, and incubated for 12-15 h at 30 °C to allow mating. The cells on each plate were resuspended with 2 mL of liquid SD Galactose (Gal)/ Raffinose (Raf)/ -Ura, -His, -Trp medium, pelleted, transferred to 100 mL of SD Gal/Raf/ -Ura,-His,-Trp liquid medium in a 500 mL flask, and incubated for 6 h at 30 °C with shaking. Cells were collected by centrifugation and resuspended in 5 ml sterile water to ~10⁸ cells/mL (OD₆₀₀~ 5.0). To select for interactors from the library mating, 100 μ L of the undiluted cells were plated on twenty SD Gal/Raff/ -Ura, -His, -Trp, -Leu plates. Plates were incubated at 30 °C for 3 days. The positive diploids were patched onto SD Gal/Raf/-Ura -His -Trp - Leu/+x- β -Gal media. For positive colonies a yeast colony PCR was

performed, the PCR product was purified and sequenced. In total, 2×10^7 diploid cells were screened with approximately 60% of mating efficiency. More than 1,000 clones showed β -Galactosidase activity. 300 clones were sequenced using the Sanger method.

2.8.2. Y2H screening for MLACC interaction partners (AIST system)

The pDEST-BTM116-MLACC₁₋₁₆₀ and pDEST-BTM116-MLACC₁₋₂₂₅ bait vectors were obtained by LR reaction between the corresponding pENTR vectors and the pDEST-BTM116 vector. The *A. thaliana* TF prey library was generated by Mitsuda et al., 2010. The screen was conducted in the group of Dr. Nobutaka Mitsuda (AIST, Japan) according to the method published in Mitsuda et al., (2010). The AIST system involves GAL4 (prey) /LexA (bait) and *HIS3* was used as reporter. The screening was conducted in a nearly binary fashion, in which up to 4 homologous TR prey constructs (e.g. bZIP family) were transformed into yeasts expressing a single bait protein. Once positive interactions were detected, individual prey construct were transformed to the respective yeasts expressing a single bait protein to confirm interactions as described in Mitsuda et al., (2010). Two independent replicates were performed for the screen involving the MLA10_{CC1-225} bait. Any interaction identified by either of the replicates was taken into account. Interactions were detected between MLACC and bZIP18, bZIP29 and bZIP30, but these interactions were not considered because the corresponding prey constructs have been shown to produce false positives in the AIST system. For similar reasons, the trihelix AT3G11100 and the bZIP VIP1 have to be considered as candidates with caution.

2.9. Dexamethasone (DEX)-inducible expression in stable *A. thaliana* transgenic lines

2.9.1. Leaf disc assays

Four to six week old plants grown under short day conditions were used. For electrolyte leakage assay, 3x4 leaf discs (5 mm diameter) from at least four independent plants were sampled with a biopsy punch, rinsed briefly in ddH₂O, dried on paper, transferred to three wells of a 24-well plate containing each 1 ml +/-10 μ M DEX + 0.001% Silwet (Lehle seeds, USA), and incubated at 20°C for the time of the experiment. The conductivity was measured along time using a LAQUAtwin COND (Horiba). For western blot analysis, six leaf discs (5 mm diameter) from at least four independent plants were sampled with a biopsy punch, transferred to 1 ml of 10 μ M DEX + 0.001% Silwet (Lehle seeds, USA), incubated at 20°C for the appropriate time, dried, and extracted with 80 μ L of 2x SDS sample buffer. Twenty μ L were used for loading onto SDS-Page gel.

In the case of LaCl₃ and diphenyleneiodonium (DPI) treatments, leaf discs were pre-incubated with 2 mM LaCl₃ or 7 μ M DPI or the respective control buffers (water and 1% DMSO respectively) for 20 min prior addition to DEX to a final concentration of 10 μ M.

In the case of PLA2A inhibitors aristolochic acid (ARA) and bromoenol lactone (BEL) treatments, leaf discs were transferred to a solution containing 30 μ M ARA or 30 μ M BEL or the respective control buffers (0.1% DMSO) and +/- 10 μ M DEX.

2.9.2. Leaf infiltration

Seeds of the F₂.BC_T progeny were sown on ½ MS agar plates containing Cla, vernalized for three days at 4°C and grown for 10 days at 22°C under short day conditions (10 h photoperiod). Afterwards, all seedlings were transferred to Jiffy pots supplemented with a fertilizer (Wuxal TopN, Aglukon Spezialdünger) and further grown under short day conditions at 22°C. Four week after germination, the two or three youngest and fully expanded leaves were infiltrated with 1 μ M DEX. For electrolyte leakage assay, 3 x 4 leaf discs (5 mm diameter) from at least five independent plants were sampled with a biopsy punch 20 min after infiltration, rinsed briefly in ddH₂O, dried on paper, transferred to three wells of a 24-well plate containing each 1 ml ddH₂O + 0.001% Silwet L-77 (Lehle seeds, USA), and incubated at 20°C for the time of the experiment. The conductivity was measured along time using a LAQUAtwin COND (Horiba). For RNA-seq, western blot analysis, trypan blue staining, and detection of phosphorylated MAPKs, six leaf discs (5 mm diameter) from at least five independent plants were sampled with a biopsy punch at the appropriate time after infiltration. The 0 h time point was taken at 3-5 min after infiltration. Samples for western blot were extracted with 80 μ L of 2x SDS sample buffer. Twenty μ L were used for loading onto SDS-Page gel.

2.10. Estradiol (ER)-inducible expression in stable *A. thaliana* transgenic lines

2.10.1. Seedling assays

Seedlings were mainly used for immunodetection of the protein encoded by the transgene and electrolyte leakage measurements. 10-14 day old seedlings grown on ½ MS agar plates were used. For immunodetection of proteins, 8 seedlings were gently transferred to 1 mL 10 μ M ER + 0.001% Silwet L-77 (Lehle seeds, USA) and incubated at 20°C for the appropriate time. Afterwards, the seedlings were dried and frozen in 1.5 mL microcentrifuge tubes containing 5 steel beads (2 mm) in liquid nitrogen for protein extraction. The samples containing 8 seedlings were extracted with 80 μ L of 2 x SDS sample buffer. For electrolyte leakage measurement, 3 x 6 seedlings were rinsed briefly in ddH₂O, dried on paper, transferred to three wells of a 24-well plate containing each 1 ml of 10 μ M ER + 0.001% Silwet L-77 (Lehle seeds, USA), and incubated at 20°C for the time of the experiment. The conductivity was measured along time using a LAQUAtwin COND (Horiba).

2.10.2. Large scale induction of older plants

For TAP and SDD-AGE analysis, large amounts of plant material were prepared. Seed batches of 50 mg were mixed with 35 mL agar 0.01% and sown onto 35 pots (7 x 7 cm). After three days at 4°C in the dark, the pots were transferred to growth chambers under short day conditions (10 h photoperiod) at 22°C covered with a lid for the first 10 days. Three-week old plants were used. The aerial parts were sampled by cutting the hypocotyl with scissors, carefully transferred to 2 L of ER 10 µM + 0.001% Silwet L-77 (Lehle seeds, USA) and incubated at 20°C for 16 h. Afterwards, the plant material was quickly drained, dried with paper towels and frozen into liquid nitrogen. The frozen material was frozen-ground with mortar and pestle into a fine powder and stored at -80°C for further use. One batch of plants usually resulted in 40-55 g plant powder.

2.11. Screening for suppressors of MLA_{CC}-mediated signalling

2.11.1. Primary screening on plates

Vapor phase-sterilised seeds (~50 seeds per batch) were sown onto vertical ½ MS agar plates containing 10 µM DEX, vernalized for three days at 4°C and transferred to a growth chamber under short day conditions (10h photoperiod) at 22°C. The seedlings able to grow were recovered at 10 dp and transferred to soil for further screening and propagation.

2.11.2. Primary screening on soil

Seeds were vernalized three days in DEX-containing agar (0.01% agar + 30 µM DEX) and subsequently sown on moist compost. The seedlings were sprayed with a DEX solution (30 µM DEX + 0.01% Silwet L-77) at 5 and 7 days after germination. The seedlings able to grow were recovered at 10 dp and transferred to soil for further screening and propagation.

2.11.3. Secondary screening

One young leaf (~2-3 mm diameter) per 16-day old plant was cut, transferred to 200 µL 10 µM DEX + 0.001% Silwet (Lehle seeds, USA), incubated at 20°C for 16 h and subsequently observed with a Axio Imager A2 fluorescence microscope (Zeiss) to score the YFP signal density in the upper leaf epidermis compared to the non-mutagenized parental line and the auto-fluorescence observed at different excitation wavelengths. The scoring for the transgene expression level was defined as follows: “++++”, more than 75% of YFP positive cells; “+++”, 50-75% of YFP positive cells, “++” 25-50% of YFP positive cells, “+”, 10-25% of YFP positive cells. The scoring for auto-fluorescence was defined as follows: “+++”, more than 90% of auto-fluorescent cells; “++”, 50-90% of auto-fluorescent cells, “+” 10-50% of auto-fluorescent cells.

2.11.4. Analysis of the M₃ and F₂.BC_T progeny

2.11.4.1. Scoring and selection of mutant plants

Seeds of the M₃ and F₂.BC_T progeny were analysed as described in the method sections 2.10.1 and 2.10.3 with some modifications. The seeds were grown on horizontal ½ MS agar plates containing 10 µM DEX +/- 2 µM 3-Deazaneplanocin A (DZNep) for 14 days prior transfer to soil.

2.11.4.2. Selection of wild-type plants in the F₂.BC_T progeny (negative segregant bulk)

Seeds of the F₂.BC_T progeny were sown on ½ MS agar plates, vernalized for three days and grown for 10 days at 22°C under short day conditions (10 h photoperiod). Afterwards, all seedlings were transferred to soil and further grown under short day conditions at 22°C. Four week after germination, two leaves per plant were infiltrated with 1 µM DEX. Plants displaying a wild-type like phenotype (i.e. like the non-mutagenized parental line) were selected based on visible leaf yellowing or tissue collapse symptoms from two to four days after infiltration.

2.12. Trypan blue staining

A. thaliana leaves were boiled for 3 min in a 1:1 mixture of ethanol and staining solution (10 ml lactic acid, 10 ml glycerol, 10 g phenol and 10 mg trypan blue, dissolved in 10 ml distilled water) for staining. The leaves were then de-stained three times in 2.5 g/ml chloral hydrate in distilled water. After destaining, the leaves were imaged on an Axio Imager.D2 fluorescence microscope (Zeiss) equipped with a Zeiss EC Plan-NEOFLUAR 5x/0.16 dry objective.

2.13. Biochemical methods

2.13.1. *A. thaliana* total protein extraction for immunoblot analysis

Plant material was frozen in liquid nitrogen in 1.5 mL microcentrifuge tubes together with 5 steel beads (2 mm diameter). Samples were homogenized 2 x 1 min at 30 Hz to a fine powder using a MM400 tissue lyser (Retsch) whose adapter racks had been pre-cooled at -80°C. 2x SDS sample buffer was added to the frozen powder (usually 80 µL for 6 leaf discs), the samples were vortexed, spun down, boiled for 4 min at 95°C, and centrifuged 10 min at 18,000 g. The supernatant was stored at -20°C if not directly loaded onto SDS PAGE.

2.13.2. Denaturing SDS-polyacrylamide gel electrophoresis (SDS-PAGE)

Denaturing SDS-PAGE was carried out using Mini-Protean system (BioRad) according to the manufacturer instructions. Tris-Glycine polyacrylamide gels, 1.5 mm thick, were prepared with the composition indicated below. After polymerization, the gels were placed in the electrophoresis tank and submerged in 1 x SDS running buffer. A pre-stained molecular weight marker and denatured protein samples were loaded onto the gel (usually 20 μ L) and run at 90-100 V until the desired separation was reached.

Composition of polyacrylamide gels (15 mL)

	10% resolving	12% resolving	5% stacking
ddH ₂ O	4 mL	3 mL	10.2 mL
30% acrylamide/bis solution 29:1	5 mL	6 mL	2.5 mL
1M Tris-HCl pH 8.8	5.7 mL	5.7 mL	-
1M Tris-HCl pH 6.8	-	-	1.9 mL
10% SDS	150 μ L	150 μ L	150 μ L
10% ammonium persulfate	150 μ L	150 μ L	150 μ L
TEMED (Biorad)	6 μ L	6 μ L	15 μ L

2.13.3. Immunoblot analysis (Western Blot)

Proteins separated by SDS-PAGE were electro-blotted onto Immobilon-P PVDF transfer membranes (Merck Millipore) in transfer buffer for 140 min at 100 V in a Mini Trans-Blot apparatus (Biorad) according to the manufacturer instructions. Equal protein transfer was monitored by staining membranes with Ponceau S for 5 min. Destained membranes were washed 3 x in TBS-T, blocked for 3 h in 5% milk TBS-T before ON incubation at 4°C with the primary antibody in 5% milk TBS-T. The membranes were washed 3 x with TBS-T, and the appropriate horseradish (HRP)-conjugated secondary antibody was applied for 2 h in 5% milk TBS-T. After 3 x washes with TBS-T, the proteins were detected using Pico or Femto chemiluminescence reagent (ECL, Pierce Thermo Scientific) and the ChemiDoc MP imaging system (Biorad).

2.13.4. Detection of phosphorylated MAPK by Western Blot

2.13.4.1. MAPK extraction

Plant material from six leaf discs (5 mm diameter) was frozen in liquid nitrogen and ground together with 5 steel beads (2 mm diameter) for 2 x 1 min at 30 Hz using a MM400 tissue

lyser (Retsch) whose adapter racks had been pre-cooled at -80°C . Proteins were extracted in $90\ \mu\text{L}$ MAPK lysis buffer, mixed and centrifuged for 15 min at 15,000 rpm at 4°C . The supernatant ($80\ \mu\text{L}$) was transferred to a fresh tube. The concentration adjusted after determination of the protein concentration with Bradford, 6x SDS samples buffer was added, boiled 5 min at 96°C and stored at -20°C until use for western blot analysis.

MAPK Lysis buffer

50 mM	Tris-HCl pH 7.5
200 mM	NaCl
1 mM	EDTA
10 mM	NaF
25 mM	beta-glycerophosphate
2 mM	sodium orthovanadate
10%(v/v)	glycerol
0.1 mM	Tween-20
0.5 mM	DTT
1 mM	PMSF
1x	Plant Proteinase Inhibitor (Roche)

2.13.4.2. Immunodetection of phosphorylated MAPKs

The immunodetection of phosphorylated MAPK was performed according to the protocol described in Method sections 2.13.2 and 2.13.3 with the differences indicated below. The samples were separated on a 10% SDS acrylamide gel. Blocking was done in 5% milk TBS-T ON at 4°C . After blocking, the membrane was extensively washed with TBS-T. Incubation with the primary antibody ($\alpha\text{-pTpY}$, 1:3000) was performed at 4°C in 5% BSA TBS-T for 5-6 h. The secondary antibody (goat $\alpha\text{-rabbit IgG-HRP}$, 1:10,000) was applied for 1 h at room temperature in 5% milk TBS-T.

2.13.5. Semi-Denaturing Detergent-Agarose Gel Electrophoresis (SDD-AGE)

The SDD-AGE was carried essentially as described in Halfmann and Lindquist, (2008). The plant material used was prepared as described in the method section 2.10.2. 400 mg frozen powder were mixed with $135\ \mu\text{L}$ of 4 x SDD buffer. The mixture was quickly vortexed, incubated for 5 min at room temperature, and centrifuged for 10 min at 16,000 g and room temperature. The supernatant ($\sim 450\ \mu\text{L}$) was collected and one fraction boiled for 4 min at 95°C . $60\ \mu\text{L}$ of each sample was loaded on a 1.5% agar gel ($8 \times 10\ \text{cm}$) containing 0.1% SDS immersed in 1 x TAE + 0.1% SDS and ran at 30 V for several hours. After separation, the gel was blotted in 1 x TBS onto a nitrocellulose membrane overnight at room temperature

following the standard procedure. After blotting, the membrane was processed following the protocol for standard immunodetection.

4X SDD buffer	TBS
2X TAE 20% glycerol 8% SDS 0.008% Bromophenol blue 1x PI Roche (added at the last moment) 2% β -mercaptoethanol (added at the last moment)	20 mM Tris 0.1 M NaCl pH 7.5

2.13.6. Tandem affinity purification (TAP) of protein complexes

The tandem affinity purification was performed as described in sections 2.2-2.4 and 3.2-3.4 of Bigeard et al., (2014). The input plant material consisted in 35-50 g of material produced as described in method section 2.10.2. Proteins were extracted as in Bigeard et al., (2014) using an extraction buffer supplemented with 0.1% SDS. An aliquot of this input extract was kept for MS analysis. The first and second affinity purification steps were performed as described. After the last elution, the eluates were directly used for subsequent MS analysis without precipitation.

2.13.7. Mass spectrometry (MS) analysis of *A. thaliana* protein extracts

2.13.7.1. Proteolytic digestion and desalting

Samples were processed using the FASP method (Wiśniewski et al., 2009) as described in detail in Hartl et al., (2015). Typically, 10-20 μ g of proteins pulled down with the TAP protocol were prepared for mass spectrometric (MS) analysis. For measurements of the extract proteome, starting material was 50 μ g protein extract. Cysteines were alkylated by incubation with 55 mM chloroacetamide in UA buffer for 30 min at room temperature in the dark followed by three washing steps with UA buffer. Incubation with LysC in UA buffer (1:50 enzyme-to-protein ratio) was performed over night at room temperature. The sample was diluted with ABC buffer (50 mM ammoniumbicarbonate) to a final urea concentration of 2 M urea. Trypsin digestion (1:100 enzyme-to-protein ratio) was performed for 4 h at room temperature. The sample was passed through the filter by centrifugation at 14,000 g for 10 min and residual peptides eluted with 50 μ l ABC. Formic acid was added to a final concentration of 0.5%. Pulldown samples were desalted with StageTips (Empore C18, 3M) as described in Rappsilber et al., (2007). For extract proteome analysis, peptides were desalted and pre-fractionated prior LC-MS/MS into three fractions using the Empore Styrenedivenylbenzene Reversed Phase Sulfonate material (SDB-RPS, 3M) as described in detail in Kulak et al., (2014).

2.13.7.2. LC-MS/MS data acquisition

Dried peptides were redissolved in 2% ACN, 0.1% TFA for analysis and adjusted to a final concentration of 0.18 $\mu\text{g}/\mu\text{l}$. Samples were analysed using an EASY-nLC 1000 (Thermo Fisher) coupled to a Q Exactive Plus mass spectrometer (Thermo Fisher). Peptides were separated on 16 cm frit-less silica emitters (New Objective, 0.75 μm inner diameter), packed in-house with reversed-phase ReproSil-Pur C18 AQ 3 μm resin (Dr. Maisch). Peptides (1 μg) were loaded on the column and eluted for 130 min (pulldowns) or 120 min (proteomes) using a segmented linear gradient of 0% to 95% solvent B (solvent A 5% ACN, 0.5% FA; solvent B 100% ACN, 0.5% FA) at a flow-rate of 300 nL/min (pulldowns) or 250 nL/min (proteomes). Mass spectra were acquired in data-dependent acquisition mode with a TOP12 (pulldowns) or TOP15 (proteomes) method. MS spectra were acquired in the Orbitrap analyser with a mass range of 300–1750 m/z at a resolution of 70,000 FWHM and a target value of 1×10^6 (pulldowns) 3×10^6 (proteomes) ions. Precursors were selected with an isolation window of 1.3 m/z . HCD fragmentation was performed at a normalized collision energy of 25. MS/MS spectra were acquired with a target value of 10^5 ions at a resolution of 17,500 FWHM and a fixed first mass of m/z 100. Peptides with a charge of +1, greater than 6, or with unassigned charge state were excluded from fragmentation for MS2, dynamic exclusion for 30s prevented repeated selection of precursors.

2.13.7.3. Data analysis

Raw data were processed using MaxQuant software (version 1.5.2.8, <http://www.maxquant.org/>) (Cox and Mann, 2008) with label-free quantification (LFQ) and iBAQ enabled (Cox et al., 2014). MS/MS spectra were searched by the Andromeda search engine against the Arabidopsis TAIR10_pep_20101214 database (ftp://ftp.arabidopsis.org/home/tair/Proteins/TAIR10_protein_lists/) supplemented with the sequences of MLA_{CC}-PC2 and mYFP-PC2. Sequences of 248 common contaminant proteins and decoy sequences were automatically added during the search. Trypsin specificity was required and a maximum of two missed cleavages allowed. Minimal peptide length was set to seven amino acids. Carbamidomethylation of cysteine residues was set as fixed, oxidation of methionine and protein N-terminal acetylation as variable modifications. Peptide-spectrum-matches and proteins were retained if they were below a false discovery rate of 1%. Subsequent quantitative statistical analyses were performed in Perseus (version 1.5.1.6, <http://www.maxquant.org/>; (Cox and Mann, 2012)). Hits were only retained if they were quantified in at least two replicates in any experimental set performed in the same background. LFQ intensities were log₂-transformed. NA values were replaced by the lowest log₂ LFQ intensity (14). Log₂-transformed LFQ ratios between the sample and the control conditions were computed for each pair of sample+control which were prepared and analysed at the same time (5 pairs in total). The average LFQ ratios were calculated from the five ratios obtained. For each protein group, a p-value was calculated using a one-sample test (t-test based on the comparison of the log₂-transformed average LFQ ratio to 0) to assess the statistical differences in the sample line compared to the control lines.

2.14. Molecular biological methods

2.14.1. Isolation of genomic DNA from *A. thaliana* (Edwards method)

This method was used for rapid DNA isolation used as a template for PCR. A piece of leaf (5 mm diameter) was placed into a 1.5 mL microcentrifuge tube together with 5 steel beads (2 mm diameter) or into a 96-well disruption vessel containing zirconia beads, frozen into liquid nitrogen and homogenized 2 x 1 min at 30 Hz in a MM400 tissue lyser (Retsch). 150 µL of Edwards Buffer (200 mM Tris-HCl pH 7.5, 250 mM NaCl, 25 mM EDTA, 0.5% SDS) was added to the powder. The sample was quickly vortexed and centrifuged for 15 min at 4°C and maximum speed. 100 µL of the supernatant was mixed with 100 µL isopropanol and centrifuged for 30 min at room temperature and maximum speed. The pellet was washed with 200 µL 70% ethanol, vortexed, and centrifuged for 10 min at room temperature and maximum speed. The ethanol was removed and the pellet allowed to air-dry before resuspension in 50 µL TE 10:1.

2.14.2. Isolation of high molecular weight genomic DNA from *A. thaliana*

For application in whole genome resequencing and genome walking, 50-100 mg of leaf material from four to six week old plants were frozen inside 1.5 mL microcentrifuge tubes in liquid nitrogen, and ground manually with a pestle to a fine powder. DNA was extracted either with the Nucleon PhytoPure kit (GE Healthcare) or with the DNeasy Plant Mini kit (Qiagen) following the manufacturer instructions, including a RNase treatment. The purified DNA was recovered in 50 µL of TE 10:0.1 pH 8.

2.14.3. Isolation of total RNA from *A. thaliana*

Total RNA was prepared from 3- to 4-week old plant material. 50-100 mg of leaf material were frozen inside 1.5 mL microcentrifuge tubes in liquid nitrogen, and ground manually with a pestle to a fine powder. Total RNA was extracted with the Plant RNeasy kit (Qiagen) according to the manufacturer instructions. On-column DNase treatment with the RNase-Free DNase Set (Qiagen) was performed according to the manufacturer instructions for the samples analysed by RNA-seq. The final RNA was eluted in 30 µL RNase-Free water.

2.14.4. Polymerase chain reaction (PCR)

Standard PCR reactions were performed using homemade *Taq* DNA polymerase. For cloning of PCR products, Pfx polymerase was used according to the manufacturer instructions. PCRs were carried out using either a GeneAmp PCR system 9700 (PE Applied Biosystems) or a T3000 thermocycler (Biometra).

2.14.5. Plasmid DNA isolation from bacteria

Standard alkaline cell lysis minipreps of plasmid DNA were carried out using the Macherey-Nagel plasmid prep kit according to the manufacturer instructions.

2.14.6. Restriction endonuclease digestion of DNA

Restriction digests were carried out according to the manufacturer instructions. Usually, reactions prepared using 1 μ L of restriction enzyme per 100 μ L reaction and the digests were conducted at the appropriate temperature for a minimum of 3 h.

2.14.7. Cloning of DNA fragments into pENTR/D-TOPO vector

All the cloning work described in this study was performed using the Gateway technology®. After synthesis by PCR, the appropriate DNA fragments were transferred into the pENTR/D-TOPO entry vector using the pENTR/D-TOPO cloning kit (Thermo Fisher Scientific) according to the manufacturer instructions. 2 μ L of the resulting product were used for transformation into *E. coli* DH5 α .

2.14.8. Site specific recombination of DNA in Gateway®-compatible vectors

LR reactions between the entry clones and the Gateway® destination vectors were performed with the Gateway LR clonase II enzyme mix (Thermo Fisher Scientific) according to the manufacturer instructions. 2.5 μ L of the resulting product was used for transformation into *E. coli* DH5 α .

In case the pENTR vector and the Gateway® destination vector carried the same antibiotic resistance marker, the pENTR was linearized using AlwNI or EcoRV restriction prior to the LR reaction.

2.14.9. Agarose gel electrophoresis of DNA

Gels were prepared with 0.8-2.5% (w/v) Seakem® LE agarose (Cambrex, USA) in TAE buffer and agarose was dissolved by heating in a microwave. Ethidium bromide was added to a final concentration of 0.3 μ g/mL into the gel during cooling down below 50°C. Samples mixed with 6 x DNA loading buffer were added to the gel after solidification and run at 100 V. Separated DNA fragments were visualized on a 312 mm UV transilluminator and photographed.

2.14.10. Isolation of DNA fragments from agarose gel

DNA fragments were excised from a separating agarose gel with a clean razor blade and extracted using the NucleoSpin® Gel and PCR Clean-up gel extraction kit (Macherey-Nagel) according to the manufacturer instructions.

2.14.11. Transformation of chemically competent *E. coli* cells

2-2.5 µL of the cloning reaction or 10 ng of purified plasmid were added to 50 µL of chemically competent *E. coli* cells. The reaction was incubated 40 min on ice, subsequently heat-shocked for 42 s at 42 °C, and transferred to ice for 2 min. After addition of 800 µL of SOC medium, the samples were incubated for 1-1.5 h at 37°C with shaking. The cell were pelleted by centrifugation for 1 min at 1,500 g and plated onto selective LB agar plates.

2.14.12. Transformation of electro-competent *A. tumefaciens* cells

50 ng of plasmid DNA were added to 25 µL of electro-competent *A. tumefaciens* cells kept on ice. The mixture was quickly transferred into an electroporation cuvette (1 mm electrode distance). Electroporation was performed with a GenePulse Xcell™ apparatus (Biorad) set to the standard *A. tumefaciens* settings (2400 V, 25 µF, 200 Ω, 1 mm cuvette). After the pulse, the cells were quickly recovered in 1 mL YEB medium and incubated for 2 h at 28°C with shaking before plating (~10 µL) onto selective YEB agar plates.

2.14.13. Genome Walking

Localization of the transgene in the *DEXp:MLAcc-mYFP* line was performed by genome walking using the GenomeWalker™ DNA Universal Kit (Clontech) according to the manufacturer instructions with the primers described in the material section 1.4. The Phusion polymerase (Thermo Fischer Scientific) was used to amplify the DNA fragments after gDNA restriction by *Stu*I or *Dra*I.

2.15. Confocal laser scanning microscopy (CLSM)

Detailed analysis of intracellular fluorescence was performed by confocal laser scanning microscopy using either a Zeiss LSM 700 or LSM780 based on an Axio Imager equipped with an argon ion laser as excitation source (Zeiss, Jena, Germany). On the LSM700, mYFP-tagged proteins were excited by a 488 nm laser line and specifically detected using a variable secondary dichroic beamsplitter (MBS 405/488/55/639, DBS1 543 nm) and a BP 490-555 band pass emission filter with a Zeiss EC Plan-Neofluar 40x/1.30 oil M27 objective. On the

LSM780, mYFP-tagged proteins were excited by a 488 nm laser line and specifically detected using a Twin gate dichroic system (MBS 488/561, MBS InVis plate, DBS1 mirror) and a BP 506-555 band pass emission filter, with a Zeiss LD C-Apochromat 40x/1.1 water M27 objective. Images were analysed with the ZEN 2011 software (Zeiss, Jena, Germany).

2.16. Microarray data analysis

Publicly available experiments using the Affymetrix ATH1-121501 platform were obtained from several data sources (Table S1-1). Only experiments including at least three biological replicates were selected. The raw .cel files were downloaded, normalized with Robust Multi-array Average (RMA) normalization as implemented in BioConductor (Gentleman et al., 2004; Irizarry et al., 2003). Probe annotation was performed using the ath1121501ACCNUM from the ath1121501.db annotation data. Probes with no or ambiguous annotations were removed. For each dataset the log₂-base fold changes (log₂FC) of treatment versus control were computed by fitting a linear model with the appropriate explanatory variables using the function lmFit (R package limma). This log₂FC was used for the comparative transcriptomic analysis described in this study. When necessary, differentially expressed genes were extracted using the R/Bioconductor package limma (Ritchie et al., 2015) with the criteria $|\log_2FC| > 1$ and $FDR < 0.05$.

2.17. RNA-seq assay

For the RNA-seq data generated in this study, mRNA sequencing libraries were prepared with barcoding using the TruSeq RNA Sample Preparation Kit (Illumina). The barcoded libraries were pooled together and sequenced by Illumina HiSeq2000 or Illumina HiSeq2500. Three biological replicates were processed and analysed by the Max Planck Genome Centre Cologne.

2.18. RNA-seq data analysis

Raw RNA-seq data were collected from public datasets, generated for this study, or obtained from collaborators (Table S1-1). Total reads were mapped to the *A. thaliana* genome (TAIR10) using TopHat2 (Kim et al., 2013). Counts per gene were calculated from the mapped RNA-seq reads using HTseq-count function, apart for our previously published 35S:MLA1 pps dataset for which the coverageBed (bedTools suite, Quinlan and Hall, 2010) was used. Genes with less than 100 reads within one dataset were discarded, and the log₂-transformed count data was normalized using the function voom from the R package limma (www.r-project.org, Smyth, 2005) resulting in log₂ counts per million. Differential gene expression between genotypes and/or treatments and/or times, were analysed by fitting a linear model with the appropriate explanatory variables using the function lmFit (R package limma). Log₂-transformed fold change (log₂FC) between sample and control at the same time point were used for most of the comparative transcriptomic analysis conducted in this study.

Statistical analysis was only performed for the *DEXp:MLACC* and the *DEXp:MLACC ppsdes* datasets. For this, moderated t-tests were performed over the contrasts of interests and the

resulting p -values were corrected for multiple testing using the Benjamini-Hochberg method. The criteria for significant differential expression were: $FDR < 0.01$ and $|\log_2FC| > 1$.

2.19. Promoter element enrichment analysis

Promoter element enrichment analysis was performed using several tools. MEME-Lab (Brown et al., 2013) was used to find the eight most enriched 6-14 bp elements in promoters of 600 bp length. Scope motif finder was used to find enriched elements in promoters of 1000 bp length, based on BEAM, PRISM, and SPACER programs (<http://genie.dartmouth.edu/scope>, Carlson et al., 2007). Weeder1.4 and Weeder2 were run under default settings to identify enriched elements in promoters of 1000 bp length (Pavesi et al., 2006; Zambelli et al., 2014). Pscan was used to assess the enrichment of already known transcription factor binding sites in promoters of 1000 bp length, based on the Jaspar 2016 database (Mathelier et al., 2015; Zambelli et al., 2009). The different outputs were compared to identify motifs consistently identified by independent methods. The RSAT DNA pattern matching tool was used to find the occurrences of the selected motifs in the gene set of interest and in all *A. thaliana* promoter sequences (TAIR10_upstream_1000_20101104.fas or TAIR10_upstream_500_20101028.fas) (Medina-Rivera et al., 2015). The resulting occurrence data was used to calculate the enrichment false discovery rate (FDR) by applying a cumulative hypergeometric distribution with Benjamini-Hochberg correction for multiple testing in R (p.hyper and p.adjust functions). WebLogo was used to draw logos of the identified motifs (Crooks et al., 2004).

2.20. Gene ontology (GO) term enrichment analysis

The Bingo 3.0.3 plug-in (Maere et al., 2005) implemented in Cytoscape 3.2.1 (Shannon et al., 2003) was used to analyse and visualise the GO enrichment according to the GO (ontology file GO_Full) or GO Slim (ontology file GOSlim_plants) categorization. The enrichment was statistically assessed by applying a hypergeometric distribution statistical testing method and Benjamini and Hochberg FDR correction.

2.21. Heatmaps

Apart from the cases mentioned below all heatmaps were generated using the heatmap.2 function in R and hierarchical clustering was performed under default settings. Heatmaps shown in Figure 1-10 and Figure S1-8 were generated with the heatmap.2 function where hierarchical clustering was performed using the daisy function for calculating the Gower's distance, together with the complete linkage method. The heatmap shown in Figure S1-4.D was generated using annHeatmap2 (Heatplus package, R).

2.22. Visualization and analysis of coexpression networks

Coexpression networks were generated for each gene cluster using NetworkDrawer (atted.8, <http://atted.jp>) based on all mutual ranking (MR) values. The resulting networks were imported into Cytoscape 3.2.1 for further visualization and identification of the hubs.

2.23. Comparative transcriptomic analysis

The comparative transcriptomic analysis was performed based on the \log_2 -transformed fold change (\log_2FC) expression between the sample and control at the same time point for the datasets described in Table S1-1. For genome-wide pairwise comparison of the expression changes, the Pearson correlation coefficient was calculated based on the \log_2FC of all commonly expressed genes.

2.24. Venn Diagrams

Venn diagrams were generated using the BioVenn online tool (Hulsen et al., 2008, <http://bioinformatics.psb.ugent.be/cgi-bin/liste/Venn/>)

2.25. Analysis of single nucleotide polymorphisms (SNP) in the candidate mutants

2.25.1. Whole genome resequencing

For whole genome re-sequencing, gDNA sequencing libraries were prepared with barcoding using the TruSeq DNA Sample Preparation Kit (Illumina). The barcoded libraries were pooled together and sequenced by HiSeq2500 to produce 100 bp paired-end reads. The samples were processed and analysed by the Max Planck Genome Centre Cologne. This resulted in 23.7-46.6 million reads per sample for the individual M_2 mutants, 47.7-61.5 million reads per sample for the $F_2.BC_T$ positive segregant bulks, and 34.0-52.6 million reads per sample for the $F_2.BC_T$ negative segregant bulks.

2.25.2. SNP mapping and analysis in the M_2 candidates

Read alignment and SNP calling were performed using Bowtie2 (version 2.1.0) and Samtools (version 0.1.19). Alignment files were generated from non-uniquely mapped reads and uniquely mapped reads to allow detailed inspection of the loci of interest with IGV Browser (Robinson et al., 2011; Thorvaldsdóttir et al., 2013). Uniquely mapped reads were used for SNP calling. The resulting variant files were annotated with snpEff according to TAIR10 annotation. SnpSift was used to filter the SNPs identified. First, homozygous SNPs located in genes or at less than 100 bp upstream or downstream were extracted. Second, SNPs with no significant effects were excluded. The resulting filtered SNP lists were further curated using a

semi-manual method to remove background SNPs. For this, all the SNP information for all genes carrying SNPs in more than two M_2 mutants was manually corrected after inspection with the IGV Browser. The SNP lists obtained after this final filtering step were used for further analysis.

2.25.3. SNP mapping and analysis in the F_2 .BC_T bulks

Mapping of the ML_{ACC} suppressor mutation was first performed using the SHOREmap pipeline (Schneeberger et al., 2009) under standard parameters based on SHOREmap 3.0 and SHORE 0.7.1. The sequence of an unrelated M_2 mutant was used as background reference. A second mapping approach based on the comparative analysis between negative and positive segregant bulks was also conducted (Xiangchao Gan, unpublished).

References

- Aarts, N., Metz, M., Holub, E., Staskawicz, B.J., Daniels, M.J., and Parker, J.E.** (1998). Different requirements for EDS1 and NDR1 by disease resistance genes define at least two R gene-mediated signaling pathways in Arabidopsis. *Proc. Natl. Acad. Sci.* *95*, 10306–10311.
- Abe, A., Kosugi, S., Yoshida, K., Natsume, S., Takagi, H., Kanzaki, H., Matsumura, H., Yoshida, K., Mitsuoka, C., Tamiru, M., et al.** (2012). Genome sequencing reveals agronomically important loci in rice using MutMap. *Nat. Biotechnol.* *30*, 174–178.
- Adams-Phillips, L., Wan, J., Tan, X., Dunning, F.M., Meyers, B.C., Michelmore, R.W., and Bent, A.F.** (2008). Discovery of ADP-Ribosylation and Other Plant Defense Pathway Elements Through Expression Profiling of Four Different Arabidopsis–*Pseudomonas* R-avr Interactions. *Mol. Plant. Microbe Interact.* *21*, 646–657.
- Ade, J., DeYoung, B.J., Golstein, C., and Innes, R.W.** (2007). Indirect activation of a plant nucleotide binding site–leucine-rich repeat protein by a bacterial protease. *Proc. Natl. Acad. Sci.* *104*, 2531–2536.
- Andersson, M.X., Kourtchenko, O., Dangl, J.L., Mackey, D., and Ellerström, M.** (2006). Phospholipase-dependent signalling during the AvrRpm1- and AvrRpt2-induced disease resistance responses in Arabidopsis thaliana. *Plant J.* *47*, 947–959.
- Ando, S., Obinata, A., and Takahashi, H.** (2014). WRKY70 interacting with RCY1 disease resistance protein is required for resistance to Cucumber mosaic virus in Arabidopsis thaliana. *Physiol. Mol. Plant Pathol.* *85*, 8–14.
- Aoyama, T., and Chua, N.H.** (1997). A glucocorticoid-mediated transcriptional induction system in transgenic plants. *Plant J. Cell Mol. Biol.* *11*, 605–612.
- Asai, T., Stone, J.M., Heard, J.E., Kovtun, Y., Yorgey, P., Sheen, J., and Ausubel, F.M.** (2000). Fumonisin B1–Induced Cell Death in Arabidopsis Protoplasts Requires Jasmonate-, Ethylene-, and Salicylate-Dependent Signaling Pathways. *Plant Cell* *12*, 1823–1836.
- Atkinson, M.M., Huang, J.S., and Knopp, J.A.** (1985). The Hypersensitive Reaction of Tobacco to *Pseudomonas syringae* pv. *tabaci*: Activation of a Plasmalemma K/H Exchange Mechanism. *Plant Physiol.* *79*, 843–847.
- Ausubel, F.M.** (2005). Are innate immune signaling pathways in plants and animals conserved? *Nat. Immunol.* *6*, 973–979.
- Axtell, M.J., and Staskawicz, B.J.** (2003). Initiation of RPS2-Specified Disease Resistance in Arabidopsis Is Coupled to the AvrRpt2-Directed Elimination of RIN4. *Cell* *112*, 369–377.
- Azevedo, C., Sadanandom, A., Kitagawa, K., Freialdenhoven, A., Shirasu, K., and Schulze-Lefert, P.** (2002). The RAR1 Interactor SGT1, an Essential Component of R Gene-Triggered Disease Resistance. *Science* *295*, 2073–2076.
- Bai, S., Liu, J., Chang, C., Zhang, L., Maekawa, T., Wang, Q., Xiao, W., Liu, Y., Chai, J., Takken, F.L.W., et al.** (2012). Structure-function analysis of barley NLR immune receptor MLA10 reveals its cell compartment specific activity in cell death and disease resistance. *PLoS Pathog.* *8*, e1002752.

- Bao, F., Huang, X., Zhu, C., Zhang, X., Li, X., and Yang, S.** (2014). Arabidopsis HSP90 protein modulates RPP4-mediated temperature-dependent cell death and defense responses. *New Phytol.* *202*, 1320–1334.
- Bari, R., and Jones, J.D.G.** (2009). Role of plant hormones in plant defence responses. *Plant Mol. Biol.* *69*, 473–488.
- Baubec, T., Pecinka, A., Rozhon, W., and Mittelsten Scheid, O.** (2009). Effective, homogeneous and transient interference with cytosine methylation in plant genomic DNA by zebularine. *Plant J. Cell Mol. Biol.* *57*, 542–554.
- Baubec, T., Dinh, H.Q., Pecinka, A., Rakic, B., Rozhon, W., Wohlrab, B., von Haeseler, A., and Mittelsten Scheid, O.** (2010). Cooperation of multiple chromatin modifications can generate unanticipated stability of epigenetic States in Arabidopsis. *Plant Cell* *22*, 34–47.
- Baxter, A., Mittler, R., and Suzuki, N.** (2013). ROS as key players in plant stress signalling. *J. Exp. Bot.* ert375.
- Bechtold, U., Albihlal, W.S., Lawson, T., Fryer, M.J., Sparrow, P.A.C., Richard, F., Persad, R., Bowden, L., Hickman, R., Martin, C., et al.** (2013). Arabidopsis HEAT SHOCK TRANSCRIPTION FACTOR1b overexpression enhances water productivity, resistance to drought, and infection. *J. Exp. Bot.* ert185.
- Bendahmane, A., Kanyuka, K., and Baulcombe, D.C.** (1999). The Rx Gene from Potato Controls Separate Virus Resistance and Cell Death Responses. *Plant Cell* *11*, 781–791.
- Bendahmane, A., Farnham, G., Moffett, P., and Baulcombe, D.C.** (2002). Constitutive gain-of-function mutants in a nucleotide binding site–leucine rich repeat protein encoded at the Rx locus of potato. *Plant J.* *32*, 195–204.
- Bent, A.F., Kunkel, B.N., Dahlbeck, D., Brown, K.L., Schmidt, R., Giraudat, J., Leung, J., and Staskawicz, B.J.** (1994). RPS2 of Arabidopsis thaliana: a leucine-rich repeat class of plant disease resistance genes. *Science* *265*, 1856–1860.
- Bernoux, M., Ve, T., Williams, S., Warren, C., Hatters, D., Valkov, E., Zhang, X., Ellis, J.G., Kobe, B., and Dodds, P.N.** (2011). Structural and Functional Analysis of a Plant Resistance Protein TIR Domain Reveals Interfaces for Self-Association, Signaling, and Autoregulation. *Cell Host Microbe* *9*, 200–211.
- Bethke, G., Unthan, T., Uhrig, J.F., Pöschl, Y., Gust, A.A., Scheel, D., and Lee, J.** (2009). Flg22 regulates the release of an ethylene response factor substrate from MAP kinase 6 in Arabidopsis thaliana via ethylene signaling. *Proc. Natl. Acad. Sci.* *106*, 8067–8072.
- Bieri, S., Mauch, S., Shen, Q.-H., Peart, J., Devoto, A., Casais, C., Ceron, F., Schulze, S., Steinbiß, H.-H., Shirasu, K., et al.** (2004). RAR1 Positively Controls Steady State Levels of Barley MLA Resistance Proteins and Enables Sufficient MLA6 Accumulation for Effective Resistance. *Plant Cell* *16*, 3480–3495.
- van der Biezen, E.A., Sun, J., Coleman, M.J., Bibb, M.J., and Jones, J.D.** (2000). Arabidopsis RelA/SpoT homologs implicate (p)ppGpp in plant signaling. *Proc. Natl. Acad. Sci. U. S. A.* *97*, 3747–3752.

- Bigeard, J., Pflieger, D., Colcombet, J., Gérard, L., Mireau, H., and Hirt, H.** (2014). Protein Complexes Characterization in *Arabidopsis thaliana* by Tandem Affinity Purification Coupled to Mass Spectrometry Analysis. In *Plant MAP Kinases*, G. Komis, and J. Šamaj, eds. (Springer New York), pp. 237–250.
- Binet, M.-N., Humbert, C., Lecourieux, D., Vantard, M., and Pugin, A.** (2001). Disruption of Microtubular Cytoskeleton Induced by Cryptogein, an Elicitor of Hypersensitive Response in Tobacco Cells. *Plant Physiol.* *125*, 564–572.
- Bigroove, S.R., Simonich, M.T., Smith, N.M., Sattler, A., and Innes, R.W.** (1994). A disease resistance gene in *Arabidopsis* with specificity for two different pathogen avirulence genes. *Plant Cell* *6*, 927–933.
- Bjornson, M., Dandekar, A., and Dehesh, K.** (2016). Determinants of timing and amplitude in the plant general stress response. *J. Integr. Plant Biol.* *58*, 119–126.
- Boller, T., and Felix, G.** (2009). A renaissance of elicitors: perception of microbe-associated molecular patterns and danger signals by pattern-recognition receptors. *Annu. Rev. Plant Biol.* *60*, 379–406.
- Bonardi, V., and Dangl, J.L.** (2012). How complex are intracellular immune receptor signaling complexes? *Front. Plant Sci.* *3*.
- Bonardi, V., Tang, S., Stallmann, A., Roberts, M., Cherkis, K., and Dangl, J.L.** (2011). Expanded functions for a family of plant intracellular immune receptors beyond specific recognition of pathogen effectors. *Proc. Natl. Acad. Sci. U. S. A.* *108*, 16463–16468.
- Bos, J.I.B., Armstrong, M.R., Gilroy, E.M., Boevink, P.C., Hein, I., Taylor, R.M., Zhendong, T., Engelhardt, S., Vetukuri, R.R., Harrower, B., et al.** (2010). *Phytophthora infestans* effector AVR3a is essential for virulence and manipulates plant immunity by stabilizing host E3 ligase CMPG1. *Proc. Natl. Acad. Sci. U. S. A.* *107*, 9909–9914.
- Boter, M., Ruíz-Rivero, O., Abdeen, A., and Prat, S.** (2004). Conserved MYC transcription factors play a key role in jasmonate signaling both in tomato and *Arabidopsis*. *Genes Dev.* *18*, 1577–1591.
- Boudsocq, M., and Sheen, J.** (2013). CDPKs in immune and stress signaling. *Trends Plant Sci.* *18*, 30–40.
- Boudsocq, M., Willmann, M.R., McCormack, M., Lee, H., Shan, L., He, P., Bush, J., Cheng, S.-H., and Sheen, J.** (2010). Differential innate immune signalling via Ca²⁺ sensor protein kinases. *Nature* *464*, 418–422.
- Boyes, D.C., Nam, J., and Dangl, J.L.** (1998). The *Arabidopsis thaliana* RPM1 disease resistance gene product is a peripheral plasma membrane protein that is degraded coincident with the hypersensitive response. *Proc. Natl. Acad. Sci. U. S. A.* *95*, 15849–15854.
- Brown, P., Baxter, L., Hickman, R., Beynon, J., Moore, J.D., and Ott, S.** (2013). MEME-LaB: motif analysis in clusters. *Bioinforma. Oxf. Engl.* *29*, 1696–1697.
- Caldo, R.A., Nettleton, D., and Wise, R.P.** (2004). Interaction-Dependent Gene Expression in Mla-Specified Response to Barley Powdery Mildew. *Plant Cell* *16*, 2514–2528.

- Camera, S.L., Balagué, C., Göbel, C., Geoffroy, P., Legrand, M., Feussner, I., Roby, D., and Heitz, T.** (2009). The Arabidopsis Patatin-Like Protein 2 (PLP2) Plays an Essential Role in Cell Death Execution and Differentially Affects Biosynthesis of Oxylipins and Resistance to Pathogens. *Mol. Plant. Microbe Interact.* 22, 469–481.
- Caplan, J.L., Mamillapalli, P., Burch-Smith, T.M., Czymmek, K., and Dinesh-Kumar, S.P.** (2008). Chloroplastic protein NRIP1 mediates innate immune receptor recognition of a viral effector. *Cell* 132, 449–462.
- Carlson, J.M., Chakravarty, A., DeZiel, C.E., and Gross, R.H.** (2007). SCOPE: a web server for practical de novo motif discovery. *Nucleic Acids Res.* 35, W259–W264.
- Century, K.S., Holub, E.B., and Staskawicz, B.J.** (1995). NDR1, a locus of Arabidopsis thaliana that is required for disease resistance to both a bacterial and a fungal pathogen. *Proc. Natl. Acad. Sci.* 92, 6597–6601.
- Cesari, S., Thilliez, G., Ribot, C., Chalvon, V., Michel, C., Jauneau, A., Rivas, S., Alaux, L., Kanzaki, H., Okuyama, Y., et al.** (2013). The Rice Resistance Protein Pair RGA4/RGA5 Recognizes the Magnaporthe oryzae Effectors AVR-Pia and AVR1-CO39 by Direct Binding. *Plant Cell Online* 25, 1463–1481.
- Chang, C., Yu, D., Jiao, J., Jing, S., Schulze-Lefert, P., and Shen, Q.-H.** (2013). Barley MLA Immune Receptors Directly Interfere with Antagonistically Acting Transcription Factors to Initiate Disease Resistance Signaling[C][W]. *Plant Cell* 25, 1158–1173.
- Cheng, C., Gao, X., Feng, B., Sheen, J., Shan, L., and He, P.** (2013). Differential temperature operation of plant immune responses. *Nat. Commun.* 4, 2530.
- Cheng, Y.T., Germain, H., Wiermer, M., Bi, D., Xu, F., García, A.V., Wirthmueller, L., Després, C., Parker, J.E., Zhang, Y., et al.** (2009). Nuclear pore complex component MOS7/Nup88 is required for innate immunity and nuclear accumulation of defense regulators in Arabidopsis. *Plant Cell* 21, 2503–2516.
- Chini, A., Fonseca, S., Fernández, G., Adie, B., Chico, J.M., Lorenzo, O., García-Casado, G., López-Vidriero, I., Lozano, F.M., Ponce, M.R., et al.** (2007). The JAZ family of repressors is the missing link in jasmonate signalling. *Nature* 448, 666–671.
- Chisholm, S.T., Coaker, G., Day, B., and Staskawicz, B.J.** (2006). Host-microbe interactions: shaping the evolution of the plant immune response. *Cell* 124, 803–814.
- Clark, R.M., Schweikert, G., Toomajian, C., Ossowski, S., Zeller, G., Shinn, P., Warthmann, N., Hu, T.T., Fu, G., Hinds, D.A., et al.** (2007). Common Sequence Polymorphisms Shaping Genetic Diversity in Arabidopsis thaliana. *Science* 317, 338–342.
- Clough, S.J., and Bent, A.F.** (1998). Floral dip: a simplified method for Agrobacterium-mediated transformation of Arabidopsis thaliana. *Plant J. Cell Mol. Biol.* 16, 735–743.
- Coll, N.S., Vercammen, D., Smidler, A., Clover, C., Van Breusegem, F., Dangl, J.L., and Epple, P.** (2010). Arabidopsis type I metacaspases control cell death. *Science* 330, 1393–1397.

- Coll, N.S., Epple, P., and Dangl, J.L.** (2011). Programmed cell death in the plant immune system. *Cell Death Differ.* *18*, 1247–1256.
- Collier, S.M., Hamel, L.-P., and Moffett, P.** (2011). Cell Death Mediated by the N-Terminal Domains of a Unique and Highly Conserved Class of NB-LRR Protein. *Mol. Plant. Microbe Interact.* *24*, 918–931.
- Cox, J., and Mann, M.** (2008). MaxQuant enables high peptide identification rates, individualized p.p.b.-range mass accuracies and proteome-wide protein quantification. *Nat. Biotechnol.* *26*, 1367–1372.
- Cox, J., and Mann, M.** (2012). 1D and 2D annotation enrichment: a statistical method integrating quantitative proteomics with complementary high-throughput data. *BMC Bioinformatics* *13*, S12.
- Cox, J., Hein, M.Y., Lubner, C.A., Paron, I., Nagaraj, N., and Mann, M.** (2014). Accurate Proteome-wide Label-free Quantification by Delayed Normalization and Maximal Peptide Ratio Extraction, Termed MaxLFQ. *Mol. Cell. Proteomics MCP* *13*, 2513–2526.
- Crooks, G.E., Hon, G., Chandonia, J.-M., and Brenner, S.E.** (2004). WebLogo: a sequence logo generator. *Genome Res.* *14*, 1188–1190.
- Cui, H., Tsuda, K., and Parker, J.E.** (2015). Effector-Triggered Immunity: From Pathogen Perception to Robust Defense. *Annu. Rev. Plant Biol.* *66*, 487–511.
- Curtis, M.D., and Grossniklaus, U.** (2003). A Gateway Cloning Vector Set for High-Throughput Functional Analysis of Genes in Planta. *Plant Physiol.* *133*, 462–469.
- Day, B., and He, S.Y.** (2010). Battling Immune Kinases in Plants. *Cell Host Microbe* *7*, 259–261.
- Day, B., Dahlbeck, D., and Staskawicz, B.J.** (2006). NDR1 interaction with RIN4 mediates the differential activation of multiple disease resistance pathways in Arabidopsis. *Plant Cell* *18*, 2782–2791.
- Dedecker, M., Van Leene, J., and De Jaeger, G.** (2015). Unravelling plant molecular machineries through affinity purification coupled to mass spectrometry. *Curr. Opin. Plant Biol.* *24*, 1–9.
- Demidchik, V., Straltsova, D., Medvedev, S.S., Pozhvanov, G.A., Sokolik, A., and Yurin, V.** (2014). Stress-induced electrolyte leakage: the role of K⁺-permeable channels and involvement in programmed cell death and metabolic adjustment. *J. Exp. Bot.* *65*, 1259–1270.
- DeYoung, B.J., and Innes, R.W.** (2006). Plant NBS-LRR proteins in pathogen sensing and host defense. *Nat. Immunol.* *7*, 1243–1249.
- Djamei, A., Pitzschke, A., Nakagami, H., Rajh, I., and Hirt, H.** (2007). Trojan Horse Strategy in Agrobacterium Transformation: Abusing MAPK Defense Signaling. *Science* *318*, 453–456.
- Dombrecht, B., Xue, G.P., Sprague, S.J., Kirkegaard, J.A., Ross, J.J., Reid, J.B., Fitt, G.P., Sewelam, N., Schenk, P.M., Manners, J.M., et al.** (2007). MYC2 Differentially

Modulates Diverse Jasmonate-Dependent Functions in Arabidopsis. *Plant Cell* *19*, 2225–2245.

van Doorn, W.G., Beers, E.P., Dangl, J.L., Franklin-Tong, V.E., Gallois, P., Hara-Nishimura, I., Jones, A.M., Kawai-Yamada, M., Lam, E., Mundy, J., et al. (2011). Morphological classification of plant cell deaths. *Cell Death Differ.* *18*, 1241–1246.

Du, L., Ali, G.S., Simons, K.A., Hou, J., Yang, T., Reddy, A.S.N., and Poovaiah, B.W. (2009). Ca(2+)/calmodulin regulates salicylic-acid-mediated plant immunity. *Nature* *457*, 1154–1158.

Durrant, W.E., Rowland, O., Piedras, P., Hammond-Kosack, K.E., and Jones, J.D.G. (2000). cDNA-AFLP Reveals a Striking Overlap in Race-Specific Resistance and Wound Response Gene Expression Profiles. *Plant Cell* *12*, 963–977.

Engelhardt, S., Boevink, P.C., Armstrong, M.R., Ramos, M.B., Hein, I., and Birch, P.R.J. (2012). Relocalization of Late Blight Resistance Protein R3a to Endosomal Compartments Is Associated with Effector Recognition and Required for the Immune Response[W]. *Plant Cell* *24*, 5142–5158.

Eulgem, T., Weigman, V.J., Chang, H.-S., McDowell, J.M., Holub, E.B., Glazebrook, J., Zhu, T., and Dangl, J.L. (2004). Gene Expression Signatures from Three Genetically Separable Resistance Gene Signaling Pathways for Downy Mildew Resistance. *Plant Physiol.* *135*, 1129–1144.

Eulgem, T., Tsuchiya, T., Wang, X.-J., Beasley, B., Cuzick, A., Tör, M., Zhu, T., McDowell, J.M., Holub, E., and Dangl, J.L. (2007). EDM2 is required for RPP7-dependent disease resistance in Arabidopsis and affects RPP7 transcript levels. *Plant J.* *49*, 829–839.

Evrard, A., Kumar, M., Lecourieux, D., Lucks, J., von Koskull-Döring, P., and Hirt, H. (2013). Regulation of the heat stress response in Arabidopsis by MPK6-targeted phosphorylation of the heat stress factor HsfA2. *PeerJ* *1*, e59.

Faris, J.D., Zhang, Z., Lu, H., Lu, S., Reddy, L., Cloutier, S., Fellers, J.P., Meinhardt, S.W., Rasmussen, J.B., Xu, S.S., et al. (2010). A unique wheat disease resistance-like gene governs effector-triggered susceptibility to necrotrophic pathogens. *Proc. Natl. Acad. Sci. U. S. A.* *107*, 13544–13549.

Fenyk, S., Townsend, P.D., Dixon, C.H., Spies, G.B., de San Eustaquio Campillo, A., Sloopweg, E.J., Westerhof, L.B., Gawehns, F.K.K., Knight, M.R., Sharples, G.J., et al. (2015). The Potato Nucleotide-binding Leucine-rich Repeat (NLR) Immune Receptor Rx1 Is a Pathogen-dependent DNA-deforming Protein. *J. Biol. Chem.* *290*, 24945–24960.

Fenyk, S., Dixon, C.H., Gittens, W.H., Townsend, P.D., Sharples, G.J., Pålsson, L.-O., Takken, F.L.W., and Cann, M.J. (2016). The Tomato Nucleotide-binding Leucine-rich Repeat Immune Receptor I-2 Couples DNA-binding to Nucleotide-binding Domain Nucleotide Exchange. *J. Biol. Chem.* *291*, 1137–1147.

Ferré-D'Amaré, A.R., and Burley, S.K. (1995). DNA Recognition by Helix-Loop-Helix Proteins. In *Nucleic Acids and Molecular Biology*, P.D.F. Eckstein, and P.D.D.M.J. Lilley, eds. (Springer Berlin Heidelberg), pp. 285–298.

- Feys, B.J., Wiermer, M., Bhat, R.A., Moisan, L.J., Medina-Escobar, N., Neu, C., Cabral, A., and Parker, J.E.** (2005). Arabidopsis SENESCENCE-ASSOCIATED GENE101 stabilizes and signals within an ENHANCED DISEASE SUSCEPTIBILITY1 complex in plant innate immunity. *Plant Cell* *17*, 2601–2613.
- Flor, H.** (1955). Host-parasite interaction in flax rust - its genetics and other implications. *Phytopathology* *45*, 680–685.
- Fowler, T., Sen, R., and Roy, A.L.** (2011). Regulation of Primary Response Genes. *Mol. Cell* *44*, 348–360.
- Frost, D., Way, H., Howles, P., Luck, J., Manners, J., Hardham, A., Finnegan, J., and Ellis, J.** (2004). Tobacco transgenic for the flax rust resistance gene L expresses allele-specific activation of defense responses. *Mol. Plant-Microbe Interact. MPMI* *17*, 224–232.
- Gabriëls, S.H.E.J., Vossen, J.H., Ekengren, S.K., Ooijen, G. van, Abd-El-Haliem, A.M., Berg, G.C.M. van den, Rainey, D.Y., Martin, G.B., Takken, F.L.W., Wit, P.J.G.M. de, et al.** (2007). An NB-LRR protein required for HR signalling mediated by both extra- and intracellular resistance proteins. *Plant J.* *50*, 14–28.
- Galbraith, M.D., and Espinosa, J.M.** (2011). Lessons on transcriptional control from the serum response network. *Curr. Opin. Genet. Dev.* *21*, 160–166.
- Gao, X., Chen, X., Lin, W., Chen, S., Lu, D., Niu, Y., Li, L., Cheng, C., McCormack, M., Sheen, J., et al.** (2013). Bifurcation of Arabidopsis NLR immune signaling via Ca²⁺-dependent protein kinases. *PLoS Pathog.* *9*, e1003127.
- Gao, Z., Gao, Z., Chung, E.-H., Eitas, T.K., and Dangl, J.L.** (2011). Plant intracellular innate immune receptor Resistance to *Pseudomonas syringae* pv. *maculicola* 1 (RPM1) is activated at, and functions on, the plasma membrane. *Proc. Natl. Acad. Sci. U. S. A.* *108*, 7619–7624.
- Garcia, A.V., and Hirt, H.** (2014). *Salmonella enterica* induces and subverts the plant immune system. *Plant Biot. Interact.* *5*, 141.
- Gentleman, R.C., Carey, V.J., Bates, D.M., Bolstad, B., Dettling, M., Dudoit, S., Ellis, B., Gautier, L., Ge, Y., Gentry, J., et al.** (2004). Bioconductor: open software development for computational biology and bioinformatics. *Genome Biol.* *5*, R80.
- Gietz, R.D., and Woods, R.A.** (2002). Transformation of yeast by lithium acetate/single-stranded carrier DNA/polyethylene glycol method. *Methods Enzymol.* *350*, 87–96.
- Glazebrook, J.** (2005). Contrasting Mechanisms of Defense Against Biotrophic and Necrotrophic Pathogens. *Annu. Rev. Phytopathol.* *43*, 205–227.
- Goda, H., Sasaki, E., Akiyama, K., Maruyama-Nakashita, A., Nakabayashi, K., Li, W., Ogawa, M., Yamauchi, Y., Preston, J., Aoki, K., et al.** (2008). The AtGenExpress hormone and chemical treatment data set: experimental design, data evaluation, model data analysis and data access. *Plant J.* *55*, 526–542.
- González-Lamothe, R., Tsitsigiannis, D.I., Ludwig, A.A., Panicot, M., Shirasu, K., and Jones, J.D.G.** (2006). The U-Box Protein CMPG1 Is Required for Efficient Activation of

Defense Mechanisms Triggered by Multiple Resistance Genes in Tobacco and Tomato. *Plant Cell* 18, 1067–1083.

Grant, M., Brown, I., Adams, S., Knight, M., Ainslie, A., and Mansfield, J. (2000). The RPM1 plant disease resistance gene facilitates a rapid and sustained increase in cytosolic calcium that is necessary for the oxidative burst and hypersensitive cell death. *Plant J.* 23, 441–450.

Gray, W.M., Muskett, P.R., Chuang, H., and Parker, J.E. (2003). Arabidopsis SGT1b Is Required for SCFTIR1-Mediated Auxin Response. *Plant Cell* 15, 1310–1319.

Greeff, M. C. (2014). Suppressing autoimmunity in *Arabidopsis thaliana* with dominant negative immune receptors. Thesis of the University of Copenhagen. <http://www2.bio.ku.dk/bibliotek/phd/>

Griebel, T., Maekawa, T., and Parker, J.E. (2014). NOD-like receptor cooperativity in effector-triggered immunity. *Trends Immunol.* 35, 562–570.

Gutierrez, J.R., Balmuth, A.L., Ntoukakis, V., Mucyn, T.S., Gimenez-Ibanez, S., Jones, A.M.E., and Rathjen, J.P. (2010). Prf immune complexes of tomato are oligomeric and contain multiple Pto-like kinases that diversify effector recognition. *Plant J.* 61, 507–518.

Halfmann, R., and Lindquist, S. (2008). Screening for amyloid aggregation by Semi-Denaturing Detergent-Agarose Gel Electrophoresis. *J. Vis. Exp. JoVE.*

Halterman, D.A., and Wise, R.P. (2004). A single-amino acid substitution in the sixth leucine-rich repeat of barley MLA6 and MLA13 alleviates dependence on RAR1 for disease resistance signaling. *Plant J. Cell Mol. Biol.* 38, 215–226.

Hartl, M., König, A.-C., and Finkemeier, I. (2015). Identification of Lysine-Acetylated Mitochondrial Proteins and Their Acetylation Sites. In *Plant Mitochondria*, J. Whelan, and M.W. Murcha, eds. (Springer New York), pp. 107–121.

Hatsugai, N., Kuroyanagi, M., Yamada, K., Meshi, T., Tsuda, S., Kondo, M., Nishimura, M., and Hara-Nishimura, I. (2004). A Plant Vacuolar Protease, VPE, Mediates Virus-Induced Hypersensitive Cell Death. *Science* 305, 855–858.

Hatsugai, N., Iwasaki, S., Tamura, K., Kondo, M., Fuji, K., Ogasawara, K., Nishimura, M., and Hara-Nishimura, I. (2009). A novel membrane fusion-mediated plant immunity against bacterial pathogens. *Genes Dev.* 23, 2496–2506.

Hatsugai, N., Yamada, K., Goto-Yamada, S., and Hara-Nishimura, I. (2015). Vacuolar processing enzyme in plant programmed cell death. *Plant Physiol.* 6, 234.

He, S.Y., Bauer, D.W., Collmer, A., and Beer, S.V. (1994). Hypersensitive response elicited by *Erwinia amylovora* harpin requires active plant metabolism. *MPMI-Mol. Plant Microbe Interact.* 7, 289–292.

Heidrich, K., Wirthmueller, L., Tasset, C., Pouzet, C., Deslandes, L., and Parker, J.E. (2011). Arabidopsis EDS1 connects pathogen effector recognition to cell compartment-specific immune responses. *Science* 334, 1401–1404.

- Heidrich, K., Tsuda, K., Blanvillain-Baufumé, S., Wirthmueller, L., Bautor, J., and Parker, J.E.** (2013). Arabidopsis TNL-WRKY domain receptor RRS1 contributes to temperature-conditioned RPS4 auto-immunity. *Front. Plant Sci.* *4*.
- Hein, I., Barciszewska-Pacak, M., Hrubikova, K., Williamson, S., Dinesen, M., Soenderby, I.E., Sundar, S., Jarmolowski, A., Shirasu, K., and Lacomme, C.** (2005). Virus-Induced Gene Silencing-Based Functional Characterization of Genes Associated with Powdery Mildew Resistance in Barley. *Plant Physiol.* *138*, 2155–2164.
- Heise, A., Lippok, B., Kirsch, C., and Hahlbrock, K.** (2002). Two immediate-early pathogen-responsive members of the AtCMPG gene family in Arabidopsis thaliana and the W-box-containing elicitor-response element of AtCMPG1. *Proc. Natl. Acad. Sci.* *99*, 9049–9054.
- Hobo, T., Asada, M., Kowyama, Y., and Hattori, T.** (1999). ACGT-containing abscisic acid response element (ABRE) and coupling element 3 (CE3) are functionally equivalent. *Plant J. Cell Mol. Biol.* *19*, 679–689.
- Hofius, D., Schultz-Larsen, T., Joensen, J., Tsitsigiannis, D.I., Petersen, N.H.T., Mattsson, O., Jørgensen, L.B., Jones, J.D.G., Mundy, J., and Petersen, M.** (2009). Autophagic components contribute to hypersensitive cell death in Arabidopsis. *Cell* *137*, 773–783.
- van der Hoorn, R.A.L., and Kamoun, S.** (2008). From Guard to Decoy: a new model for perception of plant pathogen effectors. *Plant Cell* *20*, 2009–2017.
- Hu, Z., Yan, C., Liu, P., Huang, Z., Ma, R., Zhang, C., Wang, R., Zhang, Y., Martinon, F., Miao, D., et al.** (2013). Crystal Structure of NLRC4 Reveals Its Autoinhibition Mechanism. *Science*.
- Huang, X., Li, J., Bao, F., Zhang, X., and Yang, S.** (2010). A Gain-of-Function Mutation in the Arabidopsis Disease Resistance Gene RPP4 Confers Sensitivity to Low Temperature1[W][OA]. *Plant Physiol.* *154*, 796–809.
- Hulsen, T., Vlieg, J., and Alkema, W.** (2008). BioVenn - a web application for the comparison and visualization of biological lists using area-proportional Venn diagrams. *BMC Genomics* *9*, 488.
- Humphry, M., Bednarek, P., Kemmerling, B., Koh, S., Stein, M., Göbel, U., Stüber, K., Piślewska-Bednarek, M., Loraine, A., Schulze-Lefert, P., et al.** (2010). A regulon conserved in monocot and dicot plants defines a functional module in antifungal plant immunity. *Proc. Natl. Acad. Sci.* *107*, 21896–21901.
- Hwang, C.-F., Bhakta, A.V., Truesdell, G.M., Pudlo, W.M., and Williamson, V.M.** (2000). Evidence for a Role of the N Terminus and Leucine-Rich Repeat Region of the Mi Gene Product in Regulation of Localized Cell Death. *Plant Cell* *12*, 1319–1329.
- Ichimura, K., Casais, C., Peck, S.C., Shinozaki, K., and Shirasu, K.** (2006). MEKK1 Is Required for MPK4 Activation and Regulates Tissue-specific and Temperature-dependent Cell Death in Arabidopsis. *J. Biol. Chem.* *281*, 36969–36976.
- Inoue, H., Hayashi, N., Matsushita, A., Xinqiong, L., Nakayama, A., Sugano, S., Jiang, C.-J., and Takatsuji, H.** (2013). Blast resistance of CC-NB-LRR protein Pbl is mediated by

WRKY45 through protein-protein interaction. *Proc. Natl. Acad. Sci. U. S. A.* *110*, 9577–9582.

Inzé, A., Vanderauwera, S., Hoesberichts, F.A., Vandorpe, M., Van Gaeveer, T., and Van Breusegem, F. (2012). A subcellular localization compendium of hydrogen peroxide-induced proteins. *Plant Cell Environ.* *35*, 308–320.

Irizarry, R.A., Hobbs, B., Collin, F., Beazer-Barclay, Y.D., Antonellis, K.J., Scherf, U., and Speed, T.P. (2003). Exploration, normalization, and summaries of high density oligonucleotide array probe level data. *Biostatistics* *4*, 249–264.

Ishihama, N., Yamada, R., Yoshioka, M., Katou, S., and Yoshioka, H. (2011). Phosphorylation of the *Nicotiana benthamiana* WRKY8 Transcription Factor by MAPK Functions in the Defense Response. *Plant Cell* *23*, 1153–1170.

Jacob, F., Vernaldi, S., and Maekawa, T. (2013). Evolution and Conservation of Plant NLR Functions. *Front. Immunol.* *4*.

Jones, J.D.G., and Dangl, J.L. (2006). The plant immune system. *Nature* *444*, 323–329.

Jordan, T., Seeholzer, S., Schwizer, S., Töller, A., Somssich, I.E., and Keller, B. (2011). The wheat Mla homologue TmMla1 exhibits an evolutionarily conserved function against powdery mildew in both wheat and barley. *Plant J. Cell Mol. Biol.* *65*, 610–621.

Jørgensen, J.H. (1988). Genetic analysis of barley mutants with modifications of powdery mildew resistance gene Ml-a12. *Genome* *30*, 129–132.

Kadota, Y., and Shirasu, K. (2012). The HSP90 complex of plants. *Biochim. Biophys. Acta* *1823*, 689–697.

Kazan, K., and Lyons, R. (2014). Intervention of Phytohormone Pathways by Pathogen Effectors[OPEN]. *Plant Cell* *26*, 2285–2309.

Kim, D., Pertea, G., Trapnell, C., Pimentel, H., Kelley, R., and Salzberg, S.L. (2013). TopHat2: accurate alignment of transcriptomes in the presence of insertions, deletions and gene fusions. *Genome Biol.* *14*, R36.

Kirsch, C., Logemann, E., Lippok, B., Schmelzer, E., and Hahlbrock, K. (2001). A highly specific pathogen-responsive promoter element from the immediate-early activated CMPG1 gene in *Petroselinum crispum*. *Plant J.* *26*, 217–227.

Knepper, C., Savory, E.A., and Day, B. (2011). The role of NDR1 in pathogen perception and plant defense signaling. *Plant Signal. Behav.* *6*, 1114–1116.

Kolonin, M.G., Zhong, J., and Finley, R.L. (2000). Interaction mating methods in two-hybrid systems. *Methods Enzymol.* *328*, 26–46.

Koncz, C., and Schell, J. (1986). The promoter of TL-DNA gene 5 controls the tissue-specific expression of chimaeric genes carried by a novel type of *Agrobacterium* binary vector. *Mol. Gen. Genet.* *MGG 204*, 383–396.

- Koonin, E.V., and Aravind, L.** (2000). The NACHT family - a new group of predicted NTPases implicated in apoptosis and MHC transcription activation. *Trends Biochem. Sci.* 25, 223–224.
- Krasileva, K.V., Dahlbeck, D., and Staskawicz, B.J.** (2010). Activation of an Arabidopsis resistance protein is specified by the in planta association of its leucine-rich repeat domain with the cognate oomycete effector. *Plant Cell* 22, 2444–2458.
- Kulak, N.A., Pichler, G., Paron, I., Nagaraj, N., and Mann, M.** (2014). Minimal, encapsulated proteomic-sample processing applied to copy-number estimation in eukaryotic cells. *Nat. Methods* 11, 319–324.
- Kumar, M., Busch, W., Birke, H., Kemmerling, B., Nürnberger, T., and Schöffl, F.** (2009). Heat shock factors HsfB1 and HsfB2b are involved in the regulation of Pdf1.2 expression and pathogen resistance in Arabidopsis. *Mol. Plant* 2, 152–165.
- La Camera, S., Geoffroy, P., Samaha, H., Ndiaye, A., Rahim, G., Legrand, M., and Heitz, T.** (2005). A pathogen-inducible patatin-like lipid acyl hydrolase facilitates fungal and bacterial host colonization in Arabidopsis. *Plant J.* 44, 810–825.
- Laluk, K., and Mengiste, T.** (2010). Necrotroph attacks on plants: wanton destruction or covert extortion? *Arab. Book Am. Soc. Plant Biol.* 8, e0136.
- Lamesch, P., Berardini, T.Z., Li, D., Swarbreck, D., Wilks, C., Sasidharan, R., Muller, R., Dreher, K., Alexander, D.L., Garcia-Hernandez, M., et al.** (2012). The Arabidopsis Information Resource (TAIR): improved gene annotation and new tools. *Nucleic Acids Res.* 40, D1202–D1210.
- Lange, C., Hemmrich, G., Klostermeier, U.C., López-Quintero, J.A., Miller, D.J., Rahn, T., Weiss, Y., Bosch, T.C.G., and Rosenstiel, P.** (2011). Defining the Origins of the NOD-Like Receptor System at the Base of Animal Evolution. *Mol. Biol. Evol.* 28, 1687–1702.
- Lecourieux, D., Ranjeva, R., and Pugin, A.** (2006). Calcium in plant defence-signalling pathways. *New Phytol.* 171, 249–269.
- Leister, R.T., Dahlbeck, D., Day, B., Li, Y., Chesnokova, O., and Staskawicz, B.J.** (2005). Molecular Genetic Evidence for the Role of SGT1 in the Intramolecular Complementation of Bs2 Protein Activity in *Nicotiana benthamiana*. *Plant Cell Online* 17, 1268–1278.
- Lipka, V., Dittgen, J., Bednarek, P., Bhat, R., Wiermer, M., Stein, M., Landtag, J., Brandt, W., Rosahl, S., Scheel, D., et al.** (2005). Pre- and Postinvasion Defenses Both Contribute to Nonhost Resistance in Arabidopsis. *Science* 310, 1180–1183.
- Liu, J.-J., and Ekramoddoullah, A.K.M.** (2007). The CC-NBS-LRR Subfamily in *Pinus monticola*: Targeted Identification, Gene Expression, and Genetic Linkage with Resistance to *Cronartium ribicola*. *Phytopathology* 97, 728–736.
- Lorang, J.M., Sweat, T.A., and Wolpert, T.J.** (2007). Plant disease susceptibility conferred by a “resistance” gene. *Proc. Natl. Acad. Sci. U. S. A.* 104, 14861–14866.
- Mackey, D., Holt III, B.F., Wiig, A., and Dangl, J.L.** (2002). RIN4 Interacts with *Pseudomonas syringae* Type III Effector Molecules and Is Required for RPM1-Mediated Resistance in Arabidopsis. *Cell* 108, 743–754.

- Mackey, D., Belkhadir, Y., Alonso, J.M., Ecker, J.R., and Dangl, J.L.** (2003). Arabidopsis RIN4 Is a Target of the Type III Virulence Effector AvrRpt2 and Modulates RPS2-Mediated Resistance. *Cell* 112, 379–389.
- Maekawa, T., Kufer, T.A., and Schulze-Lefert, P.** (2011a). NLR functions in plant and animal immune systems: so far and yet so close. *Nat. Immunol.* 12, 817–826.
- Maekawa, T., Cheng, W., Spiridon, L.N., Töller, A., Lukasik, E., Saijo, Y., Liu, P., Shen, Q.-H., Micluta, M.A., Somssich, I.E., et al.** (2011b). Coiled-coil domain-dependent homodimerization of intracellular barley immune receptors defines a minimal functional module for triggering cell death. *Cell Host Microbe* 9, 187–199.
- Maekawa, T., Kracher, B., Vernaldi, S., Ver Loren van Themaat, E., and Schulze-Lefert, P.** (2012). Conservation of NLR-triggered immunity across plant lineages. *Proc. Natl. Acad. Sci. U. S. A.* 109, 20119–20123.
- Maere, S., Heymans, K., and Kuiper, M.** (2005). BiNGO: a Cytoscape plugin to assess overrepresentation of gene ontology categories in biological networks. *Bioinforma. Oxf. Engl.* 21, 3448–3449.
- Maleck, K., Levine, A., Eulgem, T., Morgan, A., Schmid, J., Lawton, K.A., Dangl, J.L., and Dietrich, R.A.** (2000). The transcriptome of Arabidopsis thaliana during systemic acquired resistance. *Nat. Genet.* 26, 403–410.
- Mao, G., Meng, X., Liu, Y., Zheng, Z., Chen, Z., and Zhang, S.** (2011). Phosphorylation of a WRKY Transcription Factor by Two Pathogen-Responsive MAPKs Drives Phytoalexin Biosynthesis in Arabidopsis[C][W]. *Plant Cell* 23, 1639–1653.
- Marcotte, E.M., Pellegrini, M., Ng, H.-L., Rice, D.W., Yeates, T.O., and Eisenberg, D.** (1999). Detecting Protein Function and Protein-Protein Interactions from Genome Sequences. *Science* 285, 751–753.
- Mathelier, A., Fornes, O., Arenillas, D.J., Chen, C., Denay, G., Lee, J., Shi, W., Shyr, C., Tan, G., Worsley-Hunt, R., et al.** (2015). JASPAR 2016: a major expansion and update of the open-access database of transcription factor binding profiles. *Nucleic Acids Res.* gkv1176.
- Matzke, M.A., and Mosher, R.A.** (2014). RNA-directed DNA methylation: an epigenetic pathway of increasing complexity. *Nat. Rev. Genet.* 15, 394–408.
- Medina-Rivera, A., Defrance, M., Sand, O., Herrmann, C., Castro-Mondragon, J.A., Delerce, J., Jaeger, S., Blanchet, C., Vincens, P., Caron, C., et al.** (2015). RSAT 2015: Regulatory Sequence Analysis Tools. *Nucleic Acids Res.* gkv362.
- Meng, X., Xu, J., He, Y., Yang, K.-Y., Mordorski, B., Liu, Y., and Zhang, S.** (2013). Phosphorylation of an ERF Transcription Factor by Arabidopsis MPK3/MPK6 Regulates Plant Defense Gene Induction and Fungal Resistance[C][W]. *Plant Cell* 25, 1126–1142.
- Mengiste, T.** (2012). Plant immunity to necrotrophs. *Annu. Rev. Phytopathol.* 50, 267–294.
- Meyers, B.C., Kozik, A., Griego, A., Kuang, H., and Michelmore, R.W.** (2003). Genome-wide analysis of NBS-LRR-encoding genes in Arabidopsis. *Plant Cell* 15, 809–834.

- Michael Weaver, L., Swiderski, M.R., Li, Y., and Jones, J.D.G.** (2006). The *Arabidopsis thaliana* TIR-NB-LRR R-protein, RPP1A; protein localization and constitutive activation of defence by truncated alleles in tobacco and *Arabidopsis*. *Plant J.* *47*, 829–840.
- Mindrinos, M., Katagiri, F., Yu, G.L., and Ausubel, F.M.** (1994). The *A. thaliana* disease resistance gene RPS2 encodes a protein containing a nucleotide-binding site and leucine-rich repeats. *Cell* *78*, 1089–1099.
- Mirabella, R., Rauwerda, H., Allmann, S., Scala, A., Spyropoulou, E.A., de Vries, M., Boersma, M.R., Breit, T.M., Haring, M.A., and Schuurink, R.C.** (2015). WRKY40 and WRKY6 act downstream of the green leaf volatile E-2-hexenal in *Arabidopsis*. *Plant J. Cell Mol. Biol.* *83*, 1082–1096.
- Miranda, T.B., Cortez, C.C., Yoo, C.B., Liang, G., Abe, M., Kelly, T.K., Marquez, V.E., and Jones, P.A.** (2009). DZNep is a global histone methylation inhibitor that reactivates developmental genes not silenced by DNA methylation. *Mol. Cancer Ther.* *8*, 1579–1588.
- Mitsuda, N., Ikeda, M., Takada, S., Takiguchi, Y., Kondou, Y., Yoshizumi, T., Fujita, M., Shinozaki, K., Matsui, M., and Ohme-Takagi, M.** (2010). Efficient Yeast One-/Two-Hybrid Screening Using a Library Composed Only of Transcription Factors in *Arabidopsis thaliana*. *Plant Cell Physiol.* *51*, 2145–2151.
- Moffett, P., Farnham, G., Peart, J., and Baulcombe, D.C.** (2002). Interaction between domains of a plant NBS–LRR protein in disease resistance-related cell death. *EMBO J.* *21*, 4511–4519.
- Moghaddam, M.R.B., and Ende, W.V. den** (2012). Sugars and plant innate immunity. *J. Exp. Bot.* ers129.
- Morkunas, I., and Ratajczak, L.** (2014). The role of sugar signaling in plant defense responses against fungal pathogens. *Acta Physiol. Plant.* *36*, 1607–1619.
- Moscou, M.J., Lauter, N., Caldo, R.A., Nettleton, D., and Wise, R.P.** (2011). Quantitative and temporal definition of the Mla transcriptional regulon during barley-powdery mildew interactions. *Mol. Plant-Microbe Interact. MPMI* *24*, 694–705.
- Mukhtar, M.S., Carvunis, A.-R., Dreze, M., Epple, P., Steinbrenner, J., Moore, J., Tasan, M., Galli, M., Hao, T., Nishimura, M.T., et al.** (2011). Independently evolved virulence effectors converge onto hubs in a plant immune system network. *Science* *333*, 596–601.
- Munch, D., Teh, O.-K., Malinovsky, F.G., Liu, Q., Vetukuri, R.R., Kasmi, F.E., Brodersen, P., Hara-Nishimura, I., Dangl, J.L., Petersen, M., et al.** (2015). Retromer Contributes to Immunity-Associated Cell Death in *Arabidopsis*. *Plant Cell Online* tpc.114.132043.
- Nagy, E.D., and Bennetzen, J.L.** (2008). Pathogen corruption and site-directed recombination at a plant disease resistance gene cluster. *Genome Res.* *18*, 1918–1923.
- Narusaka, M., Kubo, Y., Hatakeyama, K., Imamura, J., Ezura, H., Nanasato, Y., Tabei, Y., Takano, Y., Shirasu, K., and Narusaka, Y.** (2013). Interfamily transfer of dual NB-LRR genes confers resistance to multiple pathogens. *PloS One* *8*, e55954.

- Narusaka, Y., Nakashima, K., Shinwari, Z.K., Sakuma, Y., Furihata, T., Abe, H., Narusaka, M., Shinozaki, K., and Yamaguchi-Shinozaki, K.** (2003). Interaction between two cis-acting elements, ABRE and DRE, in ABA-dependent expression of Arabidopsis rd29A gene in response to dehydration and high-salinity stresses. *Plant J. Cell Mol. Biol.* *34*, 137–148.
- Navarro, L., Zipfel, C., Rowland, O., Keller, I., Robatzek, S., Boller, T., and Jones, J.D.G.** (2004). The Transcriptional Innate Immune Response to flg22. Interplay and Overlap with Avr Gene-Dependent Defense Responses and Bacterial Pathogenesis. *Plant Physiol.* *135*, 1113–1128.
- Nie, H., Zhao, C., Wu, G., Wu, Y., Chen, Y., and Tang, D.** (2012). SR1, a Calmodulin-Binding Transcription Factor, Modulates Plant Defense and Ethylene-Induced Senescence by Directly Regulating NDR1 and EIN31[W][OA]. *Plant Physiol.* *158*, 1847–1859.
- Nordström, K.J.V., Albani, M.C., James, G.V., Gutjahr, C., Hartwig, B., Turck, F., Paszkowski, U., Coupland, G., and Schneeberger, K.** (2013). Mutation identification by direct comparison of whole-genome sequencing data from mutant and wild-type individuals using k-mers. *Nat. Biotechnol.* *31*, 325–330.
- Noutoshi, Y., Ito, T., Seki, M., Nakashita, H., Yoshida, S., Marco, Y., Shirasu, K., and Shinozaki, K.** (2005). A single amino acid insertion in the WRKY domain of the Arabidopsis TIR–NBS–LRR–WRKY-type disease resistance protein SLH1 (sensitive to low humidity 1) causes activation of defense responses and hypersensitive cell death. *Plant J.* *43*, 873–888.
- O’Donnell, A., Odrowaz, Z., and Sharrocks, A.D.** (2012). Immediate-early gene activation by the MAPK pathways: what do and don’t we know? *Biochem. Soc. Trans.* *40*, 58–66.
- Ohme-Takagi, M., and Shinshi, H.** (1995). Ethylene-inducible DNA binding proteins that interact with an ethylene-responsive element. *Plant Cell* *7*, 173–182.
- van Ooijen, G., van den Burg, H.A., Cornelissen, B.J.C., and Takken, F.L.W.** (2007). Structure and function of resistance proteins in solanaceous plants. *Annu. Rev. Phytopathol.* *45*, 43–72.
- Ossowski, S., Schneeberger, K., Clark, R.M., Lanz, C., Warthmann, N., and Weigel, D.** (2008). Sequencing of natural strains of Arabidopsis thaliana with short reads. *Genome Res.* *18*, 2024–2033.
- Padmanabhan, M.S., and Dinesh-Kumar, S.P.** (2014). The conformational and subcellular compartmental dance of plant NLRs during viral recognition and defense signaling. *Curr. Opin. Microbiol.* *20*, 55–61.
- Padmanabhan, M.S., Ma, S., Burch-Smith, T.M., Czymmek, K., Huijser, P., and Dinesh-Kumar, S.P.** (2013). Novel positive regulatory role for the SPL6 transcription factor in the N TIR-NB-LRR receptor-mediated plant innate immunity. *PLoS Pathog.* *9*, e1003235.
- Page, D.R., and Grossniklaus, U.** (2002). The art and design of genetic screens: Arabidopsis thaliana. *Nat. Rev. Genet.* *3*, 124–136.

- Pajerowska-Mukhtar, K.M., Wang, W., Tada, Y., Oka, N., Tucker, C.L., Fonseca, J.P., and Dong, X.** (2012). The HSF-like Transcription Factor TBF1 Is a Major Molecular Switch for Plant Growth-to-Defense Transition. *Curr. Biol.* *22*, 103–112.
- Parker, J.E., Holub, E.B., Frost, L.N., Falk, A., Gunn, N.D., and Daniels, M.J.** (1996). Characterization of *eds1*, a mutation in *Arabidopsis* suppressing resistance to *Peronospora parasitica* specified by several different RPP genes. *Plant Cell* *8*, 2033–2046.
- Pavesi, G., Mereghetti, P., Zambelli, F., Stefani, M., Mauri, G., and Pesole, G.** (2006). MoD Tools: regulatory motif discovery in nucleotide sequences from co-regulated or homologous genes. *Nucleic Acids Res.* *34*, W566–W570.
- Payne, S.H.** (2015). The utility of protein and mRNA correlation. *Trends Biochem. Sci.* *40*, 1–3.
- Pecinka, A., Abdelsamad, A., and Vu, G.T.H.** (2013). Hidden genetic nature of epigenetic natural variation in plants. *Trends Plant Sci.* *18*, 625–632.
- Perez, I.B., and Brown, P.J.** (2014). The role of ROS signaling in cross-tolerance: from model to crop. *Front. Plant Sci.* *5*.
- Pflieger, D., Bigeard, J., and Hirt, H.** (2011). Isolation and characterization of plant protein complexes by mass spectrometry. *PROTEOMICS* *11*, 1824–1833.
- Pick, T., Jaskiewicz, M., Peterhänsel, C., and Conrath, U.** (2012). Heat Shock Factor HsfB1 Primes Gene Transcription and Systemic Acquired Resistance in *Arabidopsis*. *Plant Physiol.* *159*, 52–55.
- Pieterse, C.M.J., Does, D.V. der, Zamioudis, C., Leon-Reyes, A., and Wees, S.C.M.V.** (2012). Hormonal Modulation of Plant Immunity. *Annu. Rev. Cell Dev. Biol.* *28*, 489–521.
- Pike, S.M., Zhang, X.-C., and Gassmann, W.** (2005). Electrophysiological Characterization of the *Arabidopsis* *avrRpt2*-Specific Hypersensitive Response in the Absence of Other Bacterial Signals. *Plant Physiol.* *138*, 1009–1017.
- Poovaiah, B.W., Du, L., Wang, H., and Yang, T.** (2013). Recent Advances in Calcium/Calmodulin-Mediated Signaling with an Emphasis on Plant-Microbe Interactions. *Plant Physiol.* *163*, 531–542.
- Qi, D., and Innes, R.W.** (2013). Recent Advances in Plant NLR Structure, Function, Localization, and Signaling. *Front. Immunol.* *4*.
- Qi, Y., and Katagiri, F.** (2009). Purification of low-abundance *Arabidopsis* plasma-membrane protein complexes and identification of candidate components. *Plant J.* *57*, 932–944.
- Qi, D., DeYoung, B.J., and Innes, R.W.** (2012). Structure-Function Analysis of the Coiled-Coil and Leucine-Rich Repeat Domains of the RPS5 Disease Resistance Protein. *Plant Physiol.* *158*, 1819–1832.
- Qi, Y., Tsuda, K., Glazebrook, J., and Katagiri, F.** (2011). Physical association of pattern-triggered immunity (PTI) and effector-triggered immunity (ETI) immune receptors in *Arabidopsis*: Physical association of PTI and ETI receptors. *Mol. Plant Pathol.* *12*, 702–708.

- Quinlan, A.R., and Hall, I.M.** (2010). BEDTools: a flexible suite of utilities for comparing genomic features. *Bioinforma. Oxf. Engl.* *26*, 841–842.
- Rafiqi, M., Ellis, J.G., Ludowici, V.A., Hardham, A.R., and Dodds, P.N.** (2012). Challenges and progress towards understanding the role of effectors in plant-fungal interactions. *Curr. Opin. Plant Biol.* *15*, 477–482.
- Rairdan, G., and Moffett, P.** (2007). Brothers in arms? Common and contrasting themes in pathogen perception by plant NB-LRR and animal NACHT-LRR proteins. *Microbes Infect.* *9*, 677–686.
- Rairdan, G.J., Collier, S.M., Sacco, M.A., Baldwin, T.T., Boetrich, T., and Moffett, P.** (2008). The Coiled-Coil and Nucleotide Binding Domains of the Potato Rx Disease Resistance Protein Function in Pathogen Recognition and Signaling. *Plant Cell* *20*, 739–751.
- Ramonell, K., Berrocal-Lobo, M., Koh, S., Wan, J., Edwards, H., Stacey, G., and Somerville, S.** (2005). Loss-of-function mutations in chitin responsive genes show increased susceptibility to the powdery mildew pathogen *Erysiphe cichoracearum*. *Plant Physiol.* *138*, 1027–1036.
- Rappsilber, J., Mann, M., and Ishihama, Y.** (2007). Protocol for micro-purification, enrichment, pre-fractionation and storage of peptides for proteomics using StageTips. *Nat. Protoc.* *2*, 1896–1906.
- Reina-Pinto, J.J., Voisin, D., Kurdyukov, S., Faust, A., Haslam, R.P., Michaelson, L.V., Efremova, N., Franke, B., Schreiber, L., Napier, J.A., et al.** (2009). Misexpression of FATTY ACID ELONGATION1 in the Arabidopsis Epidermis Induces Cell Death and Suggests a Critical Role for Phospholipase A2 in This Process. *Plant Cell* *21*, 1252–1272.
- Ritchie, M.E., Phipson, B., Wu, D., Hu, Y., Law, C.W., Shi, W., and Smyth, G.K.** (2015). limma powers differential expression analyses for RNA-sequencing and microarray studies. *Nucleic Acids Res.* *43*, e47.
- Roberts, M., Tang, S., Stallmann, A., Dangl, J.L., and Bonardi, V.** (2013). Genetic requirements for signaling from an autoactive plant NB-LRR intracellular innate immune receptor. *PLoS Genet.* *9*, e1003465.
- Robinson, J.T., Thorvaldsdóttir, H., Winckler, W., Guttman, M., Lander, E.S., Getz, G., and Mesirov, J.P.** (2011). Integrative genomics viewer. *Nat. Biotechnol.* *29*, 24–26.
- Saedler, R., Jakoby, M., Marin, B., Galiana-Jaime, E., and Hülskamp, M.** (2009). The cell morphogenesis gene SPIRRIG in Arabidopsis encodes a WD/BEACH domain protein. *Plant J.* *59*, 612–621.
- Saha, R.N., and Dudek, S.M.** (2013). Splitting hares and tortoises: a classification of neuronal immediate early gene transcription based on poised RNA polymerase II. *Neuroscience* *247*, 175–181.
- Salmeron, J.M., Oldroyd, G.E.D., Rommens, C.M.T., Scofield, S.R., Kim, H.-S., Lavelle, D.T., Dahlbeck, D., and Staskawicz, B.J.** (1996). Tomato Prf Is a Member of the Leucine-Rich Repeat Class of Plant Disease Resistance Genes and Lies Embedded within the Pto Kinase Gene Cluster. *Cell* *86*, 123–133.

- Sarin, S., Prabhu, S., O'Meara, M.M., Pe'er, I., and Hobert, O.** (2008). Caenorhabditis elegans mutant allele identification by whole-genome sequencing. *Nat. Methods* *5*, 865–867.
- Sarris, P.F., Duxbury, Z., Huh, S.U., Ma, Y., Segonzac, C., Sklenar, J., Derbyshire, P., Cevik, V., Rallapalli, G., Saucet, S.B., et al.** (2015). A Plant Immune Receptor Detects Pathogen Effectors that Target WRKY Transcription Factors. *Cell* *161*, 1089–1100.
- Schneeberger, K., and Weigel, D.** (2011). Fast-forward genetics enabled by new sequencing technologies. *Trends Plant Sci.* *16*, 282–288.
- Schneeberger, K., Ossowski, S., Lanz, C., Juul, T., Petersen, A.H., Nielsen, K.L., Jørgensen, J.-E., Weigel, D., and Andersen, S.U.** (2009). SHOREmap: simultaneous mapping and mutation identification by deep sequencing. *Nat. Methods* *6*, 550–551.
- Seeholzer, S., Tsuchimatsu, T., Jordan, T., Bieri, S., Pajonk, S., Yang, W., Jahoor, A., Shimizu, K.K., Keller, B., and Schulze-Lefert, P.** (2010). Diversity at the Mla powdery mildew resistance locus from cultivated barley reveals sites of positive selection. *Mol. Plant-Microbe Interact. MPMI* *23*, 497–509.
- Segonzac, C., Feike, D., Gimenez-Ibanez, S., Hann, D.R., Zipfel, C., and Rathjen, J.P.** (2011). Hierarchy and Roles of Pathogen-Associated Molecular Pattern-Induced Responses in *Nicotiana benthamiana*. *Plant Physiol.* *156*, 687–699.
- Selote, D., Shine, M.B., Robin, G.P., and Kachroo, A.** (2014). Soybean NDR1-like proteins bind pathogen effectors and regulate resistance signaling. *New Phytol.* *202*, 485–498.
- Shannon, P., Markiel, A., Ozier, O., Baliga, N.S., Wang, J.T., Ramage, D., Amin, N., Schwikowski, B., and Ideker, T.** (2003). Cytoscape: a software environment for integrated models of biomolecular interaction networks. *Genome Res.* *13*, 2498–2504.
- Shen, Q., and Ho, T.H.** (1995). Functional dissection of an abscisic acid (ABA)-inducible gene reveals two independent ABA-responsive complexes each containing a G-box and a novel cis-acting element. *Plant Cell* *7*, 295–307.
- Shen, Q.-H., Zhou, F., Bieri, S., Haizel, T., Shirasu, K., and Schulze-Lefert, P.** (2003). Recognition specificity and RAR1/SGT1 dependence in barley Mla disease resistance genes to the powdery mildew fungus. *Plant Cell* *15*, 732–744.
- Shen, Q.-H., Saijo, Y., Mauch, S., Biskup, C., Bieri, S., Keller, B., Seki, H., Ülker, B., Somssich, I.E., and Schulze-Lefert, P.** (2007). Nuclear Activity of MLA Immune Receptors Links Isolate-Specific and Basal Disease-Resistance Responses. *Science* *315*, 1098–1103.
- Shimono, M., Sugano, S., Nakayama, A., Jiang, C.-J., Ono, K., Toki, S., and Takatsuji, H.** (2007). Rice WRKY45 plays a crucial role in benzothiadiazole-inducible blast resistance. *Plant Cell* *19*, 2064–2076.
- Shirasu, K., Lahaye, T., Tan, M.-W., Zhou, F., Azevedo, C., and Schulze-Lefert, P.** (1999). A Novel Class of Eukaryotic Zinc-Binding Proteins Is Required for Disease Resistance Signaling in Barley and Development in *C. elegans*. *Cell* *99*, 355–366.
- Slootweg, E., Roosien, J., Spiridon, L.N., Petrescu, A.-J., Tameling, W., Joosten, M., Pomp, R., van Schaik, C., Dees, R., Borst, J.W., et al.** (2010). Nucleocytoplasmic

Distribution Is Required for Activation of Resistance by the Potato NB-LRR Receptor Rx1 and Is Balanced by Its Functional Domains. *Plant Cell* 22, 4195–4215.

Slootweg, E.J., Spiridon, L.N., Roosien, J., Butterbach, P., Pomp, R., Westerhof, L., Wilbers, R., Bakker, E., Bakker, J., Petrescu, A.-J., et al. (2013). Structural Determinants at the Interface of the ARC2 and LRR Domains Control the Activation of the NB-LRR Plant Immune Receptors Rx1 and Gpa2. *Plant Physiol.*

Smyth, G.K. (2005). limma: Linear Models for Microarray Data. In *Bioinformatics and Computational Biology Solutions Using R and Bioconductor*, R. Gentleman, V.J. Carey, W. Huber, R.A. Irizarry, and S. Dudoit, eds. (Springer New York), pp. 397–420.

Solomon, M., Belenghi, B., Delledonne, M., Menachem, E., and Levine, A. (1999). The Involvement of Cysteine Proteases and Protease Inhibitor Genes in the Regulation of Programmed Cell Death in Plants. *Plant Cell* 11, 431–443.

Staal, J., and Dixelius, C. (2007). Tracing the ancient origins of plant innate immunity. *Trends Plant Sci.* 12, 334–342.

Staal, J., Kaliff, M., Dewaele, E., Persson, M., and Dixelius, C. (2008). RLM3, a TIR domain encoding gene involved in broad-range immunity of Arabidopsis to necrotrophic fungal pathogens. *Plant J.* 55, 188–200.

Swiderski, M.R., Birker, D., and Jones, J.D.G. (2009). The TIR domain of TIR-NB-LRR resistance proteins is a signaling domain involved in cell death induction. *Mol. Plant-Microbe Interact.* MPMI 22, 157–165.

Takemoto, D., Rafiqi, M., Hurley, U., Lawrence, G.J., Bernoux, M., Hardham, A.R., Ellis, J.G., Dodds, P.N., and Jones, D.A. (2011). N-Terminal Motifs in Some Plant Disease Resistance Proteins Function in Membrane Attachment and Contribute to Disease Resistance. *Mol. Plant. Microbe Interact.* 25, 379–392.

Takken, F.L., Albrecht, M., and Tameling, W.I. (2006). Resistance proteins: molecular switches of plant defence. *Curr. Opin. Plant Biol.* 9, 383–390.

Tao, Y., Xie, Z., Chen, W., Glazebrook, J., Chang, H.-S., Han, B., Zhu, T., Zou, G., and Katagiri, F. (2003). Quantitative nature of Arabidopsis responses during compatible and incompatible interactions with the bacterial pathogen *Pseudomonas syringae*. *Plant Cell* 15, 317–330.

Tavernier, E., Wendehenne, D., Blein, J.P., and Pugin, A. (1995). Involvement of Free Calcium in Action of Cryptogein, a Proteinaceous Elicitor of Hypersensitive Reaction in Tobacco Cells. *Plant Physiol.* 109, 1025–1031.

Thines, B., Katsir, L., Melotto, M., Niu, Y., Mandaokar, A., Liu, G., Nomura, K., He, S.Y., Howe, G.A., and Browse, J. (2007). JAZ repressor proteins are targets of the SCF(CO1) complex during jasmonate signalling. *Nature* 448, 661–665.

Thorvaldsdóttir, H., Robinson, J.T., and Mesirov, J.P. (2013). Integrative Genomics Viewer (IGV): high-performance genomics data visualization and exploration. *Brief. Bioinform.* 14, 178–192.

- Tör, M., Gordon, P., Cuzick, A., Eulgem, T., Sinapidou, E., Mert-Türk, F., Can, C., Dangl, J.L., and Holub, E.B.** (2002). Arabidopsis SGT1b Is Required for Defense Signaling Conferred by Several Downy Mildew Resistance Genes. *Plant Cell* *14*, 993–1003.
- Tornero, P., Merritt, P., Sadanandom, A., Shirasu, K., Innes, R.W., and Dangl, J.L.** (2002a). RAR1 and NDR1 contribute quantitatively to disease resistance in Arabidopsis, and their relative contributions are dependent on the R gene assayed. *Plant Cell* *14*, 1005–1015.
- Tornero, P., Chao, R.A., Luthin, W.N., Goff, S.A., and Dangl, J.L.** (2002b). Large-Scale Structure–Function Analysis of the Arabidopsis RPM1 Disease Resistance Protein. *Plant Cell* *14*, 435–450.
- Torp, J., and Jørgensen, J.H.** (1986). Modification of barley powdery mildew resistance gene Ml-a12 by induced mutation. *Can. J. Genet. Cytol.* *28*, 725–731.
- Tsuda, K., and Katagiri, F.** (2010). Comparing signaling mechanisms engaged in pattern-triggered and effector-triggered immunity. *Curr. Opin. Plant Biol.* *13*, 459–465.
- Tsuda, K., and Somssich, I.E.** (2015). Transcriptional networks in plant immunity. *New Phytol.* *206*, 932–947.
- Tsuda, K., Sato, M., Stoddard, T., Glazebrook, J., and Katagiri, F.** (2009). Network Properties of Robust Immunity in Plants. *PLoS Genet* *5*, e1000772.
- Tsuda, K., Mine, A., Bethke, G., Igarashi, D., Botanga, C.J., Tsuda, Y., Glazebrook, J., Sato, M., and Katagiri, F.** (2013). Dual Regulation of Gene Expression Mediated by Extended MAPK Activation and Salicylic Acid Contributes to Robust Innate Immunity in Arabidopsis thaliana. *PLoS Genet* *9*, e1004015.
- Van der Biezen, E.A., and Jones, J.D.** (1998). Plant disease-resistance proteins and the gene-for-gene concept. *Trends Biochem. Sci.* *23*, 454–456.
- Vidhyasekaran, P.** (2014). *PAMP Signals in Plant Innate Immunity* (Dordrecht: Springer Netherlands).
- Walley, J.W., and Dehesh, K.** (2010). Molecular Mechanisms Regulating Rapid Stress Signaling Networks in Arabidopsis. *J. Integr. Plant Biol.* *52*, 354–359.
- Walley, J.W., Coughlan, S., Hudson, M.E., Covington, M.F., Kaspi, R., Banu, G., Harmer, S.L., and Dehesh, K.** (2007). Mechanical Stress Induces Biotic and Abiotic Stress Responses via a Novel cis-Element. *PLoS Genet.* *3*.
- Walters, D., and Heil, M.** (2007). Costs and trade-offs associated with induced resistance. *Physiol. Mol. Plant Pathol.* *71*, 3–17.
- Wang, G.-F., and Balint-Kurti, P.J.** (2015). Cytoplasmic and Nuclear Localizations Are Important for the Hypersensitive Response Conferred by Maize Autoactive Rp1-D21 Protein. *Mol. Plant. Microbe Interact.* *28*, 1023–1031.
- Waters, M.T., Brewer, P.B., Bussell, J.D., Smith, S.M., and Beveridge, C.A.** (2012). The Arabidopsis ortholog of rice DWARF27 acts upstream of MAX1 in the control of plant development by strigolactones. *Plant Physiol.* *159*, 1073–1085.

- Wei Ning, F.C.** (2004). N-acetylchitooligosaccharides elicit rice defence responses including hypersensitive response-like cell death, oxidative burst and defence gene expression. *Physiol. Mol. Plant Pathol.* *64*, 263–271.
- Whitham, S., Dinesh-Kumar, S.P., Choi, D., Hehl, R., Corr, C., and Baker, B.** (1994). The product of the tobacco mosaic virus resistance gene N: Similarity to toll and the interleukin-1 receptor. *Cell* *78*, 1101–1115.
- Wiermer, M., Feys, B.J., and Parker, J.E.** (2005). Plant immunity: the EDS1 regulatory node. *Curr. Opin. Plant Biol.* *8*, 383–389.
- William, D.A., Su, Y., Smith, M.R., Lu, M., Baldwin, D.A., and Wagner, D.** (2004). Genomic identification of direct target genes of LEAFY. *Proc. Natl. Acad. Sci. U. S. A.* *101*, 1775–1780.
- Wirthmueller, L., Zhang, Y., Jones, J.D.G., and Parker, J.E.** (2007). Nuclear accumulation of the Arabidopsis immune receptor RPS4 is necessary for triggering EDS1-dependent defense. *Curr. Biol. CB* *17*, 2023–2029.
- Wiśniewski, J.R., Zougman, A., and Mann, M.** (2009). Combination of FASP and StageTip-Based Fractionation Allows In-Depth Analysis of the Hippocampal Membrane Proteome. *J. Proteome Res.* *8*, 5674–5678.
- Wulff, B.B., Horvath, D.M., and Ward, E.R.** (2011). Improving immunity in crops: new tactics in an old game. *Curr. Opin. Plant Biol.* *14*, 468–476.
- Xiao, S., Charoenwattana, P., Holcombe, L., and Turner, J.G.** (2003). The Arabidopsis genes RPW8.1 and RPW8.2 confer induced resistance to powdery mildew diseases in tobacco. *Mol. Plant-Microbe Interact. MPMI* *16*, 289–294.
- Xu, F., Kapos, P., Cheng, Y.T., Li, M., Zhang, Y., and Li, X.** (2014). NLR-Associating Transcription Factor bHLH84 and Its Paralogs Function Redundantly in Plant Immunity. *PLoS Pathog* *10*, e1004312.
- Yadav, V., Mallappa, C., Gangappa, S.N., Bhatia, S., and Chattopadhyay, S.** (2005). A Basic Helix-Loop-Helix Transcription Factor in Arabidopsis, MYC2, Acts as a Repressor of Blue Light-Mediated Photomorphogenic Growth. *Plant Cell* *17*, 1953–1966.
- Yang, S., and Hua, J.** (2004). A Haplotype-Specific Resistance Gene Regulated by BONZAI1 Mediates Temperature-Dependent Growth Control in Arabidopsis. *Plant Cell* *16*, 1060–1071.
- Yoshimoto, K., Jikumaru, Y., Kamiya, Y., Kusano, M., Consonni, C., Panstruga, R., Ohsumi, Y., and Shirasu, K.** (2009). Autophagy negatively regulates cell death by controlling NPR1-dependent salicylic acid signaling during senescence and the innate immune response in Arabidopsis. *Plant Cell* *21*, 2914–2927.
- Yu, I., Parker, J., and Bent, A.F.** (1998). Gene-for-gene disease resistance without the hypersensitive response in Arabidopsis dnd1 mutant. *Proc. Natl. Acad. Sci. U. S. A.* *95*, 7819–7824.

- Yu, I., Fengler, K.A., Clough, S.J., and Bent, A.F.** (2000). Identification of Arabidopsis Mutants Exhibiting an Altered Hypersensitive Response in Gene-for-Gene Disease Resistance. *Mol. Plant. Microbe Interact.* *13*, 277–286.
- Yue, J.-X., Meyers, B.C., Chen, J.-Q., Tian, D., and Yang, S.** (2012). Tracing the origin and evolutionary history of plant nucleotide-binding site-leucine-rich repeat (NBS-LRR) genes. *New Phytol.* *193*, 1049–1063.
- Zambelli, F., Pesole, G., and Pavesi, G.** (2009). Pscan: finding over-represented transcription factor binding site motifs in sequences from co-regulated or co-expressed genes. *Nucleic Acids Res.* *37*, W247–W252.
- Zambelli, F., Pesole, G., and Pavesi, G.** (2014). Using Weeder, Pscan, and PscanChIP for the Discovery of Enriched Transcription Factor Binding Site Motifs in Nucleotide Sequences. *Curr. Protoc. Bioinforma.* Ed. Board **Andreas Baxevanis** *AI 47*, 2.11.1–2.11.31.
- Zhang, Q., Zmasek, C.M., and Godzik, A.** (2010). Domain architecture evolution of pattern-recognition receptors. *Immunogenetics* *62*, 263–272.
- Zhang, T., Liu, Y., Yang, T., Zhang, L., Xu, S., Xue, L., and An, L.** (2006). Diverse signals converge at MAPK cascades in plant. *Plant Physiol. Biochem.* *44*, 274–283.
- Zhang, Z., Wu, Y., Gao, M., Zhang, J., Kong, Q., Liu, Y., Ba, H., Zhou, J., and Zhang, Y.** (2012). Disruption of PAMP-Induced MAP Kinase Cascade by a *Pseudomonas syringae* Effector Activates Plant Immunity Mediated by the NB-LRR Protein SUMM2. *Cell Host Microbe* *11*, 253–263.
- Zheng, Z., Qamar, S.A., Chen, Z., and Mengiste, T.** (2006). Arabidopsis WRKY33 transcription factor is required for resistance to necrotrophic fungal pathogens. *Plant J.* *48*, 592–605.
- Zhou, J., Lu, D., Xu, G., Finlayson, S.A., He, P., and Shan, L.** (2015). The dominant negative ARM domain uncovers multiple functions of PUB13 in Arabidopsis immunity, flowering, and senescence. *J. Exp. Bot.* *66*, 3353–3366.
- Zhou, T., Wang, Y., Chen, J.-Q., Araki, H., Jing, Z., Jiang, K., Shen, J., and Tian, D.** (2004). Genome-wide identification of NBS genes in japonica rice reveals significant expansion of divergent non-TIR NBS-LRR genes. *Mol. Genet. Genomics* *271*, 402–415.
- Zhu, Y., Li, Y., Fei, F., Wang, Z., Wang, W., Cao, A., Liu, Y., Han, S., Xing, L., Wang, H., et al.** (2015). An E3 ubiquitin ligase gene CMPG1-V from *Haynaldia villosa* L. contributes to the powdery mildew resistance in common wheat. *Plant J.* n/a – n/a.
- Zhu, Z., Xu, F., Zhang, Y., Cheng, Y.T., Wiermer, M., Li, X., and Zhang, Y.** (2010). Arabidopsis resistance protein SNC1 activates immune responses through association with a transcriptional corepressor. *Proc. Natl. Acad. Sci. U. S. A.* *107*, 13960–13965.
- Zipfel, C.** (2014). Plant pattern-recognition receptors. *Trends Immunol.* *35*, 345–351.



Supplementary data

1. Supplementary figures

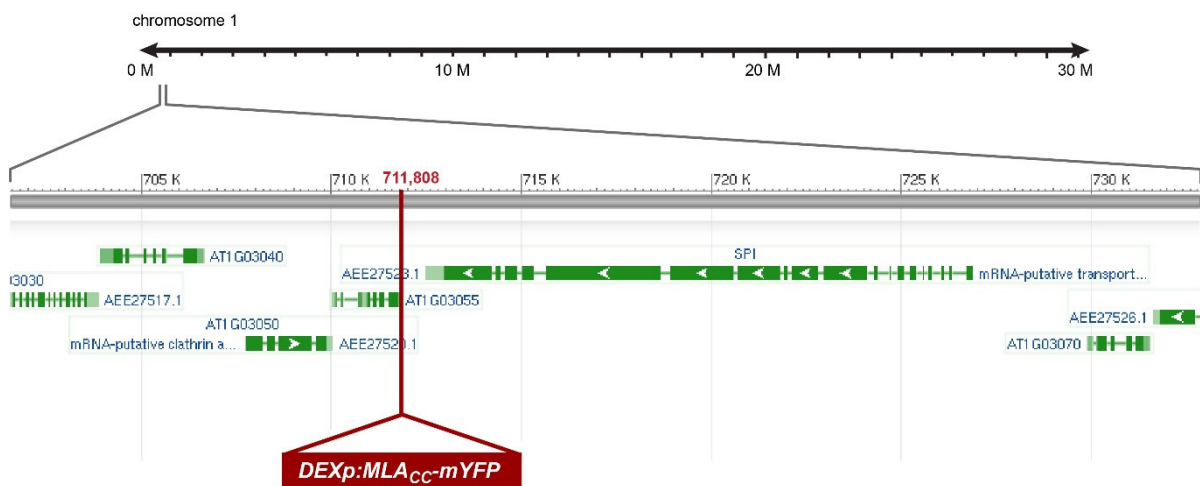


Figure S1-1: Genomic location of the *DEXp:MLAcc-mYFP* transgene in line #5.1 as defined by sequencing of the flanking regions. The location on the chromosome 1 is indicated in base pair.

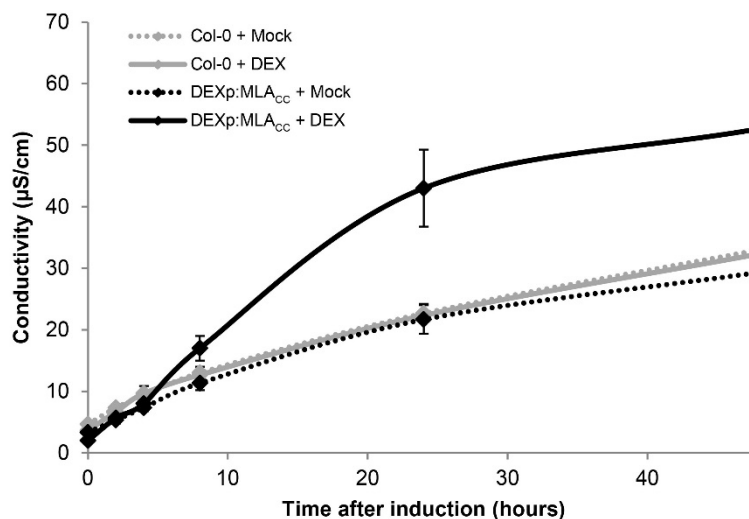
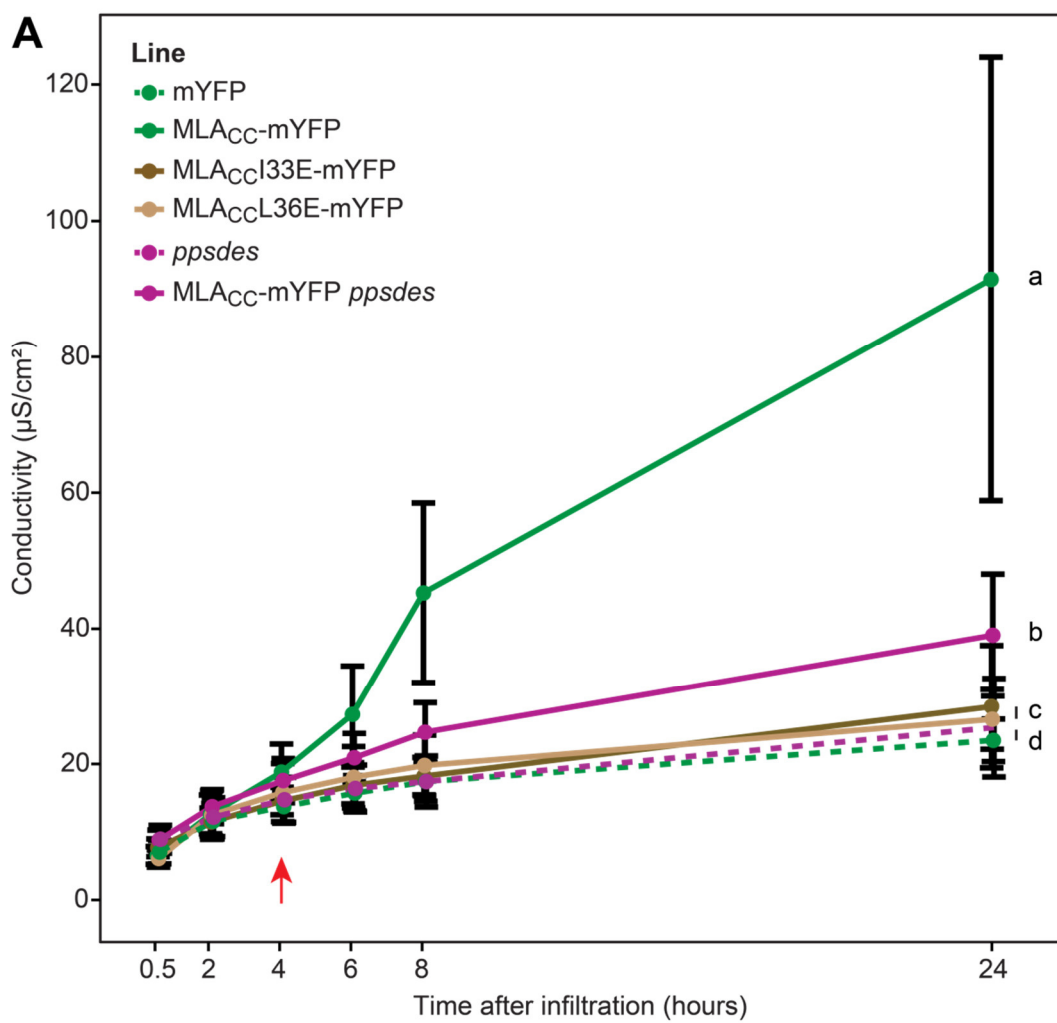


Figure S1-2: Ion leakage measure in the *DEXp:MLAcc-mYFP* line upon DEX treatment. Ion leakage was measured after immersing leaf discs of 6 week old *DEXp:MLAcc-mYFP* plants or the Col-0 wild-type control into a solution with 10 μM DEX or solvent control (mock) + 0.001% Silwet L-77. Error bars represent the standard deviation from three biological replicates from one experiment.



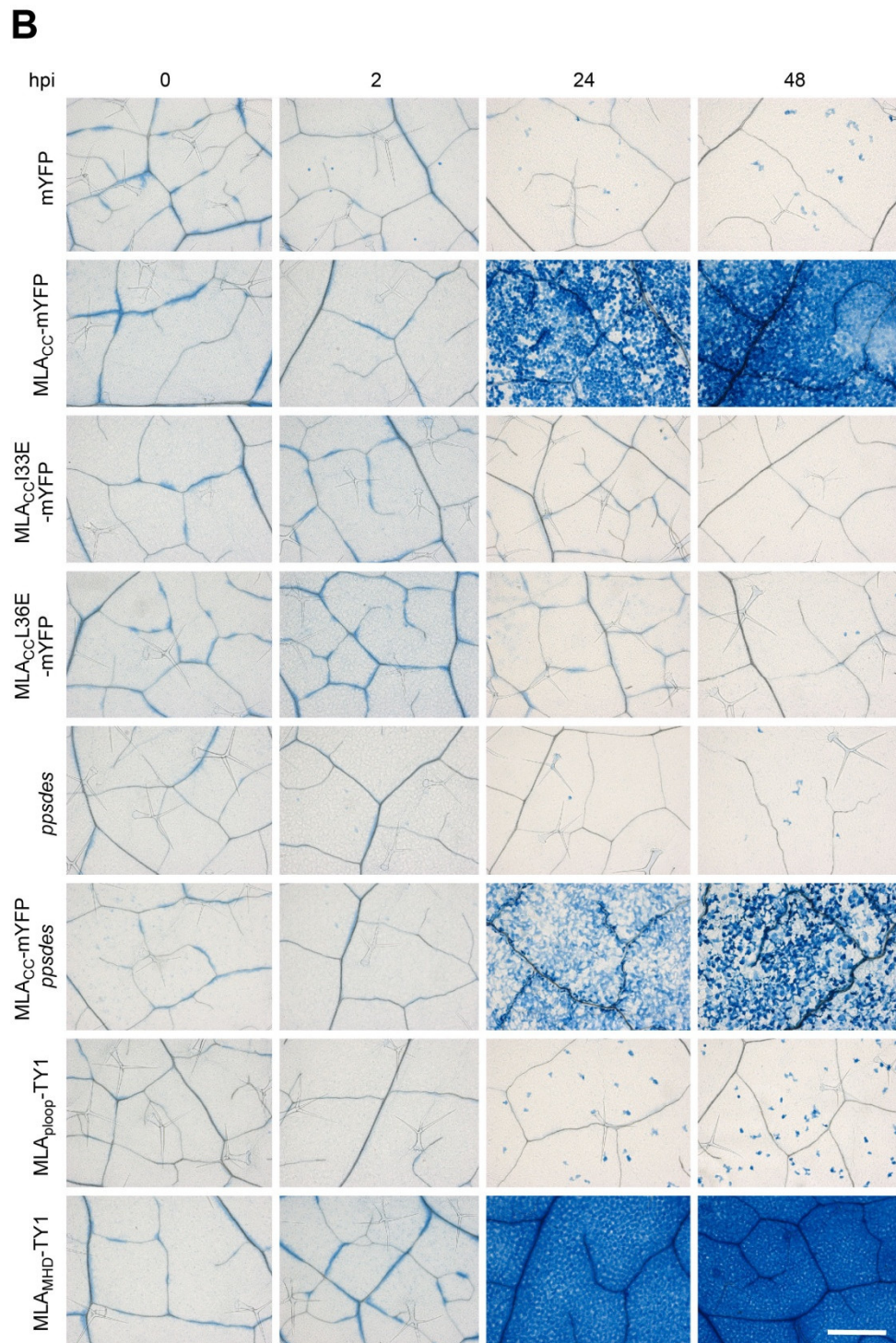
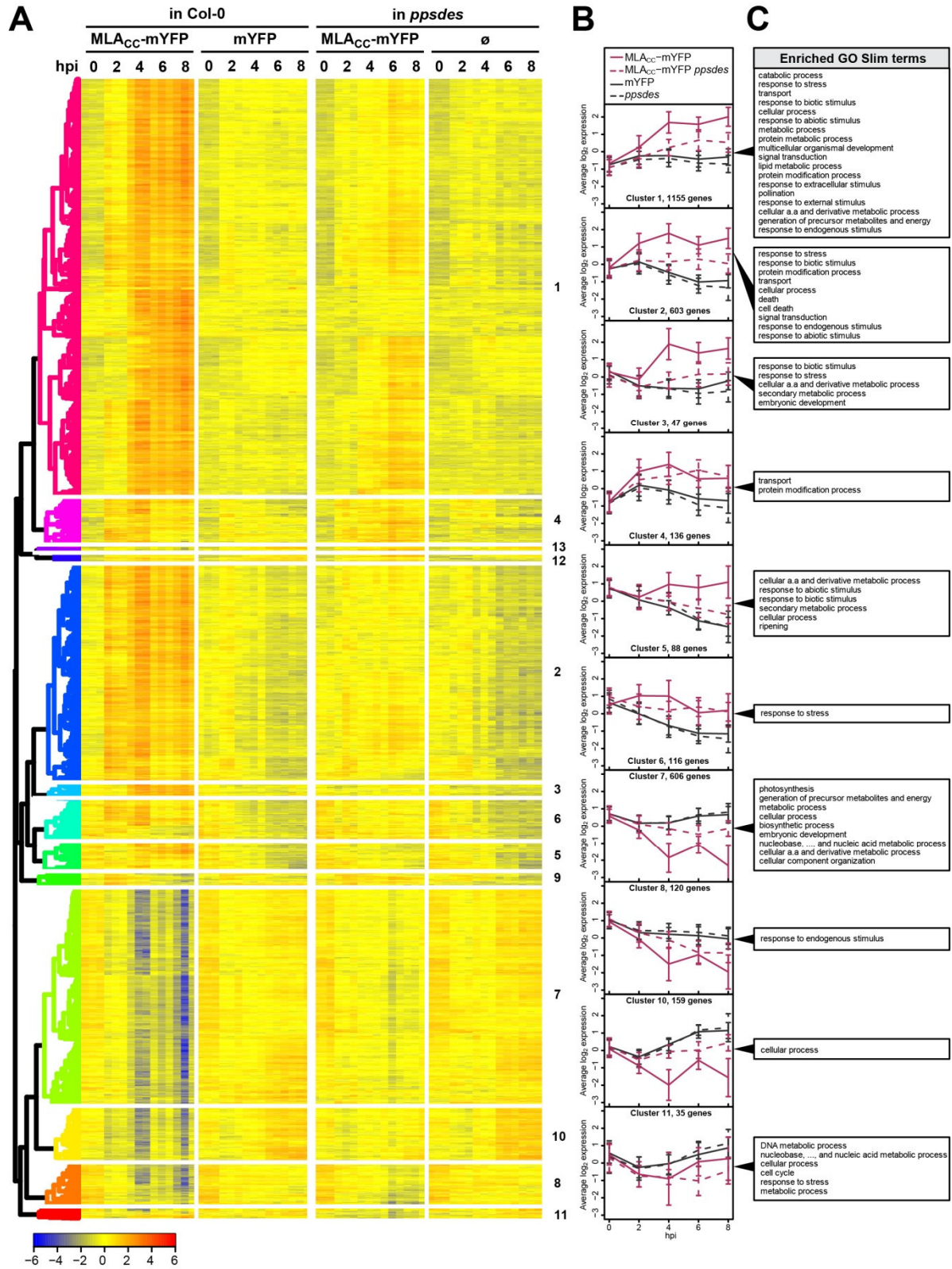


Figure S1-3: Cell death induction by MLA_{cc} and MLA_{MHD} in *A. thaliana*. Leaves of plants stably expressing the indicated construct under a DEX-inducible promoter were infiltrated with 1 μ M DEX. **A**, Ion leakage measurement after DEX infiltration. Average and standard deviation were calculated from at least four independent experiments containing at least three biological replicates each. The letters on the right indicate statistically different lines by one-way anova followed by posthoc TukeyHSD (adjusted p-value <0.01). The red arrow indicate the earliest time where a statistically significant difference can be found between the lines expressing a functional MLA_{cc} and their respective control (mYFP or ppsdes). **B**, Dead cells staining by trypan blue. The adaxial surface of trypan-stained leaves was imaged by bright field microscopy. Most of the stained cells are visible in the mesophyll layer. Scale bar: 500 μ m.



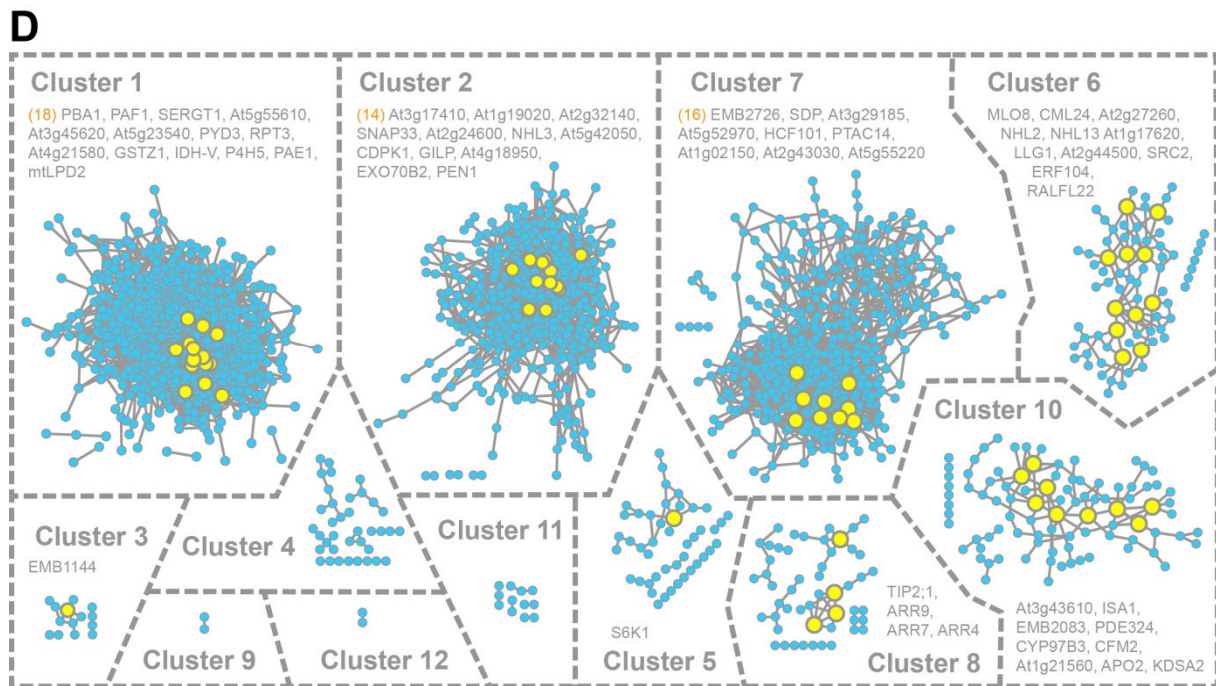


Figure S1-4: Analysis of the top 3,153 differentially expressed genes upon MLAcc expression in wild-type or *ppsdes* mutant background. **A**, Heatmap of the top 3153 (sorted by adjusted p-value) differentially regulated MLAcc-dependent genes. 13 gene clusters were defined by cutting the dendrogram at a given height and highlighted in different colors. **B**, Expression pattern of the gene clusters defined in A. The average and standard deviation were calculated from the genewise standardized log₂-transformed counts per million of all genes within each cluster. **C**, GO Slim term enrichment analysis (adjusted p-value <0.05). Only GO Slim terms for biological processes are indicated. Clusters 9, 12 and 13 contain less than 40 genes, are not enriched for any GO Slim term, and were therefore not represented here. **D**, Publicly available transcriptomic data were used to draw co-expression relationships between the genes within each cluster. Genes with a higher degree of co-expression potentially represent key regulatory hubs. Hub genes are highlighted in yellow and the corresponding gene names are indicated in grey. Unless otherwise indicated (orange numbers), the minimal number of connections used to define the hub genes was 5. No co-expressed genes were found within cluster 13. Hpi, hours post infiltration. The figures presented in A. and B. were generated by Dr. Barbara Kracher.

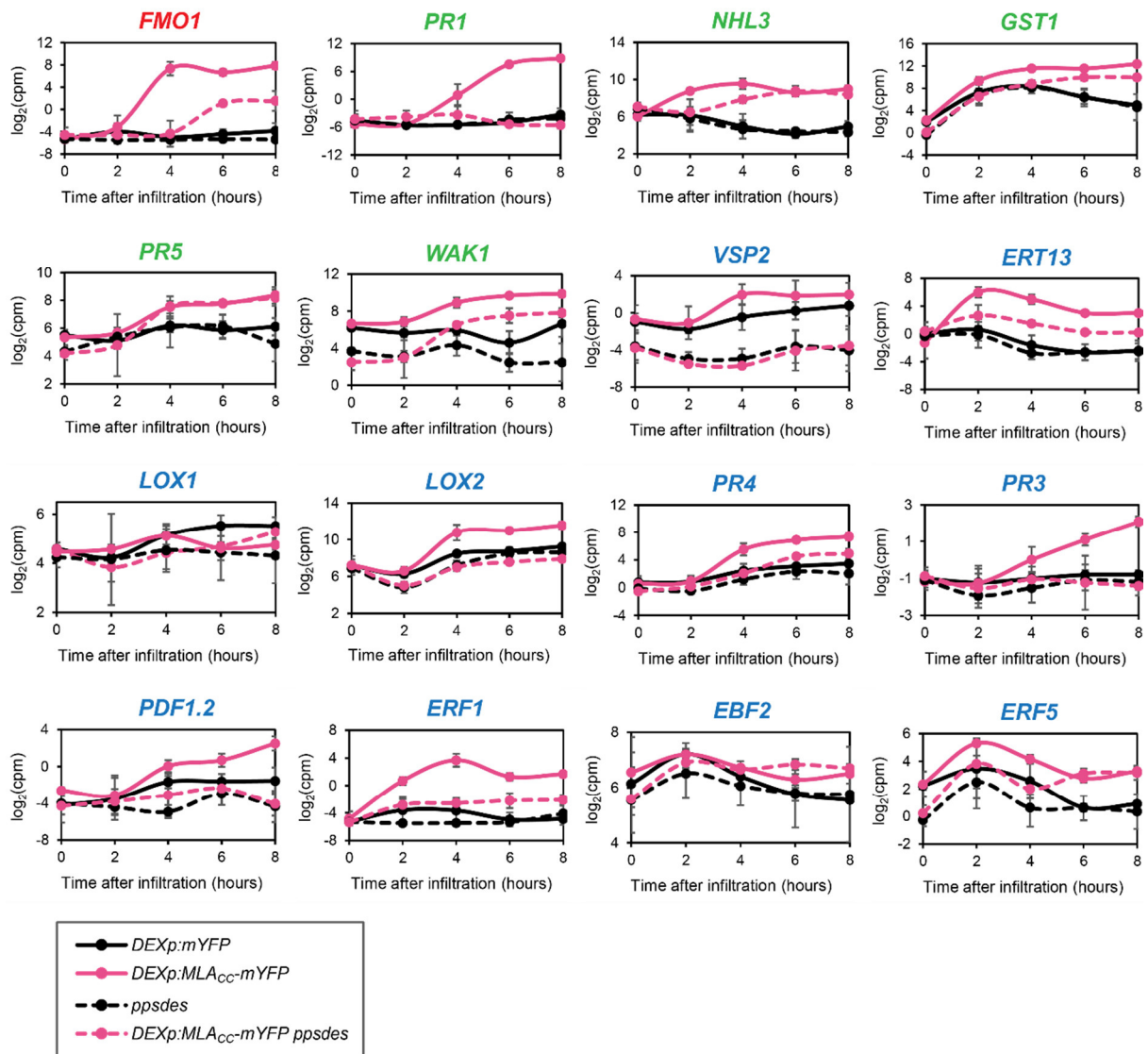


Figure S1-5: Expression profile of EDS1, SA and, ET/JA marker genes upon MLACC expression in wild-type and *ppsdes* mutant. Expression of marker genes for EDS1- (red), SA- (green), ET-/JA- (blue) mediated responses was monitored by RNA-seq over time upon MLACC expression in wild-type or in *ppsdes* mutant as compared to the *DEXp:mYFP* line or to the *ppsdes* mutant, respectively, after DEX infiltration. The selected EDS1 markers are considered to be SA-independent. The expression intensity is given in normalized \log_2 -transformed counts per million (cpm).



Figure S1-6: GO term enrichment analysis in genes differentially expressed upon MLAcc expression in wild type *A. thaliana* (Col-0) and *ppsdes* mutant background. Leaves of the indicated genotypes were infiltrated with 1 μ M DEX and analysed at different time points by RNA-seq. Go term enrichment analysis was performed on gene sets up- or downregulated. The heatmap figures the enrichment pattern of the terms enriched in at least one condition with FDR <10⁻⁶. hpi, hours post infiltration.

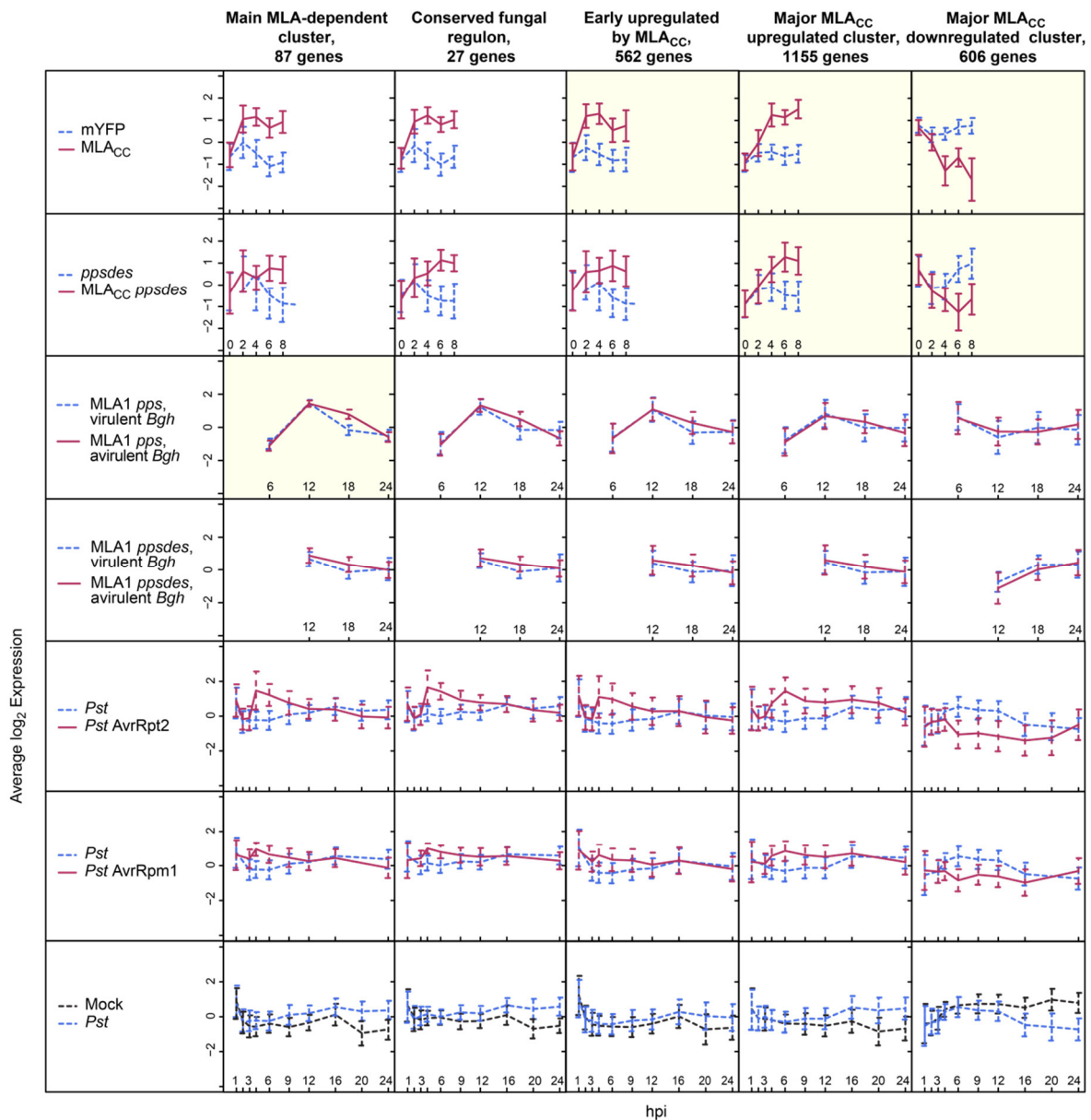


Figure S1-7: Expression profile of various gene clusters after inoculation with different pathogens and MLA_{CC} inducible expression. When represented, the dataset from which the gene cluster was originally identified is highlighted in yellow. The average and standard deviation were calculated from the genewise standardized log₂-transformed counts per million of all genes within each cluster. Hpi, hours after infiltration/inoculation. *Bgh*, *Blumeria graminis* f. sp. *hordei*. *Pst*, *Pseudomonas syringae* pv. *tomato*. This figure was generated by Dr. Barbara Kracher.

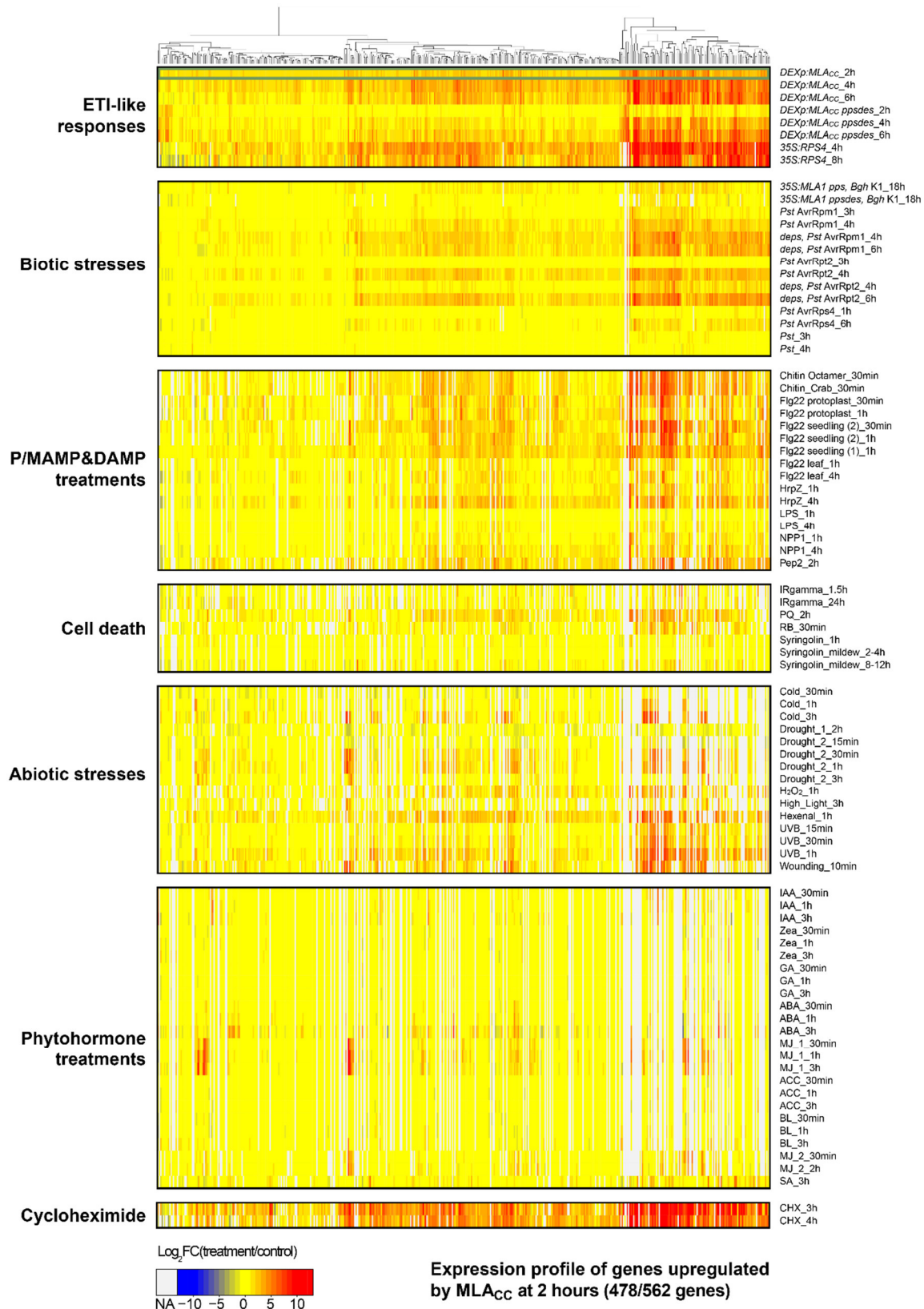


Figure S1-8: Extended expression profile of the genes rapidly induced upon MLA_{CC} expression in the early response to diverse biotic, abiotic, hormone and chemical treatments. The $\log_2FC(\text{treatment/control})$ for 478 genes out of 562 rapidly MLA_{CC}-induced genes was plotted on a heatmap. Hierarchical clustering was performed on the x-axis. NA, not available (expression not detected). A selected subset of the data is shown in Figure 1-10. For a description of the datasets used, see Table S1-1.

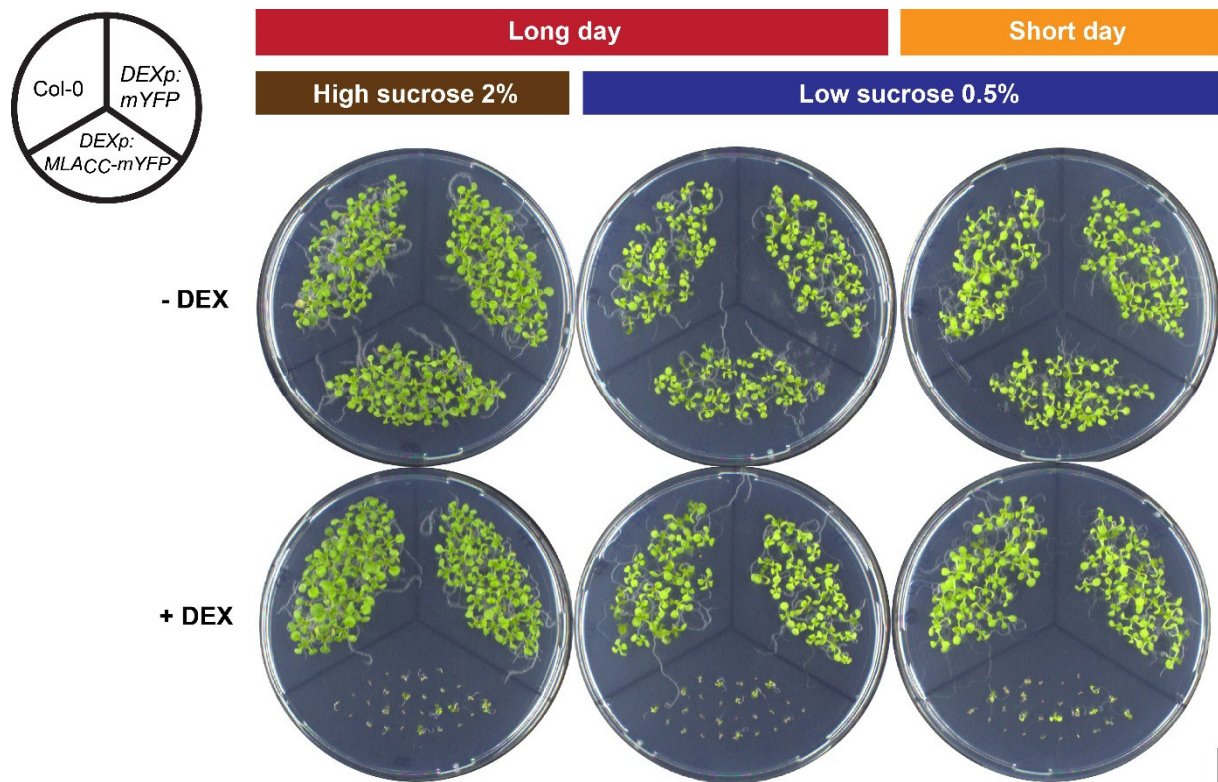


Figure S1-9: Effect of sucrose concentration and day length on the *MLACC*-mediated growth phenotype. *DEXp:MLACC-mYFP* plants were grown 14 days on MS medium supplemented with 0 or 30 μ M DEX and 0.5 or 2% sucrose under short day (8 h) or long day (16 h) conditions. Scale bar: 1 cm

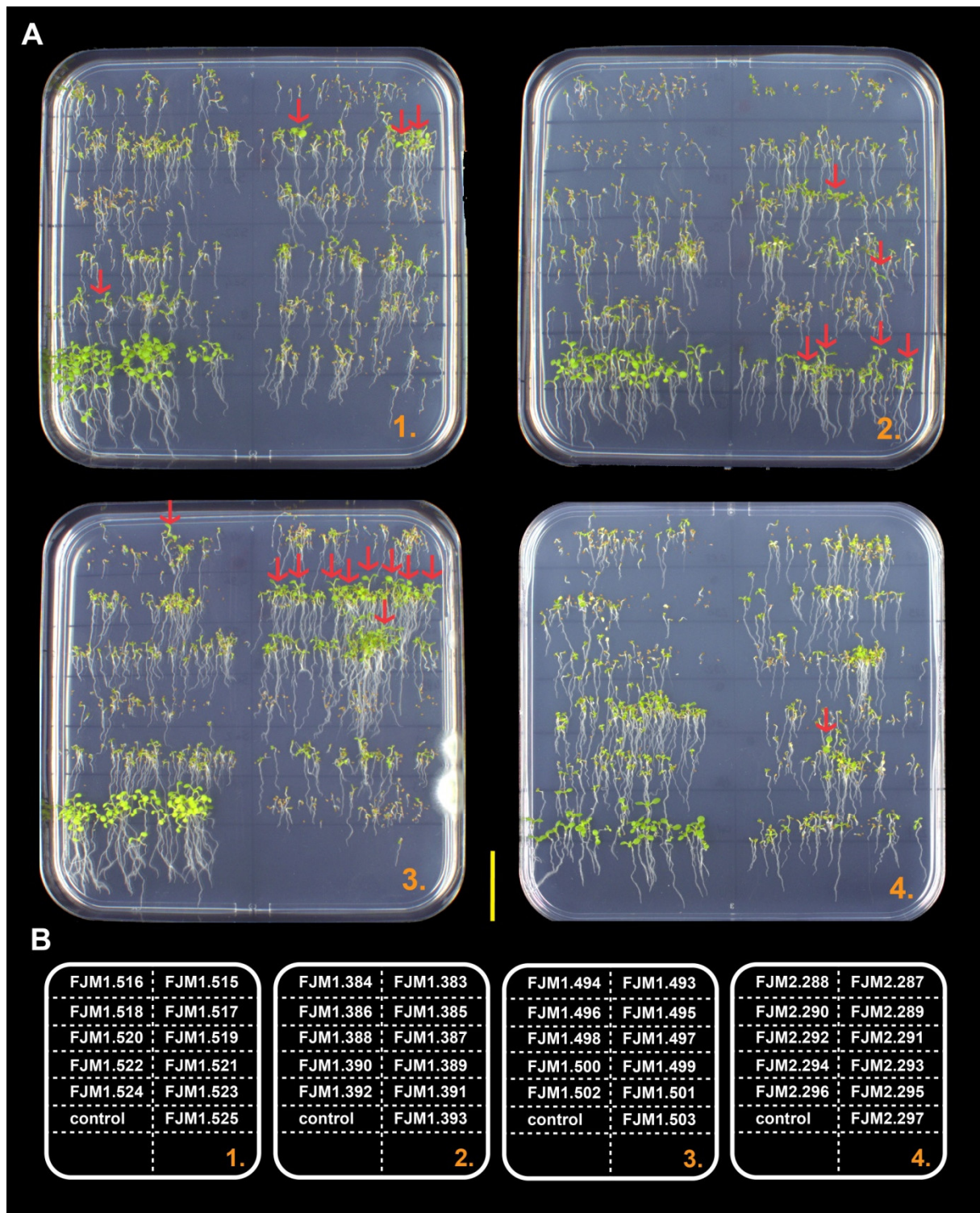


Figure S2-1: Pictures of four representative screening plates. A. Pictures of M₂ progeny grown on plates for 10 days. Red arrows, candidate suppressor mutants. Scale bar=2 cm. **B.** Sketch of the M₂ seed organisation on the plates. Controls are either Col-0 plants or *DEXp:mYFP* plants. About 50 seeds were sown for each line.

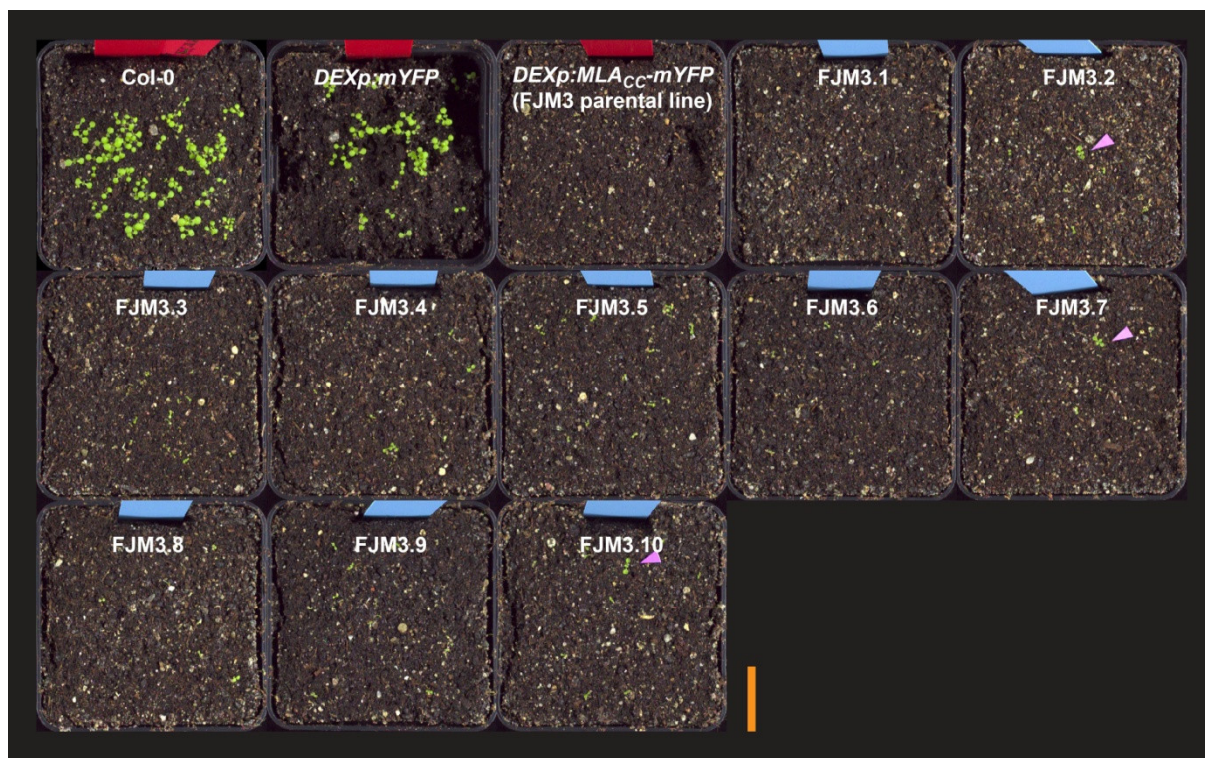


Figure S2-2: Pictures of the pilot screen conducted on soil. The seeds were stratified 3 days at 4°C in 0.01% agar + 30 μ M DEX, sown onto soil and sprayed at 5 dpg and 7 dpg with 30 μ M DEX + 0.01% Silwet L-77. The pictures were taken at 14 dpg. Pots with red labels are controls whereas pots with blue labels are independent seed progeny of FJM3. Pink arrowheads, candidate suppressor mutants. Scale bar=2 cm.

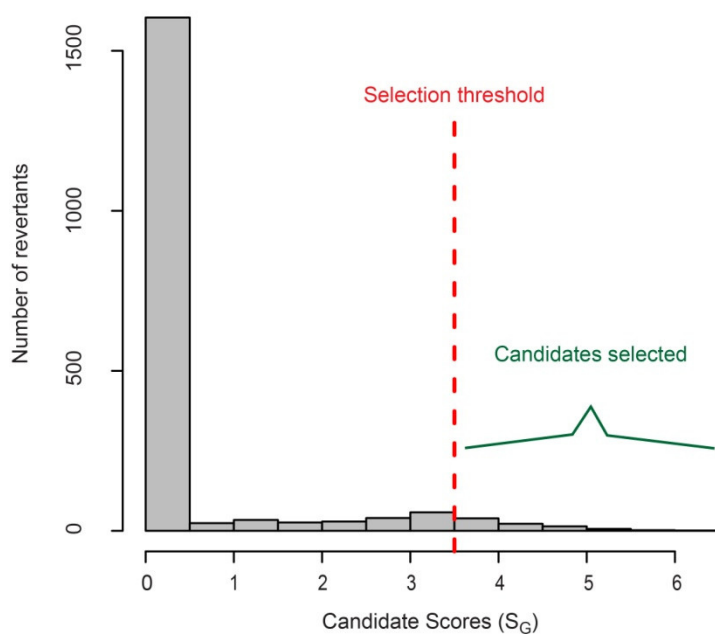


Figure S2-3: Distribution of the suppressor candidate scores. Candidate suppressor mutants with a score of at least 3.5 were selected for further characterization. The mutant population selected represents 6.9% of the suppressor mutants identified.

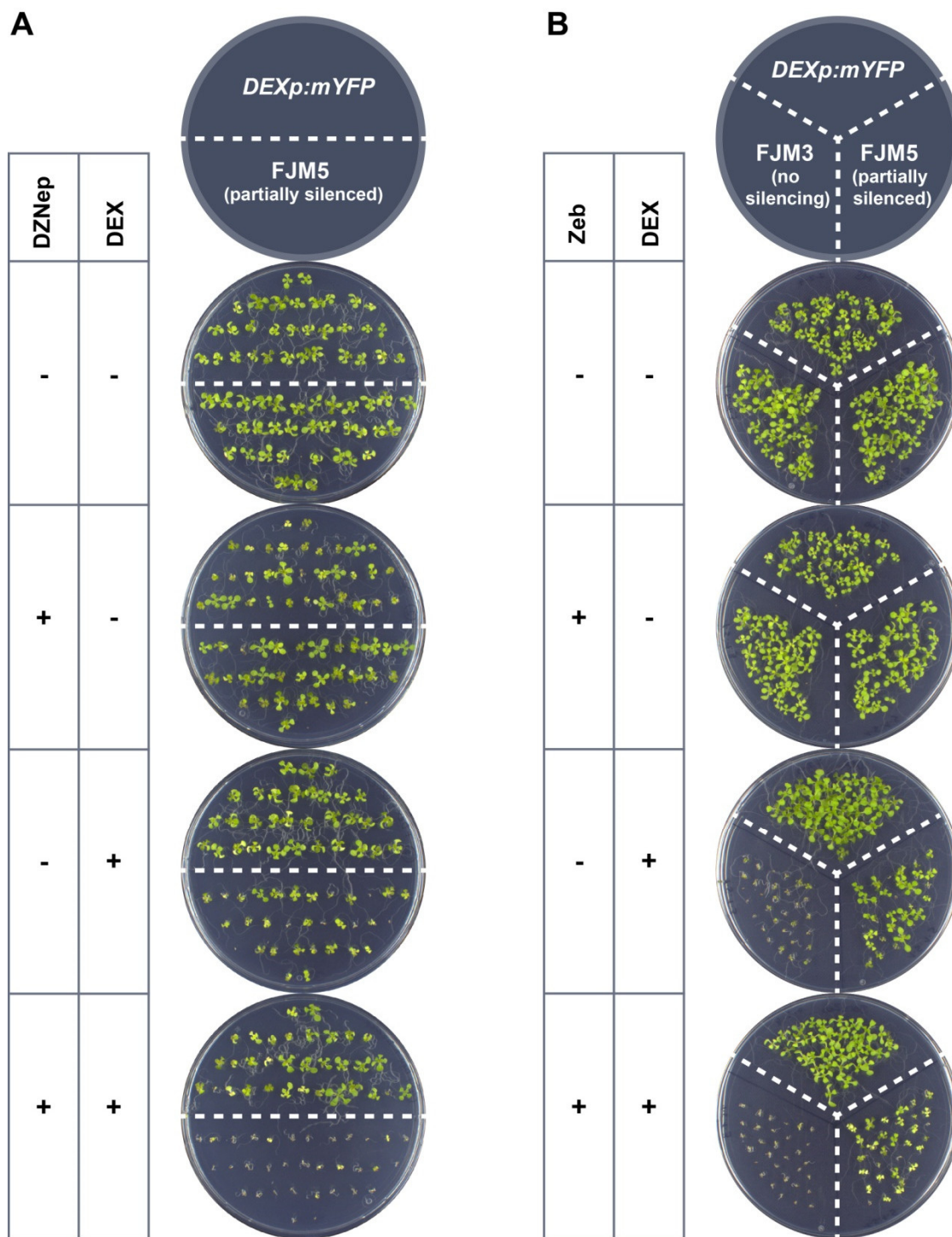


Figure S2-4: Effect of DZNep and Zeb on transgene silencing. Pictures of transgenic *A. thaliana* grown for 16 days on medium containing +/- 10 μ M DEX and +/- 2 μ M DZNep (A) or +/- 10 μ M Zeb (B). Scale bar=2 cm.

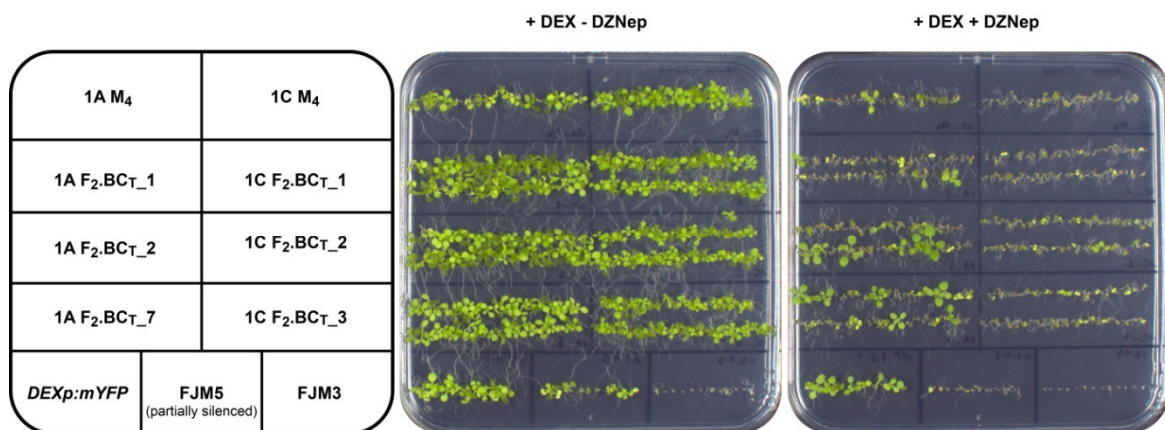


Figure S2-5: Segregation analysis of the F₂.BC_T progeny. Representative examples of F₂.BC_T progeny of candidate 1A and 1E grown for 16 days on agar plates with 10 μM DEX and +/- 2 μM DZNep.

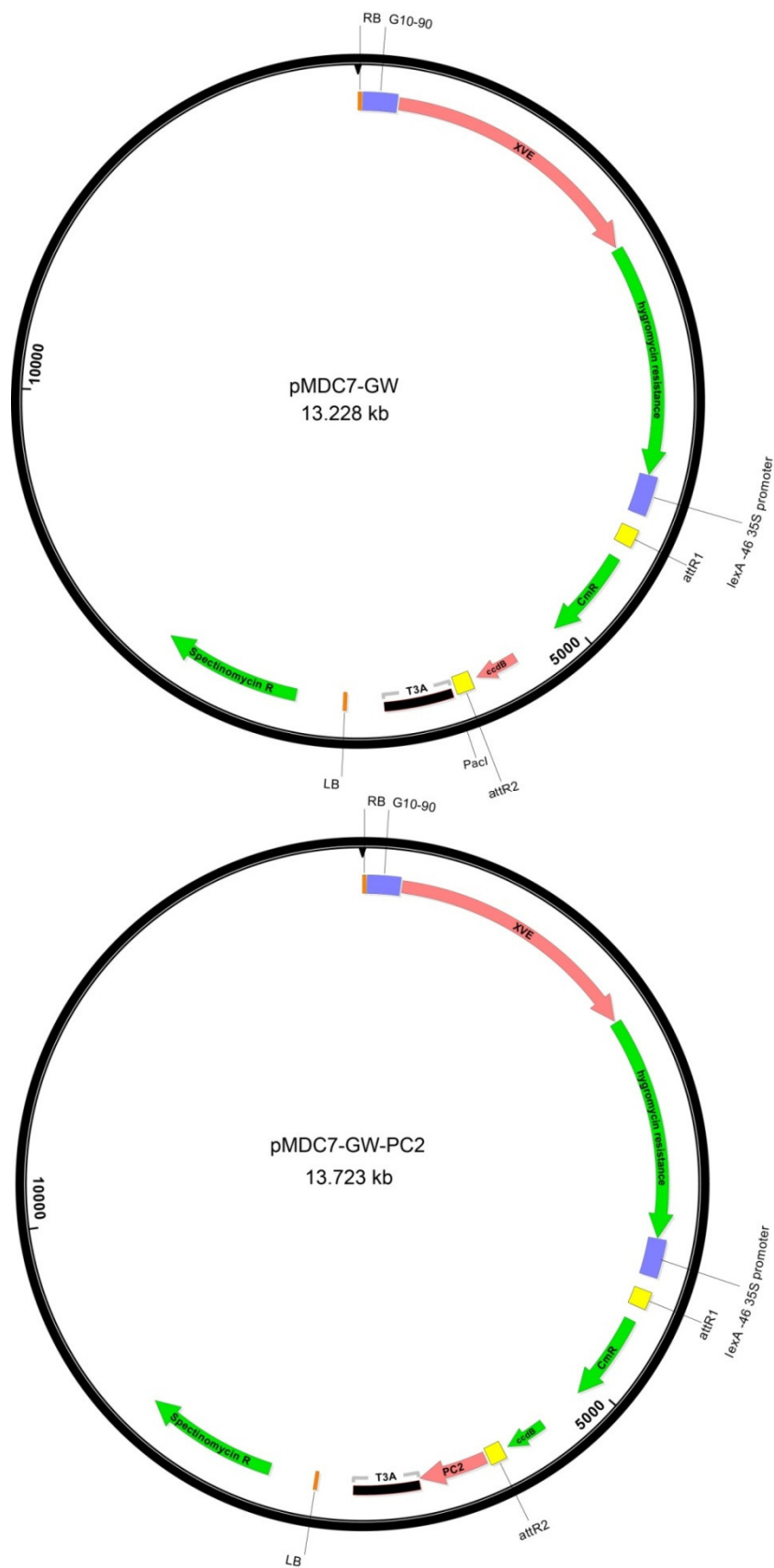


Figure S3-1: Plasmid maps of the estradiol inducible vectors used in this study. The pMDC7-GW vector was modified to introduce the PC2 TAP tag as a C-terminal fusion. This new vector was called pMDC7-GW-PC2.

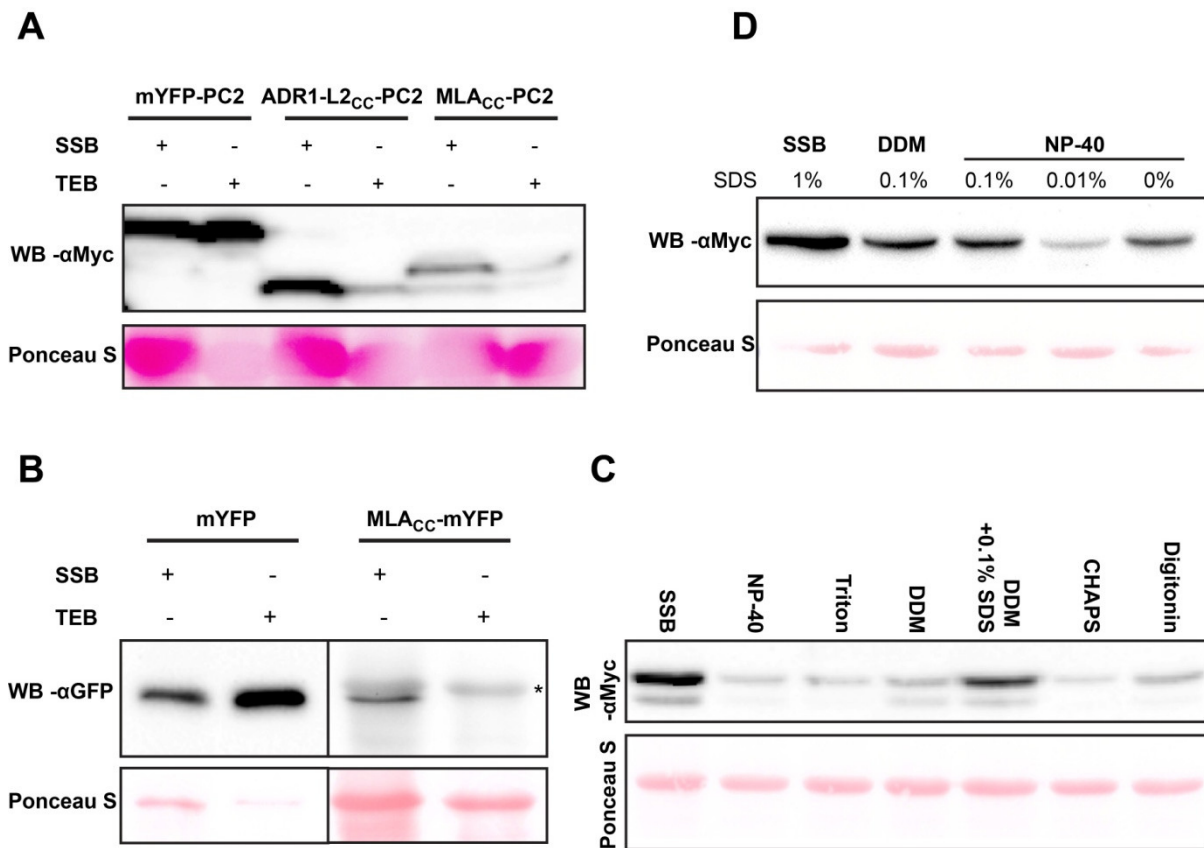
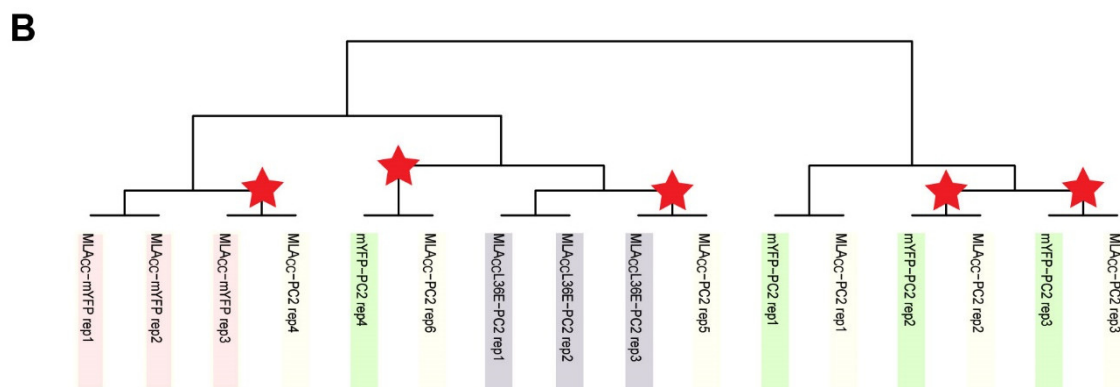
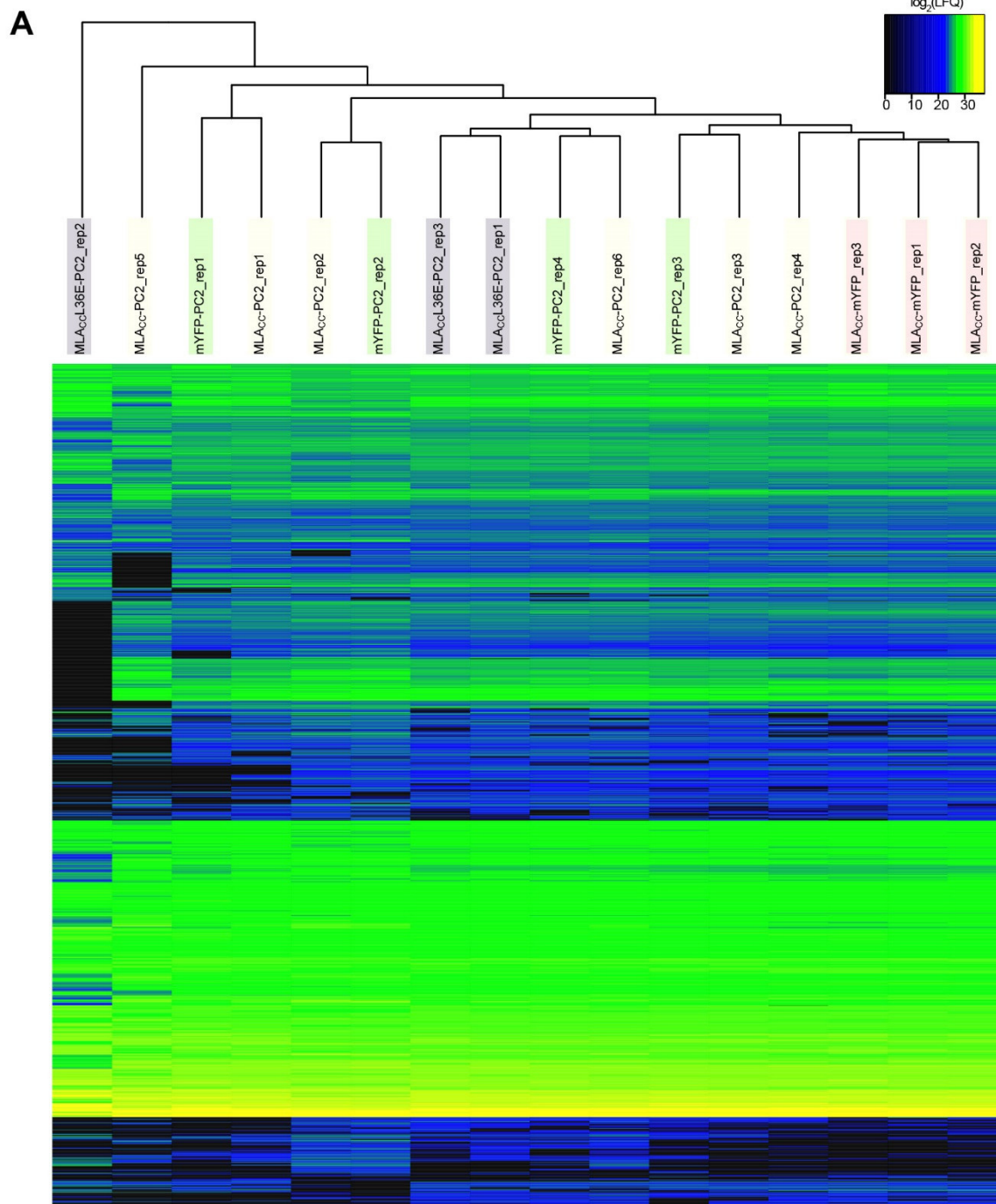


Figure S3-2: Optimization of the TAP extraction buffer composition. Leaf material from 3-4 week old plants was sampled 16 hours after induction by immersion into 10 μ M estradiol (ER) or 10 μ M dexamethasone (DEX) +0.001% Silwet L-77. Proteins were extracted with various buffers and the amount of bait protein monitored by immunoblotting (WB). **A**, comparison between the efficiency of the SDS sample buffer (SSB) and the standard TAP extraction buffer (TEB) in extracting the mYFP-PC2, the ADR1-L2_{CC}-PC2 or the MLA_{CC}-PC2 proteins. **B**, comparison between the efficiency of the SSB and the TEB in extracting the mYFP or the MLA_{CC}-mYFP. **C**, analysis of the MLA_{CC}-PC2 extraction efficiency by a modified TEB containing 1% of the indicated detergent as compared to the SSB. **D**, analysis of the MLA_{CC}-PC2 extraction efficiency using a modified TEB containing 0.1% of the indicated detergent and variable SDS concentration compared to the SSB. The asterisk indicates a non-specific signal.



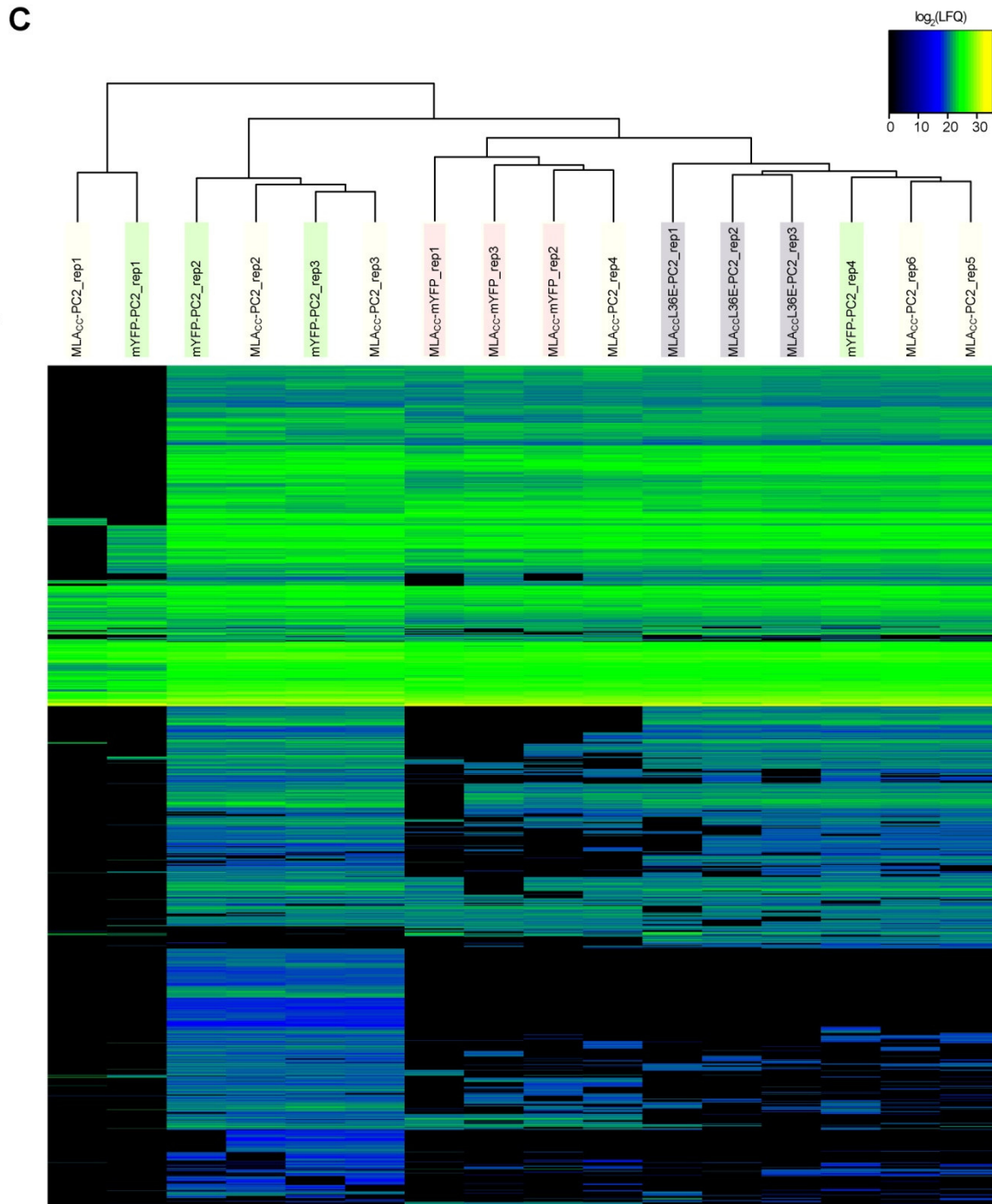


Figure S3-3: Clustering analysis of the TAP input and eluate samples. Heatmap representation of the abundance (LFQ intensities) of each protein group in the input fractions (A) or the eluate fractions (C). X-axis, TAP samples; y-axis, protein groups. Clustering was performed on both axes based on the \log_2 (LFQ intensity) distances. NaN values were replaced by 0. B, Sample clustering according to the time of preparation. All samples were processed in a pairwise manner. The pairs used for the final analysis are marked with a red star.

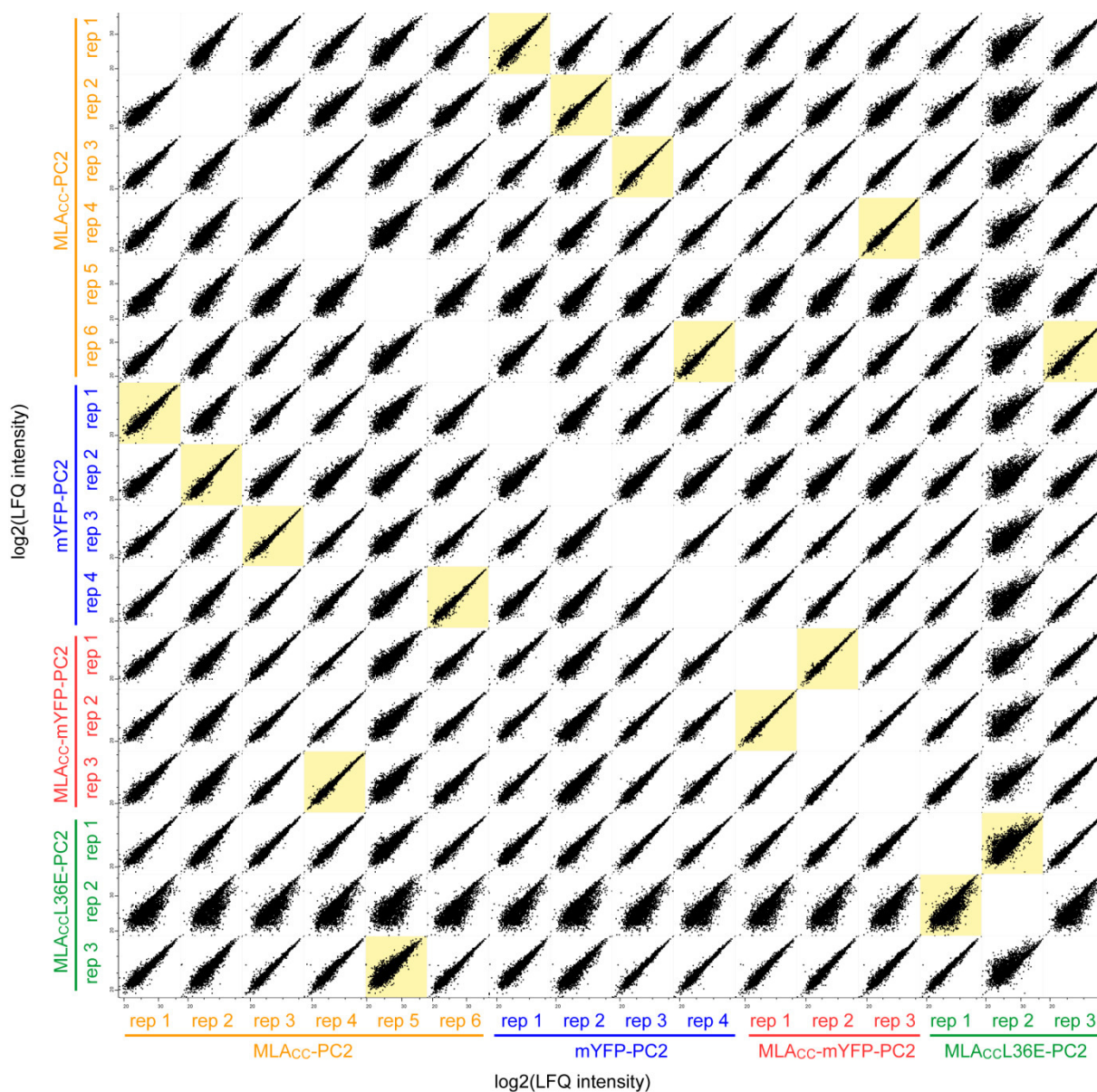


Figure S3-4: Multi scatterplot showing the correlation in protein group abundance (LFQ intensities) between all samples of the TAP input fractions. Log₂(LFQ) intensities of each protein group are plotted for all the input samples against each other. Pairs of samples processed together are highlighted in yellow.

2. Supplementary tables

Table S1-1: Description of the transcriptomic datasets used for comparative transcriptomic analysis together with the MLAcc-related transcriptomic profiling. The collected datasets are related to early responses to NLR-mediated response, biotic/abiotic stresses, hormone/chemical treatments, and cell death response.

Name	Treatment Type	Source	Database	Accession	Data type	Comparison	Description
Drought_1	Abiotic stress	PA	GEO	GSE56583	ATH1 microarray	Treated vs 0 h	Shoots of 3-week old plants exposed to air stream
H ₂ O ₂	Abiotic stress	PA	GEO	GSE56530	ATH1 microarray	Treated vs mock	Seedlings treated with H ₂ O ₂
Highlight	Abiotic stress	PA	GEO	GSE7743	ATH1 microarray	Treated vs mock	Seedlings exposed to high light intensity
Wounding	Abiotic stress	PA	GEO	GSE48676	ATH1 microarray	Treated vs mock	Wounding on 5-week old leaves
Cold	Abiotic stress	PA	TAIR	ME00325	ATH1 microarray	Treated vs mock	Shoots of 2.5-week old plants exposed to cold
Drought_2	Abiotic stress	PA	TAIR	ME00338	ATH1 microarray	Treated vs mock	Shoots of 2.5-week old plants exposed for 15 min to air stream.
UVB	Abiotic stress	PA	TAIR	ME00329	ATH1 microarray	Treated vs mock	Shoots of 2.5-week old plants exposed to UV-B
IRgamma	Cell death inducer	PA	GEO	GSE61484	ATH1 microarray	Treated vs mock	Seedlings treated with gamma irradiation
Syringolin_mildew	Cell death inducer	PA	ArrayExpress	E-MEXP-739	ATH1 microarray	Treated vs mock	Shoots of 2-week old plants inoculated with powdery mildew treated with syringolin
PQ	Cell death inducer	PA	ArrayExpress	E-ATMX-28	ATH1 microarray	Treated vs mock	Shoots of 2-week old plants treated with paraquat
RB	Cell death inducer	PA	GEO	GSE43551	ATH1 microarray	Treated vs mock	Cell culture treated with rose bengal
DEXp/MLA _{cc}	MLAcc expression	This study			RNA-seq	MLAcc vs MYFP line	Leaves of 4-week old plants infiltrated with dexanethasone
DEXp/MLA _{cc} ppsdes	MLAcc expression	This study			RNA-seq	MLAcc ppsdes vs ppsdes line	Leaves of 4-week old plants infiltrated with dexanethasone
Pst AvrRq2	Biologic stress	This study*			RNA-seq	Avirulent strain vs virulent strain	Leaves of 4-week old plants, inoculated with Pst DC3000 AvrRq2
Pst AvrRpm1	Biologic stress	This study*			RNA-seq	Avirulent strain vs virulent strain	Leaves of 4-week old plants, inoculated with Pst DC3000 AvrRpm1
Pst	Biologic stress	This study*			RNA-seq	Virulent strain vs mock	Leaves of 4-week old plants, inoculated with Pst DC3000
deps_ Pst AvrRq2	Biologic stress	This study*			RNA-seq	Avirulent strain vs virulent strain	Leaves of 4-week old deps plants, inoculated with Pst DC3000 AvrRq2
deps_ Pst AvrRpm1	Biologic stress	This study*			RNA-seq	Avirulent strain vs virulent strain	Leaves of 4-week old deps plants, inoculated with Pst DC3000 AvrRpm1
35S/MLA1 pps, Bgh K1	Biologic stress	PA	GEO	GSE39463	RNA-seq	Avirulent strain vs virulent strain	Leaves of 4-week old MLA1 pps plants inoculated with Bgh K1 (AvrMLA1)
35S/MLA1 ppsdes, Bgh K1	Biologic stress	This study#			RNA-seq	Avirulent strain vs virulent strain	Leaves of 4-week old plants inoculated with Pst AvrRPS4
Pst AvrRps4	Biologic stress	PA	NCBI SRA	SRP010938	RNA-seq	Avirulent strain vs virulent strain	Leaves of 3.5-week old plants grown at 28°C, shifted to 19°C
35S/RPS4	Biologic stress	This study†			RNA-seq	35S/RPS4 vs WT	Leaves of 3.5-week old plants treated with abscisic acid
ABA	Hormone	PA	GEO	GSE39384	ATH1 microarray	Treated vs mock	Seedlings treated with auxin
IAA	Hormone	PA	GEO	GSE39384	ATH1 microarray	Treated vs mock	Seedlings treated with zeatin (cytokinin)
Zea	Hormone	PA	GEO	GSE39384	ATH1 microarray	Treated vs mock	Seedlings treated with gibberellic acid
GA	Hormone	PA	GEO	GSE39384	ATH1 microarray	Treated vs mock	Seedlings treated with methyl jasmonate
ML_1	Hormone	PA	GEO	GSE39384	ATH1 microarray	Treated vs mock	Seedlings treated with brassinolide
ACC	Hormone	PA	GEO	GSE39384	ATH1 microarray	Treated vs mock	Seedlings treated with the ethylene precursor ACC
BL	Hormone	PA	GEO	GSE39384	ATH1 microarray	Treated vs mock	Seedlings treated with salicylic acid
SA	Hormone	PA	GEO	GSE39385	ATH1 microarray	Treated vs mock	Cell culture treated with methyl jasmonate
ML_2	Hormone	PA	ArrayExpress	E-ATMX-13	ATH1 microarray	Treated vs mock	Leaves of 3-week old plants treated with hexenol
Hexenol	Hormone	PA	GEO	GSE3957	ATH1 microarray	Treated vs mock	Seedlings treated with Pepr2
Pepr2	DAMP	PA	GEO	GSE40354	ATH1 microarray	WT vs pepr1 pepr2	Seedlings treated with crab shell chitin
Chitin_Crab	PAMP	PA	GEO	GSE2538	ATH1 microarray	Treated vs mock	Seedlings treated with chitin octamer
Chitin_Octamer	PAMP	PA	GEO	GSE2538	ATH1 microarray	Treated vs mock	Leaves of 5-week old plants treated with Fig22
Fig22 leaf	PAMP	PA	GEO	GSE615	ATH1 microarray	Treated vs mock	Leaves of 5-week old plants treated with HnZ
HnZ	PAMP	PA	GEO	GSE615	ATH1 microarray	Treated vs mock	Leaves of 5-week old plants treated with LPS
LPS	PAMP	PA	GEO	GSE615	ATH1 microarray	Treated vs mock	Leaves of 5-week old plants treated with NPP1
NPP1	PAMP	PA	GEO	GSE615	ATH1 microarray	Treated vs mock	Mesophyll protoplasts treated with Fig22
Fig22 protoplasts	PAMP	PA	GEO	GSE16472	ATH1 microarray	Treated vs 0 h	Seedlings treated with Fig22
Fig22 seedlings (2)	PAMP	PA	GEO	GSE17382	ATH1 microarray	Treated vs mock	Seedlings treated with Fig22
Fig22 seedlings (1)	PAMP	This study*			RNA-seq	Treated vs mock	Seedlings treated with cycloheximide
CHX_3h	Cycloheximide	PA	GEO	GSE39385	ATH1 microarray	Treated vs mock	Seedlings treated with cycloheximide
CHX_4h	Cycloheximide	PA	GEO	GSE911	ATH1 microarray	Treated vs mock	Seedlings treated with cycloheximide

* data obtained from Tsuda et al. (unpublished)
 # data obtained from Maekawa et al. (unpublished)
 † data obtained from Baudume et al. (unpublished)

Table S2-1: List of loci selected for the targeted analysis of the 21 M₂ candidate mutants sequenced

Gene ID	Category	Gene Name	Gene ID	Category	Gene Name	Gene ID	Category	Gene Name
AT5G52640	Required for R-gene function	HSP90.1	AT4G37260	TF	MYB73	AT1G69090	TNL	
AT5G56030	Required for R-gene function	HSP90.2	AT4G38900	TF	bZIP29	AT1G69550	TNL	
AT5G56010	Required for R-gene function	HSP90.3	AT4G38970	TF		AT1G72840	TNL	
AT5G56000	Required for R-gene function	HSP90.4	AT5G03680	TF	PTL	AT1G72850	TNL	
AT5G51700	Required for R-gene function	RAR1	AT5G05550	TF		AT1G72860	TNL	
AT4G23570	Required for R-gene function	SGT1A	AT5G07680	TF	ANAC079	AT1G72870	TNL	
AT4G11260	Required for R-gene function	SGT1B	AT5G10280	TF	MYB92	AT1G72890	TNL	
AT1G15100	Required for R-gene function	SD2	AT5G18270	TF	ANAC087	AT1G72960	TNL	
AT3G20600	Required for R-gene function	NDR1	AT5G22290	TF	ANAC089	AT1G72910	TNL	
AT3G07040	Required for R-gene function	RPM1	AT5G26950	TF	AGL3	AT1G72920	TNL	
AT2G13810	Required for R-gene function	ALD1	AT5G27130	TF	AGL39	AT1G72930	TNL	TN10
AT1G19250	Required for R-gene function	FMO1	AT5G38800	TF	bZIP43	AT1G72940	TNL	
AT1G64280	Required for R-gene function	NPR1	AT5G42520	TF	BPC8	AT1G72950	TNL	
AT5G45110	Required for R-gene function	NPR3	AT5G44190	TF	GLK2	AT2G03300	TNL	
AT4G19660	Required for R-gene function	NPR4	AT5G46760	TF	bHLH005	AT2G03300	TNL	
AT1G33560	Required for R-gene function	ADR1	AT5G47660	TF		AT2G14080	TNL	
AT4G33300	Required for R-gene function	ADR1-L1	AT5G49330	TF	MYB111	AT2G16870	TNL	
AT5G04720	Required for R-gene function	ADR1-L2	AT5G53950	TF	CUC2	AT2G17050	TNL	
AT3G40900	Required for R-gene function	EDS1	AT5G54980	TF	bHLH105	AT2G17055	TNL	
AT3G48080	Required for R-gene function	EDS1 paralogs	AT5G64750	TF	ABR1	AT2G17860	TNL	
AT3G52430	Required for R-gene function	PAD4	AT5G67300	TF	MYB44	AT2G20142	TNL	
AT5G14930	Required for R-gene function	SAG101	AT5G41030	TF	TCP6	AT2G32140	TNL	
AT4G16890	Required for R-gene function	SNC1	AT5G23280	TF	TCP7	AT3G04210	TNL	
AT1G02170	Required for R-gene function	MC1	AT1G58100	TF	TCP8	AT3G04220	TNL	
AT1G02180	Required for R-gene function	MC2	AT4G24560	TF	TCP9	AT3G05510	TNL	
AT5G64240	Required for R-gene function	MC3	AT2G37000	TF	TCP11	AT3G44400	TNL	
AT1G79340	Required for R-gene function	MC4	AT3G47620	TF	TCP14	AT3G44480	TNL	RPP1
AT1G78330	Required for R-gene function	MC5	AT1G69690	TF	TCP15	AT3G44630	TNL	
AT1G79320	Required for R-gene function	MC6	AT3G45150	TF	TCP16	AT3G44670	TNL	
AT1G78100	Required for R-gene function	MC7	AT5G51910	TF	TCP19	AT3G51560	TNL	
AT1G19420	Required for R-gene function	MC8	AT1G22110	TF	TCP20	AT3G51570	TNL	
AT5G04200	Required for R-gene function	MC9	AT5G08330	TF	TCP21	AT4G04110	TNL	
AT1G32540	Required for R-gene function	LCL1	AT1G72010	TF	TCP22	AT4G08450	TNL	
AT3G13682	Required for R-gene function	LCL2	AT1G35560	TF	TCP23	AT4G09420	TNL	
AT4G16310	Required for R-gene function	LSD1	AT1G67260	TF	TCP1	AT4G09430	TNL	
AT4G23080	Required for R-gene function	LSD1	AT4G19360	TF	TCP7	AT4G11170	TNL	RMG1
AT4G21610	Required for R-gene function	LCL2	AT1G52320	TF	TCP2	AT4G11340	TNL	
AT4G15410	Required for R-gene function	DND1	AT3G15030	TF	TCP4	AT4G12010	TNL	
AT5G54250	Required for R-gene function	DND2	AT5G66970	TF	TCP5	AT4G12020	TNL	WRKY19
AT4G37460	Required for R-gene function	SFR1	AT1G68800	TF	TCP12	AT4G14370	TNL	
AT4G36480	Required for R-gene function	TPR1	AT3G02150	TF	TCP13	AT4G18860	TNL	RPP4
AT1G69170	Required for R-gene function	SFR6	AT2G31070	TF	TCP9	AT4G18960	TNL	SNC1
AT5G46350	Required for R-gene function	WRKY8	AT5G08070	TF	TCP17	AT4G18900	TNL	
AT4G31800	Required for R-gene function	WRKY18	AT3G18550	TF	TCP18	AT4G18920	TNL	
AT1G60840	Required for R-gene function	WRKY40	AT1G30210	TF	TCP24	AT4G18930	TNL	
AT4G18170	Required for R-gene function	WRKY28	AT1G19020	CNL	LOV1	AT4G18940	TNL	
AT5G09220	Required for R-gene function	WRKY48	AT1G12210	CNL	RFL1	AT4G18950	TNL	RPP5
AT5G04870	Required for R-gene function	CPK1	AT1G12230	CNL	RPS5	AT4G18960	TNL	
AT3G10660	Required for R-gene function	CPK2	AT1G12280	CNL	SUM2	AT4G18990	TNL	RLM3
AT4G09570	Required for R-gene function	CPK4	AT1G12290	CNL		AT4G19500	TNL	
AT4G35310	Required for R-gene function	CPK5	AT1G15890	CNL		AT4G19500	TNL	
AT2G17290	Required for R-gene function	CPK6	AT1G33560	CNL	ADR1	AT4G19510	TNL	
AT1G32690	Required for R-gene function	CPK11	AT1G56160	CNL		AT4G19520	TNL	
AT5G23060	Required for R-gene function	CAS	AT1G51480	CNL	RSG1	AT4G19530	TNL	
AT4G31300	Required for R-gene function	PBA1	AT1G52660	CNL		AT4G19910	TNL	
AT3G43300	Required for R-gene function	MIN7	AT1G53350	CNL		AT4G19920	TNL	
AT1G32970	Required for R-gene function	SBT3.2	AT1G58390	CNL		AT4G19925	TNL	
AT1G32960	Required for R-gene function	SBT3.1	AT1G58400	CNL		AT4G23510	TNL	
AT1G32950	Required for R-gene function	SBT3.4	AT1G58410	CNL		AT4G23515	TNL	
AT1G32940	Required for R-gene function	SBT3.5	AT1G58602	CNL		AT4G23515	TNL	
AT2G39940	Required for R-gene function	COI1	AT1G58807	CNL		AT4G36140	TNL	
AT1G06040	TF	STO	AT1G59124	CNL		AT4G36140	TNL	
AT1G06070	TF	bZIP99	AT1G59218	CNL		AT4G36150	TNL	
AT1G06050	TF	bZIP52	AT1G59620	CNL	CW9	AT5G01250	TNL	
AT1G11510	TF		AT1G59780	CNL		AT5G17680	TNL	
AT1G14920	TF	RGAA2, GAI	AT1G61180	CNL		AT5G17880	TNL	CSA1
AT1G25440	TF	COL16	AT1G61190	CNL	RPP39	AT5G17890	TNL	DAR4
AT1G28300	TF	LEC2	AT1G61300	CNL		AT5G17970	TNL	
AT1G28520	TF	VOZ1	AT1G61310	CNL		AT5G18350	TNL	
AT1G28210	TF	TCP24	AT1G61330	CNL		AT5G18360	TNL	
AT1G31320	TF	LBD4	AT1G61350	CNL		AT5G18370	TNL	
AT1G32640	TF	MYC2	AT1G63360	CNL		AT5G22690	TNL	
AT1G43700	TF	VIP1	AT3G07040	CNL	RPM1	AT5G36930	TNL	
AT1G46408	TF	AGL97	AT3G14460	CNL		AT5G38340	TNL	
AT1G47670	TF	E2FC	AT3G14470	CNL		AT5G38344	TNL	
AT1G48150	TF		AT3G15700	CNL		AT5G38850	TNL	
AT1G49130	TF	COL8	AT3G46530	CNL	RPP13	AT5G38850	TNL	
AT1G51070	TF	bHLH115	AT3G46710	CNL		AT5G40090	TNL	CHL1
AT1G51140	TF	bHLH122	AT3G46730	CNL		AT5G40100	TNL	
AT1G53230	TF	TCP3	AT3G59950	CNL	ZAR1	AT5G40910	TNL	
AT1G53910	TF	RAP2.12	AT4G19780	CNL		AT5G41540	TNL	
AT1G68520	TF	COL6	AT4G14610	CNL		AT5G41550	TNL	
AT1G73870	TF	COL7	AT4G19060	CNL		AT5G41740	TNL	
AT1G74660	TF	MIF1	AT4G26090	CNL	RPS2	AT5G41750	TNL	
AT1G76870	TF		AT4G27190	CNL		AT5G44510	TNL	TAO1
AT2G01570	TF	RGAI	AT4G27220	CNL		AT5G44870	TNL	LAZ5
AT2G03470	TF		AT4G33300	CNL	ADR1-L1	AT5G44900	TNL	
AT2G18550	TF	HB21	AT5G04720	CNL	ADR1-L2	AT5G44910	TNL	
AT2G20570	TF	GLK1	AT5G05400	CNL		AT5G44920	TNL	TIK
AT2G21230	TF	bZIP30	AT5G35450	CNL		AT5G45000	TNL	
AT2G24300	TF	HB6	AT5G43470	CNL	RPP8	AT5G45000	TNL	WRKY16
AT2G22770	TF	NM1	AT5G43780	CNL	RSG2	AT5G45050	TNL	
AT2G23290	TF	MYB70	AT5G45740	CNL		AT5G45060	TNL	PP2-A8
AT2G24430	TF	ANAC039	AT5G45440	CNL		AT5G45070	TNL	PP2-A6
AT2G25650	TF		AT5G45490	CNL		AT5G45080	TNL	PP2-A7
AT2G26150	TF	HSFA2	AT5G47250	CNL		AT5G45090	TNL	
AT2G31980	TF	STH	AT5G47260	CNL		AT5G45200	TNL	
AT2G36340	TF		AT5G48020	CNL		AT5G45210	TNL	
AT2G40340	TF		AT5G49300	CNL		AT5G45220	TNL	
AT2G40470	TF	LBD15	AT5G66630	CNL	DAR5	AT5G45220	TNL	
AT2G40620	TF	bZIP18	AT5G66900	CNL		AT5G45230	TNL	
AT2G42280	TF	bHLH130	AT5G66910	CNL		AT5G45240	TNL	
AT2G42400	TF	VOZ2	AT1G09665	TNL		AT5G45250	TNL	RPS4
AT2G47460	TF	MYB12	AT1G11760	TNL		AT5G45260	TNL	RRS1
AT3G01470	TF	HB-1	AT1G17610	TNL	CHS1	AT5G46260	TNL	
AT3G03450	TF	RGL2	AT1G17615	TNL		AT5G46270	TNL	
AT3G11100	TF		AT1G27170	TNL		AT5G46450	TNL	
AT3G14230	TF	RAP2.2	AT1G27180	TNL		AT5G46470	TNL	RPS6
AT3G15170	TF	CUC1	AT1G31540	TNL		AT5G46490	TNL	
AT3G16770	TF	RAP2.03	AT1G47370	TNL		AT5G46510	TNL	VICTL
AT3G19860	TF	bHLH121	AT1G51270	TNL		AT5G46520	TNL	VICTR
AT3G22830	TF	AT-HSFA6B	AT1G52900	TNL		AT5G48770	TNL	
AT3G23210	TF	bHLH034	AT1G56510	TNL	ADR2	AT5G48780	TNL	
AT3G26780	TF	FUS3	AT1G56520	TNL		AT5G48780	TNL	
AT3G57800	TF	bHLH060	AT1G56540	TNL		AT5G49140	TNL	
AT3G58630	TF		AT1G57630	TNL		AT5G49140	TNL	
AT3G61630	TF	CRF6	AT1G57670	TNL		AT5G51630	TNL	
AT3G62610	TF	MYB11	AT1G57830	TNL		AT5G58120	TNL	
AT4G00290	TF		AT1G57850	TNL				
AT4G00270	TF		AT1G66020	TNL				
AT4G00390	TF		AT1G66105	TNL				
AT4G09180	TF	bHLH081	AT1G63730	TNL				
AT4G11660	TF	HSFB2B	AT1G63740	TNL				
AT4G14410	TF	bHLH104	AT1G63750	TNL				
AT4G19450	TF		AT1G63860	TNL				
AT4G27950	TF	CRF4	AT1G63870	TNL				
AT4G28530	TF	ANAC074	AT1G63880	TNL				
AT4G34680	TF		AT1G64070	TNL	RLM1			
AT4G36740	TF	HB-5	AT1G65390	TNL	PP2-A5			
			AT1G65850	TNL				

Table S2-3: Mutations identified in the candidate mapping intervals for the candidate mutants 1A, 2B and 2HHOM=homozygous, HZ=heterozygous, SSC=splice site change

Candidate	Gene	Allele frequency	Type	WT codon	Mutant codon	Genotype	M ₂	Gene Description
1A	ATTG68980	0.63	Nonsyr	V	M	HOM	HZ	MURF-1, PDE3B, APC3. Encodes AMLUE, a homology of the bacterial MURF
	ATTG68880	0.67	Nonsyr	S	N	HOM	HZ	Protein kinase superfamily protein
	ATTG67210	0.69	5' UTR	D	N	HOM	HZ	Proline-rich splicing-associated (PSP) family protein / zinc knuckle (CCHC-type) family protein
	ATTG68150	0.69	Nonsyr	D	N	HOM	HZ	WRKY9. Member of WRKY Transcription Factor: Group II-b
	ATTG68325	0.79	Nonsyr	D	N	HOM	HZ	Remoin family protein
	ATTG72310	0.69	Nonsyr	S	L	HOM	HZ	scpl4. Serine carboxypeptidase-like 4
	ATTG74380	0.67	Nonsyr	R	Q	HOM	HZ	XXT3. Xyloglucan xylosyltransferase 4
	ATTG80310	0.59	Nonsyr	G	R	HOM	HZ	MO2. Encodes a molibdate transporter which localizes to the vacuolar membrane
	ATTG80680	0.58	Nonsyr	A	T	HOM	HZ	SAF3. NUP96, PRE. HOS3. Required for the activation of downstream defense pathways by the snct1 mutation.
	AT5G33290	0.66	Nonsyr	Q	*	HOM	HOM	XGD1. Acts as a xyloglucuronan xylosyltransferase within the XGA biosynthesis pathway.
	AT5G40210	0.54	Nonsyr	G	R	HOM	HOM	Nodulin MIN2-like transporter family protein
	AT5G53410	0.64	Nonsyr	R	W	HOM	HOM	Unknown protein
	ATTG33430	0.61	Nonsyr	G	D	HOM	HOM	Leucine-rich repeat transmembrane protein kinase
	ATTG53700	0.65	Nonsyr	D	N	HOM	HOM	WAG1, PK3AT, Prclen-serine/threonine kinase
	ATTG55500	0.63	5' UTR	M	I	HOM	HOM	ECT4. Evolutionarily conserved C-terminal region 4.
	ATTG69057	0.75	Nonsyr	M	I	HOM	HOM	Unknown protein
	ATTG68220	0.59	SSC	G	D	HOM	HOM	Calcium-dependent lipid-binding (CaLB domain) family protein
	ATTG64300	0.73	Nonsyr	G	D	HOM	HOM	Protein kinase family protein
	ATTG85580	0.71	Nonsyr	T	I	HOM	HOM	FRQ3. Functions in inositol or phosphatidylinositol phosphatase activity.
	ATTG67760	0.73	5' UTR	S	F	HOM	HOM	TCP-1/cpnb0 chaperonin family protein
ATTG68060	0.69	Nonsyr	S	F	HOM	HOM	MAP70-1. Encodes a microtubule associated protein.	
ATTG71980	0.68	Nonsyr	L	F	HOM	HZ	Phobase-associated (PA) RINGU-box zinc finger family protein	
ATTG73670	0.7	Nonsyr	A	V	HOM	HZ	MPK15. Member of MAP Kinase	
AT3G03560	0.67	Nonsyr	R	K	HOM	HOM	unknown protein	
AT3G04980	0.66	Nonsyr	W	*	HOM	HOM	DNAJ1 heat shock N-terminal domain-containing protein	
AT3G05155	0.66	Nonsyr	P	L	HOM	HOM	Major facilitator superfamily protein	
AT3G07060	0.65	Nonsyr	A	V	HOM	HOM	Emh1974. Embryo defective 1974	
AT3G10040	0.65	5' UTR	A	V	HOM	HOM	sequence-specific DNA binding transcription factors	
AT3G11420	0.72	Nonsyr	E	K	HOM	HZ	Protein of unknown function (DUF604)	
AT3G12955	0.4	5' UTR	E	K	HOM	HZ?	SAUR-like auxin-responsive protein family	
AT3G13440	0.69	5' UTR	R	*	HOM	HZ	S-adenosyl-L-methionine-dependent methyltransferases superfamily protein	
AT3G14225	0.64	Nonsyr	R	Q	HOM	HZ	GLP4. Contains lipase signature motif and GDSL domain.	
AT5G02820	0.58	Nonsyr	R	Q	HOM	HZ	RHL2. BINS	
AT5G07740	0.63	Nonsyr	P	S	HOM	HOM	Actin binding	
AT5G15740	0.57	Nonsyr	A	V	HOM	HOM	O-fucosyltransferase family protein	
AT5G19980	0.55	Nonsyr	G	S	HOM	HOM	RP76a. 26S proteasome AAA-A1ase subunit	
AT5G20410	0.58	Nonsyr	A	T	HOM	HOM	MGD2. Encodes a type B monogalactosyl/diacylglycerol (MGDG) synthase.	
AT5G20450	0.57	5' UTR	P	L	HOM	HOM	Unknown protein	
AT5G21160	0.59	Nonsyr	R	C	HOM	HOM	LA RNA-binding protein	
AT5G22350	0.57	Nonsyr	R	C	HOM	HOM	ELM1. ELONGATED MITOCHONDRIA 1	
AT5G22940	0.58	Nonsyr	E	K	HOM	HOM	F8H. Homolog of FRAB (AT3G28110), a member of a member of glycosyltransferase family 47	
AT5G22960	0.57	Nonsyr	E	T	HOM	HOM	TUB8. Beta-tubulin	
2B	ATTG32080	0.65	Nonsyr	E	K	HOM	HOM	ARF791. Unknown function
	ATTG52410	0.64	SSC	D	N	HOM	HOM	TS41. TSK-ASSOCIATING PROTEIN 1. Contains a novel calcium-binding repeat sequence.
	ATTG53300	0.59	Nonsyr	D	N	HOM	HOM	TT1. TETRATRICOPETIDE-REPEAT THIOREDOXIN-LIKE 1.
	ATTG58980	0.54	Nonsyr	G	D	HOM	HOM	GLP3.GDSL-MOTIF. LIPASE 3. Contains lipase signature motif and GDSL domain.
	ATTG58410	0.56	Nonsyr	G	R	HOM	HOM	ER02. EARLY-RESPONSIVE TO DEHYDRATION 2. HSP70T-1.
	ATTG68380	0.58	Nonsyr	Q	*	HOM	HOM	NAC (No Apical Memsten) domain transcriptional regulator superfamily protein
	ATTG68170	0.6	Nonsyr	R	Q	HOM	HOM	Zinc finger, C2H2 type (RING finger) family protein
	ATTG66740	0.66	Nonsyr	R	K	HOM	HZ	SGA2. ASH1A, SP7.
	ATTG67920	0.65	5' UTR	R	H	HOM	HZ	unknown protein
	ATTG68510	0.6	Nonsyr	R	H	HOM	HZ	LBQ42. LOB domain-containing protein
	ATTG68570	0.65	Nonsyr	S	F	HOM	HZ	Doi-type zinc finger DNA-binding family protein
	ATTG71370	0.63	Nonsyr	Q	*	HOM	HZ	DEA(DH)-box RNA helicase family protein
	ATTG71891	0.66	5' UTR	Q	*	HOM	HZ	GDSL-like Lipase/cylyndriolase superfamily protein
	ATTG74380	0.51	Nonsyr	W	*	HOM	HZ	GDSL-like Lipase/cylyndriolase superfamily protein
	ATTG74380	0.62	Nonsyr	S	F	HOM	HZ	Leucine-rich repeat protein kinase family protein
	ATTG78970	0.63	Nonsyr	S	F	HOM	HZ	Taget of Myb protein 1
	ATTG77330	0.63	Nonsyr	P	S	HOM	HZ	similar to 1-aminocyclopropane-1-carboxylate oxidase GI-3385655 from (Sorghum bicolor)
	AT3G02840	0.68	Nonsyr	V	I	HOM	HOM	AR1 repeat superfamily protein
	AT3G03130	0.6	Nonsyr	Q	*	HOM	HOM	unknown protein
	AT3G06410	0.6	Nonsyr	T	I	HOM	HOM	Zinc finger C-26-C-36-C-3-H type family protein
AT3G06450	0.68	Nonsyr	A	V	HOM	HOM	HCO3- transporter family	
AT3G07660	0.6	Nonsyr	A	V	HOM	HOM	Kinase-related protein of unknown function (DUF-1296)	
AT3G12955	0.5	5' UTR	P	S	HOM	HZ?	SAUR-like auxin-responsive protein family	

Table S3-1: Top 16 differentially expressed protein groups (DEPGs) in lines expressing ML_{ACC}-PC2 compared to lines expressing mYFP-PC2.

Protein IDs	Name	Pep.	log ₂ (LFQ ML _{ACC} /mYFP)	-log ₁₀ (t-test p-value)	Brief description
AT1G33960	AIG1	3	7.88	1.23	AVRRPT2-INDUCED GENE 1, P-loop containing nucleoside triphosphate hydrolase
AT3G60420		5	7.34	1.21	Phosphoglycerate mutase family protein
AT2G26400	ARD3	5	7.19	1.36	acireductone dioxygenase 3
ATCG00790; AT2G28830	RPL16; PUB12	2	7.01	1.15	ribosomal protein L16; PLANT U-BOX 12
AT5G49570	PNG1	1	6.70	1.30	peptide-N-glycanase 1
AT2G04540		1	6.15	1.15	Beta-ketoacyl synthase
AT5G05460; AT3G11040	ENGase85A; ENGase85B	2	6.11	1.19	Endo-beta-N-acetylglucosaminidase 85A; Endo-beta-N-acetylglucosaminidase 85B
AT3G12915		15	6.04	0.78	Ribosomal protein S5/Elongation factor G/III/V
AT4G36800	RCE1	1	5.90	1.18	RUB1 conjugating enzyme 1
AT5G65910		3	5.71	0.71	BSD domain-containing protein
AT2G43950	OEP37	3	5.25	1.19	Chloroplast outer envelope protein 37
AT2G25210; AT4G31985		1	5.19	1.00	Ribosomal protein L39 family protein; Ribosomal protein L39 family protein
AT3G05520	CPA	5	-1.73	1.31	Subunits of heterodimeric actin filament capping protein Capz superfamily
AT1G10200	WLIM1	6	-6.47	1.23	GATA type zinc finger transcription factor
AT3G01850		1	-6.47	1.28	Aldolase-type TIM barrel family protein
AT2G16700	ADF5	1	-7.98	1.24	Actin depolymerizing factor 5

The DEPGs were selected based on their relative enrichment (average fold change to control) and the *p*-value thereof (volcano plot, Figure 3-6). The values given for the ML_{ACC}/mYFP ratios are log₂-transformed protein intensities (LFQ). NaN values were replaced by 14. Pep, number of peptides identified.

Table S3-2: Comparison of proteomic and transcriptomic data. Examples of genes/proteins following similar regulation in both proteomic and transcriptomic dataset upon chemically-inducible ML_{ACC} expression. FC, fold change relative to the negative control at the same time point.

ID	Name	Description	Proteomic data	Transcriptomic data (log ₂ FC)				
			log ₂ FC	average	2 hpi	4 hpi	6 hpi	8 hpi
AT1G33960	AIG1	AvrRPT2-INDUCED GENE 1	7.88	7.845	1.90	10.62	9.77	9.09
AT3G60420		Phosphoglycerate mutase family protein	7.34	5.1	3.26	5.91	6.09	5.14
AT2G26400	ARD3	acireductone dioxygenase 3	7.19	8.455	-0.29	9.14	12.95	12.02
AT1G32940	SBT3.5	Subtilase family protein	5.02	3.7625	0.09	4.84	4.84	5.28
AT5G22300	NIT4	nitrilase 4	4.97	2.9775	-0.68	3.85	3.73	5.01
AT5G06320	NHL3	NDR1/HIN1-like 3	4.62	3.94	2.65	4.59	4.48	4.04
AT3G01830		Calcium-binding EF-hand family protein	4.52	6.8875	4.27	6.55	8.14	8.59
AT2G24850	TAT3	tyrosine aminotransferase 3	4.51	9.19	6.21	7.90	11.22	11.43
AT1G30700		FAD-binding Berberine family protein	4.31	3.6575	2.37	3.21	2.85	6.20
AT1G61820	BGLU46	beta glucosidase 46	4.15	4.0875	1.78	6.70	2.94	4.93
AT1G59950		NAD(P)-linked oxidoreductase protein	3.92	6.505	3.97	7.85	6.25	7.95
AT3G21230	4CL5	4-coumarate:CoA ligase 5	3.30	5.575	2.87	7.30	5.10	7.03
AT2G29350	SAG13	senescence-associated gene 13	3.09	7.3275	1.69	7.04	10.32	10.26
AT1G14700	PAP3	purple acid phosphatase 3	-2.83	-2.8025	-0.50	-4.32	-1.91	-4.48
AT2G22980	SCPL13	serine carboxypeptidase-like 13	-3.15	-2.875	-1.04	-4.50	-1.85	-4.11

Table S3-3: Protein abundance of the 9 MLA_{CC} candidate interactors. Only the replicates included in the quantitative analysis are indicated. The abundance is indicated as a log₂-transformed label free quantification (LFQ) intensity.

ID	Log ₂ (LFQ intensity) in pull downs									
	MLA _{CC} -PC2					mYFP-PC2			MLA _{CC} -mYFP	MLA _{CC} L36E-PC2
	rep2	rep3	rep4	rep5	rep6	rep2	rep3	rep4	rep3	rep3
AT1G79600	18.75	18.53	n.d	19.24	19.35	n.d	n.d	n.d	n.d	n.d
AT5G54640	20.90	21.09	20.83	20.33	20.49	21.43	20.55	n.d	n.d	n.d
AT5G11420	20.03	20.70	20.09	20.06	20.00	20.27	20.96	n.d	n.d	n.d
AT5G45190	19.76	20.35	20.21	19.21	18.83	20.57	20.25	n.d	n.d	n.d
AT2G22400	18.51	18.61	18.59	19.41	18.98	18.57	19.36	n.d	n.d	n.d
AT5G51750	18.52	22.26	23.56	19.68	19.75	n.d	22.21	19.45	20.76	17.85
AT2G26560	23.90	23.73	22.60	23.77	22.92	21.76	21.57	22.02	22.18	22.98
AT3G48090	22.66	22.18	n.d	20.51	20.74	21.21	21.04	20.16	n.d	18.18
AT2G19800	23.22	23.82	23.62	22.81	22.49	21.93	23.65	21.71	21.16	22.19

n.d, not detected

Table S3-4: Co-expression degree between the candidates. The co-expression analysis was performed by EdgeAnnotation (atted.jp). Only the ten pairs with highest MR (mutual ranking) values are displayed. MR values lower than 1,000 are indicated in black bold.

Locus1	Name locus1	Locus2	Name locus2	MR values					
				all	tissue	abiotic	biotic	hormone	light
At2g26560	PLP2	At3g48090	EDS1	661	899	3235	485	1220	13599
At5g45190	Cyclin	At5g54640	RAT5 subtilase	1644	339	21243	910	7708	5538
At2g22400		At5g51750	1.3	1677	1439	991	4562	4481	5720
At5g11420		At1g79600		2423	1960	8693	6584	12984	22204
At3g48090	EDS1	At5g11420		2564	966	11126	19251	8360	6337
At2g26560	PLP2	At1g79600		3379	1762	7904	18569	9207	4843
At2g22400		At5g11420		5843	11833	6312	3654	2039	12436
At5g11420	DUF642	At5g51750	subtilase 1.3	6272	10100	5546	421	4112	18044
At2g19800	MIOX2	At5g54640	RAT5	6985	7830	9599	3437	345	1103
At2g19800	MIOX2	At2g26560	PLP2	7123	13987	6204	4720	6516	11847

Table S3-5: Ortholog search for the nine MLA_{CC} candidate interactors in Phytozome v10.3. The analysis is based on 36 high quality plant genomes representing all major plant taxa.

ID	Number of orthologs/paralogs in viridiplantae	Number of orthologs/paralogs in grasses	Highest a.a sequence similarity with <i>Brachypodium distachyon</i> orthologs/paralogs
AT1G79600	649	56	70.5%
AT5G54640	696	118	83.1%
AT5G11420	350	84	75.4%
AT5G45190	318	54	41.5%
AT2G22400	81	14	68.3%
AT5G51750	1177	9	73.8%
AT2G26560	415	66	75.2%
AT3G48090	227	15	50.6%
AT2G19800	135	7	80.8%

n.d, not detected.

Erklärung

Ich versichere, dass ich die von mir vorgelegte Dissertation selbständig angefertigt, die benutzten Quellen und Hilfsmittel vollständig angegeben und die Stellen der Arbeit –einschließlich Tabellen, Karten und Abbildungen –, die anderen Werken im Wortlaut oder dem Sinn nach entnommen sind, in jedem Einzelfall als Entlehnung kenntlich gemacht habe; dass diese Dissertation abgesehen von der Universität Evry Val d'Essonne/Universität Paris-Saclay noch keiner anderen Fakultät oder Universität zur Prüfung vorgelegen hat; dass sie –abgesehen von unten angegebenen Teilpublikationen –noch nicht veröffentlicht worden ist, sowie, dass ich eine solche Veröffentlichung vor Abschluss des Promotionsverfahrens nicht vornehmen werde.

Die Bestimmungen der Promotionsordnung sind mir bekannt. Die von mir vorgelegte Dissertation ist von Pr. Dr. Paul Schulze-Lefert und Pr. Dr. Heribert Hirt betreut worden.

Köln, 29/02/2016

Publikationen

Jacob, F., Vernaldi, S., and Maekawa, T. (2013). Evolution and Conservation of Plant NLR Functions. *Front. Immunol.* 4, 297.

Curriculum vitae

Adresse: 30 rue Jean Giono, 84120 Pertuis, Frankreich
Tel: +49 (0)151 238 349 28
Email: floh.jacob@gmail.com

Geburtsdatum: 16.01.1989
Nationalität: Französisch

Akademische Ausbildung

- 2011-** **PhD Projekt im Rahmen einer „Cotutelle“** an der Universität zu Köln, Deutschland (Max Planck Institut für Pflanzenzüchtungsforschung) und an der Université d'Evry Val D'Essonne, Frankreich (URGV/IPS2)
Thema: Cell death and transcriptional signalling mediated by the coiled-coil domain of the barley resistance protein MLA
- 2008-2011** **Studium in der Ecole Normale Supérieure de Lyon** (Frankreich).
2011: Master in Biowissenschaften
2010-2011: drei 15-wöchige Forschungspraktika in Japan und Deutschland (Laboratory of plant gene expression, RISH, Kyoto; Group Recognition and Signalling in Plant Innate Immunity, MPIPZ, Köln). Forschungsprojekten mit Schwerpunkt molekulare Biologie und interdisziplinären Ansätzen (Biochemie, Genetik, Physiologie, Zellbiologie).
2009: Bachelor in Biologie
2009: Ein 9-wöchiges Forschungspraktikum in Frankreich (Laboratory of Plant Developmental Biology, CEA Cadarache).
- 2006-2008** **Studium, das auf der Aufnahme in französischen Eliteschulen vorbereitet:** „Classes Préparatoires Science BCPST“ (Lycée Fermat, Toulouse, Frankreich)

Schulische Ausbildung

- 2006** **Französische Abitur mit Schwerpunkt Mathematik und Naturwissenschaften** (Lycée Val de Durance, Pertuis, Frankreich).
- 2003-2006** **Lycée Val de Durance, Pertuis, Frankreich**

Köln, den 29.02.2016,

Titre : Régulation transcriptionnelle et induction de la mort cellulaire par le domaine coiled-coil de MLA, protéine de résistance de l'orge

Mots clés : biologie végétale, phytopathologie, système immunitaire, protéine de résistance, signalisation immunitaire, réponse hypersensible

Résumé : La réponse immunitaire des plantes contre les pathogènes végétaux dépend entièrement du système immunitaire inné. La perception extracellulaire de motifs moléculaires conservés associés aux pathogènes/microbes (P/MAMP) par des récepteurs de reconnaissance de motifs moléculaires (PRR) induit un type de réponse immunitaire dénommé PTI (PAMP-triggered immunity). Certains pathogènes interceptent cette réponse en injectant, dans les cellules hôtes, des protéines appelées effecteurs. Ces effecteurs, souvent polymorphiques, peuvent être détectés par des récepteurs immunitaires intracellulaires de la famille des NLR (nucleotide-binding domain leucine-rich repeat containing). En cas de détection, les NLRs induisent une réponse immunitaire rapide, appelée ETI (effector-triggered immunity), souvent associée à la mort des cellules hôtes. Un des NLRs présents chez l'orge, MLA, confère une ETI protectrice contre *Blumeria graminis* f sp *hordei*, l'agent pathogène du mildiou. Bien que MLA n'ait d'homologues qu'au sein de la famille monocotylédone des Triticeae, MLA est fonctionnel dans une lignée transgénique chez l'espèce dicotylédone *A. thaliana*. Ceci indique que le mécanisme de résistance sous-jacent a été conservé depuis plus de 150 Ma chez les plantes dicotylédones et monocotylédones. Chez la plante dicotylédone *Nicotiana benthamiana*, l'expression transitoire du domaine coiled-coil (MLA_{CC}) qui correspond aux 160 premiers acides aminés au N-terminus de MLA, suffit à induire la mort cellulaire. Cette observation suggère que MLA pourrait initier un mécanisme de signalisation conservé, via son domaine MLA_{CC}. Le but de cette thèse a été de décrire le(s) mécanisme(s) de signalisation en aval de MLA_{CC} dans des lignées transgéniques d'*A. thaliana*. L'expression conditionnelle de MLA_{CC} induit une réponse similaire à la réponse immunitaire, et caractérisée par l'initiation d'une reprogrammation transcriptionnelle massive à ~2 h post-induction (hpi) suivie par la mort des cellules à ~4 hpi. Cette réponse est aussi induite par MLA_{CC} chez une lignée transgénique d'*A. thaliana* qui est simultanément dépourvue de trois composants

(PEN2, PAD4 et SAG101) et des trois principales phytohormones (éthylène, acide jasmonique et acide salicylique) impliqués dans la régulation immunitaire. La comparaison des profils d'expression au cours du temps chez des plantes exprimant MLA_{CC}, avec ceux induits au cours de l'ETI et de la PTI chez *A. thaliana*, a révélé des patterns largement similaires lors de la réponse précoce. Ceci suggère que la signalisation initiée par MLA_{CC}, l'ETI et la PTI pourrait converger rapidement vers une machinerie de transcription commune qui active les gènes de la réponse immunitaire. De plus, ces données indiquent que le domaine MLA_{CC} de l'orge suffit à induire la réponse immunitaire normalement associée à l'ETI chez *A. thaliana*, et que l'activation des gènes de la réponse immunitaire peut se produire indépendamment de la PTI. La plupart (> 74.7%) des 562 gènes significativement induits à 2 hpi chez des plantes exprimant MLA_{CC} sont caractéristiques des gènes de type « immediate early response » puisqu'ils sont induits rapidement sans nécessiter la synthèse *de novo* de protéine. Ces gènes pourraient donc être activés par élimination d'un répresseur à courte durée de vie. Dans les régions régulatrices en 5' de ces gènes, des motifs sont fortement enrichis qui correspondent à des sites de liaison pour des facteurs de transcription sensibles au Ca²⁺, tels que le calmodulin-binding transcription activator 3 (CAMTA3) qui est rapidement dégradé au cours de l'ETI. Ceci pourrait expliquer l'inhibition totale de la réponse médiée par MLA_{CC} en présence de LaCl₃, un inhibiteur des canaux calciques, inhibition qui a aussi été décrite par le passé concernant les réponses induites par plusieurs NLRs et P/MAMPs. J'ai effectué un crible génétique de mutants obtenus par mutagenèse chimique et identifié par ce biais trois candidats suppresseurs de la réponse médiée par MLA_{CC}. La purification des complexes protéiques associés à MLA_{CC}, ainsi qu'un crible en double-hybride chez la levure ont permis d'identifier plusieurs candidats interagissant avec MLA_{CC}. Ces approches ont révélé de nouveaux candidats impliqués dans la signalisation médiée par MLA_{CC}.



Title : Cell death and transcriptional signalling mediated by the coiled-coil domain of the barley resistance protein MLA

Keywords : plant biology, phytopathology, immune system, resistance protein, immune signalling, hypersensitive response

Abstract : Plants rely entirely on innate immunity to prevent infection by pathogens. Extracellular perception of evolutionarily conserved pathogen/microbe-associated molecular patterns (P/MAMP) by membrane-resident pattern recognition receptors (PRRs) leads to pattern-triggered immunity (PTI). Host-adapted pathogens intercept PRR-mediated immunity by delivering effectors into host cells. These polymorphic effectors can be recognized by intracellular immune receptors of the nucleotide-binding domain leucine-rich repeat (NLR) family. Upon effector recognition, NLRs trigger a rapid immune response, termed effector-triggered immunity (ETI), which is typically associated with a host cell death response. In barley, the NLR MLA confers ETI against the pathogenic powdery mildew fungus, *Blumeria graminis* f sp *hordei*. Although *MLA* orthologues are present only in the Triticeae family of monocotyledonous plants, barley *MLA* is functional in transgenic dicotyledonous *A. thaliana*, indicating that the underlying disease resistance mechanism has been evolutionarily conserved for at least 150 Mya in monocot and dicot plants. In dicotyledonous *Nicotiana benthamiana*, transient gene expression of the coiled-coil (MLA_{CC}) domain, consisting of the N-terminal 160 amino acids of the MLA receptor, was sufficient to activate a cell death response, raising the possibility that MLA initiates a conserved signalling mechanism through the MLA_{CC} domain. This thesis aimed at identifying signalling mechanism(s) acting downstream of the MLA_{CC} module in transgenic *A. thaliana*. Conditional MLA_{CC} expression triggered immune-related responses, characterized by a rapid onset of massive changes in gene expression at ~2 h post induction (hpi), followed by cell death at ~4 hpi. These MLA_{CC}-triggered responses are retained in *A. thaliana* plants simultaneously lacking the

immune components PAD4, SAG101, PEN2, and all major defence phytohormones, i.e. ethylene, jasmonic acid, and salicylic acid. A comparison of time-resolved and genome-wide transcript profiles in MLA_{CC}-expressing transgenic plants with expression profiles induced during ETI and PTI by endogenous *A. thaliana* NLRs or PRRs revealed at early time points highly similar patterns. This suggests that early signalling mediated by MLA_{CC}, ETI, and PTI converges on a common transcriptional machinery that activates immune response genes, implying that the barley MLA_{CC} domain is sufficient to stimulate an ETI-like response in *A. thaliana*. This also suggests that activation of these immune response genes can occur independently of PTI. Most (> 74.7%) of the 562 genes that were significantly upregulated at 2 hpi in MLA_{CC}-expressing plants are immediate early response genes since their induction does not depend on *de novo* protein synthesis, suggesting that these genes are activated by the removal of short-lived repressors. In the 5' regulatory regions of the early induced genes, I found a striking enrichment of *cis*-acting motifs that serve as binding sites for Ca²⁺-responsive transcription factors, including the calmodulin-binding transcription activator 3 (CAMTA3), which is known to be rapidly degraded during ETI. This might explain complete inhibition of MLA_{CC}-mediated responses by the Ca²⁺ channel inhibitor LaCl₃, which was previously also reported for several NLR-mediated and P/MAMP-triggered responses. Using chemical mutagenesis, I identified three candidate suppressor mutants of MLA_{CC}-mediated responses. Affinity purification of MLA_{CC} complexes and a yeast two-hybrid screen identified several MLA_{CC} candidate interacting proteins. Together this has revealed novel candidate components engaged in MLA_{CC} signalling.

